**Collocation of Sensing, Computing, and Actuation in Low-Power Wireless Nodes for Smart Structure Applications in Civil and Mechanical Systems**

by

R. Andrew Swartz

A dissertation submitted in partial fulfillment
of the requirements for the degree of
Doctor of Philosophy
(Civil Engineering)
in The University of Michigan
2010

Doctoral Committee:

Associate Professor Jerome P. Lynch, Chair
Professor Sherif El-Tawil
Professor Dawn M. Tilbury
Associate Professor Diann E. Brei

## DEDICATIONS

To Corrie, who makes all things possible.
To Kira, who commands the future.

## ACKNOWLEDGEMENTS

I am indebted to a great many people who have provided aid, assistance, advice, material support, funding, or some combination of the above. First and foremost, I wish to thank my wife, Corrie, for her patience and support, and my daughter, Kira, for smiling every night when I get home. Furthermore, I am indebted to my family for their help at every step along the way, particularly my parents, Terrill and Julia Swartz, my wife's parents, Robert and Leslie Guernsey, and my sister Jennifer Swartz.

I would also like to express my sincere gratitude to my advisor, Dr. Jerome Lynch, for his guidance, support, and generosity. If one were to imagine the ideal academic advisor, one would have tremendously difficulty in identifying a more apt realization of that ideal than Professor Lynch.

I would furthermore like to thank my committee members, Dr. Sherif El-Tawil (Civil and Environmental Engineering), Dr. Dawn Tilbury (Mechanical Engineering), and Dr. Diann Brei (Mechanical Engineering) for their feedback and valuable suggestions helping to make this thesis something that is more than just the sum of its parts.

I am also indebted to other members of my research group in the Laboratory for Intelligent Structural Technology (LIST). I would particularly like to thank Dr. Tsung-

Chin Hou, Dr. Kenneth Loh, Mr. Andrew Zimmerman, and Mr. Junhee Kim for their assistance and fellowship. In addition, I would like to thank and acknowledge important contributions made by Mr. Arman Kizilkale, Mr. Doekwoo Jung, Mr. Michihito Shiraishi, Ms. Stephanie Guisbert, and Mr. Roy Wang.

Furthermore, I am indebted to collaborators from institutions located literally around the world. I would like to thank the faculty and students at the National Center for Research in Earthquake Engineering (NCREE) at National Taiwan University (NTU) for their invaluable contributions of time and generous access to their unique experimental facility. In particular, I wish to thank former NCREE director, Dr. Chin-Hsiung Loh, and student Kung-Chun Lu for looking after me during five visits to Taipei. From the Institut für Statik und Dynamik at Leibniz University in Hannover Germany, I wish to thank Dr.-Ing. habil. Raimund Rolfes, Dipl.-Ing. Stephan Zerbst, and Dipl.-Ing. Johannes Reetz for their kind assistance and hospitality on the wind turbine instrumentation.

From Stanford University, I would like thank Dr. Kincho Law, Ms. Amy Askin, and Dr. Yang Wang (presently at Georgia Tech) for providing tremendous support on projects too numerous to list.

From the Los Alamos National Laboratory, I wish to thank Dr. Charles Farrar as well as Dr. Gyuhae Park for a tremendous educational experience during the Los Alamos Dynamics Summer School (LADSS). I would also like to thank my LADSS class for helping me to feel at home as the program kept me separated from my wife for two months.

From the Naval Surface Warfare Center – Carderock Division, I would like to thank Dr. Thomas Brady, Dr. Liming Salvino, and Mr. Jesus Rosario for helping to make the Sea Fighter instrumentation campaign a success. For that, I wish to thank the crew of the FSF-1 Sea Fighter as well.

From the Center for Wireless Integrated Microsystems (WIMS), I would like to thank Dr. Michael Flynn (wireless thrust leader), Dr. Dan Shi (presently with Intel), and Mr. Robert Gordenker for advice and support.

The work presented herein has been partially funded by the generous support of the National Science Foundation (through Grant Numbers 0421180 (PI: Prof. G. Parra-Montesinos), 0636300 (PI: Prof. T. Finholt), 0726812 (PI: Prof. J. P. Lynch, University of Michigan) and 0820607 (PI: Prof. J. P. Lynch, University of Michigan)) and the Office of Naval Research (Contracts N00014-05-1-0596 (PI: Prof. J. P. Lynch, University of Michigan), N00014-09-C0103 (PI: Prof. J. P. Lynch, University of Michigan), and N00014-09-1-0567 (PI: Prof. J. P. Lynch, University of Michigan)). Additional support has been received by the University of Michigan Rackham School of Graduate Studies and the Graham Environmental Sustainability Institute.

## TABLE OF CONTENTS

## LIST OF FIGURES

## LIST OF TABLES

## ABSTRACT

Effective management of civil structures requires both data and a physical means to mitigate the negative consequences of the effects of extreme loading events. This thesis presents a smart structure framework characterized by low-cost wireless nodes with collocated sensing, computing, and actuation capabilities. These nodes are intended to function as an automated first line of defense during extreme loading events, providing both rapid assessment of structural condition (*i.e.*, health) and automated response (*i.e.*, control). Low-cost wireless sensing and actuation nodes promote dense instrumentations that can provide great insight into the dynamic behavior and condition of structures. However, wireless networks should not be viewed merely as one-to-one replacements for traditional tethered systems. Rather, the goal of this thesis is to demonstrate the embedment of computationally expedient approaches for traditional smart structure tasks (*i.e.*, load estimation, structural health monitoring, and structural control) implemented within wireless sensor and actuation networks. The distributed nature of these computing resources, coupled with limitations on power and communication bandwidth, require unique decentralized data processing algorithms that can operate effectively within the decentralized wireless smart structure environment. To accomplish this goal, this thesis first presents the development and validation of a novel wireless sensing and actuation platform necessary to meet the specific requirements of this thesis work. Then, using this wireless system, a method for estimating wind loading from measured wind turbine tower

response is experimentally validated. This method can generate reference loading data that may be used to improve the design economy of future turbines. In addition, a wireless structural health monitoring method based on a physical parameterization of time-series model coefficients is presented for damage detection in post-earthquake scenarios. This method employs a physics-based method of evaluating and integrating damage indications derived from individual sensors within the network. Finally, a partially-decentralized method for wireless structural control is presented in which the wireless network dynamically trades bandwidth for performance of actuators engaged in feedback control. This method provides a means to allocate scarce bandwidth resources while still allowing the wireless controllers to improve performance by identifying and broadcasting only the most valuable feedback data over the network.

# CHAPTER 1

# INTRODUCTION

## 1.1. Motivation of Thesis Work

Civil infrastructure assets form the basis of the modern economy. Structures such as buildings, roads, bridges, dams, and levees are vital for manufacturing, transportation, trade, and most importantly, for maintaining the high quality-of-life standards in technologically developed societies. Failure of one or more of these infrastructure systems can lead to large economic losses and even fatalities. Therefore, careful management of these infrastructure assets is vitally important, especially when considering the fact that these structures are subject to deterioration and damage due to aging and extreme loading events (*e.g.*, earthquakes, hurricanes, typhoons, *etc*.).

### *1.1.1. Deterioration*

Deterioration is a major challenge for the management of civil engineering structures. Corrosion of bridges, for example, is a multi-billion dollar per year problem (Chong

2004) that, if left unchecked, can lead to catastrophic loss of structural integrity (LeRose 2001). In addition, bridges are subject to fatigue damage (Sobanjo*, et al.* 1994; Zhao and Haldar 1996), deterioration of concrete (structure and decking) (ACI Committee 345 2006), freeze-thaw induced damage (Enright and Frangopol 1998), and the effects of scour at supports submerged in waterways (Kattell and Eriksson 1998). Similarly, buildings are also subject to the detrimental effects of aging and the environment. A recent inventory of this nation's civil infrastructure initiated by the American Society of Civil Engineers (ASCE) found that over 72,000 bridges in this country are officially classified as "structurally deficient" and 89,000 bridges to be "functionally obsolete" based on estimates of their present condition (ASCE 2009). While the number of structurally deficient bridges has been shrinking in recent years due to rehabilitation efforts, ASCE still estimates that it will cost approximately $48 billion to rehabilitate fully every bridge currently in this category (ASCE 2009). In the meantime, many of these bridges must be closed or operated at reduced capacity (speed or weight) due to suspected structural deficiency (ASCE 2009). Classification of bridges relies primarily on visual inspection, a time-consuming and subjective process that is limited by the skill of the inspector as well as the level of access that the inspector has (usually limited to surface features). Correlation of visually obtained conditional data to structural performance is a major challenge and can lead to overly conservative management approaches. In addition, the high cost of inspection saps funds from the pool of money available for infrastructure management that might otherwise go to rehabilitation or replacement of structurally deficient or functionally obsolete structures.

### *1.1.2. Exposure to Extreme Loading Events*

In addition to long-term deterioration, civil structures are subject to extreme loading events such as earthquakes, hurricanes, collisions, and blast loads. In 1994, fifty-seven deaths were directly attributed to the Northridge earthquake that occurred in southern California (Chen and Scawthorn 2003). The earthquake was responsible for $30 billion in damage including 34,600 lost job-years in the immediate impact zone (valued at about $3.1 billion) and 11,450 more lost job-years ($1.0 billion) outside the region (Cho*, et al.* 2002). Also included in the damages were a large number of steel moment connections that failed despite the fact the magnitude of the Northridge earthquake was below the design level earthquake for that region (Feld and Carper 1997). These failed connections were hidden behind cladding, insulation, and fire protection and went unnoticed for months following the earthquake event (Feld and Carper 1997). In these cases, the resources available for immediate repairs of the damaged structures were not made available because the damage was not detected in a timely fashion (Mahin 1998). Buildings were left occupied and unprotected despite significant damage to their main lateral load resisting systems. In the aftermath of extreme loading events, scarcity of knowledge and scarcity of response resources present a significant hazard to public safety.

### *1.1.3. Unknown Loads*

While characterization of the effects of extreme loading events is important, characterizing the loads themselves is another challenge facing the civil engineering

community. The proper determination of design loads is vital to avoid overly conservative or unconservative designs. In cases such as earthquakes, dense instrumentation of the ground in seismically active regions helps researchers to build a statistical profile of the size and types of earthquakes endemic to the instrumented region. Those statistics can be used to generate design loads for structures based on expected earthquake ground motions and the dynamic characteristics of the structure. For other types of sites and structures, design loads may not be so easily defined. One application where this is especially true is in wind energy farms (Butterfield*, et al.* 2009). The current code requirements for wind loading are based on regionally defined basic wind speeds, converted to a pressure to be applied to the structure. Anticipated pressures are modified by factors to account for exposure, terrain, height, and directionality (ASCE 2005). While these factors work well for many building applications, turbines in wind energy farms experience complex and unique loadings due to both their distinctive geometries as well as the vortices created by upwind turbines (Hau 2006; Butterfield*, et al.* 2009). Furthermore, current trends to construct wind farms off-shore mean that these structures will be exposed to more complicated loading from wind and wave interactions, a phenomenon that is currently poorly characterized and not fully understood (Camp*, et al.* 2003). Lack of understanding of complex wind and wave interactions often leads to conservative designs that adversely affect the economic competitiveness of this form of sustainable energy (Henderson and Zaaijer 2003). As these structures are constructed, measurement and analysis of the response to these loads are important, not only to monitor the condition of the structures, but to build a database that can form the basis for

future design load determination. As such, extracting the loading information from the recorded structural response data is a key challenge.

This thesis will explore how emerging smart structure technology can help to overcome the aforementioned challenges. Smart structure technology entails the application of sensors, actuators, and computing devices to automate the process of monitoring and controlling civil infrastructure systems. This thesis will focus on some of the technological and economic hurdles that stand in the way to implementing smart structure solutions. Specifically, the thesis will demonstrate how the application of wireless technology can significantly overcome these hurdles. Wireless devices and algorithms for monitoring, feature extraction, and automated response are presented and validated both in the laboratory and in the field.

### 1.2. Smart Structures and Civil Engineering

Given the threats facing society's infrastructure assets, there is a demonstrated need for structures with the ability to sense external stimuli as well as the structural response to that stimuli. Further value still may be gained from structures that can respond autonomously to extreme loads so as to lessen their vulnerability to damage. Such structures, termed "smart structures," can serve at the front lines of defense against the effects of extreme natural events, protecting themselves and their occupants (Brownjohn 2007; Farrar and Lieven 2007). The field of smart structural technology has emerged in recent years to address concerns about long-term structural safety and reliability as well as to introduce additional functionality into structural systems. The term, "smart," is used

to delineate between structures that exist solely to span a distance and support some load from those structures that incorporate additional sensing, actuation, and computational abilities. While numerous definitions of what it means for a structure to be a "smart structure" exist (Gandhi and Thompson 1992; Adeli and Saleh 1999; Janocha 1999; Chopra 2002; Cheng, *et al.* 2008), consensus is forming around some salient characteristics (Zhang and Lu 2008). These characteristics include integrated sensing technologies, information processing, control systems, and actuators that can operate synergistically so as to allow the structure to have a sense of the external stimulus it experiences and to react appropriately and adaptively (Zhang and Lu 2008).

Smart structure technologies were initially developed for mechanical and aerospace engineering applications (Chopra 2002) but multiple applications within the civil engineering community have been found as well (Aizawa, *et al.* 1997; Yi and Dyke 2000; Cheng, *et al.* 2008). Technology for sensing civil structures has been developed using a wide variety of approaches (Doebling, *et al.* 1998; Sohn, *et al.* 2003; Brownjohn 2007) including piezoelectric transducers (PZT), optical sensors, micro-electrical mechanical systems (MEMS)-based sensors (often combined with wireless sensing technologies), and even self-sensing civil engineering materials, A non-exhaustive review of the development and application of these technologies is presented in Table 1.1. While structural monitoring systems can measure the effects of external stimuli, if such systems are provided with embedded computational capabilities, they will also be able to interrogate response data and extract damage sensitive features (Farrar and Worden 2007) that can be used to assess structural health. However, current sensor technology,

**Table 1.1.** Sensing technologies developed for civil smart structures.

| | |
|---|---|
| **Piezoelectric Transducers** | |
| Lamb-wave damage detection | (Kessler, *et al.* 2002) |
| PZT impedance based methods for SHM | (Park, *et al.* 1999) |
| PZT impedance based methods for SHM | (Park, *et al.* 2000) |
| PZT SHM reinforced concrete bridge application | (Soh, *et al.* 2000) |
| PZT impedance sensing for concrete bridge application during destructive load test | (Bhalla and Soh 2004) |
| PZT impedance based methods for SHM | (Park, *et al.* 2007) |
| Review of guided-wave methods | (Raghavan and Cesnik 2007) |
| **Optical Sensors** | |
| Application of fiber-optic sensor technologies for civil SHM | (Culshaw, *et al.* 1996) |
| Field validation on bridge structure | (Mufti, *et al.* 1997) |
| Measurement of dynamic loads | (Inaudi 2004) |
| Highway bridge load assessment | (Moyo, *et al.* 2004) |
| Bragg-grating based sensors for SHM | (Todd, *et al.* 2007) |
| **MEMS Devices** | |
| Application to civil systems | (Kiremidjian, *et al.* 1997) |
| MEMS accelerometer for civil wireless sensing | (Lynch, *et al.* 2003a) |
| Bridge monitoring using MEMS based wireless sensing | (Lynch, *et al.* 2006) |
| Large-scale bridge instrumentation | (Kim, *et al.* 2007) |
| **Wireless Sensing Technologies** | |
| Identified difficulties in application of wireless sensors as one-to-one replacements to tethered systems in terms of power consumption and bandwidth utilization | (Straser and Kiremidjian 1998) |
| Development of a wireless sensor node of SHM | (Lynch, *et al.* 2001) |
| Application of embedded algorithms in wireless network | (Lynch, *et al.* 2003c) |
| Field validation of wireless sensors on bridge structure | (Lynch, *et al.* 2003b) |
| Review of wireless "smart" sensors | (Spencer, *et al.* 2004) |
| Summary review of wireless structural health monitoring | (Lynch and Loh 2006) |
| PZT impedance based wireless sensor | (Mascarenas, *et al.* 2007) |
| Wireless PZT pitch-catch method based sensing with energy harvesting abilities | (Musiani, *et al.* 2007) |
| Decentralized wireless flexibility method analysis | (Gao and Spencer 2008) |
| Large scale bridge instrumentation using wireless sensors and multi-hopping of data | (Pakzad, *et al.* 2008) |
| **Self-Sensing Civil Materials** | |
| Piezoelectric effect of hardened cement paste | (Sun, *et al.* 2004) |
| Conductivity-based strain and damage detection in cementitious composites | (Lynch and Hou 2005) |
| Electrical impedance tomography of cementitious composites | (Hou and Lynch 2009) |

regardless of computing power provision, remains passive and sensors themselves cannot react to prevent damage.

To accomplish this final task, actuation capabilities are required. Structural control applications for civil systems are not new (Yao 1972; Soong 1990; Housner*, et al.* 1997; Spencer and Nagarajaiah 2003) and provide the means by which structures can respond to stimuli for mitigation of the effects of undesirable loadings (*e.g.,* seismic, wind, or blast). Smart structural control applications have included base isolation systems (Nagarajaiah and Narasimhan 2006), variable stiffness systems (Nagarajaiah and Mate 1998), and damping systems using adaptive materials (Dyke*, et al.* 1998; Symans and Constantinou 1999; Song*, et al.* 2004; Song*, et al.* 2006). A more exhaustive literature review for structural control may be found in *Chapter 6* of this thesis. These systems require the coordination of sensors, controllers, and actuators within the structure; see Figure 1.1 [adapted loosely from Brei (2007)].

It has been demonstrated that generic, one size fits all sensing and control systems are not well suited for smart structure applications in the civil engineering domain (Farrar*, et al.* 2006). Instead, what is needed are systems designed to meet the specific needs of the structure in which they will be installed. In addition, it is desirous to employ high sensor densities in monitoring applications to achieve statistically relevant and redundant monitoring results (Jia*, et al.* 2009). Unfortunately, the complexity and vast size of civil structures necessitate large numbers of sensors to realize this high level of sensor density. An additional benefit of high density, in both sensors and actuators, is an increase in the long-term overall system reliability (due to the avoidance of single points of failure). As will be seen in the next section, these needs introduce additional costs to the system,

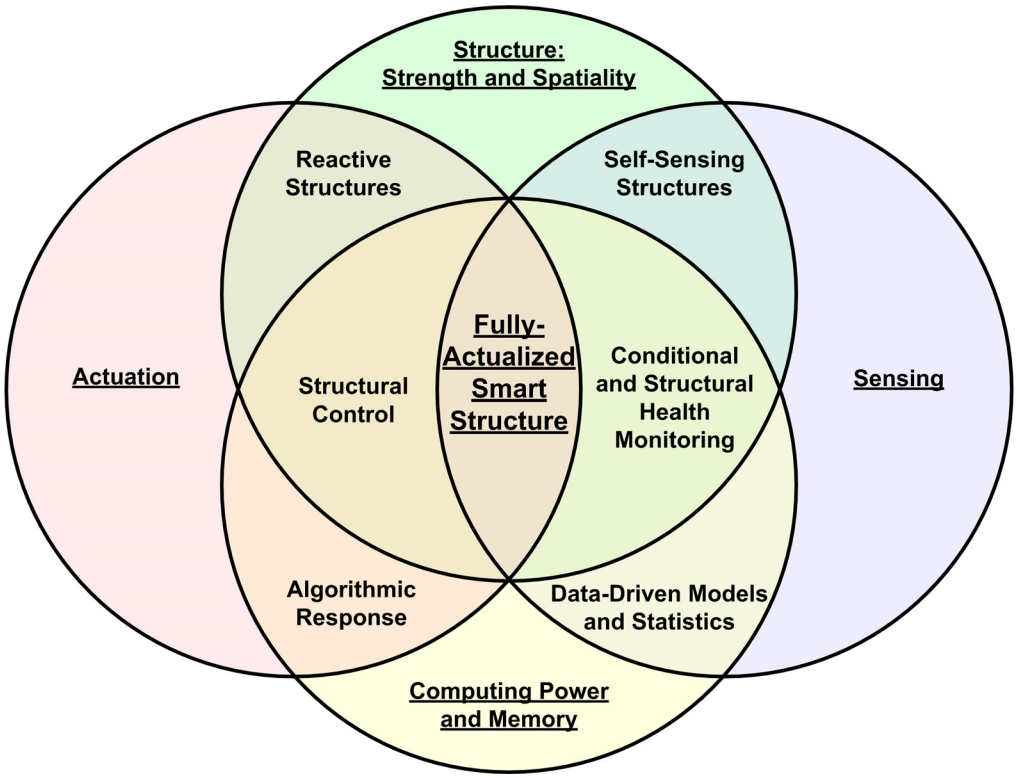


**Figure 1.1.** Interaction of the various aspects of smart structure technologies: structure, actuation, sensing, and computing [adapted from Brei (2007)].

which indirectly place a barrier to widespread commercial implementation. A wireless sensor design can reduce implementation costs which would increase the adoption of smart structure technologies in industry.

### 1.3. Wireless Smart Structure Technology

A key barrier to widespread adoption of smart structure technology in the civil engineering realm is the continual pressure to reduce system costs while increasing quantifiable benefits. Due, in part, to their relative novelty, smart structure technology tends to be somewhat costly (Gandhi and Thompson 1992). Because computing

resources are required to take full advantage of these strategically placed sensing and actuation devices, it is necessary to connect these devices to a computer. Due to the relative size of civil structures and the inaccessibility of many portions of the structure, the installation of signal cables between devices and a centralized computing center can be prohibitively expensive, often costing thousands of dollars per channel (Celebi 2002). Signal cables are also subject to damage and analog domain noise corruption which can impair the operation (and effectiveness) of the smart structure system.

Wireless sensor technology can alleviate the aforementioned cabling costs, linking sensors and actuators to computing resources at a significantly reduced cost, to the order of one hundred dollars per sensing channel. By reducing the per channel cost, wirelessly-enabled sensors and actuators enable implementation of dense networks of smart structure devices at a competitive cost. In addition, wireless devices represent a paradigm shift in smart structure technology for civil systems. Instead of viewing sensors, actuators, and computers as distinct, and often physically separated entities, wireless sensors are integrated systems that incorporate transducers (sensors and actuators), signal conditioning, computer memory, and data processing within a single package. The collocation of computing with sensors is a significant advancement because it allows automated data processing to occur at the sensor leading to early warning in the instance of structural problems (*e.g.*, damage). Fundamentally, automated data processing also avoids the accumulation of large quantities of unprocessed data, a phenomenon that plagues structural monitoring systems that lack any form of autonomous data processing.

Successful field deployments in actual civil structures over the past five years have demonstrated the feasibility and value of the technology (Lynch*, et al.* 2003b; Kurata*, et al.* 2005; Lynch*, et al.* 2006; Whelan*, et al.* 2007; Pakzad*, et al.* 2008). Research continues to advance wireless sensing with distributed computing within the wireless sensing network now emerging as a new usage strategy for the technology. Sensor-centric computing, in which wireless sensors process their own measurement data, has been illustrated for modal analysis (Lynch*, et al.* 2004) and damage detection (Tanner*, et al.* 2002; Clayton*, et al.* 2005; Hou*, et al.* 2005). More recently, network-wide computing architectures have also been proposed for mode shape estimation of civil structures (Zimmerman*, et al.* 2008). Wireless sensors with the ability to affect their surroundings are also suitable for "active" sensing applications (Chintalapudi*, et al.* 2005) thereby eliminating reliance on ambient vibrations for excitation. Once actuation is integrated into the design of a wireless sensor, it becomes possible for wireless sensors to perform feedback control functions as well. In this study, a wireless sensor capable of commanding structural actuators is proposed.

Wireless sensors however, do present their own set of unique challenges that must be addressed. Principally, challenges include: 1) the physical limitations to the amount of data that may be transmitted over a communications channel; 2) communication distance limitations (or the effect of barriers to radio frequency (RF) wave propagation); and 3) energy limitations based on the fact that many of these devices are powered by battery packs. These challenges affect the prospects for both system scalability and economy. For example, scarce bandwidth resources can be quickly saturated by transmission of raw data as the number of sensors in the network increases. One approach frequently

employed for overcoming communication distance restrictions in wireless sensor networks is the use of multi-hopping, the practice of relaying data from node to node within a network to cover long distances (Broch*, et al.* 1998; Kurata*, et al.* 2003; Nagayama 2007). This practice is very effective in overcoming communication range restrictions in wireless sensor networks, but it does have a negative effect on bandwidth utilization by the network reducing the quantity of data that may be transmitted in a fixed period of time (Callaway 2003). Multitier wireless networks (consisting of low-power data nodes collecting data and transmitting it to high-power collector nodes with greater throughput and range) can also address range issues (Kottapalli*, et al.* 2003) without significant bandwidth degradation (different tiers within the network can be allocated to separate communication channels), but still may be unable to penetrate physical barriers to microwave signals (Elliott 2003). Finally, the cost savings realized by the elimination of cables from the system will be negated if overly frequent system maintenance is required to replace batteries. An important advance in enhancing the practicality of long-term deployment of wireless sensing technology is the application of energy harvesting techniques by which wireless sensors generate power for themselves from locally ambient energy sources (Sodano*, et al.* 2004; Sodano*, et al.* 2005; Musiani*, et al.* 2007). However, energy harvesting applications are limited by the amount of energy available in the environment, as well as the mechanism by which that energy is captured and stored (Scruggs 2009). Due to that limitation, preservation of energy within wireless sensing networks is still an important concern.

Two strategies will be employed throughout different phases of this thesis to overcome or alleviate the challenges associated with wireless sensing: 1) embedded data

processing; and 2) use of hybrid wired/wireless networks. The most important strategy is the use of embedded data processing. By processing data locally within the sensing node, the need to transmit vast amounts of raw data may be eliminated, thereby saving bandwidth and energy (due to the fact that data processing is more energy efficient than transmission) (Straser and Kiremidjian 1998; Lynch and Loh 2006). This practice also preserves system scalability and attempts to prevent accumulation of unexamined data. The second strategy is to use a hybrid network consisting of wired and wireless sensors where distance and physical barriers impede the reliability of wireless communications. In a hybrid monitoring system, a relatively small number of wired sensing nodes collects data (raw or processed) from many distributed wireless nodes. The wired backbone of the hybrid system can move higher rates of data and is able penetrate radio-frequency (RF) barriers while allowing for efficient centralization of data from a large number of channels. The wireless system developed for this thesis will be designed to employ these strategies in order to meet all of the requirements for a smart structure system.

### 1.4. Development of the *Narada* Wireless Sensing and Actuation Node

At the core of this thesis is the development of a wireless sensing/actuation node specifically tailored to meet the demands of the smart structure application ontology. Creation of the *Narada* wireless sensing and actuation node (see Figure 1.2) required a hardware and firmware design that enhances its functionality in smart civil structure applications. Hardware design encompasses the selection of electrical components and the layout of a printed circuit board (PCB), which together constitute the physical node.

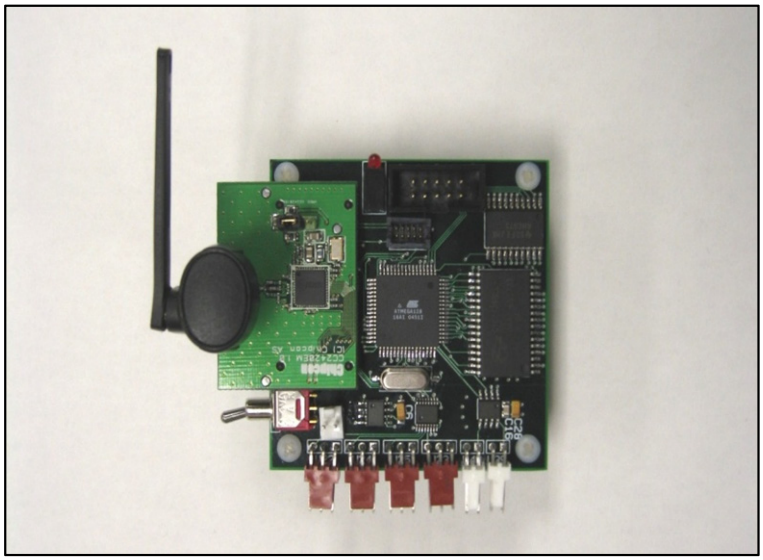

**Figure 1.2.** *Narada* wireless sensing and actuation node.

The firmware (*i.e.*, embedded software) development, which was required to produce a working prototype, includes an embedded operating system (OS) as well as engineering algorithms that interrogate data collected. The OS is composed of low-level device drivers that allow individual hardware components to work together, medium access control (MAC) definitions that define how the sensor is allowed to access the wireless communications channel, communications protocols that define how the sensors transmit information among themselves and with users, and a state-machine that governs which actions are allowable at which times. These firmware components form the basis for automation of the sensor's operation.

Firmware enables a host of embedded algorithms that form the basis of smart wireless sensing and control technology. Development of these algorithms followed a natural flow from basic algorithms to increasingly complex smart structure applications, as shown in Figure 1.3. Basic data processing algorithms for system identification (*e.g.,*

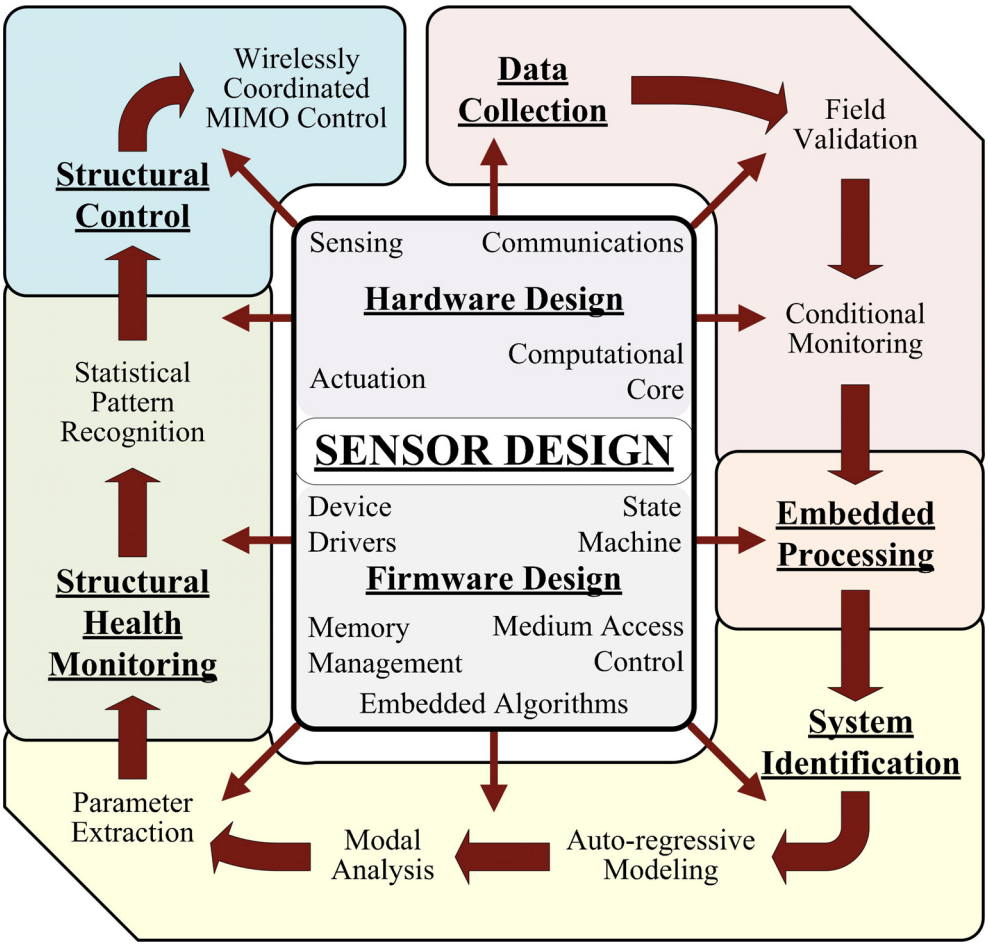


**Figure 1.3.** Schematic depicting the developmental flow of the *Narada* system.

auto-regressive time-series modeling, modal analysis, model parameter extraction, and state estimation) enable complex model-based structural health monitoring applications when combined with statistical pattern recognition algorithms. Increasing the level of complexity, the addition of real-time wireless structural control applications to the *Narada* toolbox make it a fully-active smart structure system capable of controlling physical systems (in this study, civil structures).

## 1.5. Organization of the Thesis

This thesis is organized as follows (also see Figure 1.4). *Chapter Two: Development of the Narada Wireless Sensing and Actuation Unit* presents a detailed description of the design of the *Narada* wireless sensor including a review of precursor wireless sensing units from both industry and academics. In addition, the design considerations that make *Narada* ideally suited for civil engineering smart structure applications will be presented. *Narada* is designed as a sensing, computing, and actuation platform that serves as a building block for wireless smart structure systems. The sensing interface allows for the deployment of up to four transducers per node allowing a structure with *Narada* nodes to collect and process a heterogeneous set of data regarding its state and condition. The actuation interface accommodates command lines for the operation of up to two actuators thereby allowing structures instrumented with *Narada* nodes to respond to external stimuli. In addition to hardware, *Chapter Two* also presents the development of the embedded software (termed firmware) that operates the *Narada* unit. *Chapter Two* presents some basic data collection and transmission algorithms embedded in *Narada*; higher-level embedded processing algorithms for load estimation, health assessment, and structural control are presented in subsequent chapters. The embedded engineering algorithms that process and analyze data constitute the bulk of the intellectual contributions that this thesis makes to the field.

Since its inception, the *Narada* wireless sensing and actuation node has been extensively field tested. *Chapter Three: Field Validation of Narada: Hybrid Wireless Hull Monitoring of Naval Combat Vessels* presents an in-depth field deployment case study in which the *Narada* wireless units are used for structural monitoring. This case

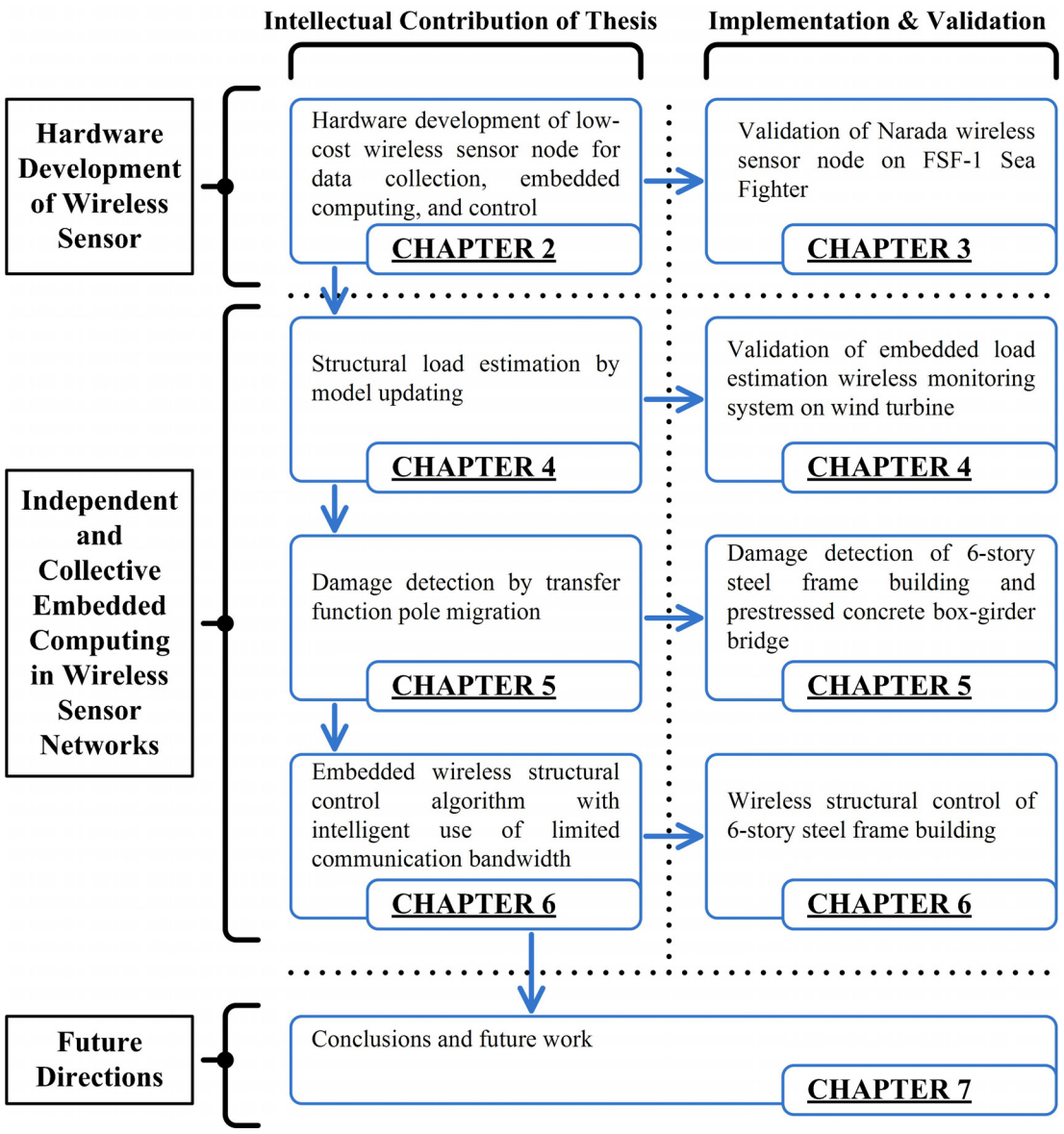


**Figure 1.4.** Thesis outline.

study provides a demonstration of an operational network of *Narada* wireless sensors as they collect data in an unsupervised manner for an extended period of time aboard a high-speed, U.S. Navy littoral combat vessel. In this case study, a hybrid wireless/wired monitoring network is employed to take advantage of the ease by which wireless sensors aggregate data from transducers installed within individual compartments of the ship and

the high data throughput and bulkhead piercing ability of the wired portion of the network. Data collected from the wireless system are verified against data collected from a traditional tethered monitoring system also installed in the ship.

In *Chapter Four: Structural Monitoring and Load Estimation of Wind Turbines Using Wireless Sensor Networks* the first true embedded data processing algorithm is presented in which a model-assisted load estimation method for wind turbine applications is embedded within the *Narada* wireless sensor. The characterization of wind loads imposed on wind turbines (structure and components) is still an open problem, particularly in large wind farm arrays and off-shore applications. Wireless sensors can be economically deployed to collect structural response data from turbines in the field; the challenge lies in extracting loading information from the response of the turbine where the turbine dynamic model is either not characterized or changes over time. In *Chapter Four*, an embedded algorithm performs an online update of a turbine tower model; then the updated model is used to estimate the loading spectra extracted from measured response data. The loading data extracted can be used to estimate the fatigue life remaining for the turbine or to improve the design of future turbine installations (topics that are beyond the scope of this thesis). This chapter includes a laboratory validation component as well as results of a field instrumentation campaign in which structural response data from operational wind turbines are collected and analyzed using the *Narada* wireless sensor.

In *Chapter Five: Wireless Structural Health Monitoring Using Migration of System Pole Locations*, a damage detection algorithm is presented to run on the distributed computing network represented by a monitoring system consisting of *Narada* wireless

sensors. Because data, memory, and computational power are distributed throughout the network, the damage detection algorithm relies primarily on sensor-level data and sensor-level processing to identify changes in the dynamic behavior of the structure that could indicate damage. By processing data, at the sensor level, the algorithm avoids transmission of large tracks of raw data thereby preserving battery energy and system scalability (the transmission of raw data over increasing numbers of data channels quickly erodes the available bandwidth of the communications channel). Single-input, single-output (SISO) time-series models (either output-only or input/output) are recursively fit to collected data at the sensor level. System poles are then extracted from the time-series models, and their complex values (corresponding to frequency and damping) are correlated to damage. The damage estimates made independently at all of the sensors in the network are then integrated by means of weighted averaging. Weights are based on the estimated signal quality as indicated by that sensor's contribution to the observability grammian in modal coordinates. *Chapter Five* presents the method in detail and demonstrates results based on changes in stiffness of a box-girder concrete bridge and a six-story steel building.

With its native actuation interface, the *Narada* wireless sensor can also provide smart civil structures with reactive capabilities. A wireless structural control method for seismic disturbance rejection is presented in *Chapter Six: Strategic Network Utilization in a Wireless Structural Control System for Seismically Excited Structures*. In this chapter, a novel decentralized feedback control method is presented by which wireless bandwidth is traded for controller performance (Yook*, et al.* 2002). Wireless sensors measure story responses, compute the entire state response of the structure, compute

control forces, and actuate collocated semi-active dampers. Each sensor employs a redundant Kalman estimator; the performance of the controller is then linked to the quality of the state estimates generated by the local estimators. Sensors are continually comparing their measured data to local estimates. When the error exceeds a predefined threshold, the unit broadcasts the measured value to the entire network to use in the calculation of control forces. By varying the broadcast threshold, the utilization of the shared wireless communication channel and performance of the control system may be varied. *Chapter Six* presents the method in detail and investigates the effects of varying this threshold as applied to the same six-story building presented in *Chapter 5*, except that the structure is now controlled by magneto-rheological (MR) dampers.

Finally, *Chapter Seven: Conclusions and Future Directions*, presents final comments on the achievements and relevance of this thesis work, its suitability for implementation and commercialization, and a discussion of the future work that can be built upon these studies. Also included in *Chapter Seven* is a broader discussion of where the field of wireless sensing for smart civil structures appears to be heading in future years and beyond.

# CHAPTER 2

## DEVELOPMENT OF THE NARADA WIRELESS SENSING AND ACTUATION UNIT

This chapter presents the development of the *Narada*[1] wireless sensing unit that has been designed as a low-cost alternative to cable-based monitoring systems in civil infrastructure applications. The *Narada* wireless sensor has been developed with embedded processing and low-power operation in mind. Initially, wireless sensors were proposed as a one-to-one replacement for tethered sensors (Straser and Kiremidjian 1998). However, by taking advantage of the inherent distributed processing power contained within a network of wireless sensing nodes, data processing and structural health monitoring activities can be fully automated by the monitoring system. In addition, a wireless system that can react in real-time to its environment is desired. Therefore the *Narada* wireless sensor is also built with an actuation interface so that it can participate in active networks and be used for embedded feedback control operations

[1] The wireless sensing unit is named for the Javanese messenger of the gods, Narada, who would warn people of impending disaster Encyclopedia Mythica, "Narada", *Encyclopedia Mythica: mythology, folklore, and religion* Retrieved Sept. 1, 2009, from http://www.pantheon.org/articles/n/narada.html, (1997).

where the wireless sensor is responsible for sensing, control force calculation, and command of actuators. In this chapter, the individual challenges inherent in wireless sensing networks are detailed, followed by a discussion of the hardware elements required in the design of a wireless sensing/actuation node. This discussion is followed by a summary of wireless sensing prototypes that predated or are contemporaries of the *Narada* design. Finally, the hardware and software components of the *Narada* wireless sensor are introduced and described including the basic sensing module. Embedded processing algorithms developed for feature extraction, structural health monitoring, and structural control are presented in later chapters (*Chapters 4*, *5*, and *6* respectively) with their associated applications.

## 2.1. Challenges in Wireless Monitoring

Wireless sensors are low-cost alternatives to traditional wired sensors due to the eradication of extensive wiring needed between traditional tethered sensors. However, the lack of the dedicated communication channel offered by a wired system presents unique challenges to the successful implementation of wireless monitoring systems in actual structures. These challenges include limited on-board power supplies as well as bandwidth constraints inherent to the wireless communication channels that exist between sensing nodes. In addition, transmission range becomes a major concern in spatially disperse networks, as is often the case in civil engineering structures that are regularly defined by dimensions of hundreds of meters. Finally, data flow over-the-air in wireless networks presents an additional security concern that must be addressed. These

challenges, and strategies for alleviating their effects, are presented in detail in this section.

### *2.1.1. Limited Power Supplies*

In some structures, such as commercial buildings, wireless sensors can be conveniently operated using AC power native to the structure. However, many civil structures do not have AC power outlets distributed throughout. Therefore, without cables to supply power, wireless sensors are reliant on battery power to function. For monitoring systems intended to operate independently in the field (perhaps for years at a time) power consumption is then a major concern. The cost savings that can be obtained by employing wireless sensing will never justify a wireless system that requires constant maintenance and battery replacement. This fact is especially true in the civil engineering environment where sensors may be out of reach, located behind cladding, or otherwise very difficult to access. The design of a wireless sensing unit must therefore incorporate low power components in its design in order to preserve battery power as much as is possible. However, lower power consumption often comes with reduced functionality: lower resolution, lower communications range, and/or reduced speed. These are all tradeoffs that must be judiciously analyzed during the design of wireless sensors in order to reduce power consumption yet obtain adequate sensor performance for the intended application.

The largest consumer of battery power in most wireless sensor hardware designs is the wireless radio. Given this fact, reducing radio use is the most effective way of preserving battery power within a well designed wireless sensing network. Because

computational operations within the sensing unit are less costly (in terms of energy drain) than data transmission, any on-board data processing that can reduce the amount of raw data transmitted wirelessly throughout the network will result in a net decrease in energy expended (Straser and Kiremidjian 1998; Lynch*, et al.* 2004b). Besides simply preserving battery life, on-board data processing is advantageous in any monitoring system as it helps to avoid data glut, the situation where a very large collection of data is compiled within a repository at a rate faster than a qualified person (*e.g.,* an engineer or trained technician) can manually process. By collocating computational power at the sensor, data can be processed as it is collected, without the added labor and expense of human interaction.

For many monitoring applications, some additional options exist to help overcome power supply limitations. First is the strategic use of a wireless sensor's sleep mode, where the sensor is powered down for a prolonged period of time. Another option is to scavenge energy from the environment, such as capturing solar power (Shinozuka 2003; Chung*, et al.* 2004) or harvesting power from mechanical vibrations (Sodano*, et al.* 2004; Scruggs 2009). For applications with little to no computational requirements, passive radio frequency identification (RFID) sensors are an additional option to consider. RFID sensors do not require a collocated power source since power is received from a reader through electromagnetic coupling (Finkenzeller 1999). Generally, appropriate power saving approaches are often application specific, and require careful thought as well as creativity on the part of the system designer.

### *2.1.2. Limited Bandwidth*

The majority of wireless sensing units today are designed to operate within the unlicensed industrial, scientific, and medical (ISM) radio band. In the United States, the Federal Communications Commission (FCC) has designated 900 MHz, 2.4 GHz, and 5.0 GHz frequency bands as unlicensed ISM frequencies for general use, but limits the output power of devices that operate within those bands to 1 W (FCC 2004). Many wireless technologies (*e.g.,* Wi-Fi, Bluetooth, Zigbee) operate within these frequency requirements. The limited number of unlicensed frequencies and the potential for interference from other wireless technologies using the same bands restricts the amount of data that can be reliably transmitted within a network during a given time period (even in cases where power consumption is not a concern). Another factor to consider is that wireless signals may be sent either as narrow-band signals (*i.e.*, modulated on a single frequency) or as a spread-spectrum signal (*i.e.*, modulated over a range of frequencies). Narrow-band signals are more susceptible to environmental interference and multi-path distortions (Mittag 2001), however spread-spectrum signals, while more reliable (Bensky 2004), monopolize more bandwidth and further limit the total amount of data that can be moved over a particular range of frequencies in a given time period.

Multiple devices sharing common bandwidth (wired or wireless) must coordinate their actions to avoid collisions that would corrupt the data they transmit. A number of medium access control (MAC) protocols are available for this purpose. A MAC protocol defines the rules a device must follow in order to access a shared communication medium; in the case of wireless sensors, that medium is a wireless channel. These rules are designed to avoid collisions and corruption of data, ensure proper data reception, and

offer uniform quality of service throughout the network (Zhao and Guibas 2004). Two MAC protocols that are popular for wireless sensing applications include carrier sense multiple access with collision avoidance (CSMA/CA) and time division multiple access (TDMA). CSMA/CA avoids collisions by enabling sensors to detect when another unit is utilizing the wireless channel; collisions are then avoided by having any unit detecting another unit's use of the channel to back off for a random period of time before attempting to send its data packet. TDMA is a more straight forward (and deterministic) approach by which guaranteed time slots for communication are allocated to each wireless sensor. In large civil structures, the ability for multiple sensors to share a single medium is especially important when taking into account limitations on transmission range between nodes.

### *2.1.3. Transmission Range*

As previously mentioned, the power levels of transmissions made within unlicensed frequency bands are limited by the FCC to 1 W. Limiting the output power also limits the effective communication ranges of devices that use these bands. In open spaces, wireless signals lose power in proportion to their wavelength and in inverse proportion to the square of their distance from the transmitter (Rappaport 2002). Boundaries such as floors and walls also attenuate the wireless signal; this effect is called path loss. In civil engineering structures, the size of the structure can be considerably larger than the effective range of low-power wireless devices. Nodes may be able to communicate with neighboring nodes but not distant sensors. A number of solutions are available to overcome range restrictions. First, altering the antenna can produce substantial

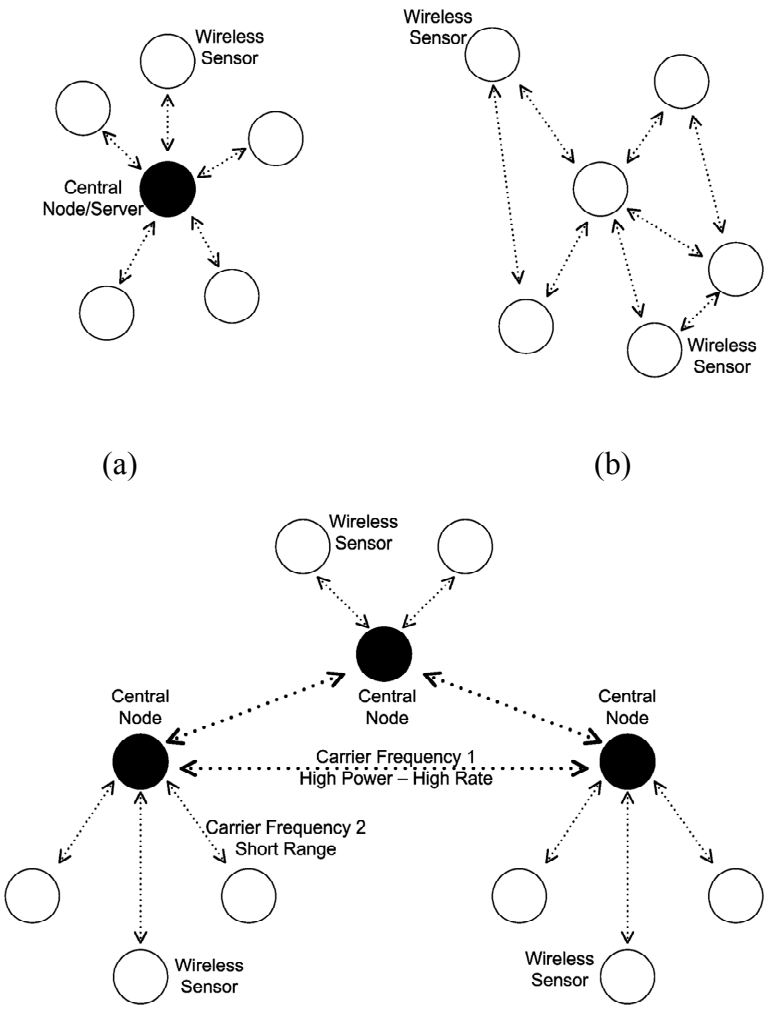


**Figure 2.1.** Wireless communication topologies: (a) star network, (b) peer-to-peer, (c) multi-tiered networks, adapted from (Lynch and Loh 2006).

improvements. High-gain and directional antennas can increase the effective range of wireless sensor nodes, but these may be expensive solutions. High power broadcasts would also drain available battery power quickly. Such solutions are ideal for star networks (Figure 2.1(a)) in which a single unit seeks to communicate with all other units in the wireless sensor network.

Where time is not critical, multi-hopping, peer-to-peer networks (Figure 2.1(b)) can transmit data from node to node over the entire length of the network. However, the delay induced in multi-hopping, peer-to-peer networks increases rapidly as the network grows larger, effectively limiting its node-to-node data rate. Assuming 100% reliable communication between the nodes, the total energy expended by multi-hop network will be less than in star topologies because lower power data transmissions are used (Zhao and Guibas 2004). However, if link quality is poor and frequent re-transmission of data is necessary, multi-hop networks lose their advantage and can actually consume more power than a star network with higher-power radios.

Finally, a multi-tier network architecture (Figure 2.1(c)) may be employed in which high-power, high-throughput central nodes (wired or wireless) serve as intermediaries for lower-power wireless sensor nodes. The central nodes, powered from a structure's electrical grid, collect data from their local sub-network and transmit aggregated data to other central nodes on either a second carrier frequency (Mitchell*, et al.* 2002) or using a traditional wired network.

### *2.1.4. Security*

As owners of Wi-Fi networks are well aware, wireless networks are vulnerable to security threats, both passive and active. Passive attacks come in the form of attempts to steal data as it is transmitted over the airwaves (Perrig*, et al.* 2004). One type of active attack involves the transmission of malicious data into the network to negatively impact its performance (Karlof and Wagner 2003). Both of these forms of attack may be defeated by use of an effective encryption algorithm (Karlof and Wagner 2003; Karlof*, et*

*al.* 2004). Encryption increases the time and energy overhead involved in wireless transmissions, computation, and memory but may be necessary in critical applications where security is a chief concern (Perrig*, et al.* 2002). The other form of active attack that might be perpetrated against a wireless sensing network is jamming which is the flooding of the communications bandwidth range with interfering signals that are intended to block communications (Karlof and Wagner 2003). In such cases, unless the power output of the network radios can be increased dramatically, this kind of attack will be debilitating to a wireless network. In applications with a reasonable possibility of suffering such an attack, and where communications between nodes are critical, wireless networks are probably not an ideal means of data acquisition. Susceptibility to this kind of attack is a fundamental limitation of the wireless sensing approach.

## 2.2. Hardware Requirements for Wireless Sensors for Structural Monitoring and Control

The primary task of wireless sensors is to collect and transmit sensor data using a wireless channel. In order for wireless sensor nodes to communicate with one another, digital wireless radios are readily available and will be used. However, because the outputs from most sensors are analog, signals at some point must be converted into the digital domain in order to be transmitted using the digital radio. To accomplish the task of digitization of the analog sensor data, a sensing interface must also be included in the design of a wireless sensor node. Prior to sending data to the digital radio, the data must be packaged in a packet that is used to route the data in the wireless network. Therefore, a computational core containing a microcontroller is necessary for packetizing sensor data prior to communication. Hence, wireless sensors typically contain three primary

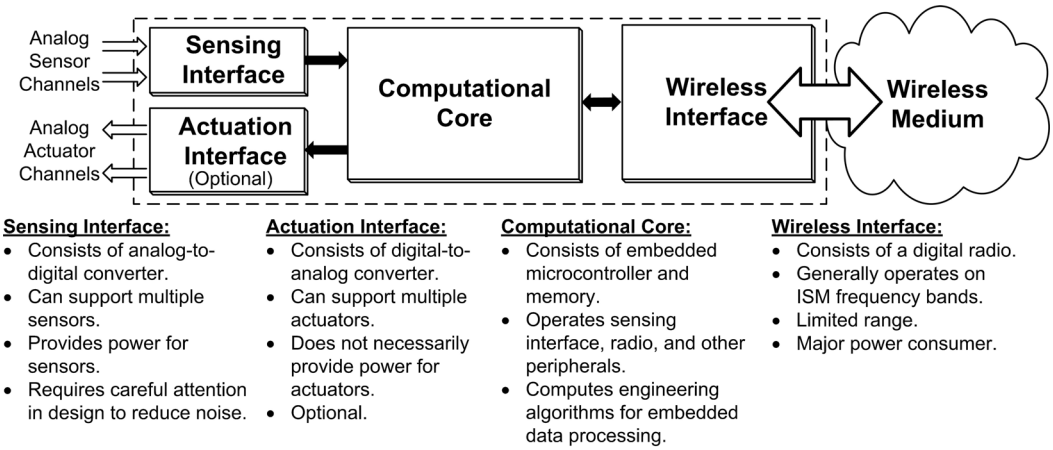


**Figure 2.2.** Wireless sensing node architectural diagram.

functional modules: sensing interface, communications interface, and computational core as depicted in Figure 2.2. All of the academic and commercial wireless sensors previously explored for structural monitoring have been designed with these three modules. This thesis will attempt to extend the functionality of the wireless sensor by allowing it to interact with its physical environment (or function as an "active sensor"). As a result, a fourth functional element is proposed: the actuation interface. This interface will take digital signals originating from the microcontroller and convert them into analog voltage signals that can command a host of actuators (*e.g.*, hydraulic, piezoelectric, and electric actuators). The compositions and roles of each of these functional elements are described in this section with an emphasis on providing solutions to the aforementioned challenges associated with wireless structural health monitoring.

### *2.2.1. Sensing Interface*

The sensing interface is responsible for converting analog voltage output signals from transducers interfaced to a wireless sensor unit into digital signals that can be processed

by a digital processor. Many types of transducers commonly used for monitoring of civil structures (*e.g.* linear variable differential transformers, geophones, accelerometers, *etc*.) output analog signals that are not immediately usable by digital circuitry. Therefore, an analog-to-digital converter (ADC) is needed to transform these analog signals into a digital format. Key considerations when selecting an ADC are resolution, maximum sampling frequency, allowable input voltage range, and noise characteristics.

Resolution is especially important in civil applications because structural responses to ambient conditions can be quite small. Here, high resolution is required in order to adequately differentiate low energy signals from electrical noise inherent to the sensor. Most commercially available wireless sensing units implement low resolution ADCs in the range of 10 to 12-bits. Higher resolution (16-bits or higher) is more suitable for civil monitoring applications, particularly for ambient excitation studies where the signal level is quite low and important features may be difficult to distinguish from the noise floor.

The voltage range of the ADC is also important to consider. For example, signals outside of the ADC allowable input range will not be measured correctly. Furthermore, using a large input range to record data from low voltage signals wastes valuable resolution. As a result, the voltage range of the transducer should be properly matched to the input voltage range of the ADC. Otherwise, amplification (or de-amplification) circuits may be necessary to add between the sensor and ADC (Wang 2007).

In addition to voltage range, the noise characteristics of the sensing interface will impact the final measurement resolution that a wireless sensor can realize. Hence, electrical noise outside the ADC should be kept as low as possible to preserve the ADC resolution. Generally, electrical noise finds its origin in the digital circuitry that

surrounds the actual ADC component; therefore, careful circuit layout is mandatory when integrating high resolution ADCs in the wireless sensor circuit.

Secondary considerations for the design of the sensing interface include number of sensing channels, power consumption, and cost. Providing multiple sensing channels per node allows one node to collect data from more than one sensor resulting in amortization of the unit cost over more channels. Low power consumption is vitally important for wireless monitoring applications. However, low power components often come with performance tradeoffs in terms of speed, resolution, noise, and other factors. For applications that rely solely on battery power, it is prudent to select the lowest power ADC meeting the minimum requirements of the intended application.

### *2.2.2. Computational Core*

The microprocessor selected for the computational core is one of the most important components of the wireless sensor design. The programming that operates the sensing node is contained within the computational core. More specifically, this programming runs on a microcontroller. The microcontroller is a low-power computing platform capable of executing complex tasks reliably and efficiently. The microcontroller is responsible for operation of the peripheral devices (*e.g.*, ADC, transceiver, *etc*.) on the sensing node, coordination of wireless communications between sensors, embedded data processing, and power management. For some applications, the memory required for data storage or embedded processing exceeds the capacity of the microcontroller. In these cases, external memory may be added for additional data storage capacity. The microcontroller may also include built-in peripherals that may form the basis of the other

interfaces (*e.g.*, an integrated ADC might serve as the basis for a sensing interface). Key properties in selecting a microcontroller include power consumption, clock speed, memory, number and type of peripheral communication buses, timers, and cost.

### *2.2.3. Communications Interface*

Sensors must communicate with the end-user of the monitoring system and, in some cases, with other sensors in the network for collaborative data analysis. Communicating data, or the results of embedded algorithms, is accomplished by the communications interface. A two-way wireless radio (*i.e.*, transceiver) contained within this interface provides the primary communication link for the node. Key parameters for wireless transceiver selection include transmission data rate, transmission range, power consumption, operational frequency band, compliance with communications standards, and cost.

### *2.2.4. Actuation Interface*

For active sensing applications (*e.g.,* ultrasonic inspection or feedback control) in which the wireless sensing unit must interact with its environment, a fourth interface is required to command actuators. For motor based actuators, a pulse-width modulator (PWM) interface can supply the command signal. The PWM interface is provided as a built-in peripheral of many microcontrollers, though amplification may be necessary. Most other actuators are commanded using analog voltage signals necessitating a digital-to-analog converter (DAC) to bridge the gap between the microprocessor and an actuator. A DAC converts discrete time digital signals into continuous analog signals, generally

via zero-order hold outputs. Key properties in DAC selection include resolution, output voltage range, power consumption, number of channels, settling time, and cost. Considering civil structures, it is often the case that the resolution is not as critical for the actuation interface as it is for the sensing interface, as civil engineering actuators are rarely high-precision instruments. Output range, settling time, and power consumption are usually more important properties to consider for structural engineering applications.

## 2.3. Wireless Sensing Prototypes

Since the late 1990's many wireless sensing unit prototypes have been developed for both academic and commercial applications. With different intended applications and priorities in mind, wireless sensor designers have gone in a myriad of different directions with their developments. Depending on the goals of the designers, node design may emphasize speed, transmission range, reliability of communications, security, versatility, sensitivity, power consumption, cost, or some combination of those factors. Clearly, it is impossible to emphasize all of these objectives in a single, generic design. Furthermore, the best sensing unit design for one application is not necessarily the best design for another. With that fact in mind, Tables 2.1 through 2.4, adapted from tables compiled by Lynch and Loh (2006), present published specifications of wireless sensors developed in academia, as well as industry, that illustrate the development of wireless sensing units from 1998 to 2009. Tables 2.1 and 2.2 present seventeen academic wireless sensing units developed since 1998 ranging from short-range, low-power mites (Mitchell*, et al.* 2002), to powerful and versatile behemoths (Allen 2004; Farrar*, et al.* 2005). Table 2.3 presents commercial sensors while Table 2.4 presents active wireless sensing units that include

actuation interfaces in their design (including the *Narada* wireless sensor designed during the course of this thesis). These tables help to put the *Narada* wireless sensor into the context of the existing wireless sensing hardware at the time of its inception and facilitate comparison to sensor platforms that follow.

*Narada* shares many hardware attributes (and even functional components) with precursor and contemporary wireless sensing platforms; but it is *Narada*'s unique combination of these attributes that make it the ideal platform for performing the embedded sensing, processing and control tasks in the following chapters of this thesis. At its inception, very few wireless sensing units feature high-resolution (16-bit or greater) sensing interfaces; but, as of the writing of this thesis, additional systems with this ability have been developed (Pakzad*, et al.* 2008; Rice and Spencer 2008). While many commercial and academic wireless sensing networks now support low-power, ad-hoc wireless networking (Sazonov*, et al.* 2004; Kling 2005; Pakzad*, et al.* 2008), particularly using wireless transceivers that conform to the IEEE 802.15.4 communication standard, *Narada* does so with a modular communication interface allowing longer communication ranges (over 300 m) to be achieved when installed on larger civil structures.

Most critically, in reactive structures, the ability to command actuators is a necessary component that is embedded directly with the *Narada* wireless sensing and actuation node. Sensor units configured for impedance interrogation of structures equipped with piezoelectric transducers are included in Table 2.4 as "active" sensors; they are only active in the sense that they provide their own local excitation. Their actuation interface is not configured to directly command typical analog actuators meaning that these systems are primarily effective for sensing alone. Active sensing units, such as that

**Table 2.1.** Academic prototype wireless sensors: 1998-2003.

| | Straser and Kiremidjian (1998) | Bennett, *et al.* (1999) | Lynch, *et al.* (2001; 2002a; 2002b) | Mitchell, *et al.* (2002) | Kottapalli, *et al.* (2003) | Lynch, *et al.* (2003a; 2004a) | Aoki, *et al.* (2003) | Wang *et al.* (2003) Gu *et al.* (2006) |
|---|---|---|---|---|---|---|---|---|
| **Data Acquisition Module** | | | | | | | | |
| ADC Channels | 8 | 4 | 1 | | 5 | 1 | | 8 |
| Sample Rate | 240 Hz | | 100 kHz | 20 MHz | 20 MHz | 100 kHz | | > 50 Hz |
| ADC Resolution | 16-bit | 16-bit | 16-bit | 16-bit | 8-bit | 16-bit | 10-bit | 12-bit |
| Digital Inputs | 0 | | 2 | | 0 | 2 | | multiple |
| **Embedded Computing Capabilities** | | | | | | | | |
| Processor | Motorola 68HC11 | Hitachi H8/329 | Atmel AVR8515 | Cygnal 8051 | Microchip PIC16F73 | Atmel AT90 S8515 AVR MPC555 PowerPC | Renesas H8/ 4069F | Analog Devices ADu-C832 |
| Bus Size | 8-bit | 8-bit | 8-bit | 8-bit | 8-bit | 8-bit/32-bit | 8-bit | 8-bit |
| Clock Speed | 2.1 MHz | 4.9 Hz | 4 MHz | | 20 MHz | 4 MHz/20 MHz | 20 MHz | |
| Program Memory | 16 kB | 32 kB | 8 kB | 2 kB | 4 kB | 8 kB/26 kB | 128 kB | 62 kB |
| Data Memory | 32 kB | | 32 kB | 128 kB | 192 kB | 512 Kb/448 kB | 2 MB | 2 kB |
| **Wireless Communications Specifications** | | | | | | | | |
| Radio | Proxim ProxLink | Radio-metrix | Proxim RangeLan 2 | Ericsson Bluetooth | BlueChip RBF915 | Proxim RangeLan2 | Realtek RTL-8019AS | Linx Techno-logies |
| Frequency Band | 900 MHz | 418 MHz | 2.4 GHz | 2.4 GHz | 900 MHz | 2.4 GHz | | 916 MHz |
| Wireless Standard | | | | IEEE 802.15.1 | | | | |
| Spread Spectrum | Yes | | Yes | Yes | Yes | Yes | | No |
| Outdoor Range | 300 m | 300 m | 300 m | 10 m | 500 m | 300 m | 50 m | 152 m |
| Indoor Range | 150 m | | 150 m | 10 m | 200 m | 150 m | 50 m | 61 m |
| Data Rate | 19.2 kbps | 40 kbps | 1.6 Mbps | | 10 kbps | 1.6 Mbps | | 33.6 kbps |
| **Assembled Unit Attributes** | | | | | | | | |
| Dimensions | 15x13x 10 cm | 15x15x 30 cm | 10x10x5 cm | 5x3.8x1.2 cm | 10x5x1.5 cm | 12x10x2 cm | 30x6x8 cm | |
| Power | | | | 120 mW | 100 mW | | | |
| Power Source | Battery (9V) | Battery (6V) | Battery (9V) | Battery | Battery (9V) | Battery (9V) | | Battery |

**Table 2.2.** Academic prototype wireless sensors: 2004-2009.

| | Mastr-oleon, *et al.* (2004) | Shino-zuka, (2003); Chung, *et al.* (2004) | Ou, *et al.* (2004) | Sazanov, *et al.* (2004) | Farrar, *et al.* (2005); Allen (2004) | Wang, *et al.* (2005) | Pei, *et al.* (2005) | Super Node, Huang, *et al.* (2008) | Pakzad, *et al.* (2008) |
|---|---|---|---|---|---|---|---|---|---|
| Data Acquisition Module | | | | | | | | | |
| ADC Channels | 5 | | 4/2 | 6 | 6 | 4 | | 8 | 4 |
| Sample Rate | 480 Hz | | | | 200 kHz | 100 kHz | 100/500 Hz | | 50 Hz (over-sampled) |
| ADC Resolution | 16-bit | | 8-bit/ 10-bit | 12-bit | 16-bit | 16-bit | 10/12/ 16-bit | 12-bit | 16-bit |
| Digital Inputs | 0 | | 2 | 16 | | 0 | | | |
| Embedded Computing Capabilities | | | | | | | | | |
| Processor | Micro-chip PIC-micro | | Atmel AVR ATMega 8L | Texas Instru-ments MSP430 -F1611 | Intel Pentium/ Motorola | Atmel AVR ATMeg a 128 | Moto-rola 68HC-11 | TI MSP-430 | Atmel AVR ATMega 128L |
| Bus Size | 16-bit/ 8-bit | | 8-bit | 16-bit | 16-bit | 8-bit | 8-bit | 16-bit | 8-bit |
| Clock Speed | | | | | 120/233 MHz | 8 MHz | | 8 MHz | 8 MHz |
| Program Memory | | | 8 kB | 16 MB | 256 MB | 128 kB | 32 kB | 48 kB | 128 kB |
| Data Memory | | | 1 kB | | Compact Flash | 128 kB | 32 kB | 1024 kB | 512 kB |
| Wireless Communications Specifications | | | | | | | | | |
| Radio | Blue-Chip RFB-915B | | Chipcon CC1000 | Chipcon CC2420 | Motorola neuRFon | Max-stream 9XCite | Max-Stream X-stream | Uniband UZ2400 | Chipcon CC2420 |
| Frequency Band | 900 MHz | 2.4 GHz | 433 MHz | 2.4 GHz | 2.4 GHz | 900 MHz | 900 MHz/ 2.4 GHz | 2.4 GHz | 2.4 GHz |
| Wireless Standard | IEEE 802.15.1 | IEEE 802.11b | | IEEE 802.15.4 | IEEE 802.15.4 | | | IEEE 802.15.4 | IEEE 802.15.4 |
| Spread Spectrum | Yes | Yes | Yes | Yes | Yes | Yes | Yes | Yes | Yes |
| Outdoor Range | 200-300 m | 250 m | | 75 m | 9.1 m | 300m | | 100 m | 75 m |
| Indoor Range | | | | | 9.1 m | 100 m | | 30 m | 20 m |
| Data Rate | 19.2 kbps | | 76.8 kbps | 250 kbps | 230 kbps | 38.5 kbps | | 250 kbps | 250 kbps |
| Assembled Unit Attributes | | | | | | | | | |
| Dimensions | 8x8x2 cm | 6x9x3.1 cm | | | | 10x6x4 cm | | | |
| Power | | | | 75 mW | 6 W | | | 75 mW | 350 mW |
| Power Source | | Battery + Solar | Battery | | | Battery (7.5V) | Battery (9V) | | Battery (9V) |

**Table 2.3.** Four families of commercial wireless sensors: 1999-2009.

| | UC Berkeley Cross-bow WeC: 1999 | UC Berkeley Crossbow Rene: 2000 | UC Berkeley Crossbow MICA: 2002 | UC Berkeley Crossbow MICA2: 2003 | Intel iMote Kling (2003) | Intel/ Crossbow iMote 2, Kling (2005) (2008) | Micro-strain, Galbr-eath (2003) | Rock-well, Agre (1999) |
|---|---|---|---|---|---|---|---|---|
| Data Acquisition Module | | | | | | | | |
| ADC Channels | 8 | 8 | 8 | 8 | | 4 | 8 | 4 |
| Sample Rate | 1 kHz | 1 kHz | 1 kHz | 1 kHz | | Variable | 1.7 kHz (1 channel) | 400 Hz |
| ADC Resolution | 10-bit | 10-bit | 10-bit | 10-bit | | 12-bit | 12-bit | 20-bit |
| Digital Inputs | | | | | | | | |
| Embedded Computing Capabilities | | | | | | | | |
| Processor | Atmel AT90LS 8535 | Atmel ATMega 163L | Atmel ATMega 103L | Atmel ATMega 128L | Zeevo ARM-7TDMI | PXA271 XScale | Micro-Chip PIC-16F877 | Intel Strong-ARM 1100 |
| Bus Size | 8-bit | 8-bit | 8-bit | 8-bit | 32-bit | 32-bit | 8-bit | 32-bit |
| Clock Speed | 4 MHz | 4 MHz | 4 MHz | 7.383 MHz | 12 MHz | 13-416 MHz | | 133 MHz |
| Program Memory | 8 kB | 16 kB | 128 kB | 128 kB | 64 kB | 256 kB | | 1 MB |
| Data Memory | 32 kB | 32 kB | 512 kB | 512 kB | 512 kB | 32-64 MB | 2 MB | 128 kB |
| Wireless Communications Specifications | | | | | | | | |
| Radio | TR1000 | TR1000 | TR1000 | Chipcon CC1000 | Wire-less BT Zeevo | Chipcon CC2420 | RF Mono-lithics DR-3000-1 | Con-exant RDSSS 9M |
| Frequency Band | 868/916 MHz | 868/916 MHz | 868/916 MHz | 315, 433, or 868/ 916 MHz | 2.4 GHz | 2.4 GHz | 916.5 MHz | 916 MHz |
| Wireless Standard | | | | | IEEE 802.15.1 | IEEE 802.15.4 | | |
| Spread Spectrum | No | No | No | Yes | Yes | Yes | | Yes |
| Outdoor Range | | | | | | 30 m | | |
| Indoor Range | | | | | | 50 m | | 100 m |
| Data Rate | 10 kbps | 10 kbps | 40 kbps | 38.4 kbps | 600 kbps | 250 kbps | 75 kbps | 100 kbps |
| Assembled Unit Attributes | | | | | | | | |
| Dimensions | 2.5x2.5x 1.3 cm | | | | | 3.6x4.8 | | 7.3x7.3 x8.9 cm |
| Power | 575 mAh | 2850 mAh | 2850 mAh | 1000 mAh | | | | |
| Power Source | Coin Cell | Battery (3V) | Battery (3V) | Coin Cell | Battery | Battery | Battery (3.6V) | Battery (two 9V) |

**Table 2.4.** Active wireless sensors: 2003-2009.

| | Lynch, *et al*. (2003b; 2004c) | Grisso, *et al*. (2005) | Allen (2004) | *Narada*, Swartz, *et al.* (2005) | SHiMmer, Musiani, *et al*. (2007) | Masca-renas, *et al*. (2007) | TelosB (2008) |
|---|---|---|---|---|---|---|---|
| Data Acquisition Module | | | | | | | |
| ADC Channels | 32 | 8 | 6 | 4 | 16 | 1 | 8 |
| Sample Rate | 40 kHz | >50 kHz | 200 kHZ | 10 kHz | 10 MHz | 1 MHz | |
| ADC Resolution | 10-bit | 16-bit | 16-bit | 16-bit | 12-bit | 12-bit | 12-bit |
| Digital Inputs | 0 | 1 | | 0 | | | 0 |
| Actuation Module | | | | | | | |
| DAC Channels | 1 | Impe-dance | Impe-dance | 2 | 16 PZT Interface | Impedance | 2 |
| Sample Rate | 40 kHz | | | 10 kHz | 1 MHz | | |
| DAC Resolution | 12-bit | | | 12-bit | 12-bit | | 12-bit |
| Voltage Outputs | ± 5 V | | | 0-4.095 V | ± 15 V | | |
| Embedded Computing Capabilities | | | | | | | |
| Processor | Motorola MPC555 PowerPC | Diamond Systems PC 104 | Pentium | Atmel ATMega 128 | TI TMS320-R2811 | Atmel ATMega 128L | TI MSP-430 |
| Bus Size | 32-bit | | 32-bit | 8-bit | 32-bit | 8-bit | 16-bit |
| Clock Speed | 40 MHz | 100 MHz | 133 MHz | 8 MHz | | 8 MHz | 8 MHz |
| Program Memory | 448 kB | 64 kB | 256 MB | 128 kB | 128 kB | 128 kB | 48 kB |
| Data Memory | 512 kB | 32 MB | Compact Flash | 128 kB | 1 MB | 4 kB | 1024 kB |
| Wireless Communication Specifications | | | | | | | |
| Radio | Proxim ProLink | Radio-metrix | Motorola neuRFon | Chipcon CC2420 | Chipcon CC1100 | Max-Stream XBee | Chipcon CC2420 |
| Frequency Band | 902-928 MHz | 480 MHz | 2.4 GHz | 2.4 GHz | 433 MHz | 2.4 GHz | 2.4 GHz |
| Wireless Standard | | | IEEE 802.15.4 | IEEE 802.15.4 | | IEEE 802.15.4 | IEEE 802.15.4 |
| Spread Spectrum | | Yes | Yes | Yes | Yes | Yes | Yes |
| Outdoor Range | 300 m | 1,000 m | 9.1 m | 50/300 m | | 90 m | 75 m |
| Indoor Range | 150 m | | 9.1 m | 20/100 m | | 30 m | 20 m |
| Data Rate | 2.4 kbps | 5 kbps | 230 kbps | 250 kbps | | 250 kbps | 250 kbps |
| Assembled Unit Attributes | | | | | | | |
| Dimensions | 7x7x2.5 cm | | | 6x6x2 cm | | | 6.5x3.1x0.6 cm |
| Power Source | Battery (9V) | Battery (9V) | Battery (9V) | 200 mW Battery (9V) | 0.68-3.5 W Vibrations | 212 mW RF Power | Battery (3V) |

presented by Lynch, *et al*. (2003b, 2004c) as well as *Narada*, are capable of commanding a host of actuators that are useful in structural control. Of the two, Narada is a lower power device, higher sampling resolution, and supports a significantly faster communication data rate. In recent years, the TelosB commercial platform has also become available, consumes very low levels of energy, and may be appropriate for some wireless structural control applications in which sensing resolution is not a critical concern.

## 2.4. The *Narada* Wireless Sensor

The *Narada* wireless sensor (Figure 2.3) was developed at the University of Michigan in 2004, explicitly for structural monitoring and feedback control applications (Swartz*, et al.* 2005). It was designed for use in low-cost, high-density sensor networks where the high cost of cable installation makes traditional tethered sensor and actuator networks undesirable. Furthermore, it was intended to be able to run on battery power for a long period of time (up to two years, depending on the duty cycle of use) in the absence of a power supply native to the monitored structure; therefore, it was designed to be a very low-power device. To meet the low-cost requirements, its design takes advantage of commercial, off-the-shelf (COTS) technology for all of its functional components. Finally, to participate in active sensing and control activities, an actuation interface is included in the design. The complete design of the *Narada* wireless node is broken down into two parts: hardware design and software design.

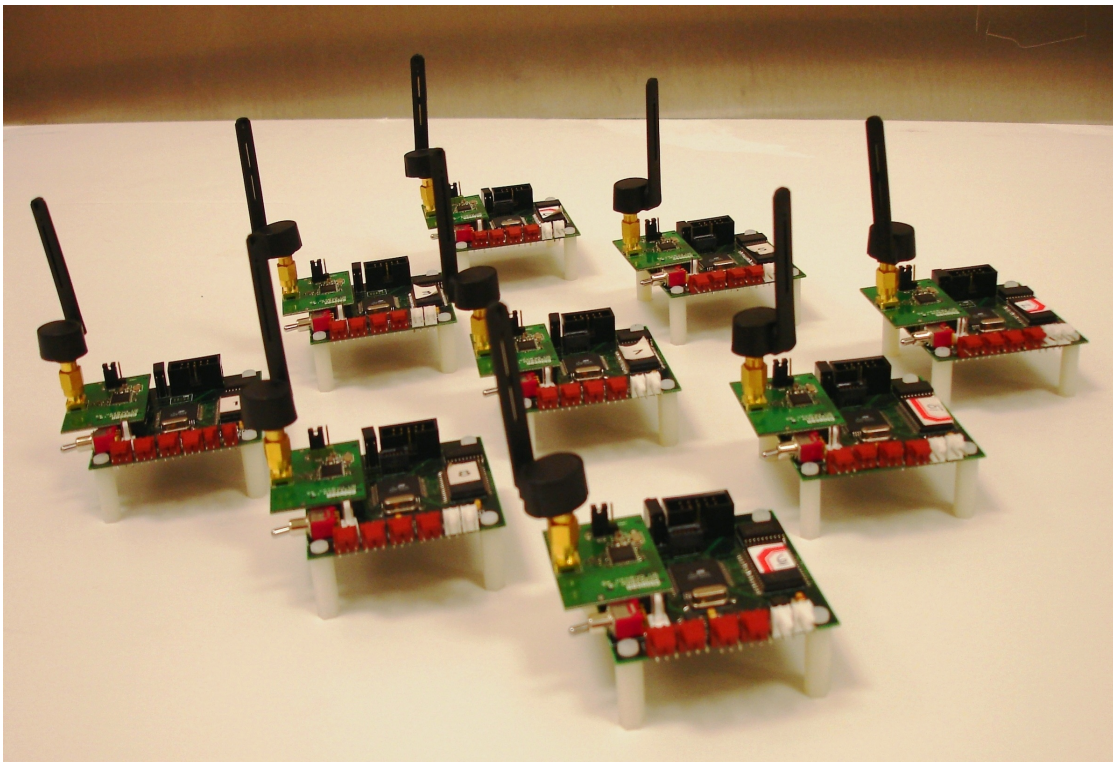

**Figure 2.3.** *Narada* wireless sensing nodes.

*2.4.1. Narada Hardware Design*

The sensor node itself includes four functional modules (Figure 2.4). The first module is the computational core which is defined by the microcontroller (Atmel Atmega128) and is responsible for the autonomous operation of the device. The Atmega128 (Atmel 2009) is a low-power, 8-bit microcontroller with 128 kB of flash memory, 4kB of Static Random Access Memory (SRAM), and 4 kB of Electrically Erasable Programmable Read-Only Memory (EEPROM). Embedded software, termed firmware, is stored within the microcontroller. The firmware includes two categories of software: first, an operating system (OS) is embedded for the configuration and operation of peripheral components on the sensor, as well as for real-time allocation of processing

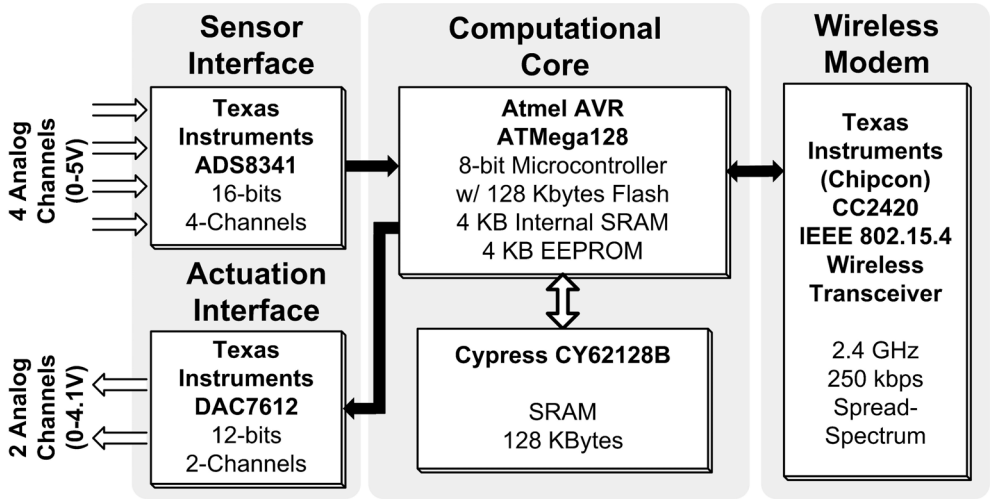


**Figure 2.4.** *Narada* wireless sensing node architectural schematic.

power. Second, application software is installed consisting of specific engineering algorithms that are responsible for local data processing of interest to the end-user. An additional 128 kB of external SRAM has also been added to the computational core in order to enhance local data buffering and computational capabilities within the sensor.

The second module is the sensing interface. It consists of a Texas Instruments ADS8341 (Texas Instruments 2003) which is a 4-channel, 16-bit analog-to-digital converter (ADC) with an input range of 0-5 V. This interface allows the sensing system to measure data from up to four transducers per sensing node (channels numbered 0 through 3) and gives considerable flexibility in the type of transducer used. The resolution of the ADC is unique for a wireless sensing platform as it is unusually high (*i.e.*, most commercial wireless sensors employ 10 to 12-bit ADC interfaces). *Narada* was designed with a high resolution ADC to allow for low signal data collection; low signals may be lost in the noise floor of the sensor if the ADC resolution is not sufficiently high. The *Narada* four-layer printed circuit board (PCB) has been carefully

designed (*e.g.*, careful separation of power and ground planes servicing analog and digital components of the node circuitry) to preserve this resolution resulting in true 16-bit performance where the quantization error is just one bit (1/65536th of the input analog voltage range). The maximum sample rate of the *Narada* node using this interface is 10,000 Hz and is limited by the speed of the data bus between the ADC and the microprocessor in the computational core.

The third module in the *Narada* design is the communications interface. The wireless interface consists of a Texas Instruments CC2420, which is a wireless transceiver that meets the IEEE 802.15.4 communications standard for dense, adaptive wireless networking (Texas Instruments 2008). The wireless transceiver is a spread-spectrum device that operates within the 2.4 GHz Federal Communications Commission (FCC) defined unlicensed industrial, scientific, and medical (ISM) communications frequency band. It also operates below the FCC established power limit of 1 W, defined for such devices. The transceiver is capable of maintaining an over-the-air communications rate of 250 kbps and can reliably communicate over a range of 50 m. A useful feature of the CC2420 transceiver is that the output wireless signal can be varied from weak to strong (Texas Instruments 2008). Reducing the output power of the radio results in reduced power consumption and range. Similarly, if long communication range is necessary, the radio can be commanded to have high output power to meet range requirements but resulting in greater power consumption. Smart communication schemes can vary the transmission power level as required depending on the distance to the target receiving node(s) as well as the quality (*i.e.*, noise level) of the communication bandwidth.

The communications interface sits on a modular daughter board that can be removed from the rest of the sensing unit to allow the user to install alternative communication modules, if necessary. A power-amplified version of the radio board has also been developed to provide increased communications range for applications that require it. The power-amplified radio daughter board is described in greater detail in the following section.

The final module of the sensor node design is the actuation interface consisting of a DAC7612 (Burr-Brown 1999), a 2-channel, 12-bit Texas Instruments digital-to-analog converter. The DAC has an output range of 0-4.1 V and gives the sensor actuation capabilities so that it can, if desired, participate in active sensing or even feedback control activities. The maximum actuation rate of the DAC is comparable to the maximum sample rate of the ADC (10,000 Hz) which is limited by the speed of the data bus between the DAC and the microcontroller. As the ADC and the DAC share this data bus, this rate is for one of these interfaces at a time. The maximum combined sample/actuate rate is one half of the independent rate (5,000 Hz).

The power draw of the *Narada* wireless sensor is 200 mW, assuming all components are operating simultaneously (250 mW using the power-amplified wireless transceiver board). Power savings can be accomplished by putting portions of the sensor (or the entire sensor) into sleep mode. The sensor is designed to run on 6 AA size nickel-metal hydride (NiMH) rechargeable batteries. Without being placed in sleep mode, the fully-active sensor will exhaust the rated life of the batteries in just over 5 days. Turning off various components when not used will also extend this life span. Full duty-cycle operation using only the microcontroller will allow for just over 12 days before depleting

**Table 2.5.** *Narada* wireless sensor performance characteristic summary.

| Performance Characteristics | |
|---|---|
| Cost | $175 per unit |
| Form Factor | 6 cm x 6 cm x 2 cm |
| Energy Source | 6 AA Ni-Metal Hydride Batteries |
| Peak Power | 200 mW (250 mW power-amped) |
| Range | 50 m (500 m power-amped) |
| Data Rate | 250 Kbps |
| Sample Rate | 10 kHz |

the batteries. Adding the ADC reduces this time to just over 11 days. Adding the external memory reduces this time to 6.8 days. The transceiver is responsible for the bulk of the remaining power consumption. Using an appropriate duty cycle, the battery life can be extended to one or two years, limited by the storage losses of the batteries. Table 2.5 summarizes the characteristics of the *Narada* wireless node.

### *2.4.2. Modular Power-Amplified Radio Option*

The IEEE 802.15.4 standard defines a wireless personal area network (WPAN) technology (IEEE 2006). Such networks are, by nature, relatively low-range. Wireless devices based on transceivers designed to meet this standard have relatively limited communication distances, on the order tens of meters. Some examples include communications ranges of 30 m for the *Imote2* (Crossbow Technology 2007) and of 50 m for the *Narada* wireless sensor using its native communication interface. In civil applications, where the size of the instrumented structures may necessitate that data be transmitted distances on the order of hundreds of meters, short-range communications

will necessitate unduly large numbers of transmission "hops" (the serial retransmission of data by multiple units in a network to route it over distances in excess of the originating unit's range). The redundant data transmissions that characterize multi-hop networks erode the available bandwidth on the wireless communications channel thereby limiting the total data throughput of the network as a whole (Raghavendra*, et al.* 2004). Where data throughput is critical, bandwidth may be recovered by increasing the transmission range of individual units and reducing the number of hops required by the system.

Increased range can usually be achieved through increased transmitted signal strength by changing the location of the transmitter and receiver antennas with respect to their surroundings (*i.e.*, more favorable use of physical wave guides or obstacles) or reduction of ambient RF noise. In the deployment of a wireless sensor network, designers often have limited control over the second and third of these parameters, but transmitted signal strength may be readily increased through application of improved-range antennas (*i.e.*, high-gain and directional antennas), increased transmission power, or both. To take advantage of the benefits of higher transmission power, in applications where range is an important network design consideration as well as the benefits of lower power consumption, in shorter range applications, the CC2420 wireless transceiver has eight different output power setting ranging from 28 mW to 57 mW (Texas Instruments 2008). This option allows the network designer to tailor the output power level to specific applications.

In addition to this native ability of the wireless transceiver, the *Narada* wireless sensor unit has been equipped with a modular communication interface that sits on a removable daughter-board. Using its native interface (Texas Instruments CC2420),

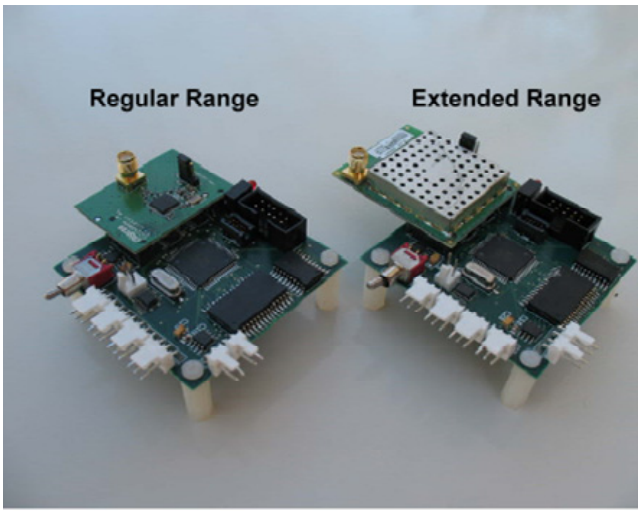


**Figure 2.5.** *Narada* wireless sensing unit with both regular and extended range radio transceivers.

transmission power to the antenna is limited at 1.0 mW (0 dBm) from 57 mW of power drawn from the batteries. That communication interface may be swapped out for a power-amplified daughter board (Figure 2.5) that can transmit at power levels up to 10 mW (10 dBm) from 114 mW of power drawn from the batteries. The modular nature of the transceiver board allows it to be used only in high-range applications, saving battery life when it is not necessary. The power-amplified module doubles the strength of transmissions emanating from the unit increasing both range and the reliability of communications in noisy communication environments. This extra range, of course, comes at the expense of additional energy consumption. In addition, standard-gain omni-directional antennas as well as high-gain, directional antennas are available for the *Narada* wireless sensor. With the addition of high-gain directional antennas, the maximum range of the *Narada* system (in the strong direction of the directional antenna) is over 500 m.

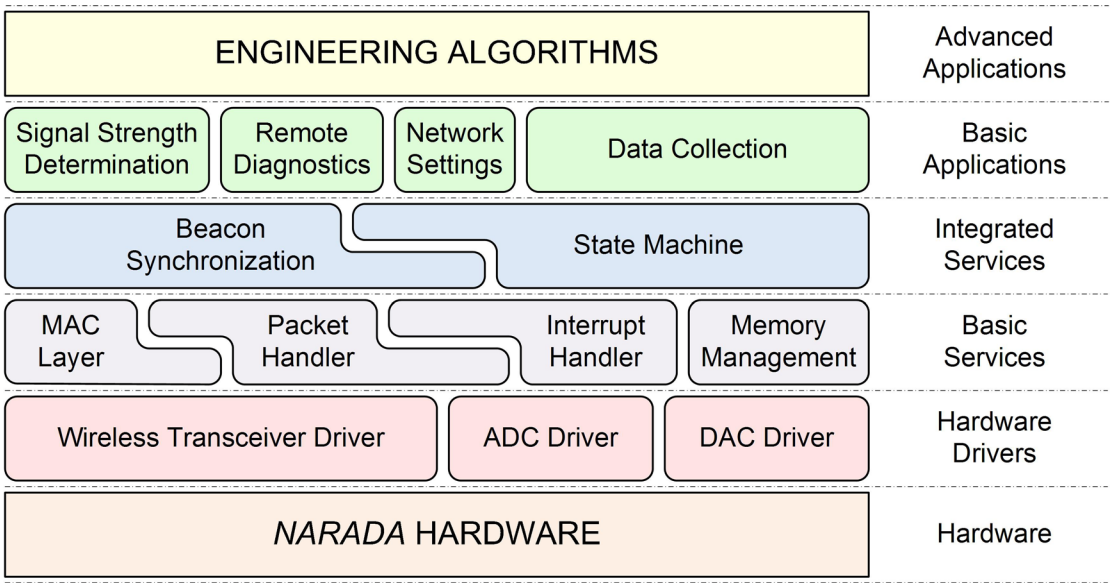


**Figure 2.6.** Graphical overview of the *Narada* embedded operating system.

### *2.4.3. Narada Software Design*

Embedded software for the wireless sensors (termed firmware) is made up of two general categories: the operating system (OS) that controls the node, and engineering analysis algorithms that perform local processing of raw sensor data. The operating system is responsible for both coordinating the operation of the wireless sensor and for providing device drivers that operate peripheral sensor components (*e.g.,* ADC, wireless transceiver, DAC). One popular operating system used on many commercial and academic wireless sensors is TinyOS, an open-source operating system originally designed at University of California, Berkley (Levis*, et al.* 2004; Ruiz-Sandoval*, et al.* 2006). TinyOS is a generic platform intended to operate on a broad variety of hardware platforms for multiple applications.

In this study, a custom OS is embedded within the *Narada* sensor (Figure 2.6). This OS is tailored to meet the needs of smart civil infrastructure applications, allows access to

the sensing, actuation, and communications interfaces on *Narada*, and provides basic services including sensor diagnostics, measurement of communication quality of service, management of device settings, and establishment of network synchronization. In addition, the OS defines the memory allotment given to operational tasks as well as engineering algorithms. The OS must also provide timely access to computational resources (*i.e.*, memory and the processor) to embedded engineering algorithms that accomplish tasks necessary for monitoring and control. Below, a description of the Narada OS and basic data collection package is presented including a discussion of multi-tasking, application specific memory mapping, network synchronization, data collection, and data transmission.

One important feature of operating systems for wireless sensing (*Narada* included) is the ability to simultaneously execute multiple tasks. This ability, called multi-threading (or multi-tasking), is similar to the multi-tasking operation of a personal computer. In wireless sensors, multi-threading can be an indispensible feature, allowing them to transmit data within the network while not interrupting sensing (or actuation) activities. To keep the overall footprint of the OS as small as possible, a prioritized event-driven multi-tasking scheme is adopted (similar to that developed for later versions of TinyOS (Levis 2006)) by which high-priority tasks, such as data sampling, data reception, or actuation, can interrupt lower priority tasks, such as data processing. By use of the event-driven multi-tasking method, the *Narada* OS avoids the need for a computationally-intensive software-driven event sequencer.

To achieve the best performance possible on the *Narada* wireless sensor, the operating system has been tailored to both the hardware platform it runs on and the

application for which it has been designed. This practice is to reduce the size of the operating system within the sensor memory and to minimize non-deterministic OS related delays in code execution. Inefficient or overly generic operating systems can consume memory, thereby reducing the memory space available for the storage of data and engineering algorithms. Depending on the application, large blocks of memory may be required to run the necessary algorithms. Additional memory may be added to augment the on-processor memory, but accessing external memory requires additional clock cycles (and power consumption) compared to what is required to access internal memory; this delay in reading and writing to external memory may become a problem in time-critical applications.

In addition to memory concerns, another major challenge in wireless sensing (as well as in utilization of data collected over a computer network) is data synchronization (Raghavendra*, et al.* 2004). Unlike in a traditional data collection system, defined by a single computer operating on a single clock that can initiate data collection from multiple sensors, a wireless sensing network is composed of multiple computers each operating according to its own local clock. Synchronization of the clocks within these multiple devices must take place using the available communication media. However, synchronization by wireless communications is dependent upon the propagation and processing of synchronization messages broadcast between the networked processors. This task is made more difficult in wireless networks where signal propagation times are stochastic, and direct communications between all units in the network may not be possible (Raghavendra*, et al.* 2004). Errors in synchronization will lead to corruption of the phase information inherent within the data signals that may necessary for correct

computation of certain processing algorithms, including modal analysis (Ginsberg 2001), input-output or multiple-output models (Ying, *et al.* 2005), or feedback control algorithms (Lian, *et al.* 2005). While methods do exist to correct for existing synchronization error in collected data (Nagayama 2007; Yan, *et al.* 2009), minimization of the error at the outset (to a value that is significantly smaller than the sampling time step) can eliminate the need for synchronization correction algorithms and their associated computational overhead.

Data collected on the *Narada* wireless sensor is synchronized through means of a beacon packet initiated by a central server. Long-range packet transmission options developed for the *Narada* platform allow networks distributed over areas with diameters as large as 1000 m to be initiated in this manner (centered on the server). Synchronization errors resulting from beaconing are the result of differential signal propagation times as well as differential processing times. Due to multi-path effects, the differential signal propagation times are stochastic, but are limited by the signal propagation range of the system (1000 m divided by the speed of light, or 3.3 μs). On *Narada*, differential processing time is limited by restricting the actions of the wireless sensor at the beginning of a data collection test. Specifically, the sensing units in the network are placed in a wait state, composed of a "while" loop, that will execute (at most) four assembly level instructions before a beacon packet is serviced. This practice limits the differential processing time to four clock cycles on the microprocessor (operating at 8.0 MHz) plus the potential differential delays in wireless transceiver processing (which are in turn limited by the size of the digital data buffer located within the transceiver). The synchronization error due to differential processing time has been

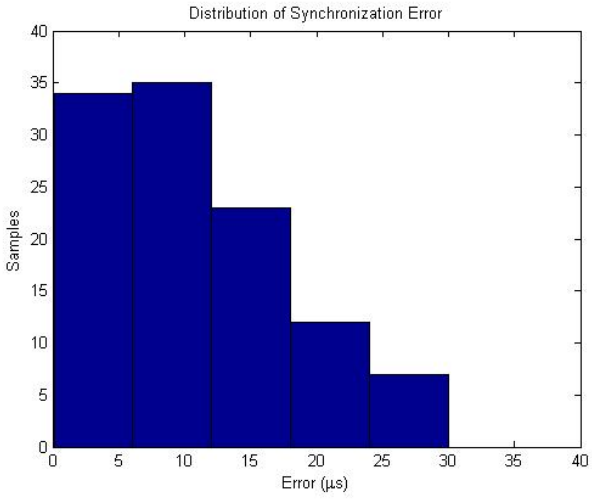


**Figure 2.7.** Distribution of measured differential beacon processing synchronization error for a *Narada* wireless sensor network.

characterized experimentally by use of multiple, collocated sensing nodes programmed to raise a digital logic line when the first data point is ready (after successful reception of the start beacon). The differential processing time is then measured on a digital oscilloscope. The average differential processing time synchronization error on *Narada* is found to be 10.8 μs, with variance of 7.4 μs, and a peak observed value of 30 μs. The distribution of these errors is depicted in Figure 2.7. Considering 200 Hz as a typical sampling frequency for civil engineering applications, these results indicate a maximum synchronization error of less than 0.7% of a time step on the *Narada* system without use of post-processing synchronization correction algorithms.

As part of the operating system, a basic data collection module was developed. The module supports data collection for up to 65,534 wireless sensing devices that collect data and transmit it back to a personal computer (PC) for archival. The connection to the PC is accomplished through use of a CC2420DBK Texas-Instruments wireless radio development board that uses a CC2420 wireless transceiver connected to an ATmega128

microprocessor. Received IEEE802.15.4 packets are transmitted to the PC via the board's RS-232 (serial) port and, likewise, serial data received from the PC is converted to wireless packets and broadcast over the air. The upper limit of the network size is dictated by the number of unique node identification numbers supported by the IEEE802.15.4 standard, but wireless bandwidth and communication range impose a practical limitation on network size far below that limit. To maximize the number of data channels that can be supported on a single network, a single-hop, TDMA communications standard has been developed for this application. The basic data collection module supports sampling rates up to 10,000 Hz with a limit of 30,000 data points that can be buffered on the wireless sensor at a given time. In single-cycle mode, the sensing units collect a finite amount data (less than the local buffer limit) and transmit it back to a server program running on the PC. In this mode, data transmission is not time-critical and does not impose any special limitations on network size. In continuous collection mode, the units will buffer data locally until queried by the server. Each sensing unit in the network is polled in turn, transmitting data back in 50 point packets (one sensing channel at a time) until the buffer is empty (the buffer size can be selected by the user). The network size in this mode is limited by the wireless communications channel and depends on the sampling rate and quality of communication. For example, at 100 Hz, a single wireless channel can support 16 sensor channels of data (on anywhere from 4 to 16 sensing units) if there is little to no communication noise. As of this writing, the largest single network of *Narada* sensing units deployed is sixty.

## 2.5. *Narada* Development Conclusions

In this chapter the *Narada* wireless sensor that has been tailored for smart civil infrastructure applications is presented. The system boasts low per-channel costs (comparable to many commercial wireless systems, considerably less expensive than traditional cable-based systems) and is easy (and inexpensive) to install due to its use of wireless communication technology rather than traditional (and expensive) cabled technology. These cost attributes encourage the use of high-density sensor networks in future wireless monitoring systems. Furthermore, the system includes a high resolution (16-bit) analog-to-digital converter within its sensing interface that allows it to differentiate low-level ambient vibrations from the electrical noise inherent within the sensor. The *Narada* system also includes an actuation interface consisting of a digital-to-analog converter that give the sensor the ability to command a wide range of analog actuators necessary for automated response of the smart structure to external stimuli. Finally, the sensor also contains a computational core running the operating system that coordinates the activities of the communication, sensing, and actuation interfaces, as well as defining communication protocols, memory and processor allotment, and the organization for a basic data collection algorithm.

The development of hardware and an operating system for the wireless sensor are only part of the solution. Central to the wireless monitoring architecture is the fact that sensors are essentially collocated with embedded computing resources, namely processing power and memory. This fact implies that the sensors can do more than merely collect and report data. Therefore, another critical step is the development of a library of embedded algorithms that may be combined for monitoring operations such as

modal analysis, auto-regressive modeling, model updating, damage detection, and feedback control. Both the operating system and the engineering algorithms may be written in a high-level programming language, C, with only the most time-critical operations requiring assembly level instructions that are microprocessor specific. A host of building block algorithms are developed to run within the *Narada* wireless network to support high-level embedded analysis and control applications. Novel applications of these embedded engineering algorithms for smart civil structures are presented in the following chapters.

# CHAPTER 3

## FIELD VALIDATION OF *NARADA* WIRELESS SENSORS: HYBRID WIRELESS HULL MONITORING OF NAVAL COMBAT VESSELS

Wireless sensors for smart structures must operate successfully, not only in the laboratory, but for extended periods of time in the field. Ultimately, smart structures must be able to operate independently (*i.e.*, without supervision), many times in difficult operational environments, in order to realize their potential for low-cost, autonomous protection of infrastructure assets. In this chapter, a two-month, autonomous field validation study is performed employing the *Narada* wireless sensing system as part of a hybrid wireless hull monitoring system aboard a U.S. Navy littoral combat vessel. Also, as there is increasing interest by the naval engineering community in permanent monitoring systems that can monitor the structural behavior of ships during their operation at sea, this study also seeks to reduce the cost and installation complexity of hull monitoring systems by introducing wireless sensors into their architectural designs. Wireless sensor networks also provide other advantages over their cable-based counterparts such as adaptability, redundancy, and weight savings. While wireless sensors can enhance functionality and reduce cost, the compartmentalized layout of most

ships requires some wired networking to communicate data globally throughout the ship. In this study, 20 *Narada* wireless sensing nodes are connected to a ship-wide fiber-optic data network to serve as a hybrid wireless hull monitoring system on a high-speed littoral combat vessel (FSF-1 Sea Fighter). The wireless hull monitoring system is used to collect acceleration and strain data during unattended operation during a one-month period at sea. The key findings of this study include that wireless sensors can be effectively used for reliable and accurate hull monitoring. Furthermore, the fact that they are low-cost can lead to higher sensor densities in a hull monitoring system thereby allowing properties, such as hull mode shapes, to be accurately calculated as will be presented.

### 3.1. Field Validation Introduction

The U.S. Navy is currently exploring novel ship design concepts optimally suited for future littoral (shallow-water) combat operations. For example, the joint high-speed vessel (JHSV) and littoral combat ship (LCS) acquisition programs are focused on high-speed ships constructed from light-weight materials such as aluminum alloys (Hess 2007). In addition to the use of new materials, many of the vessels under investigation in the JHSV and LCS acquisition programs employ non-conventional hull forms including the use of multi-hull catamarans. The combination of lightweight aluminum and multi-hull forms provide ships with the speed and maneuverability necessary for littoral combat operations. However, high-performance aluminum ships also provide a number of operational challenges to the naval engineering community. First, the use of aluminum in the construction of the hull will lead to higher incidences of fatigue cracking (Donald

2007); in addition, once fatigue cracks initiate, their growth in aluminum will be significantly greater than those in steel hulls. Other challenges associated with aluminum materials is stress-corrosion cracking and material sensitization during high operational temperatures (Katsas*, et al.* 2007). Second, multi-hull ship designs can lead to complex dynamic behavior during high-speed operation in demanding sea conditions (Hess 2007). Furthermore, the unique design of these ships increases the probability that crews will operate them near, or even beyond, their safe operating envelops due to the loss of "feel" for the vessel's response to seaway loads (Pran*, et al.* 2002).

Historically, the hulls of U.S. Navy ships are inspected by the crew and port engineer to ensure the hull is in a state of good health. While this approach has proven effective in the past, the method does suffer from some inherent drawbacks. First, visual inspection is labor-intensive. As the Navy continues to reduce manning on future naval vessels (Lively*, et al.* 2008), the manning requirements of visual hull inspections will grow increasingly difficult to satisfy. Second, visual inspection can only observe obvious damage conditions. For example, hairline cracks with small dimensions are difficult to identify visually, even when using dye penetrants (Zoughi and Kharkovsky 2008). In the case of ships constructed of aluminum, thick insulation is commonly installed to protect the aluminum hull from heat and fire. Visual inspection would require removal and reinstallation of the insulation, which adds significant complexity and cost to the inspection process. The U.S. Navy is therefore interested in the development of permanent hull monitoring systems that monitor the anticipated performance and health of high-performance aluminum vessels. This interest is in response to the maintenance

issues (*e.g.*, fatigue cracking) and inspection difficulties associated with high-speed aluminum ships.

Hull monitoring systems in use in the commercial shipping industry typically consist of foil strain gauges, accelerometers and gyroscopes installed throughout a vessel to measure the ship rigid-body motion and hull deformations to seaway loads. Crews provided with real-time hull response data can pilot the ship in a manner that minimizes overloading during extreme seaway conditions (Pran*, et al.* 2002). Commercial hull monitoring systems consisting of a handful of sensors can cost, on average, $50,000 per system to purchase and install (Slaughter*, et al.* 1997). A large fraction of the system cost is associated with the installation of coaxial wiring used for the communication of sensor data to the hull monitoring system central processing unit. In addition to being expensive to install, cables add weight to the vessel, which is a critical issue for vessels designed to be light-weight, such as high-speed aluminum vessels. Furthermore, wires installed in a combat vessel are vulnerable to detriments such as heat, moisture, and toxic chemicals common in harsh military operational environments (MacGillivray and Goddard 1997). For multi-hulled aluminum ships, the costs affiliated with the installation of a hull monitoring system grows higher because of the thick insulation layers covering the aluminum hull for protection from heat and fire (Sielski 2007).

Provided the challenges associated with wired hull monitoring systems, wireless sensors can be explored for use within monitoring system architectures. Wireless sensors have emerged in recent years as low-cost alternatives to tethered sensors; their use is especially attractive for structures with large dimensions or with difficult to access spaces (Lynch and Loh 2006). In this study, a hull monitoring system is designed using wireless

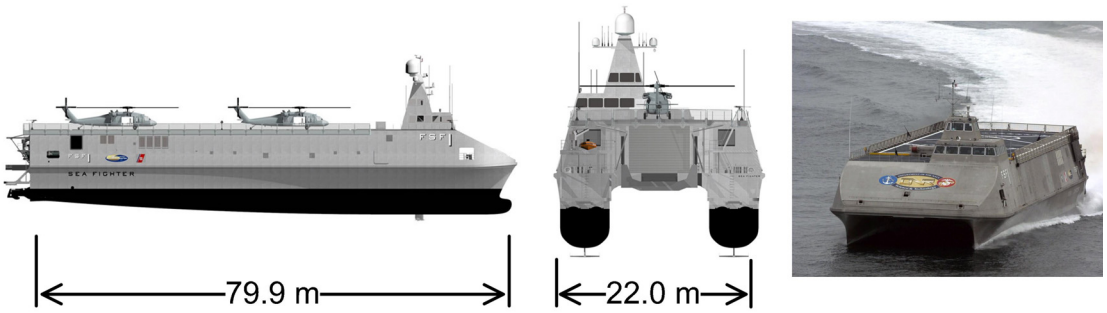


(a) (b) (c)

**Figure 3.1.** The FSF-1 Sea Fighter, a high-speed aluminum ship designed to support future littoral combat operations of the U.S. Navy: (a) side view (courtesy U.S. Navy), (b) back view (courtesy U.S. Navy), and (c) view of the Sea Fighter in operation at sea (courtesy U.S. Navy).

sensors to measure the response of a high-speed aluminum vessel undergoing seakeeping trials. Specifically, a two-tiered hull monitoring system is proposed in the study. At the lowest layer of the system architecture, wireless sensors capable of reliable short-range communication within ship compartments are installed to collect strain and acceleration measurements of the hull. Wireless sensor networks are then connected to a ship-board fiber-optic data network which serves as the hull monitoring system's second tier. The fiber-optic layer of the system architecture is necessary to establish communication between spatially distributed clusters of wireless sensors contained within different ship compartments. The fiber-optic network also facilitates the use of a central server to control and operate the multiple wireless sensor clusters as a single, global hull monitoring system.

The FSF-1 Sea Fighter (Figure 3.1), a high-speed littoral combat vessel designed with a wave-piercing catamaran aluminum hull, is used to demonstrate the efficacy of the proposed hybrid wireless hull monitoring system in a realistic marine environment. The strain and acceleration response of the ship is continuously and autonomously (*i.e.,*

without user intervention) collected by the hull monitoring system during a one-month transit from Panama City, Florida to Portland, Oregon. As part of the study, a comparison between hull response data recorded by the experimental wireless hull monitoring system and those identically recorded by the ship's permanent tethered (*i.e.*, wired) hull monitoring system is made to assess the accuracy of the experimental wireless system. Finally, acceleration hull response data collected from the wireless monitoring system is used to perform a modal analysis of the ship including identification of the ship's global modal frequencies and operational deflection shapes. First, the chapter presents a detailed description of the Sea Fighter and the wired hull monitoring system installed on-board prior to this study. Then, the hybrid wireless hull monitoring system designed and installed for this study is presented in detail. The third part of the chapter presents raw data collected by both hull monitoring systems along with the modal characteristics of the ship derived from the raw data presented. Finally, concluding remarks about the effectiveness of the hybrid wireless hull monitoring system in the shipboard environment are presented along with a description of the lessons learned during the study.

### 3.2. FSF-1 Sea Fighter

The FSF-1 Sea Fighter (Figure 3.1) is a 79.9 m long, multi-hull catamaran-style ship designed for high-speed littoral combat missions. The ship was designed by BMT Nigel Gee (Southampton, U.K.) and constructed in 2003 by Nichols Brothers Boat Builders (Freeland, WA) (Bachman*, et al.* 2007). To provide the ship with speed, the hull is constructed from aluminum, thereby keeping the total weight of the ship down. The Sea

**Figure 3.2.** FSF-1 Sea Fighter mission bay. While an open space, the bay is occupied by large steel shipping containers as seen in this photo.

Fighter's hull consists of 61 identical aluminum frames evenly spaced (1.2 m apart) along the length of the ship; six of these frames serve as water-tight bulkheads. The ship is designed with three main levels: 1) the main deck, 2) the bridge, and 3) machinery and tank spaces below the main deck. Using both diesel and gas turbine propulsion systems, the Sea Fighter is nominally capable of operating at speeds up to 50 knots and in conditions up to sea state 5. Sea Fighter is also equipped with a sophisticated ride control system (active rear interceptors and forward T-foils) which enhances the ship's maneuverability at high speed (Bachman*, et al.* 2007).

Designed as a multi-purpose sea-based combat platform, the ship's main deck is relatively open for the secure housing of modular shipping containers that contain gear and equipment specific to a variety of littoral combat missions. The main deck area for

storing these containers is referred to as the mission bay (Figure 3.2). The mission bay runs from the stern of the ship, 52 m forward, and spans the entire width of the vessel (22.0 m). The inside of the mission bay is generally protected from the sea environment, but does have some small openings above the ship waterline to the outside.

As Sea Fighter is an experimental vessel, the Naval Surface Warfare Center (NSWC) elected to install a permanent hull monitoring system during and after the ship's construction in 2003. The monitoring system, referred to as the Scientific Payload Data Acquisition System (SPDAS) is designed by the Technology Management Group, Inc. (TMG). In its design, the hull monitoring system is intended to capture data pertaining to the performance of Sea Fighter during seakeeping trials. The SPDAS system has been in operation, collecting data on ship behavior during operation at sea since 2006. In this study, it will serve as a baseline to which the proposed hybrid wireless hull monitoring system performance will be compared.

### *3.2.1. SPDAS*

As an experimental vessel, the Sea Fighter is closely monitored using an extensive hull monitoring system custom designed by TMG for the U.S. Navy. The Scientific Payload Data Acquisition System (SPDAS) is a wired hull monitoring system featuring 10 tri-axial accelerometers (Columbia 307-HPTX), over 100 metal-foil strain gauges (Micro Measurements), and a wave height measurement system (TSK) installed on the ship bow (Bachman*, et al.* 2007). The accelerometers are intended to measure the rigid body dynamics of the ship while the strain gauges are used to measure the strain response

of the hull. The TSK wave height measurement system is installed on the ship hull to measure wave height and period.

The accelerometer and strain gauges are installed throughout the ship and are interfaced to local data collection units known as data acquisition "bricks". The bricks locally filter and digitize (using internal analog-to-digital converters) the sensor data before it is communicated on the ship's high-speed fiber-optic network. While accelerometers can be interfaced directly to the SPDAS bricks, an amplification bridge circuit is necessary to take strain measurements using metal-foil strain gauges. For this purpose, each strain gauge is connected to a Wheatstone bridge circuit (with a gain of 100) contained in an enclosure called a "stamp" module. To limit load resistance, each stamp module is installed within one meter of the gauge that it services. Then, shielded coaxial wiring is used to communicate the voltage output of the stamp module to a brick where data is digitized and communicated to the server via the fiber-optic network. Measurement data communicated by the hull monitoring system's 28 bricks are aggregated at a single data server connected to the network in a lower deck of the ship. A LabView visualization client running on a Windows 2000 operating system is located on the ship bridge to query the server for real-time data (*e.g.*, peak hull strain, wave height, among others) to be presented to the crew. The system is designed to provide users with a rich set of response parameters associated with hull monitoring. The seakeeping parameters include 6-degree of freedom ship motion measurements, strain responses, wind and wave measurements, as well as ship control parameters.

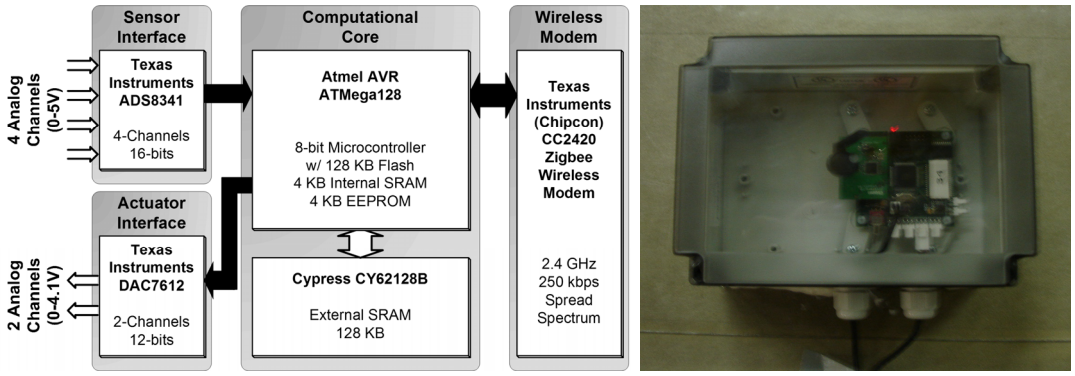


(a) (b)

**Figure 3.3.** *Narada* wireless sensing unit: (a) architectural schematic, (b) top-view of fully assembled prototype.

## 3.3. Field Validation Experimental Setup

In this section, the prototype hybrid wireless hull monitoring system developed for the Sea Fighter is described in detail. First, a brief review of the *Narada* wireless sensor platform is presented as a building block of the two-tiered hull monitoring system (for a full description of the *Narad*a system and its development, see *Chapter 2*). Following that is a description of the hybrid wireless/fiber-optic network developed for the system's upper tier to aggregate data from wireless sensors installed across the ship. Finally, unattended operation of the experimental system is described in detail.

### *3.3.1. Narada Wireless Sensors*

The *Narada* wireless sensor (Figure 3.3), developed at the University of Michigan (see *Chapter 2*), is designed for use in low-cost, high-density sensor networks where the high cost of cable installation makes traditional tethered sensor networks undesirable. Furthermore, it is intended to be able to run on battery power for a long period of time

(*e.g.*, for up to two years using a low duty cycle) in the absence of a power supply native to the monitored structure; therefore it is designed to be a very low-power device. Finally, to meet low-cost requirements, its design takes advantage of commercial, off-the-shelf (COTS) technology for all of its functional components.

The sensor node itself includes four modules (see Figure 3.3(a)). The first module is the computational core which is defined by the microcontroller (Atmel Atmega128) and is responsible for operation of the device. Embedded software, termed firmware, is stored within the microcontroller. The firmware includes two categories of software: first, an operating system (OS) is embedded for the configuration and operation of peripheral components on the sensor, as well as for real-time allocation of processing power. Second, application software is installed consisting of specific engineering algorithms that are responsible for local data processing of interest to the end-user. The sensor also includes three other modules: the sensing interface, actuation interface, and communication interface. A full description of the *Narada* wireless sensor, with information regarding the function of both hardware and firmware, may be found in *Chapter 2* of this thesis.

### *3.3.2. Hybrid Multi-Tiered Network*

Due to their compartmentalized nature, naval vessels present some challenges to centralization of measurement data from wireless sensors distributed throughout the ship. First, wireless sensors can be installed in high density because of their low costs and modular installations. However, available wireless bandwidth limits the total amount of data that can be transmitted on a given frequency channel over a given time period since

only one device can transmit at a time. This fact will effectively limit the channel count that can simultaneously operate on the same wireless channel. In addition, communication reliability can be guaranteed if nodes acknowledge reception of data; this practice places greater demand on the limited wireless bandwidth. In an example of the effects of these limitations, the *Narada* wireless sensor network configured to sample measurement data at 100 Hz can reliably transmit 12 to 15 channels of real-time data continuously on a single communication channel. The exact number of channels depends on the level of interference present in the wireless channel since interference requires packets to be occasionally retransmitted. To help alleviate the burden on a single communication channel, the IEEE 802.15.4 standard defines 16 communication channels within the 2.4 GHz frequency band (spanning from 2.405 to 2.485 GHz in increments of 0.005 GHz) that can be accessed simultaneously in the same space without interference with each other (IEEE 2006), thereby increasing the amount of data that may be moved through a network in a fixed space of time. By use of sub-networks (subnets) of wireless sensors on different communication channels, the achievable sensor channel count in the total monitoring system may be dramatically increased.

The second shipboard challenge, transmission of data between compartments, is more problematic for wireless sensor networks. Decks and watertight bulkheads made of conductive materials (*e.g.*, steel or aluminum) that enclose ship compartments naturally function as Faraday cages, reflecting virtually all incident electromagnetic waves (Harvey 1963). To overcome this inherent challenge of the shipboard environment, existing fiber-optic Ethernet network cables installed on Sea Fighter are utilized to form a wired upper tier of the hull monitoring system architecture. The fiber-optic system offers a high-data

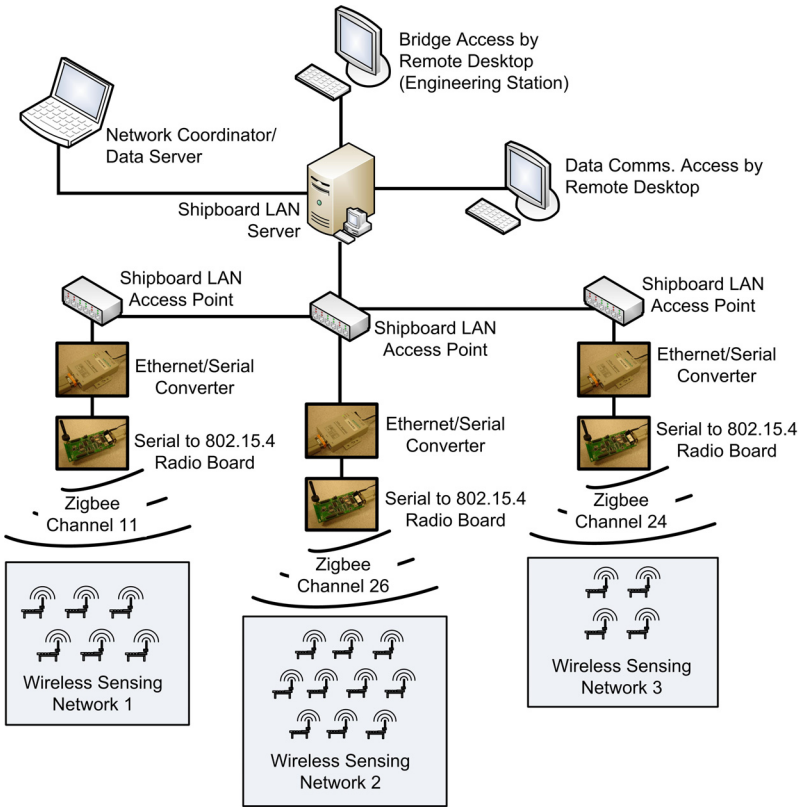


**Figure 3.4.** Overview of the multi-tiered, hybrid wireless/wired network installed on Sea Fighter.

rate connection between the wireless subnets (contained in separate compartments) in the lower tier, and the data server remotely located below deck. On Sea Fighter, the SPDAS system has access points to the fiber-optic Ethernet network at the fore and aft ends of the mission bay. Access to this network provides linkage to other important areas of the ship including the SPDAS data server located below deck, the secure communications room located behind a water-tight bulkhead on the main deck, and the bridge. A diagram depicting the multi-tier, hybrid monitoring system is presented in Figure 3.4.

*3.3.3. System Installation*

Installation of the wireless hull monitoring system aboard the Sea Fighter takes place over four days at the Naval Surface Warfare Center, Panama City Division, in Panama City, Florida. A network consisting of 20 *Narada* wireless sensors is installed along with sensing transducers (namely accelerometers and interfaces to existing strain gauges) and receiver hardware that enables communication between the wireless sensors and a centralized data repository. These instruments are removed while the ship is in dry-dock at the Cascade General Shipyard in Portland, Oregon, after two months of combined seakeeping trials and port time.

The flexural response of the Sea Fighter is measured by the wireless hull monitoring system using strain gauges. Strain measurements are taken from preexisting metal-foil strain gauges (Micro Measurements) previously installed as part of the SPDAS seakeeping system during construction of the vessel. Metal-foil strain gauges indicate changes in strain through a coupling of electrical resistance and mechanical strain (Window 1992). Measurement of these changes generally requires power and conditioning circuitry (*e.g.*, Wheatstone bridge and amplification) to convert the change in metal-foil resistance into a measurable analog voltage signal. These circuits are already included in the SPDAS stamp enclosures that are installed with the strain gauges. The outputs of the SPDAS stamp enclosures located both below deck and in the superstructure above the mission bay are routed to bricks located throughout the ship. At the SPDAS bricks, analog signals are converted into the digital domain, using on-board analog-to-digital converters, and sent via the shipboard local area network to the data repository situated below deck. As a result, the output of the wireless sensors used to

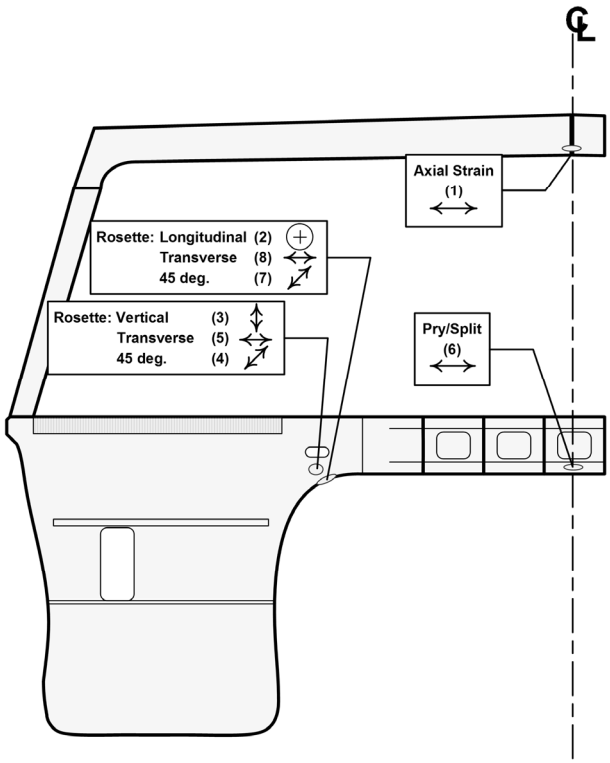


**Figure 3.5.** Layout of metal-foil strain gauges on Frame 20 measured by the proposed hybrid wireless hull monitoring system.

record strain of the hull are installed close to the SPDAS hull monitoring system bricks where the voltage signal from the stamp enclosures are collected. Eight strain gauge channels from Brick 19 are spliced in order to feed them into the wireless sensor nodes; the gauges selected for this study are physically located on Frame 20 (see Figures 3.5 and 3.6). The voltage output levels of the SPDAS strain channels are between 0 and 5 V which perfectly meet the input requirements for the *Narada* sensing interface. Preliminary tests of the SPDAS strain/*Narada* interface suggest some high-frequency noise contamination due to the splicing of the cable at the brick. As a result, each strain gauge sensor channel is provided with a low-pass, four-pole, Butterworth filter, each having a cutoff frequency of 25 Hz, prior to the interface with the *Narada* nodes. The

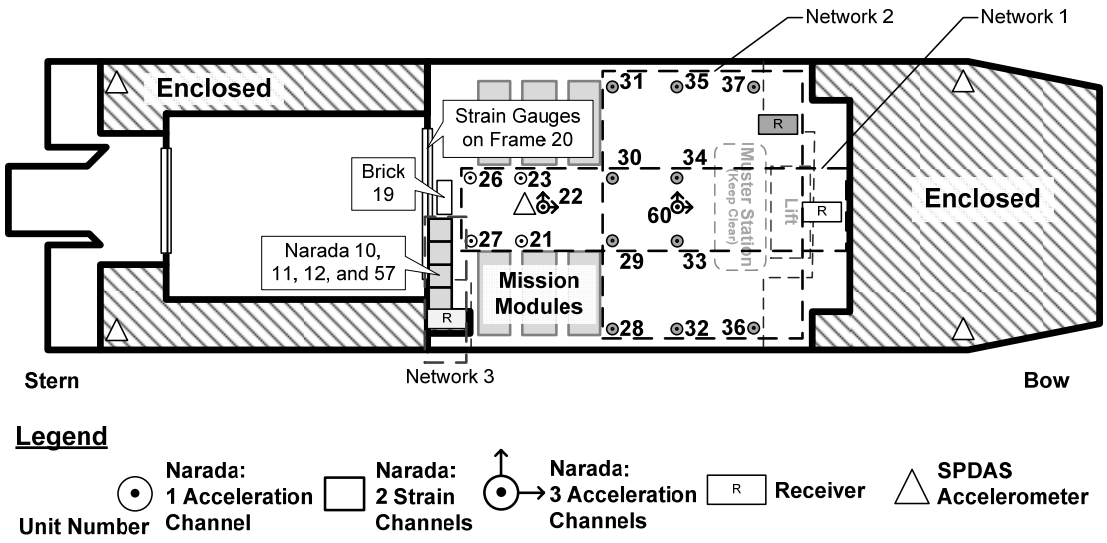


**Figure 3.6.** Layout of the wireless sensing network divided into three subnets in the Sea Fighter mission bay.

filters are assembled on a solderless breadboard and installed in weatherproof enclosures with the wireless sensors (Figure 3.7a). Four *Narada* wireless sensor nodes are used to record the eight strain measurements; each sensor node is configured to collect two channels of strain data.

Acceleration is recorded using micro-electro-mechanical systems (MEMS) accelerometers installed throughout the mission bay (Figure 3.6). Vertical-only acceleration measurements are collected using Crossbow CXL02LF1Z accelerometers. The CXL02LF1Z has an input range of ±2 g, a sensitivity of 1 V/g, a DC-offset of 2.5 V, an output range between 0 and 5 V, and a noise floor of 1 mg (RMS). Crossbow CXL02TG3 ultra-low noise, tri-axial accelerometer arrays are also provided along the centerline of the ship. The performance characteristics of the CXL02TG3 include an input range of ±2 g, a sensitivity of 0.833 V/g, a DC-offset of 2.5 V, an output range between 0.5 and 4.5 V, and a noise floor of 0.6 mg (RMS). For temporary installation of

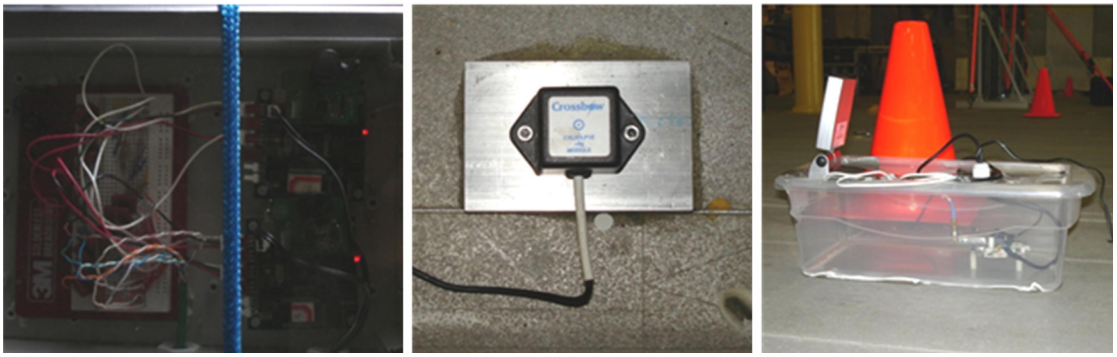

(a) (b) (c)

**Figure 3.7.** Details of the wireless sensor installation on Sea Fighter: (a) Four-pole Butterworth filter with Narada nodes for strain gauge de-noising; (b) Accelerometer bonded to mission bay deck by epoxy; (c) Wireless sensor within an enclosure with directional antenna installed in the mission bay.

accelerometers, mechanical connections such as screws are best so that the transducer is not damaged during removal. Since drilling holes for screws in the deck is deemed unacceptable, accelerometers are instead screwed to 1.2 cm thick aluminum mounting plates that are securely bonded to the deck by epoxy (Figure 3.7b). Protection of the accelerometers from crew activity is provided by rubber traffic cones placed over the top of the accelerometers and epoxied in place (Figure 3.7c). The layout of the ut PSD, and □□□□n a regular grid pattern is intended to generate response data for analysis of the ship.

A laptop computer that coordinates seakeeping data collection runs and archives wireless sensor data is installed below deck (in the hull's machinery and tank space) in close proximity to the SPDAS data server. This laptop controls the wireless sensor subnets through a pair of bridge devices (Figure 3.4). A commercial wireless transceiver development kit (Texas Instruments CC2420DBK) is commonly used by a central data server to wirelessly communicate with the wireless sensor nodes. The development kit

has a CC2420 transceiver (just like the *Narada* nodes) supported by an Atmel Atmega128 microcontroller for wireless communications. The microcontroller is connected to a serial (RS-232) port and is configured simply to pass data from the serial port to the radio. Similarly, data packets received from the wireless radio are read, reformatted, and sent out the serial port. Unfortunately, in the proposed hull monitoring system, the laptop is not collocated within the compartment containing the wireless sensor nodes. This requires use of the ship fiber-optic network to communicate data between the laptop and the wireless transceiver development kit placed in the sensors' compartment. To connect the transceiver to the Ethernet network, a commercial serial-to-Ethernet converter box (Moxa Nport DE-311) is used as a bridge. This connector is a very powerful device because its internal firmware allows it to appear to the laptop as a local serial port even though it is remotely located on the Ethernet network. Hence, the Nport device driver handles all of the networking details when establishing communication between the laptop and the transceiver. As shown in Figure 3.4, a total of three Nport converters are used to connect these wireless transceiver development kits to the network; each Nport/transceiver pair is packaged in a weatherproof container and installed in the mission bay.

The layout of the transducers, sensing nodes and receivers within the mission bay is depicted in Figure 3.6. Twenty *Narada* wireless sensing units, collecting the 8 channels of strain data and 20 channels of acceleration data, are organized into three subnets operating on three different IEEE 802.15.4 communications channels (channels 11, 24, and 26). Dividing the wireless sensors into three subnets represents an efficient use of the wireless bandwidth which is critical for allowing reliable continuous data streaming

from the wireless sensor nodes during operation of the hull monitoring system. These sensing units are allocated into the three subnets based on their location within the mission bay, as well as their functionality (*e.g.*, strain versus acceleration data collection). Subnets 1 and 2 (denoted in Figure 3.6) include *Narada* sensing nodes measuring acceleration and have their receivers located forward in the mission bay. Subnet 1 contains two *Narada* sensing units collecting tri-axial acceleration near the center of gravity of the ship. In addition, subnet 1 contains eight *Narada* nodes, each collecting uni-axial vertical acceleration. Subnet 2 contains ten *Narada* sensing units collecting vertical acceleration from the forward part of the mission bay. As previously mentioned, subnet 3 consists of four *Narada* nodes recording two strain channels each. Because their communication distance is greater, directional patch antennas are used on sensor nodes in subnet 1 while omni-direction quarter-wave dipole antennas are sufficient for subnets 2 and 3. Subnet 3 is located aft of subnet 1 near SPDAS brick 19 with the receiver and Nport converter located nearby (see Figure 3.6).

### *3.3.4. Data Collection*

The proposed hybrid wireless hull monitoring system is set to continuously collect hull response data and operate in an autonomous mode, without human intervention. The *Narada* nodes are all set to collect data at a rate of 100 Hz. To begin data collection, a start beacon is initiated by the laptop serving as network coordinator and is broadcast from the wireless transceiver boards servicing each sensor subnet. Network synchronization is handled through this beacon. Before the start command is transmitted, the *Narada* units are put in a wait state where their embedded microprocessors cycle

through four assembly instructions waiting for the server command. Limiting the actions of the embedded OS in this way limits the discrepancy between processing times that may occur within the sensing nodes upon receipt of the beacon. This practice effectively limits the synchronization error between nodes. The upper bound on synchronization error in this system is defined by the sum of the difference in wireless propagation times from receiver to sensor (wireless signal path length divided by the speed of light) and the differential processing times for the beacon packet within the sensor. Differential processing times may arise from stochastic delays in the fiber-optic network, wireless transceiver or within the microcontroller (Maróti*, et al.* 2004). Observations made on the differential processing times (absolute value) between units (measured using a digital oscilloscope in the laboratory) yield a distribution with an average synchronization error of 10 μs, a variance of 8 μs, and peak observed value of 30 μs. Assuming 1000 m in differential path length (the high end of the system's communication range), the upper bound on the synchronization error from the beaconed network is less than 35 μs. This error level is negligible when considering sampling in the low kHz range, or less.

Once the system is time synchronized, data is then buffered within the wireless sensor nodes until 30,000 samples are collected. After 300 seconds, the network coordinator queries the sensing units, one at a time, and requests the data in packets of 50 data points each. Received packets are then archived in the data server. Because the timing within each *Narada* wireless node is not exact (each sensor basis of time is derived from a crystal oscillator that exhibits slow drifts, thereby adding additional synchronization error as data collection progresses) the system is configured to stop collecting data every half-hour so that the monitoring system can briefly resynchronize before it re-initiates its data

collection activities. Oscillators on the *Narada* wireless sensing nodes operate at 8.0 MHz and are rated to have stability of 2.0 parts per million (ppm) or better. This level of stability yields a worst-case clock drift of 9 ms during the 30 minute inter-synchronization periods.

## 3.4. Results

Results of this study are presented in this section in three parts. First, data collected by the experimental wireless hull monitoring system is compared to data collected using the SPDAS wired hull monitoring system. Second, wireless reliability of data transmitted in the experimental system is discussed. Finally, results derived from modal analysis of the Sea Fighter are presented.

### *3.4.1. Comparison of wireless hull monitoring system to SPDAS system*

Wirelessly collected data compares well to identical data collected by the SPDAS system. On the strain channels where the *Narada* system and the SPDAS record the same signal, the signals recorded and archived are nearly identical. Figures 3.8 and 3.9 show strain comparisons between the *Narada* derived strain time histories and those recorded by the SPDAS system of strain gauges 2 and 3 (as numbered in Figure 3.5), respectively, measuring hog/sag bending of the twin-hull structure. A slamming event (*i.e.*, wave impact on the ship bow) is evident in Figure 3.9. In addition, some minor spikes are evident in the *Narada* signal in Figure 3.9 (*e.g.*, at time indices 304 and 306 seconds) due to imperfect connections in the breadboard filter readings from the strain

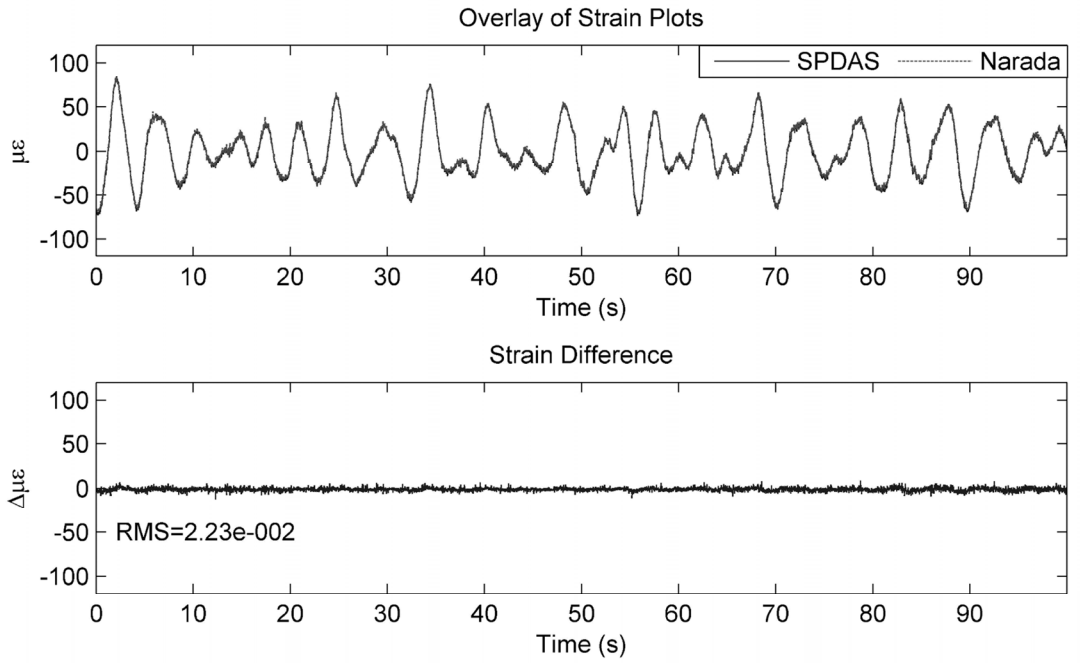


**Figure 3.8.** Time history response of the ship hull (top) during rough seas (sea state 3) as measured by the *Narada* and SPDAS based hull monitoring systems (corresponding to strain gauge 2 in Figure 3.5). The difference in the two measured time-histories is shown below.

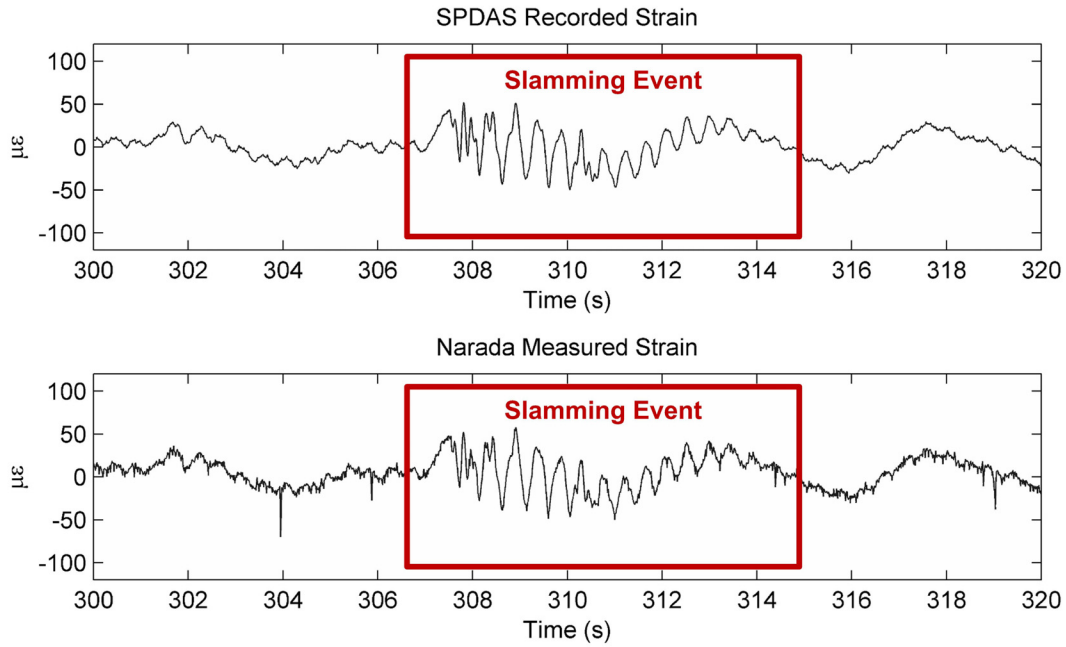


**Figure 3.9.** Strain comparison between strain measured at strain gauge 3 (in Figure 3.5) by the SPDAS (top) and wireless (bottom) hull monitoring systems. A slamming event is evident at 307 seconds in a transient vibration response.

gauge channel. Vibrations and shock loadings generated at sea will affect the quality of these connections and corresponding noise levels. Even at the higher levels though, noise levels are within acceptable limits. Of the eight strain channels recorded by *Narada*, one of the strain gauges (or its associated power circuit) fails before the ship disembarked for its sea trials resulting in zero voltage levels recorded by both the SPDAS and the *Narada* systems for that channel (strain gauge 6). Also, one Butterworth low-pass filter fails during installation (strain gauge 7). Hence, during the sea keeping trials, the wireless hull monitoring system has six operational channels of high-quality strain measurements (strain gauges 1 through 5 and 8 in Figure 3.5). In general, the error between the wireless and wired strain readings is less than 0.03 με (or about 5%), as shown in Figure 3.8.

The *Narada* sensing nodes recording hull acceleration do not share a channel directly with the SPDAS hull monitoring system. However, each system does have a tri-axial accelerometer located at the ship center-of-gravity (COG). The wireless array is located on the top surface of the mission bay deck while the SPDAS tri-axial array is mounted directly beneath on the underside of the deck. Comparison of the acceleration signals measured by these two accelerometers shows excellent agreement with errors less than 0.5 milli-g (or about 1%; Figures 3.10 and 3.11). Both noise level and time synchronization compare favorably between the two systems. Even in the presence of a slamming event (see the zoomed-in time history of Figure 3.11), the fidelity between the two systems is excellent. This result further demonstrates that the wireless sensing system can indeed operate independently of the wired monitoring system and collect high-quality data measurements.

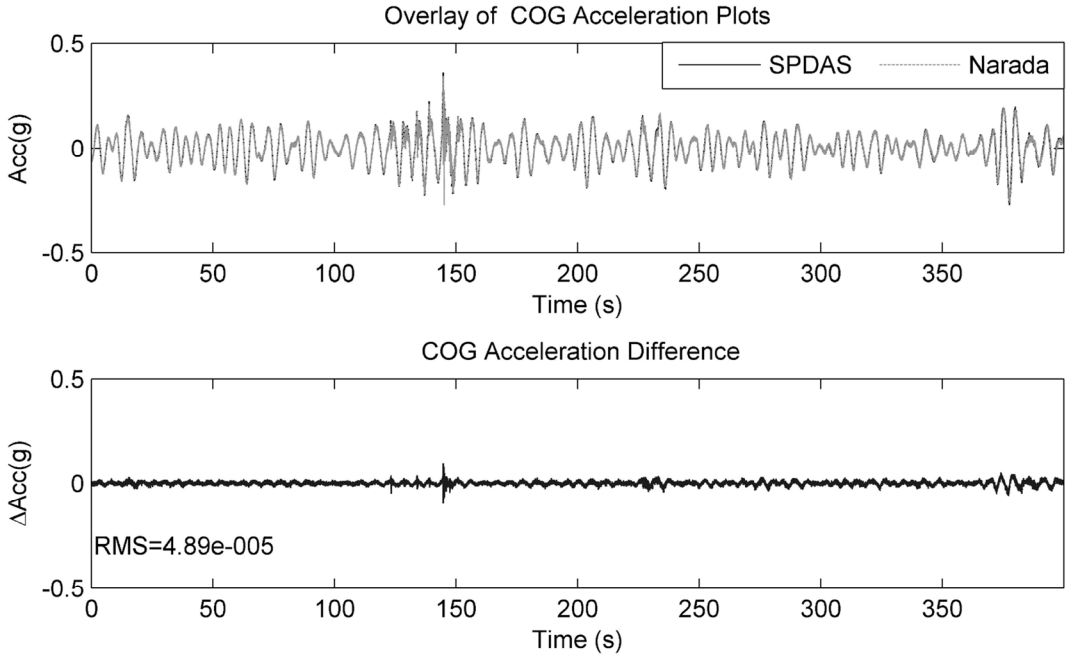


**Figure 3.10.** Comparison of *Narada* center-of-gravity (COG) vertical acceleration measurement to that independently measured and recorded by the SPDAS system (top). The difference in measured acceleration is presented below.

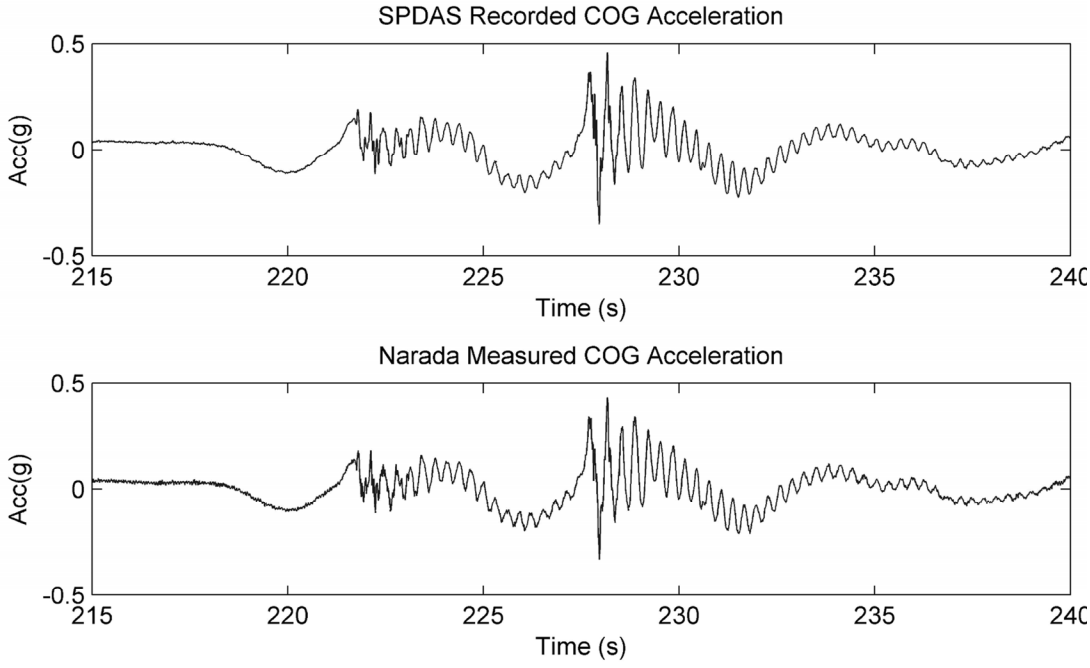


**Figure 3.11.** Center-of-gravity (COG) response of Sea Fighter during a slamming event on the ship bow as measured by the SPDAS (top) and wireless (bottom) systems.

### 3.4.2. Wireless Reliability

Wireless reliability is evaluated in terms of data packets delivered to the server over the wireless communication channels, not including the effects of data loss due to timing errors brought about by contention on the wired network. Data loss is defined as data never received by the data acquisition coordinator. It does not include data lost on one transmission, but successfully received on a retransmission as part of the wireless communication resend/acknowledge protocol. In this regard, data delivery in the strain subnet (subnet 3) is very good. The communications range for all *Narada* units measuring strain is relatively constant, approximately 3 m. For these units, data loss on the wireless communication channel ranges from 0 to 3%. It is worth noting that, during early testing, units exhibited poor performance when located very close to a metal bulkhead due to their increased exposure to signal reflections. Moving them away from the bulkhead early in the voyage results in greatly improved reliability in subnet 3.

On the other hand, subnets made up of acceleration-based *Narada* nodes include large variability in unit communication distances, multipath effects, and antenna configurations, providing very interesting results. Subnet 1, which has communication ranges as far as 30 m, is equipped with directional, high-gain, patch antennas. The directional antennas provide robust communications as a result of increased signal strength in the direction of desired wave propagation, reduced multipath effects, and increased clear distance between the antenna and the metal deck. Data loss on the subnet 1 wireless communication channel is between 0 and 5% during the transits under normal conditions. Additional data loss occurs during some transient, adverse conditions. For example, if the steel doors of the shipping containers in the mission bay are open in close

proximity to a wireless sensing node (within 0.5 m or less), the line-of-sight then between the sensing node and the receiver could be obstructed resulting in data loss as high as 50%. This result indicates that the gain in effective transmission range achieved through use of directional antennas comes at a cost of a loss in redundant wireless transmission paths. In addition, one sensing node in subnet 1 located in a very high-traffic area is damaged catastrophically very early in the transit (the node is stepped on by a crew member) and subsequently, communicates only sporadically and returns corrupted data.

Subnet 2 enjoys a shorter average distance between the receiver and sensing units than subnet 1, but sensors are equipped with omni-directional, quarter-wave dipole antennas. Sensors in this subnet exhibit both the best and worst sustained communication loss rates observed during this study. As a result of both the antennas and the geometry, data loss on the wireless channel (on average) is higher than the other two subnets due to a combination of range and multipath interference effects. For sensors closest to the receiver, data loss is minimal, with about 0 to 1% of packets lost during the entire course of the study. For the other sensors in subnet 2 that are farthest from the receiver, their data loss rate is as high as 7%. In particular, two units performed particularly poorly (these units are later replaced to test if there is some hardware malfunction with no effect). These units are physically closer to its receiver than the better performing units of subnet 1 but, due to its lower-gain, non-directed antenna, data loss is significantly higher. Other units located nearly as far from the server, but with more advantageous positioning with regards to reducing negative multi-path, give much better communications results, with only 2% data loss over the course of the study. A node by node list of wireless data delivery performance is presented in Table 3.1. This data

**Table 3.1.** Percentage data loss, by unit number, in the wireless hull monitoring network.

| Unit Number | Data Loss (%) | Data Type | Antenna Type | Unit Number | Data Loss (%) | Data Type | Antenna Type |
|---|---|---|---|---|---|---|---|
| 10 | 1 | Strain | Omni | 30 | 0 | Acc. | Omni |
| 11 | 1 | Strain | Omni | 31 | 2 | Acc. | Omni |
| 12 | 3 | Strain | Omni | 32 | 4 | Acc. | Omni |
| 21 | 4 | Acc. | Directional | 33 | 2 | Acc. | Omni |
| 22 | 1 | Acc. | Directional | 34 | 0 | Acc. | Omni |
| 23 | 3 | Acc. | Directional | 35 | 1 | Acc. | Omni |
| 26 | 5 | Acc. | Directional | 36 | 3 | Acc. | Omni |
| 27 | Broken | Acc. | Directional | 37 | 3 | Acc. | Omni |
| 28 | 6 | Acc. | Omni | 57 | 2 | Strain | Omni |
| 29 | 7 | Acc. | Omni | 60 | 0 | Acc. | Directional |

corresponds to communication performance measured over a one-week period of seakeeping trials.

### *3.4.3. Operational Deflection Shape Results*

Besides simple data collection, it is desirable to use the hybrid wireless hull monitoring system for system identification of the ship, which is the first step in many structural health monitoring applications (Doebling*, et al.* 1998). Since wireless sensors have collocated memory and processing, they have the ability to process data as soon as it is collected (Straser and Kiremidjian 1998). This practice has two main advantages: it eliminates the potential glut of unprocessed data that has been collected but is never analyzed, and it can alleviate bandwidth congestion if processed, low-bandwidth engineering results can be transmitted in lieu of high-bandwidth raw data. In battery powered sensor networks, this practice also saves battery power as embedded computing consumes less power than does data transmission (Lynch and Loh 2006). In this study, testing the ability of the wireless hull monitoring system to collect and archive vibrational

data is of primary interest, so the modal analysis is done offline (validation of embedded processing methods are presented in later chapters) using the Frequency Domain Decomposition (FDD) method (Brincker*, et al.* 2001).

This study utilizes acceleration data from the wireless sensors and the FDD method to determine mode shapes from the identified modal frequencies. In the FDD method developed by Brincker, *et al*. (2001), modal frequencies are determined from the peaks of the fast Fourier transform (FFT) of the recorded output response functions. The method assumes that the input to the system is a stationary broad-band excitation (*e.g*., impulse or white-noise). Singular value decomposition (SVD) is used to decompose the spectral density matrix at modal frequencies into single degree-of-freedom systems in the frequency domain. By decomposing the system in the frequency domain, the FDD method is very useful in determining closely spaced modes. To execute the FDD method, the power spectral density (PSD) matrix of the measured outputs, $\boldsymbol{G_{yy}}(j\omega)$, is necessary. The PSD matrix satisfies the input ($x$) and output ($y$) relationship:

$$\boldsymbol{G}_{yy}(j\omega) = \boldsymbol{H}^{*}(j\omega)\boldsymbol{G}_{xx}(j\omega)\boldsymbol{H}^{\mathrm{T}}(j\omega) \tag{3.1}$$

where $\boldsymbol{G}_{xx}(j\omega)$ is the input PSD, and $\boldsymbol{H}(j\omega)$ is the transfer function between the known output and the unknown input. Since the input and transfer function are unknown, the following estimate of the output PSD is used instead of $\boldsymbol{G_{yy}}(j\omega)$ (Allemang 1999):

$$\widehat{\boldsymbol{G}}_{yy}(j\omega_i) = F_y(j\omega_i)\left(F_y^{*}(j\omega_i)\right)^{\mathrm{T}} \tag{3.2}$$

where $\widehat{\boldsymbol{G}}_{yy}(j\omega_i)$ is the estimate of the output PSD at frequency $\omega_i$ and $F_y(j\omega_i)$ is an array of FFT values of the outputs at frequency $\omega_i$. The next step is to determine the SVD of the output PSD matrix:

$$\widehat{\boldsymbol{G}}_{yy}(j\omega_i) = \boldsymbol{U}_i \boldsymbol{S}_i \boldsymbol{U}_i^{\mathrm{H}} \tag{3.3}$$

where $\boldsymbol{S}_i$ is the diagonal matrix of singular values at frequency $\omega_i$, and $\boldsymbol{U}_i$ is the matrix of singular vectors.

$$\boldsymbol{U}_i = [\boldsymbol{u}_{i_1} \quad \boldsymbol{u}_{i_2} \quad \cdots \quad \boldsymbol{u}_{i_{1m}}] \tag{3.4}$$

The singular values indicate the relative amount of energy associated with each singular vector with the most energy at that frequency associated with the first singular value. Thus, from the first singular vector, an estimate of the mode shape at that frequency may be determined.

$$\widehat{\boldsymbol{\phi}}_i \approx \boldsymbol{u}_{i_1} \tag{3.5}$$

While the FDD method has been successfully implemented in a distributed fashion within a *Narada* wireless sensor network (Zimmerman*, et al.* 2008), due to the complicated and unknown nature of the ship structure, the FDD method employed in this study is applied offline.

Mode shape determination from data collected aboard the Sea Fighter is particularly challenging due to the nature of the input to the system. The input is highly colored, not broadband, and further influenced by the ship's ride control system that mitigates the effects of the sea upon the vessel rigid-body dynamics. Due to these difficulties, it cannot be stated with certainty that any frequency dependent deflection shapes identified from the data are indeed mode shapes, therefore the more technically accurate term "operational deflection shapes" will be referred to in lieu of mode shapes. However, operational deflection shapes are known to be closely correlated to mode shapes. One aid in the search for operational deflection shapes that are likely to be mode shapes is the presence of slamming events. Slamming events act as impulse-like loads (*i.e.*, nearly

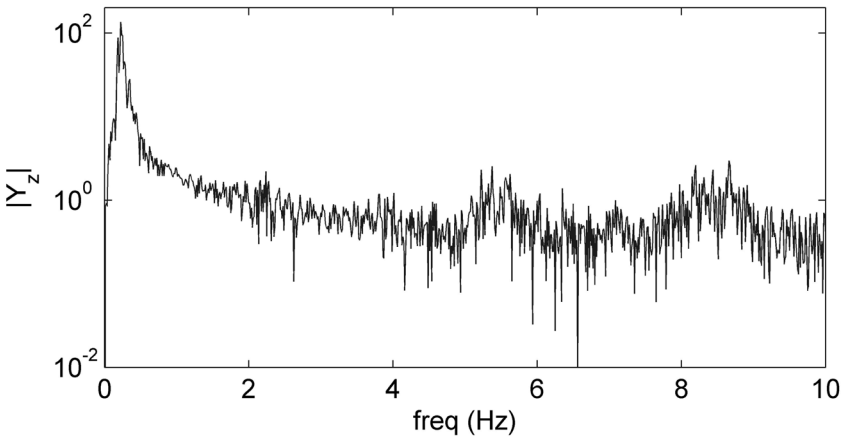


(a)

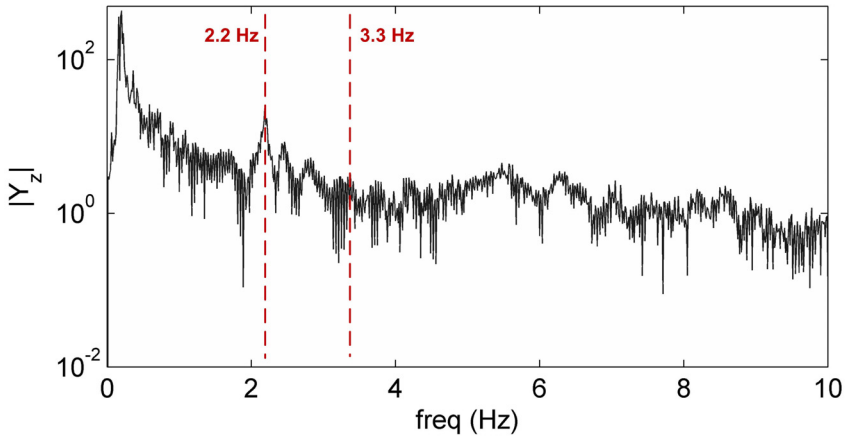


(b)

**Figure 3.12.** Response spectra of the Sea Fighter measured at accelerometer location 35 (in Figure 3.6): (a) without slamming event, (b) with slamming event.

broad-band) that excite all of the hull's modes. This effect can be seen in two frequency spectra identified from wirelessly collected acceleration data in the presence of and in the absence of a slamming event (Figure 3.12). With a slamming event present, peaks in the response spectra at 2.2 Hz and 3.3 Hz are evident (Figure 3.12b); without those events, those peaks are extremely difficult to discern (Figure 3.12a).

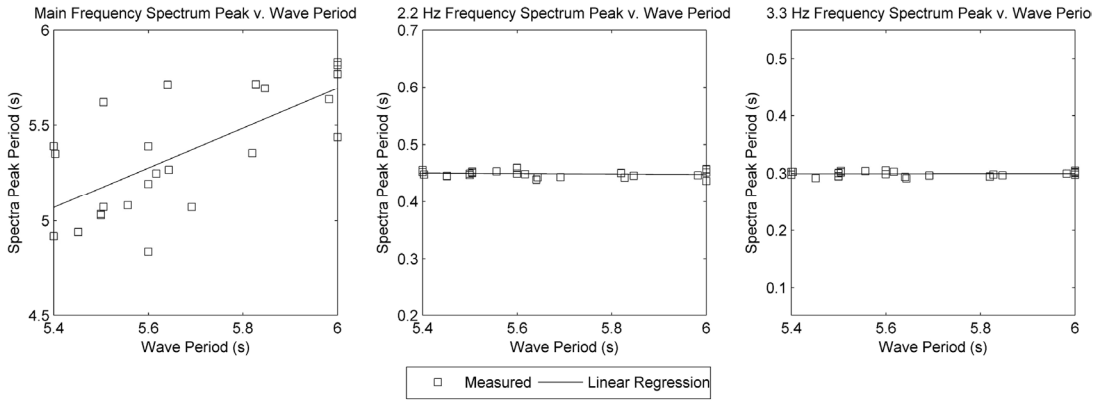


**Figure 3.13.** Correlation of identified spectra peak period to wave period using data collected during the transit between Long Beach and San Francisco.

Figure 3.12 also shows that, regardless of the presence or absence of slamming events, the effect of the predominant wave period dominates the response spectra. Throughout the transit, wave periods are measured by the TSK wave height sensor at approximately 5.0 s which corresponds to the peak in the response spectra at 0.2 Hz. If the peaks at 2.2 and 3.3 Hz do represent flexure modes of the hull, they should be invariant despite changes in ship speed and wave period. Furthermore, if the peak at 0.2 Hz is due to the wave loading, it should vary with wave period. While variance in the wave period at 0.2 Hz is relatively small, there is some variance over the course of the transit. There is however, almost no variance in the resonant frequencies near 2.2 and 3.3 Hz. The location of the dominant peak in the frequency spectrum (near 0.2 Hz), on the other hand is variable, and strongly correlated to the wave period and ship speed. Specifically, that period is correlated to wave period and the inverse of ship speed. The correlation between spectra peak period and the seaway wave period is plotted in Figure 3.13 (a). The linear regression between the wave period and main peak period is almost one-to-one

(slope = 1.0366) while it is nearly uncorrelated (slope = -0.0041 and slope = 0.0002, respectively) for the 2.2 and 3.3 Hz peaks.

As shown in Figure 3.14, the two operational deflection shapes calculated using FDD at 2.2 and 3.3 Hz correspond to torsion and hog-sag modes of the ship, respectively. It should be noted that the accelerometers interfaced to the wireless hull monitoring system correspond to the central section of the ship. However, the SPDAS hull monitoring system has accelerometers at the four corners of the ship, as well as at the ship center of gravity, which would provide a more comprehensive view of the global operational deflection shape. The operational deflection shapes obtained by applying FDD to the combined acceleration measurements from the experimental hybrid wireless system and the SPDAS hull monitoring system (time synchronized in post-processing using the COG acceleration measurement as a reference) are shown in Figure 3.15. The two operational deflection shapes obtained from the combined data set help to confirm the findings obtained by the wireless hull monitoring system alone.

### 3.5. Field Validation Conclusions

For this study a wireless sensing network, based on the *Narada* wireless sensor developed in *Chapter 2*, is installed and tested on the FSF-1 Sea Fighter during its transit from Panama City, Florida, to Portland, Oregon. Twenty *Narada* sensors recording twenty-eight channels of strain and acceleration data are installed on three subnets in the Sea Fighter mission bay. These sensors communicate with receiver boxes that are interfaced with the existing shipboard Ethernet network via serial-Ethernet converters

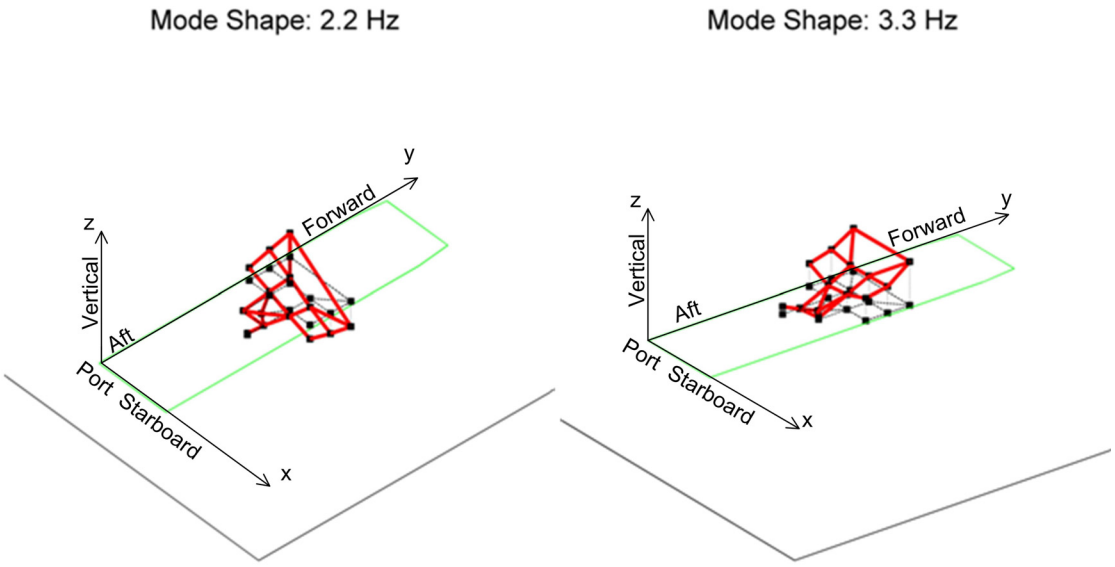


**Figure 3.14.** Operational deflection shapes determined from *Narada* collected acceleration data.

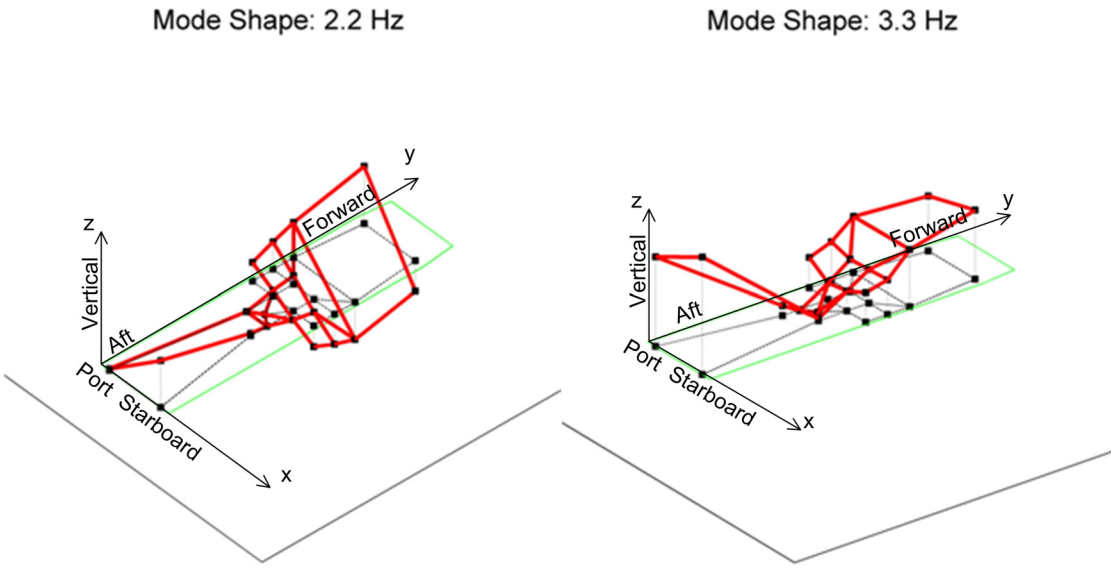


**Figure 3.15.** Operational deflection shapes determined from combined *Narada* and SPDAS collected acceleration data.

that abstract the networking details from the network coordinator. The network coordinator server is below deck and is accessed via remote desktop from the ship's secure communications room as well as from the bridge. This experimental validation of

a hybrid sensing network composed of wired and wireless tiers demonstrates the value of combining the strengths of both technologies in a single system. Wireless sensors are used to collect hull response data from transducers located throughout a ship's compartment. Once consolidated at a receiver box, a high-bandwidth wired system carries the sensor data through bulkheads to a central repository below deck.

Wirelessly collected data compares well with data collected by the wired system. Comparisons between the strain signals recorded by the SPDAS monitoring system and the proposed hybrid wireless hull monitoring system show little difference between the two. Errors observed are, on average, in the range of 0.023 micro-strain, RMS. In these cases, the SPDAS and the proposed wireless hull monitoring systems share use of the same transducers. Comparisons of acceleration data between the SPDAS and the proposed wireless hull monitoring systems (each collecting data measured from independent transducers) also show very good agreement, with representative errors less than 50 μg, RMS. These results demonstrate the high-fidelity of the hybrid wireless hull monitoring system.

Data is transmitted successfully with little data loss due to use of a robust send/acknowledgement protocol when wirelessly communicating. The reliability results obtained in this study demonstrate that high quality wireless communication can be achieved in the shipboard environment, but a number of factors influence success and can greatly impact the quality of the wireless communication system. The most critical component in most wireless applications is transmission power (strongly correlated to range), but in many shipboard applications, compartments are small enough that range is not a factor. However, the mission bay, which is nearly 60 m long, is an exception. Just

as important as range on Sea Fighter (and likely more important on vessels lacking large, open bays) are multipath effects. Multipath effects can be harmful as well as helpful. They are harmful when primary and secondary transmission waves reach a receiver antenna simultaneously, resulting in decoding errors by the wireless receiver. Negative multipath effects are significantly alleviated on subnet 1 by use of directional antennas. However, some of the useful aspects of multipath effects are mitigated as well including the provision of redundant signal paths that can overcome transient conditions such as physical obstructions along the primary line-of-sight pathway between transmitter and receiver. Wireless sensors located near their receivers or those that used directional antennas performed extremely well in the sea trials. Sensors relatively far from receivers using omni-directional antennas did not perform as well, suggesting that wireless communication issues arose as a result of a combination of range and multipath effects. Greater use of directional and high-gain antennas (where appropriate) and power amplified radios will improve performance where data loss is an issue. Creating clear space, wherever possible, between decks (or bulkheads) and the antennas attached to the *Narada* nodes, will also help in improving the reliability of the wireless channel. As such, this study identifies sensing node placement, receiver placement, and antenna selection as non-trivial tasks in shipboard installations.

Improvements in communication can be accomplished by taking advantage of additional board features and additional testing. One feature of the CC2420 wireless modem employed by the *Narada* wireless sensor is that it returns to the microcontroller a measurement of the received wireless signal strength whenever it decodes a packet. This information can be used to provide to the network a real-time map of network reliability

given transient conditions. This information can be used at the time of installation to optimize sensor node location and antenna orientation for maximum performance. Second, leveraging the computational abilities of the sensor for embedded data processing can greatly improve robustness and reliability of the wireless communication channels as well as save battery power (where necessary) as data transmission is an energy intensive operation for the wireless unit (Lynch*, et al.* 2004). Even so, some level of interference and lost data packets is inevitable; therefore, reduction of the sensor channel load per communication channel to a conservative level (below the theoretical upper limit) is important to help ensure system reliability. In this environment, ten sensor channels per communication channel streaming data collected at 100 Hz is identified as a practical upper limit. Distributed over the sixteen communication channels defined by the IEEE 802.15.4 communication standard, this practice would limit the sensor count to 160 sensor channels. However, with adequate spatial separation and signal blocking due to bulkheads, these channels may be employed in different zones of the vessel without interference. Furthermore, since communication of raw data over the wireless communication channels consumes a large amount of bandwidth and is a practice that scales poorly as sensor networks grow in size. Communicating a reduced set of processed data alleviates stress on the available bandwidth, thereby increasing the time window available for multiple, robust resend/acknowledge protocols to help ensure that data is delivered.

Future work should include even larger sensor networks, defined by hundreds of sensor channels with both greater physical resolution and scope (*i.e.,* a denser sensor network located throughout the entire length of the ship). Greater reliance on embedded

data processing will alleviate demand on the crowded wireless communication band, increase system scalability, and reduce the system's reliance on the data servers that serve as potential single points of failure. The use of wirelessly collected acceleration data for modal analysis of the ship demonstrates the value of the hull response data. Leveraging the ability of wireless sensors to serve as a platform for economical, high-density sensing networks can also help in making automated ship-board hull health monitoring systems a reality.

# CHAPTER 4

## STRUCTURAL MONITORING AND LOAD ESTIMATION OF WIND TURBINES USING WIRELESS SENSOR NETWORKS

Monitoring of alternative energy generators such as wind turbines is becoming increasingly critical; however, acquisition of the dynamic output and load data can be a time-consuming and difficult process. At the same time, new off-shore and deep-water turbine installations are pushing the bounds of current turbine designs as towers increase in height, and push the limits of the industry's knowledge with regard to loading in these unique environments. In such cases, monitoring becomes doubly important, both to characterize structural performance of the turbine, and to build a statistical database of environmental loads acting on the structure over time. In recent years, low-cost wireless sensors have emerged as an enabling technology for structural monitoring applications. In this chapter, the wireless sensor network developed in *Chapter 2* and field validated in *Chapter 3* is installed in three operational turbines in order to demonstrate their efficacy in this unique operational environment. Data collected from these turbines is used for validation of a novel model-assisted load estimation algorithm developed for autonomous execution within a wireless sensor network.

## 4.1. Introduction of Load Estimation

One of the most critical elements in the design of any new structure is the proper development of design loads. Design loads depend on the structure's composition, location, as well as intended function, and are based on physics, historical loading data, and professional experience. Design load guidelines developed by a consensus of professional opinion have been codified for use by the design engineer (ASCE 2005; ICC 2006). For stochastic loads, particularly wind and seismic loads, the profession's collective database of historical load information is particularly vital to development of appropriate design loads (loads that are neither under nor overly conservative). As novel and innovative structures (*e.g*., very tall buildings or wind turbines) are developed in increasingly challenging environments (*e.g*., offshore), it becomes necessary to add new loading data representative of these novel.

Direct measurement of lateral loads is often quite challenging. Seismic events can be indirectly captured by recording ground acceleration from which the effects of the recorded seismic movement may be inferred. However, the characterization of wind loads imposed on structures is a difficult problem to solve (Schueeller*, et al.* 1983), particularly in large wind farm arrays and off-shore applications (Veers and Butterfield 2001; Butterfield*, et al.* 2009). In wind turbine applications, wind measurements taken at ground level do not accurately represent the conditions that occur at the level of the nacelle or blades, thus meaningful measurements must be taken from sensors located many meters above the ground. Wind sensors (*i.e*., anemometers) located on the tower itself can be helpful in load estimation, but due to the fact that turbines are designed to

"face" the wind, anemometers on the tower can only measure wind that has already been disturbed through its interaction with the turbine blades. Passive measurement towers may be constructed upwind from the turbine and can provide a reasonable, undisturbed measurement of the wind conditions (*e.g.*, speed, direction, temperature, and density) at appropriate heights above the ground. Unfortunately, such towers represent a significant expense. Furthermore, large wind farms, defined by many turbines arranged in multiple rows, will require a large number of sensor towers that can adequately capture the complex loadings that occur due to turbine interactions via turbulence and wake effects (Hau 2006).

Recently, a variety of new sensor solutions have been proposed for wind measurements in the wind energy arena. One innovative sensing technology viable for spatial sensing of wind conditions in wind farms is atmospheric light detection and ranging (LIDAR) mapping (Smith*, et al.* 2006). LIDAR operates on the principles of scattered light to estimate wind speed, direction, and density (Yoe*, et al.* 2003). While capable of measuring wind conditions as far away as 10 km, LIDAR can be an expensive device to obtain.

These constraints make potential load estimation using the vibrations of the turbine structures themselves an attractive prospect. This form of load measurement takes advantage of the existing structure as a sort of "load sensor". Load estimation from the measured response of mechanical and civil structures has been an active area of research as far back as the 1980s (Stevens 1987). Observer based methods for extracting loads on rotating machinery have been investigated by Gibson and Stein (1996) as well as Kim, *et. al*. (2006). These methods have been advanced to estimate unwanted loads (*i.e.*,

disturbances) in the control community for devices under feedback control (Abidi, *et al.* 2004; Ronkanen, *et al.* 2007; Nurung, *et al.* 2009). In addition, impact load estimation of passive systems (*e.g.*, aircraft wings) has been studied by Liu, *et al*. (2000). In the civil engineering community, load estimation methods have been developed for stochastic loads including bridge traffic (Yu and Chan 2007), stadium crowd loading (Ellis and Littler 2004), as well as wind loads on roofs (Uematsu, *et al.* 1996; Uematsu, *et al.* 2001), shells (Li and Tamura 2005), towers (Ma, *et al.* 2003; Law, *et al.* 2005; Hwang, *et al.* 2009), buildings (Hwang, *et al.* 2009), and wind turbine blades (White, *et al.* 2009).

Extracting loading information from structural response necessitates the use of some model of the structure. High fidelity finite element models such as those used by Uematsu, *et al*. (1996; 2001) can provide good results but are impractical for embedment in resource-constrained wireless sensor networks. Furthermore, this method and other methods using reduced complexity models (Ma, *et al.* 2003; Law, *et al.* 2005; White, *et al.* 2009) assume that very accurate models that reflect the true dynamics of the structure (including environmental effects) are available. Hwang, *et al*. (2009) present methods that take modeling uncertainty into account through use of the Kalman filter to minimize error. However, the method presented in this chapter attempts to address this issue more directly, by developing a wind load estimation algorithm that includes an explicit system identification step to update a model of the structure online, then uses that updated model to make the input force estimation. Furthermore, the method relies on a frequency-domain structural model that is both computationally undemanding (relative to high-order finite element models) in order to allow it to be embedded in low-power wireless sensing

nodes, and is based on the physical parameters of the structure so as to restrict it to realistic models.

### 4.2. Application to Wind Turbines

Due to their importance and exposure to wind loadings, wind turbines are identified as an ideal subject for this study. With the recent rise in public consciousness regarding renewable and carbon-neutral energy sources, wind energy is gaining popularity as perhaps the most technologically developed and practical alternative energy source available today. Recent studies put the annual wind energy generation capacity of the United States at 11,575 megawatts (Leopold 2007) with a growth rate of 30% annually (Southern 2007). Technological improvements (*e.g.* larger, more powerful generation turbines) and federal tax subsidies have increased investment in wind energy technology to the point where 33 states host sizable wind farms, 19 of which are significant with capacities over 100 MW (DOE 2006). Despite those accomplishments, wind energy only accounts for 0.8% of the United State's total energy supply (Leopold 2007). This number pales in comparison to other developed nations such as Germany which already realizes a full 7% of its energy supply from wind (Wiser and Bolinger 2007). By substantially increasing its wind power capacity, the United States could drastically reduce its own carbon emissions by as much as 2 billion tons by 2050, if it were to generate 20% of its energy by wind (DOE 2006).

Improvements to the cost/benefit ratio of wind turbine construction can come through the aggressive pursuit of efficient turbine designs. Longer and lighter blade designs using novel materials (*e.g.*, fiberglass composites) will yield better performance (Schulz and

Sundaresan 2006). Frequently reversing wind loads and blade orientation with respect to gravity subject blades to high levels of fatigue that have the potential to cause sudden failure (Pitchford, *et al.* 2007). Typically, blades experience damage requiring repair or even replacement, on average, five times per year (Rolfes, *et al.* 2006), a fact that negatively affects the long-term profitability of wind turbines. In addition, undetected damage can propagate into sudden and catastrophic failure. A sheared blade presents a substantial risk to anyone on the ground and unbalances the entire nacelle, potentially resulting in damage to internal gears and the energy plant (Schulz and Sundaresan 2006). For example, an on-shore turbine experienced sudden blade failure in Dunbar, Scotland in 2005, resulting in £1.25 million in repair costs and significant downtime (Tweedie 2005). Other reported damage mechanisms in wind turbines include corrosion (particularly for turbines sited near bodies of salt water), foundation failures, and fatigue cracking in the steel turbine tower (Hau 2006). As future wind farms go off-shore, damage may not be detected as promptly, resulting in more extensive damage, longer downtimes, and reduced profitability.

Installation of sensors, whether temporary or permanent, can provide turbine response data from which the wind energy field can greatly benefit. First, data pertaining to the dynamic response of turbines exposed to wind and wave loads (as in the case of off-shore turbines) may be collected. Such data can be used to better understand the behavior of turbines under complex loading scenarios. Fused with an analytical model of the structure, such data may also yield information related to the loading to which these structures are subjected (as will be the subject of this chapter). The end results are

improved analytical models and a statistical database of loading data; both results would lead to more cost-efficient design procedures for future turbine systems.

Permanently installed sensors can also serve as the basis for a structural health monitoring (SHM) system. Such systems would provide turbine owners with data from which damage could be detected and quantified. Early warning of damage can lower the cost of repairs and reduce turbine downtime; the result is an increase in the long-term profitability of wind energy. While the many benefits provided by monitoring are evident, few operational turbines have extensive sensor instrumentations due to cost restrictions. With cable-based monitoring systems being challenging and costly to install, alternative sensor technologies should be considered. Furthermore, installation of dense sensor arrays in turbine blades are restricted by the availability of data communication lines in the turbine slip ring. In particular, wireless sensors are considerably less-expensive to purchase and easier to install than traditional cable-based systems (Lynch and Loh 2006). In the case of turbine blades, wireless communication eradicates a need to move data through the slip ring interface, which can be technically difficult as well as costly. Furthermore, wireless sensors may be rapidly installed for temporary installation in turbine towers should the need arise. Indeed, a preliminary study applying a wireless module to a fiber optic sensor interface installed in the blades of a research wind turbine structure returned very promising results demonstrating the usefulness of wireless sensors for overcoming the connectivity challenges at the slip ring (Turner*, et al.* 2009).

In this study, a wind load estimation algorithm for embedment in a low-power, wireless sensor network (*Narada*, introduced in *Chapter 2*) is developed and experimentally verified in the laboratory and demonstrated using data wirelessly

collected in the field from operational wind turbines. The objectives of this study are to: 1) employ high-quality turbine response data for load estimation of operational turbines based on the response of the structure; 2) illustrate the utility of wireless sensors in wind turbines; and 3) quantify the wireless communication reliability in turbine applications. This chapter begins with a conceptual method that can estimate structural loading from measured vibrational response. The method is intended to be computationally efficient to ensure that it fits within the computational platform integrated with the *Narada* wireless sensor node. A description of a laboratory study follows in which a turbine analog is subjected to a known loading, the response measured by wireless sensors, and a model-assisted loading estimation algorithm employed for load characterization. A controlled laboratory environment with a measurable input force is critical for validation of the method. Finally, to illustrate the utility of wireless sensors installed in wind turbines, the proposed sensor technology is installed in three operational turbines in Germany. The load estimation method is also applied to turbine response data obtained from the operational turbine structures tested.

### 4.3. Model-Assisted Load Estimation from Output Measurements

The measured responses of a structure to wind loading can be thought of as outputs, $\boldsymbol{Y}(j\omega)$, to a dynamical system with a linear transfer function, $\boldsymbol{H}(j\omega)$, and the wind force as the input, represented at a point by $W(j\omega)$. The turbine structure acts as a linear filter of that wind signal, effectively coloring the input signal and producing the measured outputs, $\boldsymbol{Y}(j\omega)$ (Figure 4.1). The measured vibrations of the structure will be dependent on the wind loading $W(j\omega)$, the structural properties of the tower (encapsulated in $\boldsymbol{H}(j\omega)$),

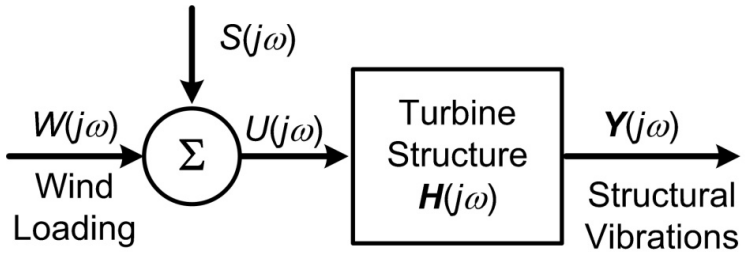


**Figure 4.1.** Block diagram depicting turbine input/output system.

as well as by the properties of the blades and the gyroscopic rotation of the blades that introduce a lateral force, $S(j\omega)$. Here, a model-assisted method is proposed for estimating the loading on the tower portion of the turbine structure, $U(j\omega)$, from the response outputs, $\boldsymbol{Y}(j\omega)$. The method seeks to develop a model of the turbine that can be used to identify the loading as seen by sensors located within the tower (as the space within the turbine tower is significantly more accessible than the space within the blades). This loading estimate includes the effect of the wind as well as the lateral loads created by the rotation of the turbine blades, represented in Figure 4.1 as a disturbance to the system.

In this study, a model of a turbine as a tapered cantilevered Bernoulli-Euler beam with hollow circular cross section and eccentric tip mass with rotational inertia, will be identified (Figure 4.2). Loading on the turbine model will be assumed to occur as a point load acting on the tip mass; structural parameters to be estimated are depicted in Figure 4.2. With the model of the system defined, the loading input can be measured from an arbitrary output according to the transfer function:

$$U(j\omega) = \frac{Y_i(j\omega)}{H_i(j\omega)} \tag{4.1}$$

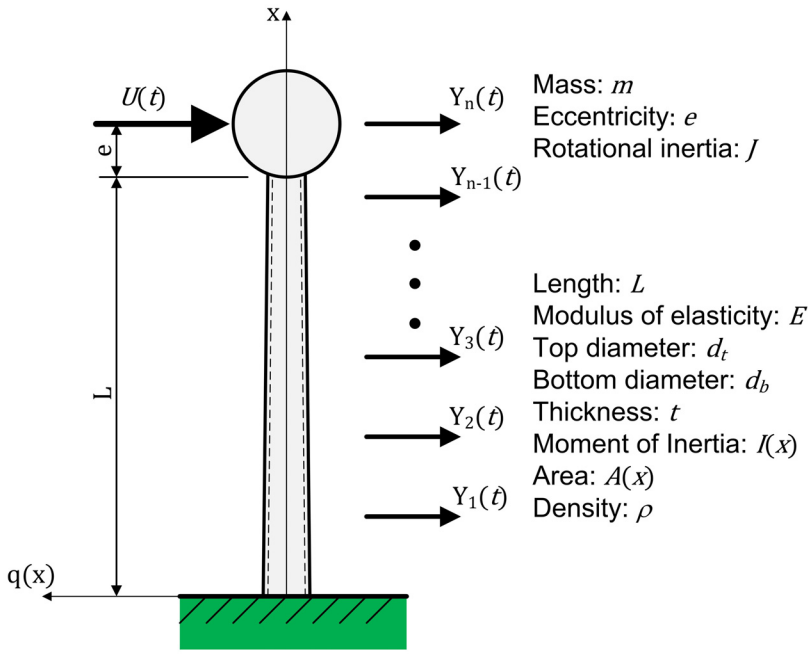


**Figure 4.2.** Wind turbine model to be identified.

The transfer function model of the structure used in this study is derived in state-space from the modal frequencies and modes shapes and converted to the transfer function form of Equation 4.1 (Chen 1999). For a system with $n$ degrees of freedom (DOFs) and $p$ measured outputs, the state-space representation is based on an $2n$ dimensional state vector, $\boldsymbol{x}(t)$, composed of lateral displacements and velocities of the tower degrees-of-freedom (DOF) coinciding with sensor locations, plus one additional DOF collocated with the tip mass at the top of the structure (if no sensor exists there):

$$\begin{aligned} \dot{\boldsymbol{z}}(t) &= \boldsymbol{A}\boldsymbol{z}(t) + \boldsymbol{B}u(t) \\ \boldsymbol{y}(t) &= \boldsymbol{C}\boldsymbol{z}(t) + \boldsymbol{D}u(t) \\ \boldsymbol{z}(t) &= [\boldsymbol{v}(t)^{\mathrm{T}} \quad \dot{\boldsymbol{v}}(t)^{\mathrm{T}}]^{\mathrm{T}} \end{aligned} \tag{4.2}$$

Here, $\boldsymbol{v}(t) \epsilon \mathbb{R}^{n\times 1}$ is the lateral displacement vector of the system DOFs, $\boldsymbol{A} \epsilon \mathbb{R}^{2n\times 2n}$ is the system matrix, $\boldsymbol{B} \epsilon \mathbb{R}^{2n\times 1}$ is the input matrix, $\boldsymbol{C} \epsilon \mathbb{R}^{p\times 2n}$ is the output matrix, and $\boldsymbol{D} \epsilon \mathbb{R}^{p\times 1}$

is the feedthrough matrix. For systems employing acceleration measurements, assuming that there is one input that is located at the top DOF, the state-space matrices are:

$$\boldsymbol{A} = \begin{bmatrix} [\boldsymbol{0}] & [\boldsymbol{I}] \\ [-\boldsymbol{M}^{-1}\boldsymbol{K}] & [-\boldsymbol{M}^{-1}\boldsymbol{C_d}] \end{bmatrix}, \boldsymbol{B} = \begin{bmatrix} [\boldsymbol{0}] \\ [\boldsymbol{M}^{-1}\boldsymbol{T}] \end{bmatrix}, \boldsymbol{T} = \begin{bmatrix} 0 \\ 0 \\ 0 \\ \vdots \\ 1 \end{bmatrix} \tag{4.3}$$

where $\boldsymbol{M} \epsilon \mathbb{R}^{n \times n}$ is the mass matrix for the structure, $\boldsymbol{K} \epsilon \mathbb{R}^{n \times n}$ is the stiffness matrix, $\boldsymbol{C_d} \epsilon \mathbb{R}^{n \times n}$ is the damping matrix. In addition the observation matrix, $\boldsymbol{C}$, defines the sensor outputs; assuming the sensors are accelerometers, then $\boldsymbol{C}$ is composed of the rows of $\boldsymbol{A}$ corresponding to the DOFs at which accelerometers are placed. Similarly, $\boldsymbol{D}$ is composed of the rows of $\boldsymbol{B}$ corresponding to the DOFs at which accelerometers are placed.

Identification of the unknown terms of $\boldsymbol{A}$ in Equation 4.3 is the result of an on-line modal analysis algorithm. If the modal frequencies and mode shapes can be identified, then terms of the $\boldsymbol{A}$ matrix can be approximated using:

$$\begin{aligned} [\boldsymbol{M}^{-1}\boldsymbol{K}] &= [\boldsymbol{\Phi}][\boldsymbol{\Omega}][\boldsymbol{\Phi}]^{-1} \\ [\boldsymbol{M}^{-1}\boldsymbol{C_d}] &= a_1 + a_2[\boldsymbol{M}^{-1}\boldsymbol{K}] \end{aligned} \tag{4.4}$$

where $\boldsymbol{\Phi}$ is a matrix whose columns are the identified mode shapes (*i.e.*, eigenvectors) corresponding to the chosen degrees-of-freedom of the structural model, $\boldsymbol{\Omega}$ is the spectral matrix corresponding to the eigenvalues of the structure (estimated from the structure's modal frequencies), and $a_1$ and $a_2$ are Rayleigh damping coefficients as described in Caughey (1960). The state-space representation may be converted into the transfer function representation for the $i^{th}$ output of Equation 4.1 by:

$$H_i(j\omega) = \boldsymbol{C}_i(j\omega \boldsymbol{I}_{2n} - \boldsymbol{A})^{-1}\boldsymbol{B} + D_i \tag{4.5}$$

where $\boldsymbol{C}_i$ and $D_i$ correspond to the i$^{th}$ row of $\boldsymbol{C}$ and $\boldsymbol{D}$ respectively. Finally, in order to formulate the state-space model, accurate modal frequencies, mode shapes, and mass estimations are necessary. As it is often difficult to extract true modal frequencies and mode shapes from output-only data sets in which the unknown input is non-white, these parameters will be estimated from a model based on the assumed modes method.

### *4.3.1. Assumed Modes Method*

The assumed modes method (AMM), proposed by Merovitch (1986), is an energy-based, approximate method for determining modal frequencies and mode shapes of continuous beams, and is quite useful because it requires neither the solution of a fourth-order beam bending equation, nor knowledge of the natural (non-essential) boundary conditions of the beam (Merovitch 1986). The method works by creating "mass" and "stiffness" matrices, $\widetilde{\boldsymbol{M}}$ and $\widetilde{\boldsymbol{K}}$ respectively, based on kinetic energy and potential energy approximations that are in turn based on an assumed set of continuous user-defined basis functions, $q(x)$. Rather than defining the relationship between forces and displacements, as standard mass and stiffness matrices do, AMM "mass" and "stiffness" matrices define the relationship between elements of the user-defined basis functions. These basis functions must satisfy the geometric (essential) boundary conditions of the beam as well as form a complete basis for the fourth-order beam bending equation. For the cantilever beam of Figure 4.2, the geometric boundary conditions that must be satisfied are:

$$q(0) = 0, \quad \frac{dq(0)}{dx} = 0 \tag{4.6}$$

Satisfying those conditions, the basis functions may be superimposed to represent any arbitrary, reachable deformation pattern for the beam, in the same way that mode shapes may be superimposed for the same purpose. As such, there exists a linear combination of these basis functions to represent all possible beam deformation patterns, including the full set of mode shapes (Merovitch 1986). It is also important to stress that, while the mode shapes form a basis for the representation of the deformation of a beam taking into account its full set of boundary conditions (both geometric and natural), the AMM basis functions form a basis for the representation of the deformation of an arbitrary beam satisfying only the geometric boundary conditions. As such, any set of basis functions that satisfies the geometric boundary condition and completeness constraints will suffice. The set of basis functions used in this study satisfies the completeness requirement for a fourth-order differential equation, as demonstrated by Storch and Strang (1988), and is represented by:

$$q_1(x) = x^2, \quad q_2(x) = 1 - \cos\left(\frac{\pi x}{L}\right), \; q_3(x) = 1 - \cos\left(\frac{2\pi x}{L}\right), \cdots, q_n(x) = 1 - \cos\left(\frac{(n-1)\pi x}{L}\right) \tag{4.7}$$

Here, $L$ corresponds to the height of the cantilever and $x$ is the length variable along the cantilever height. An infinite number of basis functions are necessary to represent the complete set, though a smaller number may be used to identify modes of interest. The AMM generates one mode shape for every basis function employed (the size of the $\widetilde{\boldsymbol{M}}$

and $\widetilde{\boldsymbol{K}}$ matricies are also equal to the number of basis functions employed). The AMM "mass" and "stiffness" matrices based on these basis functions come from the kinetic and potential energy equations (respectively) associated with the basis functions:

$$\begin{aligned} \widetilde{M}_{i,j} &= \int_0^L \rho\, A(x) q_i(x) q_j(x) dx + m q_i(L+e) q_j(L+e) + J \frac{dq_i(L)}{dx} \frac{dq_j(L)}{dx}, \\ \widetilde{K}_{i,j} &= \int_0^L EI(x) \frac{d^2 q_i(x)}{dx^2} \frac{d^2 q_j(x)}{dx^2} dx \end{aligned} \tag{4.8}$$

Here, $EI(x)$ is the flexural rigidity of the cantilever, $\rho$ is the mass density of the material, $A(x)$ is the area of the cross-section, and $m$ and $J$ are the mass and rotational inertia of the tip mass respectively. The generalized eigenvalue problem of the $\widetilde{\boldsymbol{M}}$, $\widetilde{\boldsymbol{K}}$ system can be formulated:

$$\widetilde{\boldsymbol{M}}\widetilde{\boldsymbol{\Phi}} = \widetilde{\boldsymbol{K}}\widetilde{\boldsymbol{\Phi}}\widetilde{\boldsymbol{\Omega}} \tag{4.9}$$

where the matrix $\widetilde{\boldsymbol{\Omega}}$, whose diagonal elements are the eigenvalues (modal frequencies squared), and the matrix $\widetilde{\boldsymbol{\Phi}}$, whose columns contain the linear combination scaling factors for the basis functions necessary to compute the continuous mode shape associated with the modal frequency represented in the corresponding column of $\widetilde{\boldsymbol{\Omega}}$. In this way, any number of mode shapes may be determined equal to the number of shape functions used. The complete set of infinitely many shape functions represents an exact solution, though it is not necessary to use an infinite number of basis functions in the analysis. It is recommended to use at least twice as many shape functions as the number of modes of interest based on the convergence properties of the method (Merovitch 1986).

The modal frequencies and mode shapes are thus determined by the assumed structural properties (*e.g.*, $E$, $I$, $\rho$, $A$, *etc*.) used to form $\widetilde{\boldsymbol{M}}$ and $\widetilde{\boldsymbol{K}}$ (by Eqn. 4.8). In this study it is assumed that these values are not known exactly but are only known within some range. Therefore values within the candidate range must be selected by the embedded algorithm. To accomplish this task, a comparison between the operational deflection shapes (ODS), generated from output-only sensor data, and the mode shapes, generated by the AMM model, is made and the structural parameters that minimize the error between the two are used. This numerical global error minimization is accomplished using a simulated annealing algorithm previously developed for *Narada* in another study (Zimmerman and Lynch 2009).

### *4.3.2. Model Updating Step Using Simulated Annealing*

Simulated annealing is a numerical method devised to search a parameter space for the combination of assignments to those parameters that minimize a given error or cost function (Kirkpatrick*, et al.* 1983). It is a mathematical analog for the annealing process by which physical materials achieve an optimal thermal state as they cool (Metropolis*, et al.* 1953). The method is an iterative process by which the parameters are treated as random variables and random assignments to those random variables are made. Often, the assignments yielding the smallest cost function values are retained for the next iteration. However, at each step there exists a random chance that suboptimal assignments will be selected; this practice is to help the algorithm avoid convergence on local minima. During the next iteration, the random variables are reassigned and a new set of assignments is generated. This process is repeated as a numerical analog for

temperature is reduced. This temperature analog defines the number of suboptimal solutions that are accepted by the algorithm. By decreasing the temperature analog slowly, the global minimization of the error function may be determined from many local minimums (Kirkpatrick*, et al.* 1983). The process continues until no new assignment sets are accepted at a given temperature step and the process is essentially "frozen". The simulated annealing process has the advantage that it parallelizes well to multiple processors (due to branched processes and low memory requirements) to take advantage of networked computing resources such as those found in wireless sensor networks (Greening 1990). Furthermore, it has been previously validated on the *Narada* wireless sensor network by Zimmerman and Lynch (2009) and demonstrated to be effective for model updating of civil structural systems.

For load estimation of wind turbines, the simulated annealing algorithm is used to solve for the realization of the structural parameters that minimizes the error between the AMM of the previous section, and the operational deflection shapes (ODS) identified using the frequency domain decomposition (FDD) method previously detailed in Chapter 3 and implemented in the *Narada* wireless sensor by Zimmerman, *et al*. (2008). The ODS are based on the output-only power spectral density matrix corresponding to the measured output signals. It should be noted that they are not true mode shapes, but for fairly broad-band excitation, they are closely correlated to mode shapes. However, they do represent the best estimate of mode shapes available from the data taking into account the non-white nature of the unmeasured input. The comparison between the AMM modes and the FDD operational deflection shapes is made based on modal assurance criterion (MAC) which takes the length of the projection of one potential mode shape

onto another, and varies between zero (indicating no similarity between shapes) and one (indicating that the shapes are scaled versions of each other) (Allemang and Brown 1982). Also included in the objective function is a measure of peakness that penalizes solutions that generate models with modal frequencies not occurring at or near peaks of the measured output spectra. The peakness measure, $p(\omega)$, is generated for every discrete frequency point in the output FFT calibrated within a range around the point:

$$p(\omega) = \frac{\sum_{k=-r}^{r} |Y(\omega + k \cdot d\omega)|}{\sum_{k=-3r}^{3r} |Y(\omega + k \cdot d\omega)|} \tag{4.10}$$

where $r$ is a peakness radius and is set depending on the closeness of the peaks in the output spectra; in this study, $r$ is set to 8. The peakness functions are calculated from the sensor data collected by the wireless system and averaged over the full set of sensor data to produce global peakness function that varies from near zero (no peak) to one (the largest peak measured). The objective function minimized by the simulated annealing function also includes a first modal frequency term to penalize solutions that yield unrealistic frequencies of the primary structural mode. This term does require an *a priori* estimate of the first structural mode, but this value is generally available from the turbine manufacturer or can be accurately estimated from rough structural parameters. In this study, the modes with frequencies falling below the Nyquist frequency of the collected output data are used in the objective function. If $m$ modes occur below the Nyquist frequency, the objective function ($\mathcal{O}$) is:

$$\mathcal{O} = w_1 \frac{|\omega_{m1a} - \hat{\omega}_{m1}|}{\omega_{m1a}} + w_2 \sum_{k=1}^{m} (1.0 - MAC_k) + w_3 \sum_{k=1}^{m} (1.0 - p(\omega_k)) \tag{4.11}$$

where $\omega_{m1a}$ is the *a priori* estimate of the first modal frequency, $\widehat{\omega}_{m1}$ is the first modal frequency generated by the AMM model, and $w_1$, $w_2$, and $w_3$ are weighting values. The selection of the weighting values requires some engineering judgment, but a $w_1$ weight that is at least two times the magnitude of the largest of $w_2$ or $w_3$ will ensure that the simulated annealing algorithm returns a model with a close first modal frequency match. To aid in convergence, the parameter search space is restricted to a realistic range around the suspected true value. That is to say, true parameter values are estimated and, depending on the degree of confidence in their estimate, the search space is restricted. The model updating algorithm is thus given more leeway in making assignments to less well characterized parameters, but never more than 50% deviating from the estimated value.

The mode shapes and modal frequencies produced by the AMM model using parameters identified by the simulated annealing process are used to identify the combined mass/stiffness and mass/damping terms in Equation 4.4. The simulated annealing method also yields the tip mass that is the final term in $\boldsymbol{B}$ and $\boldsymbol{D}$ in Equation 4.3. The remaining mass terms representing the distributed mass of the tower may be approximated as zero without a meaningful loss in accuracy. With the state-space model formed, the transfer functions relating measured outputs to the inputs may be estimated by Equation 4.5 and input estimates (one generated from each measured output) may be estimated using Equation 4.1. Finally, the multiple input estimates are averaged to produce the system-wide estimate of the input spectra. The complete algorithm is depicted in Figure 4.3. A laboratory validation experiment is presented in the next

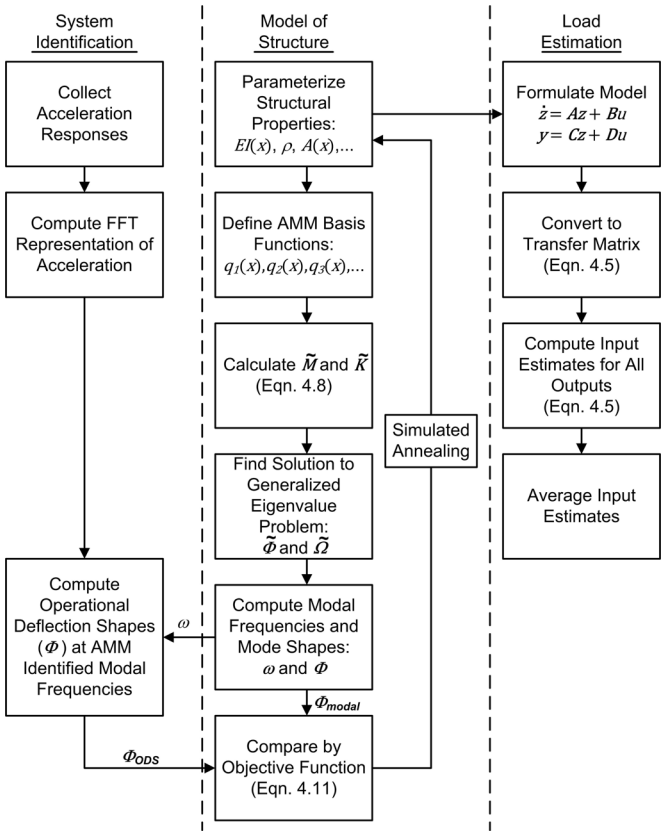


**Figure 4.3.** Graphical depiction of load estimation algorithm.

section to demonstrate the effectiveness the method on a turbine analog structure with known structural properties and measurable loading.

## 4.4. Laboratory Validation of Load Estimation Method

Validation of the load estimation method occurs in the laboratory using a test structure designed to be a turbine analog that has known parameters and can be excited using known loading. The turbine analog structure is composed of a 3.1 m long, nominal

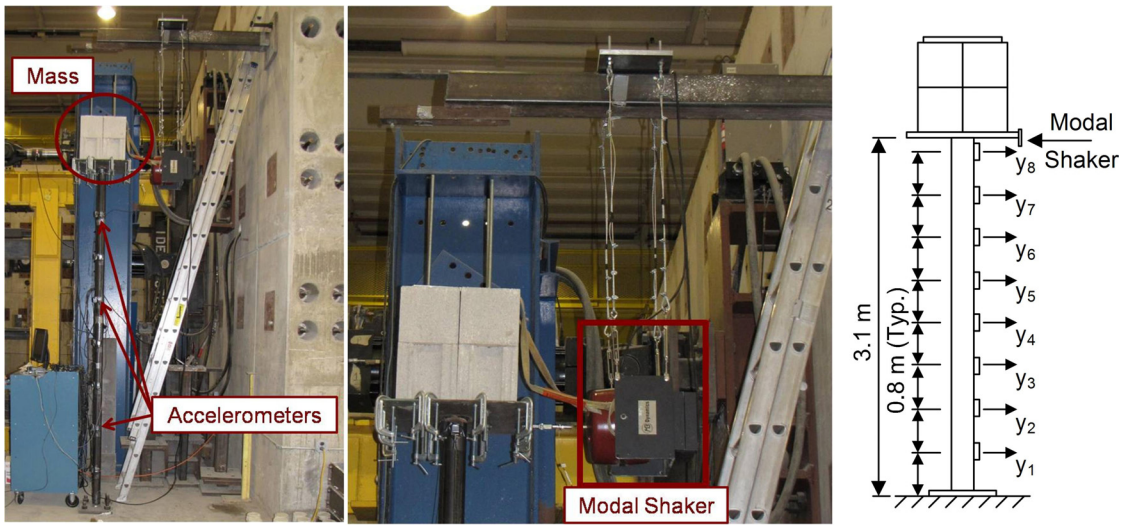


(a) (b) (c)

**Figure 4.4.** Laboratory validation structure: (a) full structure view; (b) attachment and support of modal shaker; (c) instrumentation.

2.5 inch (6.35 cm) schedule-40 steel pipe, to represent the turbine tower that is welded to a 1 inch (2.54 cm) thick base-plate and a 3/8 inch (0.952 cm) thick cap-plate. The cap-plate supports four normal-weight, two-core concrete masonry units (CMU) that represent the eccentric tip mass of the turbine nacelle and blades. These CMUs are arranged in two layers and held in place vertically by a top plate with four through bolts, and are clamped around their perimeter to restrain lateral movement relative to the cap-plate. The base-plate is bolted to the strong-floor of the University of Michigan Structures Laboratory. An MB Dynamics 110 modal shaker is suspended at the height of the cap-plate from a cantilever beam supported by the lab's strong-wall and is connected to the cap-plate by a stinger. The lab structure and modal shaker are depicted in Figure 4.4.

The laboratory structure tower is instrumented along its height with eight Crossbow CXL02LF1Z accelerometers oriented laterally in the direction of excitation and evenly

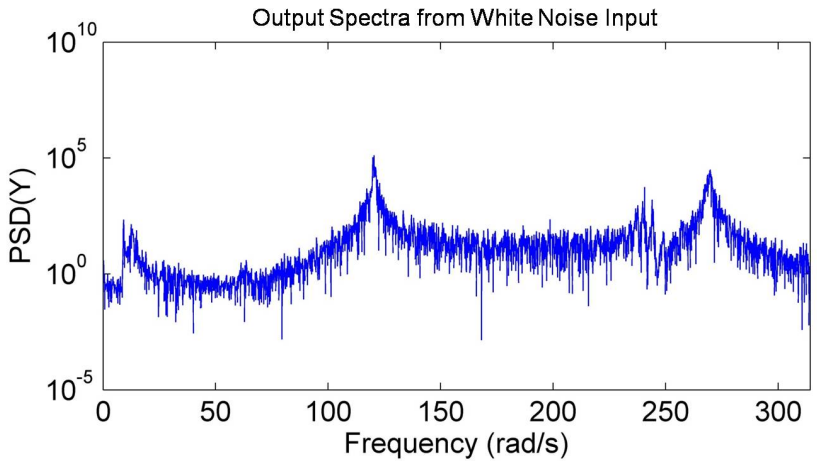


**Figure 4.5** Measured acceleration output spectra from sensor level four mounted on the tower of the laboratory validation structure under white-noise loading.

spaced (by 80 cm on center) between the base and the tip mass. Another set of eight accelerometers is installed oriented in the orthogonal lateral direction to measure incidental out of plane vibrations. Accelerometers are also mounted to the sides of the modal shaker, oriented laterally in the direction of excitation. An Omega DLC101 dynamic load transducer is mounted in series between the modal shaker stinger and the structure to provide a direct measure of input loading applied to the structure.

The modal shaker is used to provide arbitrary loadings to the laboratory structure. Both white noise loadings as well as artificially colored-noise loadings are applied. White noise loading provides excellent excitation of structural modes and does not interject additional peaks into the frequency spectra (Figure 4.5). This loading is used in preliminary studies to characterize the modal parameters of the structure. Using the white-noise loading, modal frequencies are identified at 10.7 rad/s, 121 rad/s, and 269 rad/s. However, input spectra from wind loadings rarely approximate those of white-noise inputs (Holmes 2007). A more challenging colored noise loading with peaks representing the effects of the rotating blades, out-of-plane modes, and other sources of

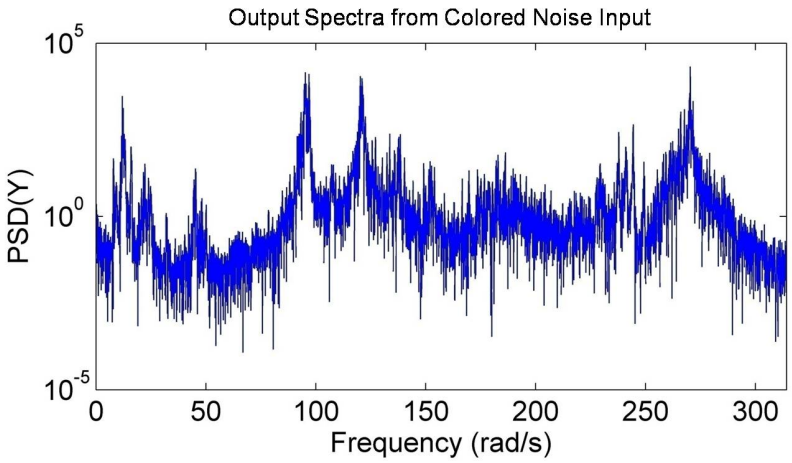


**Figure 4.6.** Measured acceleration output spectra from sensor level four mounted on the tower of the laboratory validation structure under colored-noise loading.

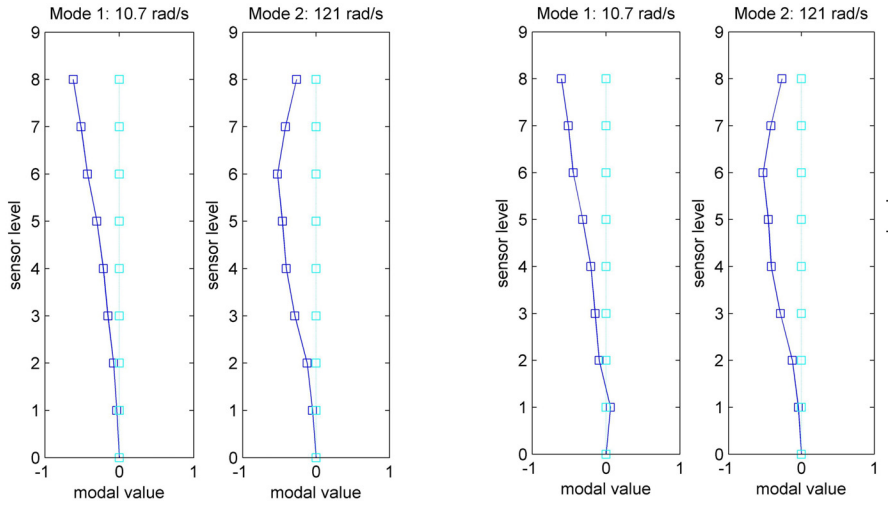


(a) (b)

**Figure 4.7.** Discrepancies in operational deflection shapes generated from output signals resulting from both white noise and colored noise inputs: (a) white noise input; (b) colored noise input.

harmonic noise contamination is then applied to the structure to be estimated. The resulting output spectra measured at level 4 is shown in Figure 4.6 where modal frequencies are significantly less clear than in Figure 4.5. Operational deflection shapes are also distorted by the application of colored noise (Figure 4.7).

**Table 4.1.** Estimated structural parameters of laboratory validation structure.

| **Parameter** | $E$ (GPa) | $\rho$ (kg/m$^3$) | $d_t$ (cm) | $d_b$ (cm) | $t$ (cm) | $L$ (m) | $e$ (cm) | $M$ (kg) | $J$ (kg m$^2$) |
|---|---|---|---|---|---|---|---|---|---|
| **Value** | 200 | 7850 | 7.3 | 7.3 | 0.5 | 3.1 | 20 | 78 | 4.8 |
| **Estimated Value** | 205 | 7901 | 8.0 | 8.0 | 0.5 | 3.4 | 25 | 85 | 5.2 |

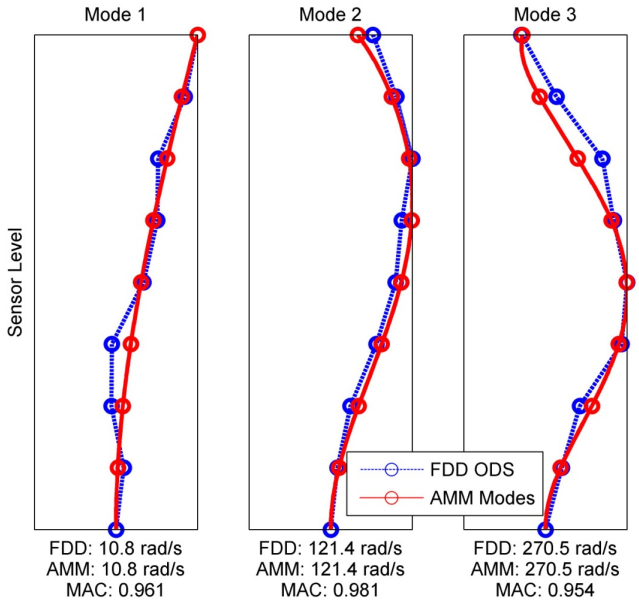


**Figure 4.8.** Identified mode shapes of the laboratory validation structure.

These challenges of output-only system identification of structures with non-white excitation necessitate identification by a model-based method such as that presented in the previous section. Structural response data are collected at a sampling frequency of 200 Hz using the *Narada* wireless sensing units. Then, peakness and operational deflection shapes are computed for 2048 discrete frequency points between zero and the Nyquist frequency (100 Hz). The simulated annealing algorithm is then used to update the assumed modes method model parameters, the results of which are presented in Table 4.1. The three identified mode shapes from the AMM that fall below the Nyquist frequency are presented in Figure 4.8 with the colored noise operational deflection shapes. Identified modal frequencies (including the first mode assumed, *a priori*, to be

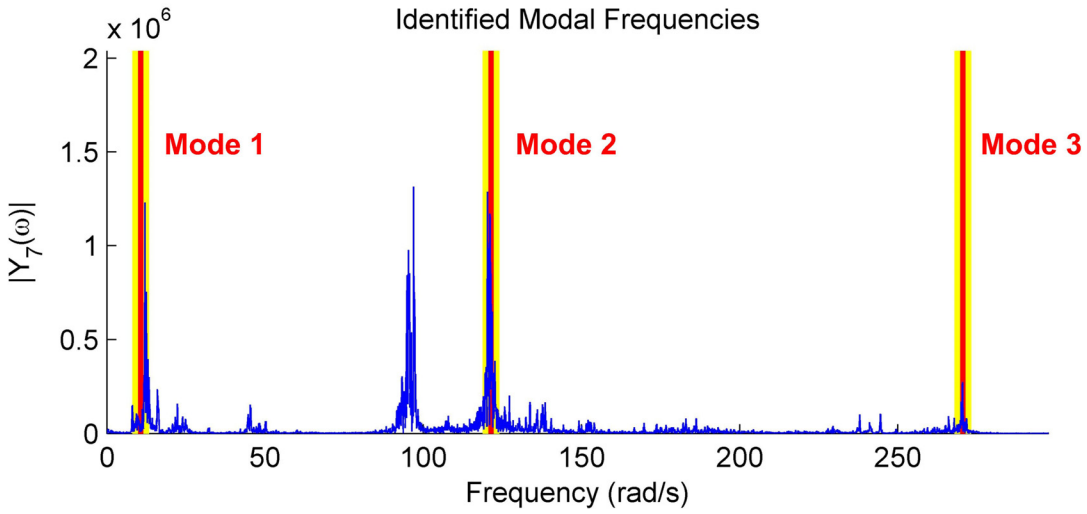


**Figure 4.9.** Modal frequencies identified as part of the load estimation algorithm overlaid with the output spectra measured at sensor level 7.

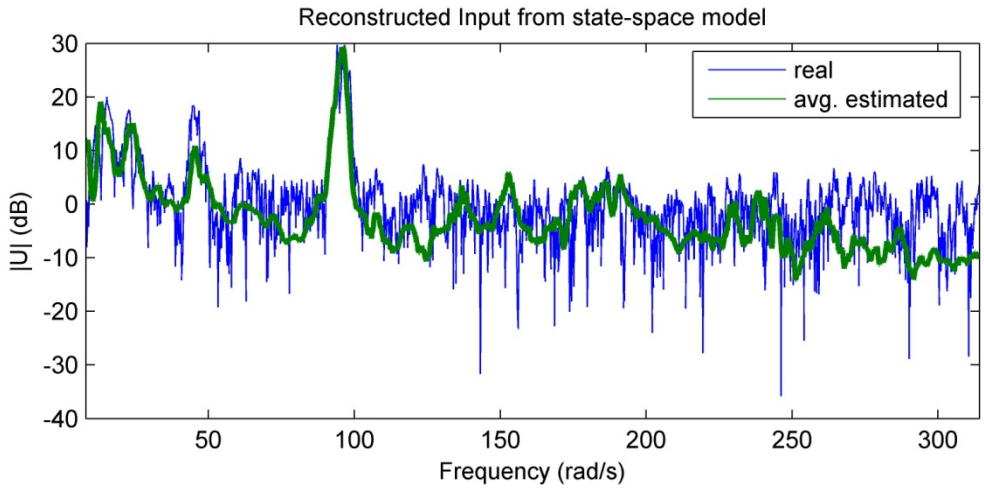


**Figure 4.10.** Estimated input spectra for the laboratory validation structure overlaid with the "real" measured input.

10.7 rad/s) are presented with the measured acceleration output spectra in Figure 4.9. Finally, a plot of the average estimated input spectra is presented in Figure 4.10 with the measured real input spectra. Figure 4.9 shows excellent agreement between the measured and estimated input spectra demonstrating the effectiveness of the method in the laboratory setting. Also investigated is the effect of error in the *a priori* estimate of the first modal frequency as modeling error and environmental effects will affect its

accuracy. Since the objective function penalizes models that result in first modal frequencies that are different than the assumed frequency, incorrect assumptions do tend to cause errors in first frequency returned by the algorithm. Errors of up to 5% are investigated and result in only minor localized errors in the final load estimation spectra. Over this range, the proper identification of higher order modes is not affected. This result validates the theory behind the method, but a demonstration on a full-scale operational wind turbine is also necessary. In the next section, the load estimation method is applied to an operational turbine as part of a field turbine wireless instrumentation study.

### 4.5. Wind Turbine Instrumentation

The subjects of this portion of the study are three wind turbines: two 78 m tall, 2 MW Vestas V-80 turbines, Figure 4.11(a and c), and one 40 m tall, 250 kW NEG-Micon 250 turbine, Figure 4.11(b). All three are circular steel towers bolted to concrete foundations with power generators and nacelles located at the top. Internally, the towers are hollow with periodic steel platforms intended to prevent workers from accidentally falling the entire tower height. The instrumentation of each tower included in this study is designed to fulfill specific objectives in order to demonstrate the effectiveness of wireless sensors in this environment. The instrumentation and the objective of each campaign is detailed for each turbine in the following sub-sections, as well as in Table 4.2.

In this study, two sensors are interfaced to the *Narada* wireless sensor: a MEMS accelerometer (Crossbow CXL01) and metal foil strain gauge (Texas Measurements YFLA-5-5L). The accelerometer has a low sensitivity of 1.0 V/g which means its output

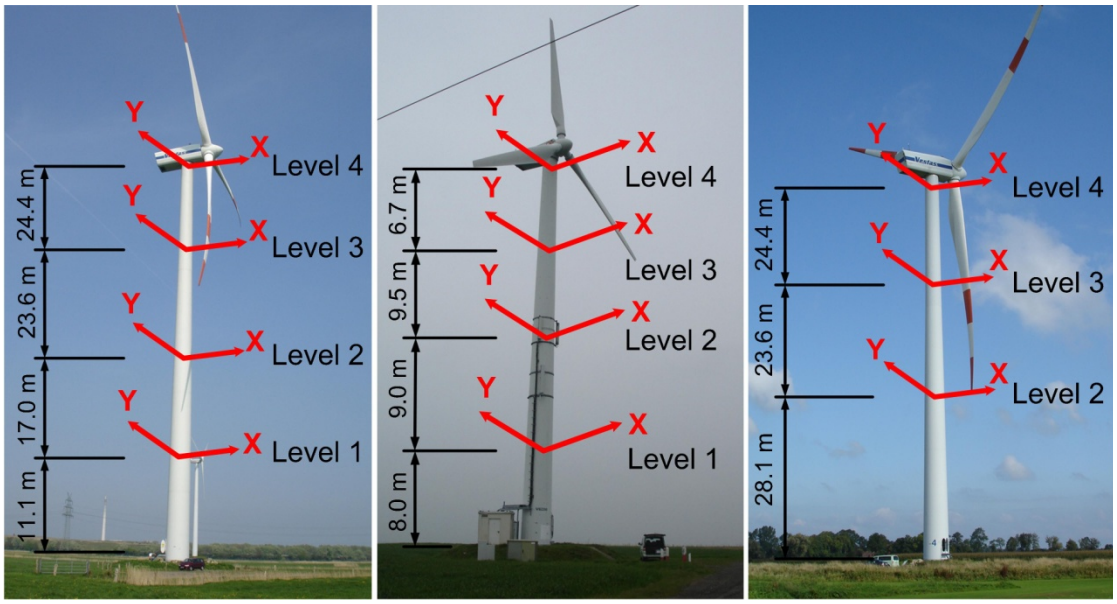


(a) (b) (c)

**Figure 4.11.** Location of wireless sensors within the (a) Vestas #1 (located near Wilhelmshaven, Germany), (b) Vestas #2 (located near Jever, Germany), and (c) Micon (located nein Langeln, Germany) turbines.

**Table 4.2.** Summary of turbine installation objectives.

| Turbine, Location | Vestas V-80, Wilhelmshaven | NEG-Micron 250, Langeln | Vestas V-80, Jever |
|---|---|---|---|
| **Testing Objectives** | Basic Wireless Functionality | Impulse Loading | Wireless Range Testing/Reliability |
| | Side-by-Side Wired Comparison | Modal Analysis | Strain Sensing |
| | | Mode Shapes | Load Estimation |

will be small during ambient excitation of the turbines. Hence, a signal conditioning board custom designed for ambient vibration measurements (Figure 4.12(a)) is also employed (Wang 2007). The signal conditioning circuit serves two functions; it serves as a band-pass (0.03 to 25 Hz) anti-aliasing filter and amplifies the sensor output voltage by a factor of twenty so as to better utilize the full input range of the ADC. Amplification is especially important when recording the output of accelerometers deployed for ambient response measurements. Unlike most sensors, strain gauges do not output a voltage

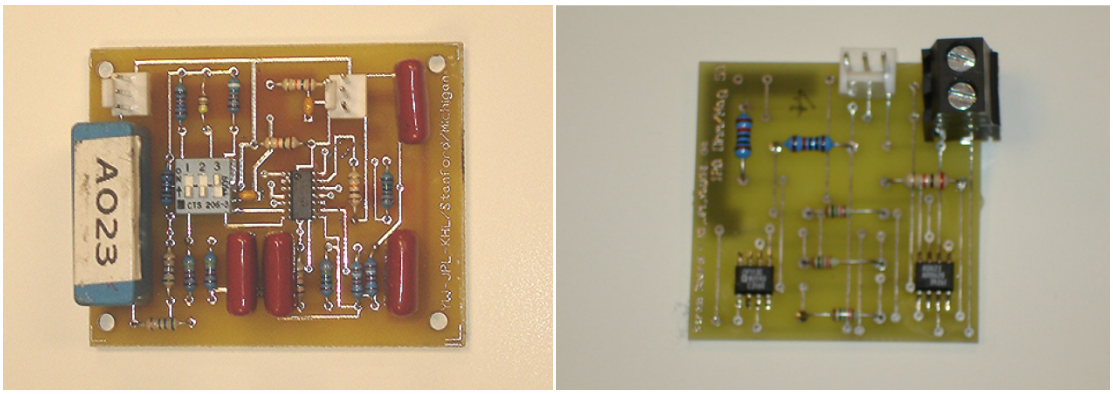


(a) (b)

**Figure 4.12.** Signal conditioning circuitry, (a) Signal conditioning board for amplifying and band-pass filtering of low-amplitude acceleration signals; (b) Wheatstone bridge circuit for conversion of strain gauge resistance changes to voltage signals.

signal directly. Rather, a bridge circuit is necessary to convert changes in gauge resistance to a voltage signal. A Wheatstone bridge circuit is designed (Figure 4.12(b)) to convert the strain gauge resistance changes to a voltage signal that can be digitized by the wireless sensor ADC.

### *4.5.1. Vestas Turbine Installation 1*

The first turbine instrumentation presented in this study is one of the 2 MW Vestas V-80 turbines. This turbine is located in a rural area outside of Wilhelmshaven, Germany and is sited on the German Wind Energy Institute testing site. The objectives of the first instrumentation are to: 1) demonstrate that wireless sensors will operate within the turbine tower, 2) collect and transmit acceleration data, and 3) demonstrate that the data collected compare favorably with similar data collected via a traditional tethered data acquisition (DAQ) system installed in parallel. To accomplish these goals, four wireless

sensor nodes are located at different levels within the tower, one at each of the steel platforms; connected to each wireless sensor node are two accelerometers measuring lateral acceleration in orthogonal directions (denoted as X and Y in Figure 4.11(a)), for a total of eight accelerometers. Amplification and filtering circuitry (previously detailed) is also provided for each transducer. In the Vestas turbine, wireless sensors are placed at heights of 11.1 m (Level 1), 28.1 m (Level 2), 51.7 m (Level 3), and 76.1 m (Level 4) above the ground level. The locations of the wireless sensors with respect to the height of the tower may be seen in Figure 4.11(a). Data collected at a variety of sampling frequencies (50, 100, 500 Hz) are transmitted to a laptop PC located at the base of the tower. To better facilitate transmission of data within the tower, hatches in the steel platforms are kept open during testing. For comparison purposes, PCB 3701 accelerometers are connected by coaxial wire to a commercial DAQ installed in parallel to the wireless sensors. Data runs are coordinated between the two systems to facilitate direct comparison.

### *4.5.2. Micon Turbine Installation*

The next part of the field validation study focuses on the Micon turbine; this turbine is located in Langeln, Germany. In the Micon turbine, controls are available to the operator to engage a braking mechanism on the hub of the turbine. Hard braking provides an "impulse-like" loading to the entire structure. This ability is important for modal analysis of structures with unmeasurable inputs or structures that are excited by ambient excitation sources (*e.g.* wind) that do not generally manifest themselves as white-noise (Holmes 2007). With the presence of the impulse-like load, proper excitation

of modal frequencies is assured thereby allowing the identification of true mode shapes whereas, in the previous two instrumentations, only identification of operational deflection shapes is possible. Again, four wireless sensor nodes are located in the towers, each with two accelerometers measuring lateral acceleration in orthogonal X and Y directions. In the Micon turbine, these sensors are located at heights of 8 m (Level 1), 17 m (Level 2), 26.5 m (Level 3), and 33.2 m (Level 4) above the base (ground) level. The locations of the wireless sensors with respect to the height of the Micon tower are presented in Figure 4.11(b). Data are collected both wirelessly (sampled at 100 Hz) and with the parallel tethered DAQ system (sampled at 200 Hz) under both ambient and impulse-like loadings.

To find the modal properties of the wind turbines, the DIAMOND software package (developed at Los Alamos National Laboratory for MATLAB) is adopted. The DIAMOND package was developed to help simplify modal analysis for practitioners of experimental mechanics (Doebling*, et al.* 1997). The program takes as its inputs, the time-history data, frequency response functions, the coherence function matrix, cross and auto-power spectra, and geometry data for the structure. With user input, modal frequencies are selected by either peak-picking, the eigenfunction realization algorithm (ERA), complex exponential, or rational polynomial methods. For this study, ERA is used to identify potential modal frequencies and mode shapes by identifying a state-space model of the structure from its Hankel matrices. Once identified by ERA, the model frequencies are examined for closely spaced modes using the rational polynomial methods to reconstruct transfer functions for each output. Finally, the modes are verified

using peak-picking. With the modal frequencies identified, the imaginary parts of the frequency response functions at that frequency form the operational deflection shape.

### *4.5.3. Vestas Turbine Installation 2*

The final turbine instrumentation presented in this study involves the second of the 2 MW Vestas V-80 turbines; this turbine is located outside of Jever, Germany. The objectives of this instrumentation are to: 1) quantify the performance of the wireless sensing system within the turbine tower, 2) to add strain sensors to the network in order to generate useful data regarding the performance of the structure at its base (where lateral acceleration signals would be minimal), and 3) to estimate loading from the measured response of the turbine. Acceleration instrumentation in this part of the study is similar to the previous section except that this turbine has one fewer internal platform (Level 1 is not present); there are three sensor nodes located directly above the internal bulkheads measuring two accelerometers each in orthogonal X and Y directions, see Figure 4.11(c). In this portion of the study, an additional wireless sensor is located at the bottom of the tower measuring two channels of flexural strain response. Wheatstone bridge circuitry (previously introduced) is also provided to convert the change in resistance of the strain gauges into a measurable voltage signal before interfacing with the wireless sensor. A typical sensing node installation is shown in Figure 4.13(a) with a detailed accelerometer installation view in Figure 4.13(b) and strain gauge installation detail in Figure 4.13(c). A strain gauge connected to a traditional DAQ system is installed in parallel to the wirelessly enabled strain gauge as shown in Figure 4.13(c).

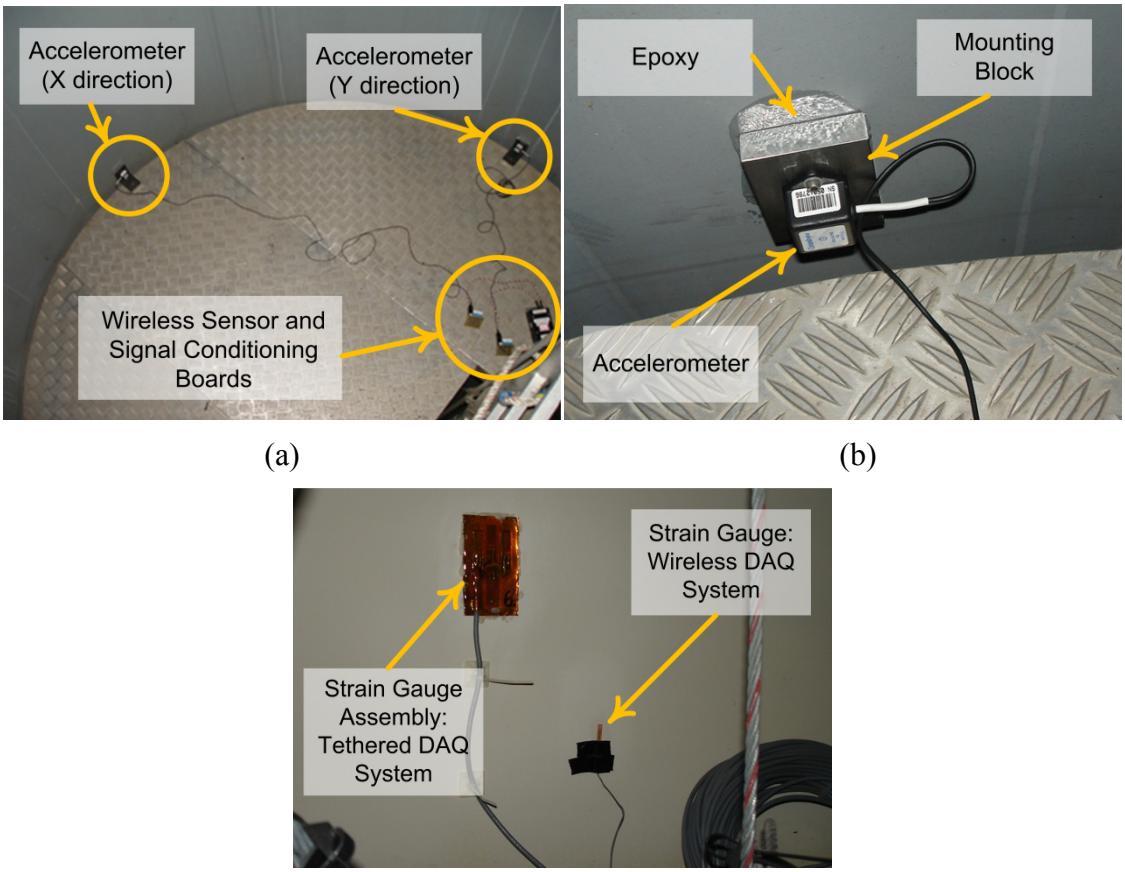


**Figure 4.13.** Installation of the wireless sensing system in the Vestas #2 turbine: (a) one sensing node with two accelerometers, (b) accelerometer installation detail, and (c) strain gauge installation detail.

Data from these sensing nodes (again collected at 50, 100, and 500 Hz) are transmitted to a laptop located at the base of the structure. A second laptop passively monitors and records network traffic. During the wireless tests, data packets transmitted from a sensor to the server must be successfully acknowledged by the server. The record of network traffic shows where multiple attempts are made to send individual data points. In the event that the network monitor misses a packet, one can still infer its presence based on the expected timing of the packets and their embedded (consecutive) sequence numbers. After the data collection, an off-line analysis of this record is performed to

quantify the percentage of packets requiring additional transmissions before they successfully generate and receive an acknowledgement from the server. This analysis will quantify the reliability of the wireless communication channel within the turbine tower. The parallel tethered DAQ system is again installed for comparison.

The load estimation algorithm is implemented using the data collected from the second Vestas turbine installation. Here, operational deflection shapes are identified via FDD algorithm over the range of discrete frequencies from zero to the Nyquist frequency. These operational deflection shapes are compared to mode shapes obtained from the assumed modes method model for a given set of structural properties. The model producing the best match between model-driven mode shapes and data-driven operational deflection shape (that also has modal frequencies corresponding to peaks in the output spectra) is identified via a parallel simulated annealing search. Identified modal frequencies, mode shapes, and the mass estimate are used to build a state-space representation of the system from which transfer functions mapping the input to the measured outputs can be constructed. These transfer functions are then used with the output spectra to estimate the loading spectra (one estimate from each sensor). These estimates are averaged to form a final estimate of the loading.

### *4.5.4. Wind Turbine Monitoring Results and Discussion*

Results from the first Vestas turbine installation demonstrate that wireless sensors can indeed function effectively in the wind turbine environment. The wireless sensing system effectively measures effects of ambient (wind) excitation on the turbine during normal operation. Additionally, wireless sensors are capable of communicating data

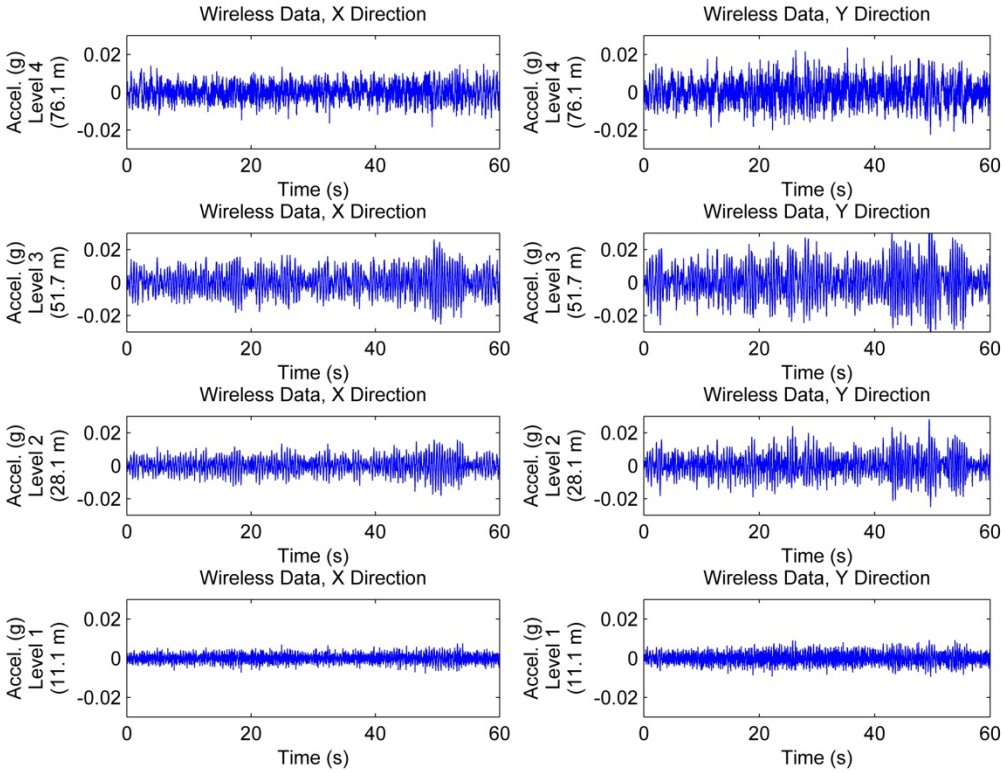


**Figure 4.14.** Sample acceleration data collected on the wireless sensor network in the Vestas #1 turbine.

from all levels of the tower to a server located at the base of the structure. For example, time history accelerations from all 8 channels are shown in Figure 4.14. A comparison between the wirelessly collected data and that recorded by a traditional tethered system shows very good agreement between the two (see sample ambient data in Figure 4.15), thus validating the viability of the wireless sensing system in this application. Some minor differences in noise levels are evident due to minor analog domain corruption of the wired system signals in imperfectly shielded cable runs down the height of the tower as well as differing low-pass anti-aliasing filter designs used in each system. Finally,

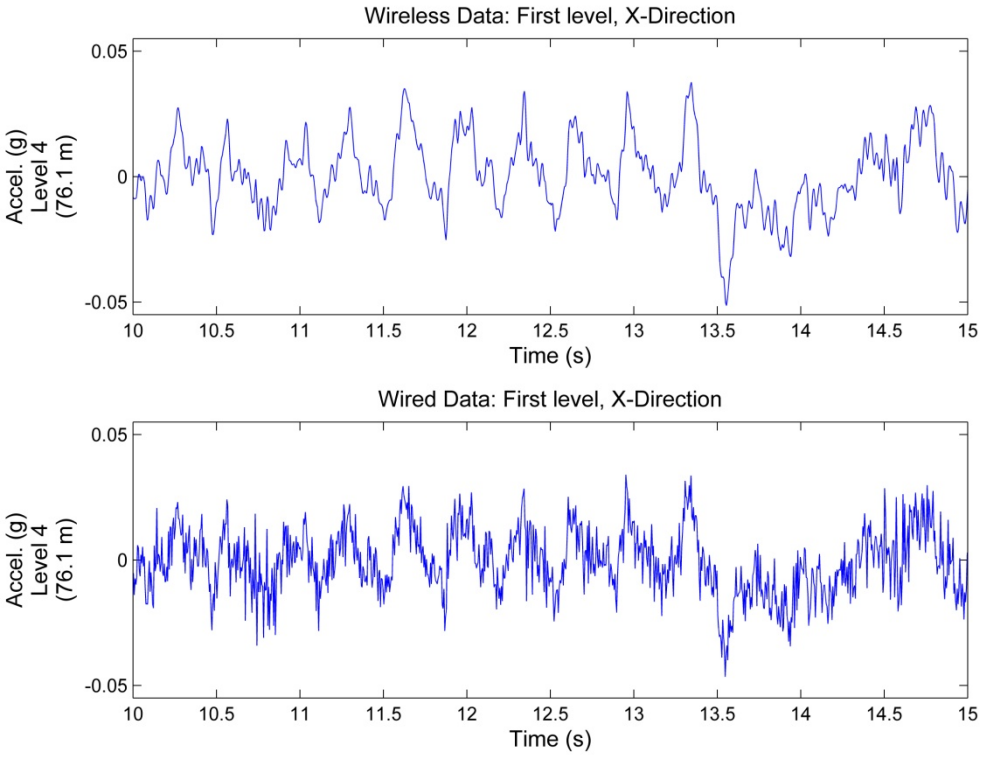


**Figure 4.15.** Comparison of wired and wirelessly obtained data from the Vestas #1 turbine. Acceleration data shown is for Level 4.

natural frequencies are evident in the frequency domain realization of the wirelessly collected data (Figure 4.16).

Example time history plots that include blade braking within the nacelle are presented for the Micon turbine in Figure 4.17. During these runs, the brake is activated for a short pulse which instantaneously stops the blades from turning, resulting in an impulse-like loading upon the tower. Figure 4.18 presents the fast-Fourier transform (FFT) and the covariance estimate of the discrete-time power spectral density (PSD) calculated for data measured at Level 4 of the Micon turbine. These processed signals are used in DIAMOND for the modal analysis portion of the study. Modal shape results for the Micon turbine are presented in Figure 4.19. Modal frequencies identified (0.89 and 4.24

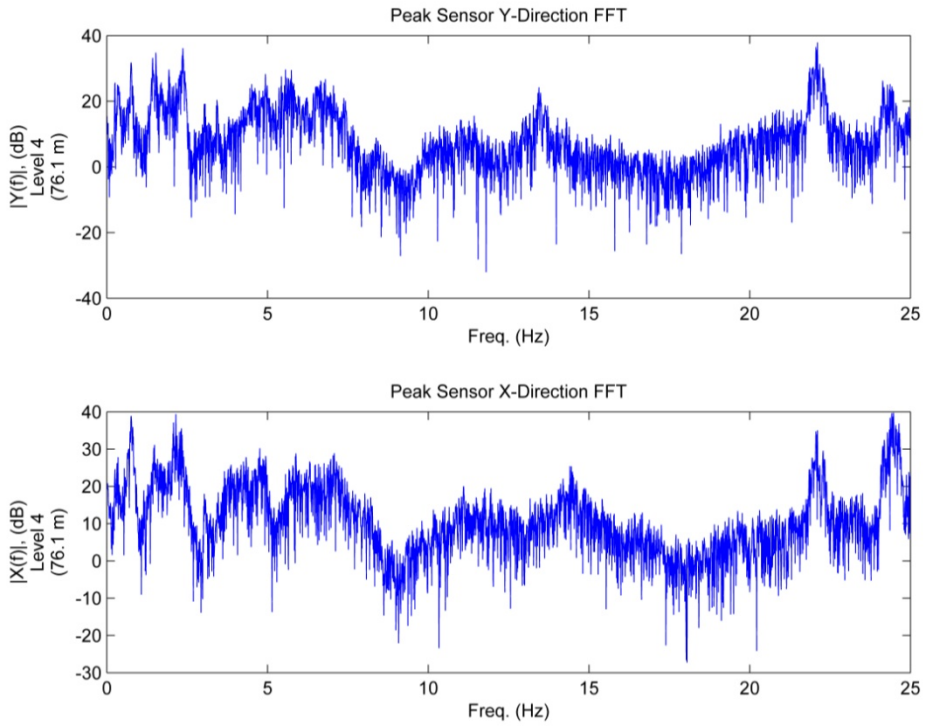


**Figure 4.16.** FFT results from the Vestas #1 turbine, Level 4 accelerations.

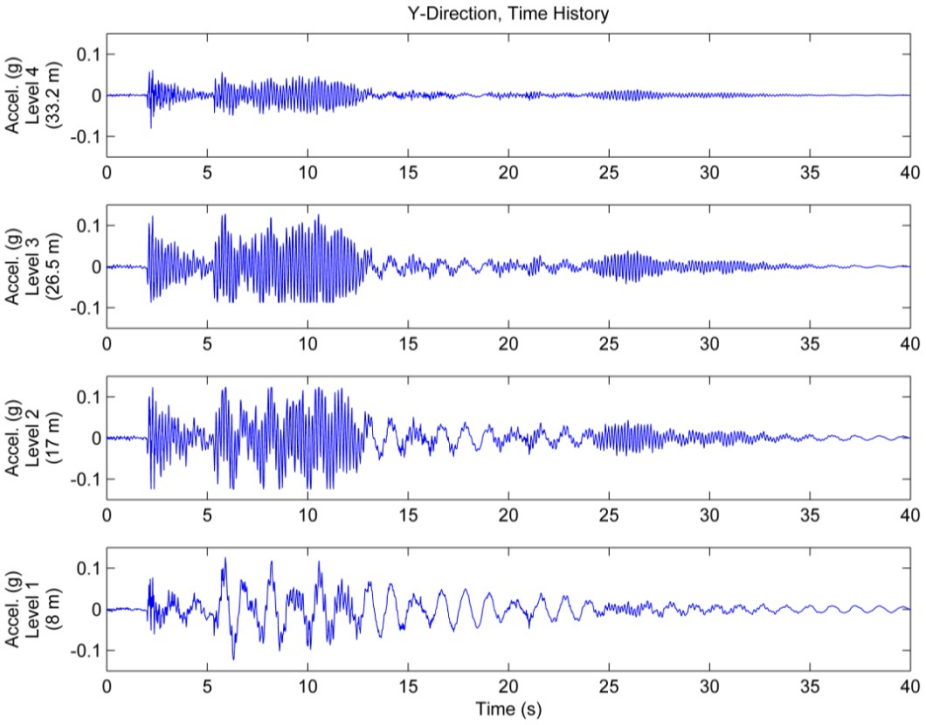


**Figure 4.17.** Time history response of Micon tower under "impulse" loading.

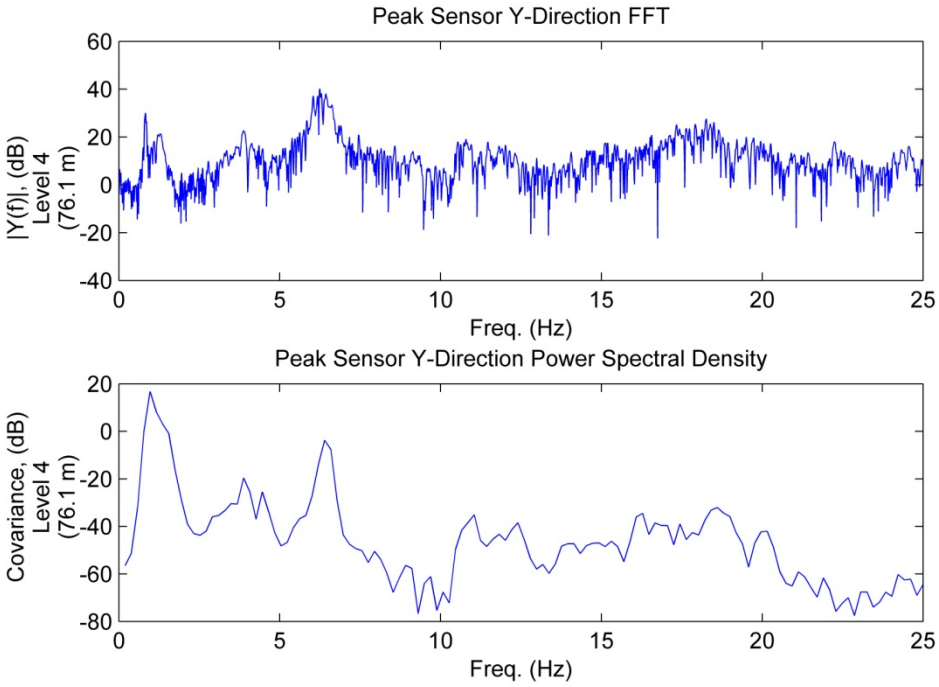


**Figure 4.18.** FFT and PSD results from the Micon turbine.

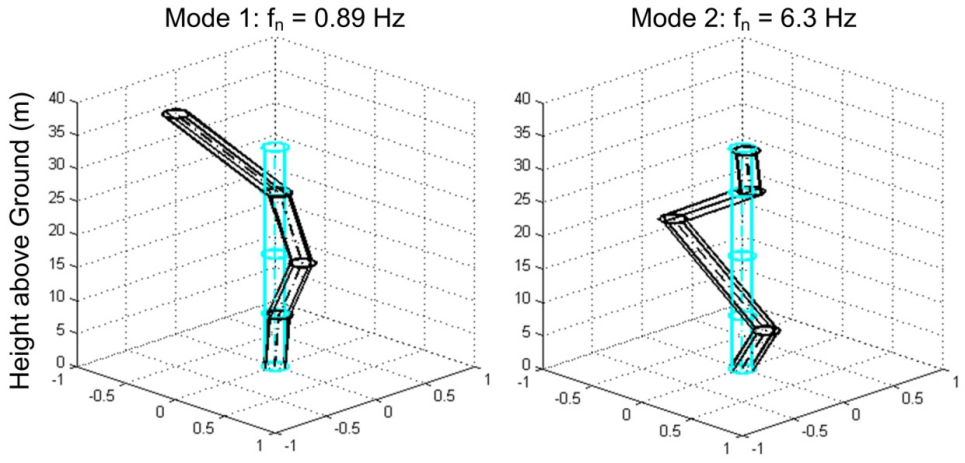


**Figure 4.19.** First two (3-dimensional) modes of the Micon turbine.

Hz) in this study for the Micon turbines compare well with those found for the same structure using finite element updating methods, as reported in Rolfes, *et al*. (2007).

Finally, the goals of the second Vestas installation are to quantify wireless network performance as well as to generate an estimate of the loading spectra using the method validated in the lab. With regard to wireless reliability, interference in the digital wireless channel will manifest itself as dropped packets (that must be retransmitted) rather than as corrupted data. A second laptop computer, acting as a network monitor, observed two levels of performance: one level for the sensors located at the base, and another for those located further up the tower. At the base, 3-4% of the packets require multiple attempts to send before an acknowledgement packet is received. Because of the relatively short distance between antennas (less than 2 m), losses here are primarily due to interference from the electrical equipment located at the base of the tower as well as adverse multipath effects. Sensors located at higher levels record a slight drop in reliability, with 5-6% of packets requiring multiple transmission attempts. Internal bulkheads do not appear to degrade the wireless transmissions; for instance, Level 4 performance is not significantly different than Level 2 performance due to numerous openings in the bulkheads and an air gap between the bulkhead and the tower shell. Because in the wireless system the sensor signal is digitized directly at its source, there is less opportunity for analog domain corruption of the signal than in a traditional tethered system. Another objective of testing in the second Vestas turbine was the ability to collect strain data using wireless sensors. Strain gauge data collected from the base of the second Vestas turbine is also presented (Figure 4.20) to demonstrate successful collection of vibrational strain data from the base of the structure.

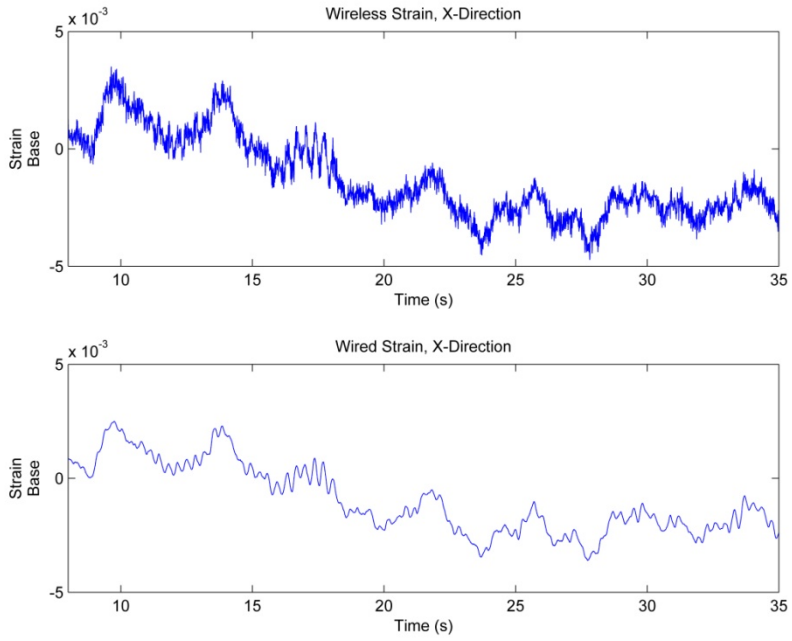


**Figure 4.20.** Wireless strain comparison between the wired and wireless systems in the Vestas 2 turbine.

### *4.5.5. Load Estimation of Vestas 2 Wind Turbine*

The second Vestas turbine is also used to test the load estimation method. The output spectra computed from the acceleration data in the x-direction (Figure 4.11(c)) are colored by the loading, the response of the tower to the loading, as well as the effects of the rotating blades. The modal frequencies identified as part of the load estimation method are overlaid with the output spectra measured at three locations along the tower height in Figure 4.21, including the first mode that is estimated *a priori* at 2.6 rad/s. The corresponding model mode shapes are presented in Figure 4.22 and are plotted against the operational deflection shapes computed from the output-only FDD method at frequencies corresponding to the modal frequencies identified during the execution of the simulated annealing algorithm. The structural properties identified using the simulated

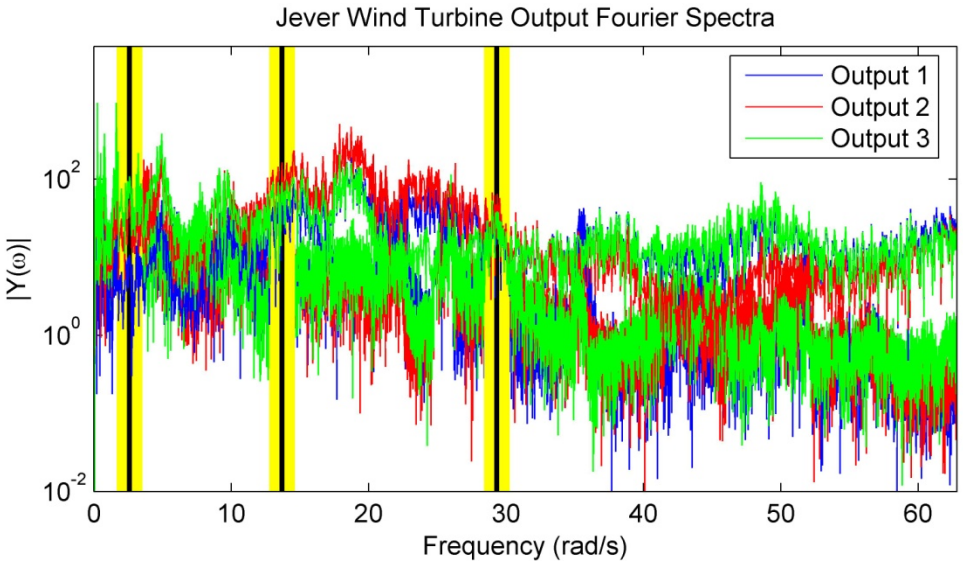


**Figure 4.21.** Identified modal frequencies superimposed on the measured output spectra from three levels in the Vestas #2 turbine.

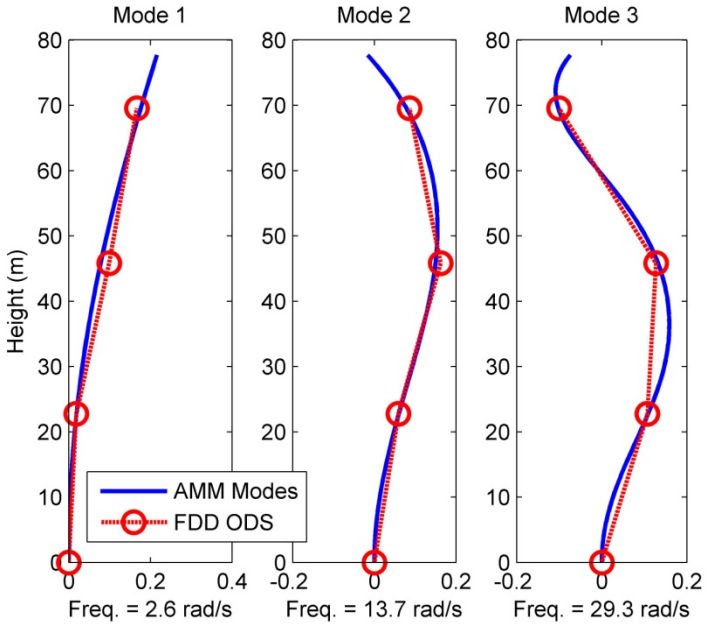


**Figure 4.22.** Mode shapes and operational deflection shapes for the Vestas #2 turbine as identified by the load estimation algorithm.

annealing algorithm that form the basis of the modal model are presented in Table 4.3 and appear to be quite reasonable. Also presented are estimated structural values obtained from the turbine blueprints. Those mode shapes and frequencies (as well as the

**Table 4.3.** Estimated structural parameters of Vestas #2 turbine.

| **Parameter** | $E$ (GPa) | $\rho$ (kg/m$^3$) | $d_t$ (m) | $d_b$ (m) | $t$ (cm) | $L$ (m) | $e$ (m) | $M$ (kg) | $J$ (kg m$^2$) |
|---|---|---|---|---|---|---|---|---|---|
| **Value** | 200 | 7850 | 2.3 | 4.4 | 5.0 | 78.2 | 2.0 | -- | -- |
| **Estimated Value** | 197 | 7804 | 2.4 | 4.4 | 5.2 | 77.7 | 2.4 | 125 x10$^3$ | 7.81 x10$^6$ |

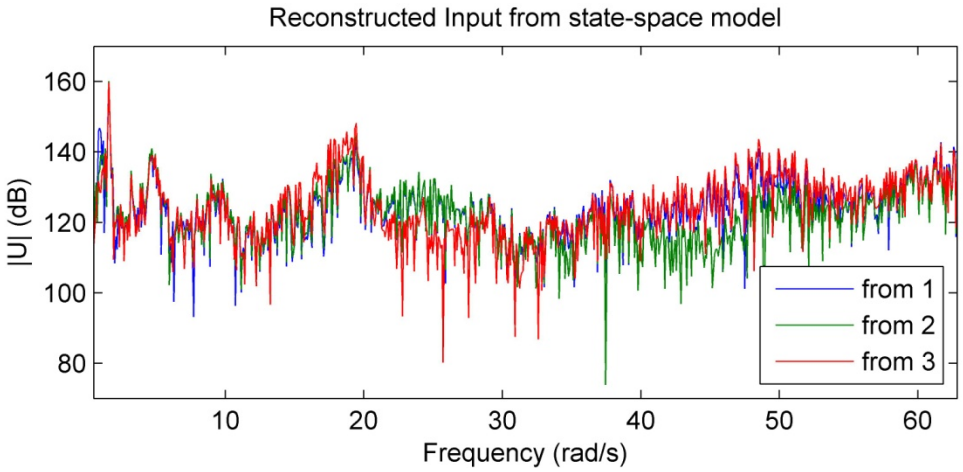


**Figure 4.23.** Estimated input spectra as estimated from sensor outputs at three levels of the Vestas #2 turbine.

top mass estimate) are then used to generate state-space and transfer function matrix models of the turbine tower. Input loadings estimated using each accelerometer's output are presented in Figure 4.23 and show very good consistency between the individual estimates conducted at each node. These estimated loading spectra are averaged into a final loading spectra estimate as seen in Figure 4.24. The plot in Figure 4.24 represents the best guess as to what the true loading of the turbine is during the instrumentation campaign. In the estimated input spectra, peaks corresponding to the peaks in the transfer function at resonant frequencies have been canceled out, but loading peaks remain. In Figure 4.24, loading peaks are evident at multiples of 1.63 rad/s (0.26 Hz). These peaks correspond to the observed rotational frequency of the turbine blades. Effects of coupling

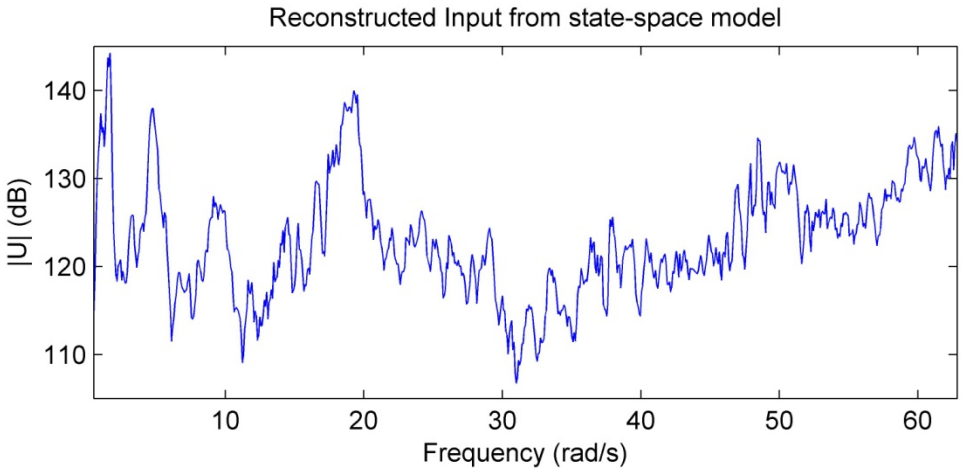


**Figure 4.24.** Average estimated input spectra from all three sensor outputs measuring acceleration in the x-axis of the Vestas #2 turbine.

between the x-direction and y-direction modes are also evident in the estimated input as the estimate method is only applied for modes in the x-direction.

### 4.6. Wind Turbine Load Estimation and Monitoring Conclusions

Characterization of dynamic loads and their interaction with wind turbine towers are vital for the future development of this promising energy technology. This chapter presents a frequency-domain model-aided method for wind load estimation with application to wind turbine towers. As opposed to prior methods, this method explicitly takes into account uncertainties in the available model to avoid bias. It updates an assumed physical model using wirelessly collected data before finding the load estimate. The method does require an *a priori* estimate of the first modal frequency in order to reliably converge on the correct model of the system. However, it has been found that the method is resilient in the face of error in that first modal frequency estimate but, if possible, that error should be small (within 5%). It is also important to bound the model

update parameter search range to values that are realistic (i.e., values over 50% in error from the estimated true value should be omitted) to aid in convergence.

Wireless sensor networks provide a low-cost and easy to install platform from which to collect the data required to build these necessary models. In addition, wireless sensors, with their inherent on-board data processing abilities, can be used to automate monitoring, load estimation, and damage detection in large-scale wind turbines in an economical manner. By demonstrating the effectiveness of wireless sensors in the wind turbine environment for data collection, building dynamical models of the structures, and load estimation, this study represents the first phase of their implementation for improving the design and economic viability of wind power technology.

Future work should focus in three new directions. First, long-term monitoring using permanent monitoring systems is an important step in the study of loads and structural responses of turbines over a large range of conditions and turbines, especially off-shore turbines that require additional study of both their dynamic behavior and the loadings to which they are subjected. In particular, the combination of wind and wave loads on the turbine structure remains a challenging environment for the economical design of off-shore turbines. For such turbines, dense sensor instrumentation will be necessary to measure the dynamic response of the system to wind and wave loads and build a statistical database of estimated loading conditions experienced by the structure over an extended period of time.

Second, a two dimensional version of the load estimation method would be advantageous to separate from sensor outputs the effects of the structural response both parallel and perpendicular to the wind loading direction. Wind turbines are designed to

turn into the wind through rotation of the nacelle atop the tower. Sensors installed within the tower are fixed in a set orientation that may not reflect the orientation of the blades. Because the orientation of the nacelle has a strong effect on the orientation of the mode shapes, the measured operational deflection shapes will change as the nacelle rotates. Decoupling the modes that are parallel to the wind direction and those perpendicular to the wind direction is difficult and affects the quality of the load estimation. A load estimation method that employs a three dimensional model would help to address this problem.

Finally, damage detection algorithms must be included in the computing cores of the wireless sensors to provide automated monitoring of the condition of turbine towers, nacelles, and blades and report failures, both after the fact and, if possible, incipient. With this information, the cost and risk inherent in building these structures may be reduced, increasing their attractiveness to the energy industry and to the public as a whole. A damage detection algorithm suitable for parallelization in a wireless sensor network is presented in the next chapter of this thesis.

# CHAPTER 5

# WIRELESS STRUCTURAL HEALTH MONITORING USING MIGRATION OF SYSTEM POLE LOCATIONS

In this chapter, a novel wireless approach to the characterization of structural damage in civil structures is presented. The proposed method is scalable, automated, and well suited for implementation within a low-power, low-cost wireless sensor network. Structural damage often results in subtle changes to structural stiffness and damping properties that are manifested by changes in the location of transfer function characteristic equation roots (poles) upon the complex plane. Using structural response time-history data collected from instrumented structures, transfer function poles can be estimated using traditional system identification methods with minimal communication between sensing nodes. Comparing the location of poles corresponding to the structure in an unknown structural state to those of the undamaged structure, damage can be accurately identified and its severity estimated. Pattern classification methods that have been increasingly popular in recent years for damage detection are leveraged to quantify damage existence, location, and severity. A novel method for evaluation and integration

of damage detection results realized by individual sensor nodes is also presented. Both input/output and output-only versions of this method are presented.

## 5.1. Motivation and Background

Autonomous monitoring of civil infrastructure systems can produce vital information regarding the condition of these complex engineered systems in real-time. The process of collecting and interrogating data to infer the damage state of a structure is referred to as structural health monitoring (SHM). Due to the potential of SHM to provide continuous and autonomous assessments of the damage state of structures, SHM is an extremely active research field with many applications to civil, mechanical, military, and aerospace structures. Methods for SHM vary widely and are categorized by the type of structure to which they are applied, the type of damage expected in the monitored structure, the physical parameter measured from the structure, the type of damage sensitive feature extracted from collected data, the assumptions made regarding the availability of high-fidelity structural models (*e.g.*, finite-element models), the type of underlying model assumed for the structure (high-fidelity or reduced-order as well as explicit or implicit), the availability of data collected from the structure in its healthy (or baseline) state, and the scale (*i.e.*, local versus global detection abilities). Extensive summary reviews of SHM methods are available in the literature including reviews of vibration based methods (Doebling*, et al.* 1998; Carden and Fanning 2004), a general review of SHM literature (Sohn*, et al.* 2003), a review of impedance based methods (Park*, et al.* 2003), a review of methods utilizing wireless sensors (Lynch and Loh 2006), reviews of SHM applications

for civil structures (Chang, *et al.* 2003; Brownjohn 2007), and a review of methods based on guided waves (Raghavan and Cesnik 2007). The reader is encouraged to refer to these references for a comprehensive review of the current state of the art.

This chapter attempts to address two major challenges within the broader SHM framework and that is economical collection of the data required for SHM analysis, as well as automation of the processing of this data to avoid the accumulation of unprocessed data that, if unexamined, is ultimately wasted. The large number of sensors necessary to collect sufficient and localized response data in order to build a complete picture of the system behavior (Farrar, *et al.* 2003) can be prohibitively expensive to install. Because the cost of cable installation can be in the range of thousands of dollars per channel (Celebi 2002), wireless sensor networks equipped with low-cost MEMS accelerometers (Lynch, *et al.* 2003) are gaining popularity as a means of controlling installation costs as monitoring systems grow in size (*i.e.*, total number of sensor channels employed). A unique aspect of wireless sensing is that each sensor has a small amount of collocated memory and processing power, meaning that a wireless sensor network has decentralized memory and computing resources (Straser and Kiremidjian 1998; Nagayama and Spencer 2007). Furthermore, collected data is also distributed throughout the network. Consolidation of this data in a centralized server will incur a communication overhead in terms of energy expended and bandwidth utilized, effectively placing limits on battery life and scalability of the network. Embedded processing of data limits the communications load, preserving both energy and network scalability. For many applications, wireless sensors must be able to operate for an extended period of time on battery power necessitating low-power design. Tradeoffs made in this design

will necessitate some reduction in functionality (particularly in terms of processing speed) versus a computing platform designed to run using power supplied by the electrical grid. These tradeoffs result in the need to identify reduced order models of monitored structures versus more processor intensive models such as those based on the finite element method that would require unacceptable long computational periods for fast response applications after a major disaster. Additionally, within a single wireless sensor, memory limitations restrict the model size and number of data points that can be used in many batch-type system identification methods, including batch least-square, subspace identification, and the eigenvalue identification algorithm (ERA), necessitating care when selecting an identification algorithm to be embedded.

With these challenges in mind, this chapter presents a health monitoring method tailored for wireless sensing applications in civil infrastructure systems based on time-series models. Unlike methods based on mode shapes (or their derivatives) centralization of data collected from spatially distributed transducers is not a requirement. Nor is it assumed that a high-fidelity model of the structure is available (Fassois and Sakellariou 2007). Instead, time-series methods leverage the embedded processing power of the wireless sensors and employs, primarily, sensor-level computing, (*i.e.*, processing within a sensor on locally collected data). The use of autoregressive time-series models for SHM is first proposed by Brinker, *et al*. (1995a; 1995b) that extracted modal frequencies from acceleration data as damage sensitive features. A later study by Sohn and Farrar (2001) identifies time-series coefficients from structural response data and uses them to construct a predictor model. The error between a recorded time-series data set and the estimate generated by the model is presented as the damage-sensitive feature. Here,

explicit use of structural properties (e.g., modal frequencies) is avoided due to their dependence on environmental conditions, but the predictor model used to generate the damage feature is dependent on the structural properties (modal frequency and damping) as demonstrated by Brinker, *et al*. (1995a), though the dependence on damping is not exploited until a method proposed by Lynch (2004; 2005) demonstrates that migration of systems poles in the complex plane (that inherently indicates changes in both modal stiffness and modal damping) can be indicative of damage. Other follow-up studies have applied variants of autoregressive time-series modeling in different contexts (Montalvao, *et al.* 2006; Fassois and Sakellariou 2007) including Wei, *et al*. (2005) who present a nonlinear autoregressive model, Lu and Gao (2005) who use response measurements as artificial inputs to their model, and Lynch, *et al*. (2006) who present a wireless validation study for time-series based SHM using the autoregressive coefficients themselves as damage features. Because the approach by Lynch, *et al*. (2006) uses the autoregressive coefficients as damage features, it has the advantage of providing additional damage features per data set than predictor error based methods. However, it is demonstrated that only some of these features are sensitive to the forms of damage applied in their study. Without a physical interpretation, it is difficult to provide a rationale for why some coefficients exhibit sensitivity nor establish an *a priori* means to predict which coefficients will be the most useful.

In this study, data collected by a wireless network is used to fit a time-series model by a recursive least-squares algorithm, converting the time-series coefficients into equivalent parametric damage features by transformation into the discrete-time Z-domain where they can be converted into equivalent system poles (see Lynch (2004; 2005)). Pole

locations within the complex-plane contain information about the modal frequencies and damping ratios of the system; changes in their location over time reflect changes in these modal properties. Once a sensor within the network has computed a set of system poles, it compares them to a saved baseline set and quantifies the degree of their migration in the form of a damage index. The relationship between the damage sensitive features (equivalent system poles) and structural modes will be exploited in the integration step to identify the relative quality of damage indices produced by different sensors from their local identified pole locations. Damage indices resulting from individual sensors are then integrated through use of a weighted average based on the modal form of the observability grammian. This average is calculated by the network and produces a network-level estimate of the degree of damage with a minimum of raw data transmission.

The structure of the chapter is as follows. First, the theory behind input/output and output-only time-series modeling and their relationship to system poles and structural vibrational behavior are presented. Next, three damage indices for the identified system poles are introduced that measure the movement of poles on the complex plane over time. This discussion is followed by the presentation of a system for integrating damage assessment results from multiple damage indices computed from poles corresponding to multiple vibrational modes as well as integration of damage indices computed by multiple sensing nodes. The method is then illustrated on two test structures: a three-span, prestressed concrete box-girder bridge and a six-story, lumped-mass, steel structure. The box-girder bridge utilized in this study is the Z24 bridge located between Utzenstorf and Koppigen in Switzerland. In 1998 researchers had unprecedented access to the

bridge prior to its scheduled demolition; they were able to instrument and monitor the bridge as it was progressively damaged. By doing so, they produced a set of vibrational data representative of a real structure subject to multiple, realistic damage modes. While the data set acquired from the Z24 bridge has the advantage of having a high degree of realism, the demolition of the bridge makes it impossible to go back and instrument the bridge with *Narada* wireless sensors. To test the method embedded inthe wireless sensors, a six-story laboratory steel structure is used for experimental validation. Applications of the method to the Z24 data set as well as the six-story structure are presented including modeling concerns, pole identification, and classification results. The chapter ends with concluding remarks and a discussion of the effectiveness of the proposed wireless structural health monitoring strategy.

## 5.2. Theory for Pole Identification

### *5.2.1. Time-Series Models*

Model selection for resource-constrained computing environments native to wireless sensor networks requires special care due to power and memory limitations coupled with the fact that data collected within the network is decentralized. The linear difference equation model is well suited for application in wireless sensing networks as it is relatively simple to calculate and is easy to decompose by each system degree-of-freedom. Considering a single-input, single-output (SISO) system at time $k$, a discrete-time linear difference equation consisting of $m$ and $n$ observations of past outputs, $y[k\text{-}i]$, and past inputs, $u[k\text{-}i]$, (respectively) would be written as:

$$y[k] + a_1 y[k-1] + \cdots + a_m y[k-m] = b_0 u[k] + b_1 u[k-1] + \cdots + b_n u[k-n] + e[k] \quad (5.1)$$

where $a_i$ and $b_i$ are weighting terms applied to the $i^{th}$ past output and input observations, and $e[k]$ is the error that arises from measurement noise as well as physical effects not captured within the image of the model (high order terms and non-linearities). The model can be rearranged to serve as an optimal linear predictor of the $k^{th}$ output:

$$\hat{y}[k] = -a_1 y[k-1] - \cdots - a_m y[k-m] + b_0 u[k] + b_1 u[k-1] + \cdots + b_n u[k-n] \quad (5.2)$$

which is in the form of an autoregressive with exogenous input (ARX) time-series model that may be transformed into a linear difference equation using the discrete time equivalent of the Laplace transform, the Z-transform (Proakis and Manolakis 1996). After application of the Z-transform, the more familiar form of the discrete-time linear difference equation emerges:

$$H(z) = \frac{Y(z)}{U(z)} = \frac{b_0 z + b_1 z^{-1} + \cdots + b_n z^{-n}}{1 + a_1 z^{-1} + \cdots + a_m z^{-m}} \quad (5.3)$$

The polynomial in the denominator of Equation (5.3) is the characteristic equation of the model, the roots of which are the identified system poles that encapsulate information regarding global modal frequencies and damping of the system. The roots of the numerator are referred to as zeros of the system and are specific to the input and output used.

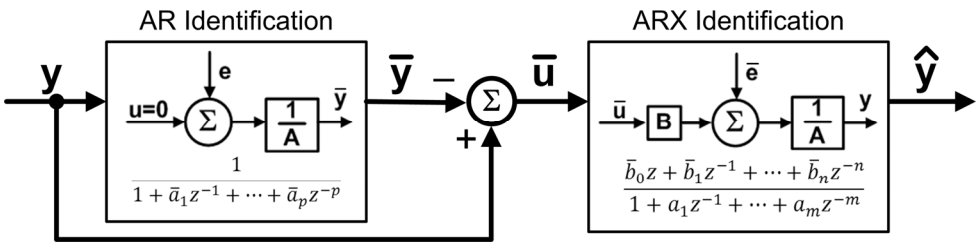


**Figure 5.1.** Practical implementation of an ARMA least-squares fit.

Because it is often difficult, or costly, to command synthetic dynamic inputs in civil structural applications, system identification is often performed under ambient excitation conditions. In such a case, modeling excitations as discrete inputs may not be appropriate. In these applications, it often becomes necessary to assume ambient excitations are approximately stationary, white noise processes. Provided that the input is relatively broad-banded, a reasonable model can still be fit to the data using an autoregressive, moving average (ARMA) model. The most popular implementation of the ARMA fit is a two-step process detailed by Ljung (1999) and depicted in Figure 5.1. In the first step, a high-order ($p > m$), output-only autoregressive (AR) model is fit to the data:

$$\hat{y}[k] = -a_1 y[k-1] - \cdots - a_m y[k-m] \tag{5.4}$$

followed by the second step in which the resulting AR error signal, $e$, is treated as in input to a second, lower-order ($m$) ARX model (Ljung 1999). The linear difference equation is drawn from the lower-order ARX model. The use of AR and ARX steps in the identification process leads some to refer to this as an AR-ARX model (Sohn and Farrar 2001).

*5.2.2. Fast Transversal Filter*

To determine the weighting coefficients ($a$ and $b$ in input/output models or $\bar{b}$ in output-only models), typically least-squares methods are used. For example, if large amounts of memory and computational throughput are available, a batch least-squares solution will be adequate. However, if one desires to implement the batch least-squares methods in resource-constrained computing environments (e.g. wireless sensors) real-time or near real-time execution would likely not be possible. An alternative approach to AR and ARX model determination would be through the use of recursive methods such as the fast transversal filter (FTF) (Haykin 1996).

In this study, the FTF is employed for embedment in wireless sensors because it represents a significant reduction in computational overhead compared to many of the other recursive least-squares algorithms available. In the FTF, the number of computations needed and the required memory increase linearly with the model order, O($p$), unlike classical recursive least-squares, which increase by the square of the model order, O($p^2$) (Juang 1994). In low-power wireless sensor applications, these computational savings are necessary to compute the transfer function with reasonable speed. The FTF takes advantage of the shifting property, including a forward-time and backward-time output estimator (Cioffi and Kailath 1984). The coefficients of the forward-time estimator are the model coefficients that define the transfer function to be identified. The FTF employs the *a priori* and *a posteriori* errors in the backward and forward time estimators to update the estimators and the estimator update gains. A complete derivation of the FTF may be found in Cioffi and Kailath (1984) or Haykin

(1991).

A description of the FTF derived for a single-input single-output (SISO) system with a direct transmission term is given by Juang (1994) and presented in Table 5.1. A single time step in the FTF algorithm begins when a new data point becomes available. The data history vector, $\boldsymbol{v_p}$, is updated (Equation 5.5) using existing data, and the new data vector, $\boldsymbol{y_{\vec{u}}}$, can be formed (Equation 5.6). These updated vectors may then be used to update the forward-time *a priori* error, $\vec{\boldsymbol{e}}_{\boldsymbol{p}}^{-}$, using the matrix of forward-time observation weights, $\hat{\vec{\boldsymbol{Y}}}_{\boldsymbol{p}}$, derived from the previous step (Equation 5.7). A conversion factor, $\gamma_p$, in Equation 5.8 relates the *a priori* error to the forward-time *a posteriori* error, $\vec{\boldsymbol{e}}_{\boldsymbol{p}}^{+}$ (*i.e.*, an estimation error derived from the observation weights after they are updated). This conversion factor is derived in the backward-time estimation step. The cumulative forward time error is then updated in the forward-time error squares term, $\vec{\boldsymbol{\varepsilon}}_{\boldsymbol{p}}$ (Equation 5.9). The *a priori* error vector and the gain matrix, $\boldsymbol{G_p}$, are used to update the matrix of coefficient weights (Equation 5.10). An augmented gain matrix, $G_{p+1}$ (Equation 5.11), and augmented conversion factor, $\gamma_{p+1}$ (Equation 5.12), are formed that are shared by both the forward and backward time estimation steps and are used to update the gain matrix, $\boldsymbol{G_p}$, and conversion factor, $\gamma_p$, respectively using parameters found in the backward-time estimation step (Juang 1994). These steps are depicted in Equations 5.14 through 5.19.

**Table 5.1.** Summary of FTF Algorithm.

| | | |
|---|---|---|
| **Forward-time Estimation** | | |
| data history vector, $v_p[k\text{-}1]$ | $\boldsymbol{v_p}[k-1]=\begin{bmatrix} u[k] \\ y[k-1] \\ u[k-1] \\ \vdots \\ y[k-p] \\ u[k-p] \end{bmatrix}$ | (5.5) |
| new data vector, $\boldsymbol{y_{\vec{u}}}[k]$ | $\boldsymbol{y_{\vec{u}}}[k]=\begin{bmatrix} u[k+1] \\ y[k] \end{bmatrix}$ | (5.6) |
| *a priori* error, $\vec{\boldsymbol{e}}_{\boldsymbol{p}}^{-}[k]$ | $\vec{\boldsymbol{e}}_{\boldsymbol{p}}^{-}[k]=\boldsymbol{y_{\vec{u}}}[k]-\hat{\vec{\boldsymbol{Y}}}_{\boldsymbol{p}}[k-1]\boldsymbol{v_p}[k-1]$ | (5.7) |
| *a posteriori* error, $\vec{\boldsymbol{e}}_{\boldsymbol{p}}^{+}[k]$ | $\vec{\boldsymbol{e}}_{\boldsymbol{p}}^{+}[k]=\gamma_p[k-1]\,\vec{\boldsymbol{e}}_{\boldsymbol{p}}^{-}[\boldsymbol{k}]$ | (5.8) |
| error squares, $\vec{\boldsymbol{\varepsilon}}_{\boldsymbol{p}}[k]$ | $\vec{\boldsymbol{\varepsilon}}_{\boldsymbol{p}}[k]=\vec{\boldsymbol{\varepsilon}}_{\boldsymbol{p}}[k-1]+\vec{\boldsymbol{e}}_{\boldsymbol{p}}^{+}[\vec{\boldsymbol{e}}_{\boldsymbol{p}}^{-}]^{\mathrm{T}}$ | (5.9) |
| observation weights, $\hat{\vec{\boldsymbol{Y}}}_{\boldsymbol{p}}[k]$ | $\hat{\vec{\boldsymbol{Y}}}_{\boldsymbol{p}}[k]=\hat{\vec{\boldsymbol{Y}}}_{\boldsymbol{p}}[k-1]+\vec{\boldsymbol{e}}_{\boldsymbol{p}}^{-}[k]\boldsymbol{G_p}[k-1]$ | (5.10) |
| augmented gain, $G_{p+1}[k]$ | $G_{p+1}[k]=\left[[\vec{\boldsymbol{e}}_{\boldsymbol{p}}^{+}[k]]^{\mathrm{T}}\vec{\boldsymbol{\varepsilon}}_{\boldsymbol{p}}^{\,-1}[k] \quad \boldsymbol{G_p}[k-1]-[\vec{\boldsymbol{e}}_{\boldsymbol{p}}^{+}[k]]^{\mathrm{T}}\vec{\boldsymbol{\varepsilon}}_{\boldsymbol{p}}^{\,-1}[k]\hat{\vec{\boldsymbol{Y}}}_{\boldsymbol{p}}[k]\right]$ | (5.11) |
| augmented conversion factor, $\gamma_{p+1}[k]$ | $\gamma_{p+1}[k]=\gamma_p[k-1]-[\vec{\boldsymbol{e}}_{\boldsymbol{p}}^{+}[k]]^{\mathrm{T}}\vec{\boldsymbol{\varepsilon}}_{\boldsymbol{p}}^{\,-1}[k]\vec{\boldsymbol{e}}_{\boldsymbol{p}}^{+}[k]$ | (5.12) |
| decompose augmented gain | $\boldsymbol{G_{p+1}}[k]=\left[\boldsymbol{G}_{\boldsymbol{p+1}}^{(r)}[k] \quad \boldsymbol{G}_{\boldsymbol{p+1}}^{(a)}[k]\right]$ | (5.13) |
| **Backward-time Estimation** | | |
| data history vector, $v_p[k]$ | $\boldsymbol{v_p}[k]=\begin{bmatrix} u[k+1] \\ y[k] \\ u[k] \\ \vdots \\ y[k-p+1] \\ u[k-p+1] \end{bmatrix}$ | (5.14) |
| data vector, $\boldsymbol{y_u}[k-p]$ | $\boldsymbol{y_u}[k-p]=\begin{bmatrix} y[k+p] \\ u[k-p] \end{bmatrix}$ | (5.15) |
| *a priori* error, $\overleftarrow{\boldsymbol{e}}_{\boldsymbol{p}}^{-}[k]$ | $\overleftarrow{\boldsymbol{e}}_{\boldsymbol{p}}^{-}[k]=\boldsymbol{y_u}[k-p]-\hat{\overleftarrow{\boldsymbol{Y}}}_{p}[k-1]\boldsymbol{v_p}[k]$ | (5.16) |
| gain, $\boldsymbol{G_p}[k]$ | $\boldsymbol{G_p}[k]=\dfrac{\boldsymbol{G}_{\boldsymbol{p+1}}^{(r)}[k]+\boldsymbol{G}_{\boldsymbol{p+1}}^{(a)}[k]\hat{\overleftarrow{\boldsymbol{Y}}}_{p}[k-1]}{1-\boldsymbol{G}_{\boldsymbol{p+1}}^{(a)}[k]\overleftarrow{\boldsymbol{e}}_{\boldsymbol{p}}^{-}[k]}$ | (5.17) |
| observation weights, $\hat{\overleftarrow{\boldsymbol{Y}}}_{p}[k]$ | $\hat{\overleftarrow{\boldsymbol{Y}}}_{p}[k]=\hat{\overleftarrow{\boldsymbol{Y}}}_{p}[k-1]+\overleftarrow{\boldsymbol{e}}_{\boldsymbol{p}}^{-}[k]\boldsymbol{G_p}[k]$ | (5.18) |
| conversion factor, $\gamma_p[k]$ | $\gamma_p[k]=\dfrac{\gamma_{p+1}[k]}{1-\boldsymbol{G}_{\boldsymbol{p+1}}^{(a)}[k]\overleftarrow{\boldsymbol{e}}_{\boldsymbol{p}}^{-}[k]}$ | (5.19) |
| *a posteriori* error, $\overleftarrow{\boldsymbol{e}}_{\boldsymbol{p}}^{+}[k]$ | $\overleftarrow{\boldsymbol{e}}_{\boldsymbol{p}}^{+}[k]=\gamma_p[k]\overleftarrow{\boldsymbol{e}}_{\boldsymbol{p}}^{-}[k]$ | (5.20) |
| error squares, $\overleftarrow{\boldsymbol{\varepsilon}}_{\boldsymbol{p}}[k]$ | $\overleftarrow{\boldsymbol{\varepsilon}}_{\boldsymbol{p}}[k]=\overleftarrow{\boldsymbol{\varepsilon}}_{\boldsymbol{p}}[k]+\overleftarrow{\boldsymbol{e}}_{\boldsymbol{p}}^{+}[k][\overleftarrow{\boldsymbol{e}}_{\boldsymbol{p}}^{-}[k]]^{\mathrm{T}}$ | (5.21) |

Similar to the forward-time step, the backward time data history vector, $v_p$ (Equation 5.14), and data vector, $\boldsymbol{y_u}$ (Equation 5.15), are updated using the newly available data point and a backward-time *a priori* error, $\overleftarrow{\boldsymbol{e}}_{\boldsymbol{p}}^{-}[k]$, can be determined (Equation 5.16). A decomposed version of the augmented gain matrix (Equation 5.13) is then used to update the gain matrix, $\boldsymbol{G_p}$, in Equation 5.16 also using the backward-time observation weights,

$\widehat{\overleftarrow{\boldsymbol{Y}}}_p[k]$ which are then updated in Equation 5.17. Also, the updated conversion factor, $\gamma_p$, may be found (Equation 5.19) from the augmented conversion factor and augmented gain decomposition from the forward-time estimation step. Equations 5.20 and 5.21 include some bookkeeping for the backward-time estimation step including update of the backward-time *a posteriori* error, $\overleftarrow{\boldsymbol{e}}_{\boldsymbol{p}}^{+}[k]$, and error squares matrix, $\overleftarrow{\boldsymbol{\varepsilon}}_{\boldsymbol{p}}[k]$, but are not strictly necessary in this implementation where the desired end result is the updated matrix of forward-time observation weights of the AR or ARX model.

The FTF may be initialized from theoretical values, assuming zero initial conditions (Haykin 1991), or based on an offline batch least-squares solution using pre-recorded data (Juang 1994). In this study, the latter approach is utilized, employing a forgetting factor, λ, multiplying the old error squares terms in Equation 5.8 and Equation 5.20 to de-emphasize older observations so that new trends will become apparent.

While the FTF can be executed faster than the standard recursive least-squares algorithm, it does suffer from instabilities when implemented on a finite precision computer. Unstable modes exist within the filter that are not excited by infinite precision arithmetic. In real systems with finite precision, the stability of the filter is dependent upon both the degree of precision of the processor as well as the characteristics of the excitation signals (Slock and Kailath 1991; Haykin 1996). This effect is exacerbated if a forgetting factor is used (Binde 1995). Slock and Kailath (1991) present a stabilization solution for the FTF taking advantage of quantities in the FTF algorithm that are computed using both the forward-time and backward-time estimator. In infinite precision systems these quantities will be calculated to be the same for both estimators. As precision errors are introduced, there exists an error between the forward-time and

backward-time calculations. Slock and Kailath essentially use these errors as feedback signals to stabilize the FTF filter. A less computationally intensive method presented by Binde (1995) is used in this study. In this method, "leakage correction factors" that are less than, but nearly equal to, 1 are introduced into the filter Equations 5.9 and 5.17 to control the propagation of errors. Soh and Douglas (1997) confirm the effectiveness of the leakage correction method for real-world signals and forgetting factors ($\lambda$) that are also nearly 1.

### *5.2.3. Pole Extraction*

Extraction of system poles from the identified characteristic equation requires identification of the complex roots of the characteristic polynomial. Solving for the roots of higher order polynomials in an automated fashion can present some numerical difficulties. In this study, the roots are found from the companion matrix of the characteristic polynomial, $\mathcal{C}(\mathfrak{p})$:

$$\mathcal{C}(1 + a_1 z^{-1} + \cdots + a_m z^{-m}) = \begin{bmatrix} 0 & 0 & \dots & 0 & -a_m \\ 1 & 0 & \dots & 0 & -a_{m-1} \\ 0 & 1 & \dots & 0 & -a_{m-2} \\ \vdots & \vdots & \ddots & \vdots & \vdots \\ 0 & 0 & \dots & 1 & -a_1 \end{bmatrix} \tag{5.22}$$

A companion matrix has for its eigenvalues, the roots of the associated polynomial (Edelman and Murakami 1995). The companion matrix is easily formed and its eigenvalues may be determined by use of LQ-decomposition, so long as there are no repeated roots (Press, *et al.* 1992).

In this study, system poles are extracted from the recursively identified time-series models (*e.g.*, input/output ARX and output-only ARMA) described above. Changes in the location of these poles in the complex plane are then experimentally correlated to damage. Model order is based on the accuracy of the estimator (as determined using separate fit and validation data sets) as well as the match between the identified poles and pole locations determined from a modal identification study (see sections 5.3.2 and 5.4.2). Multiple sets of poles identified using multiple data runs are identified. These poles form natural clusters of increasing frequency based on the modal properties of the structure. The clustering effect is due to variability in the identified pole location due to environmental effects, sensor noise, nonlinear effects, and also damage. Because the autoregressive models used in this chapter (*i.e*, ARX and ARMA) are not constrained to adhere to the specific underlying model degrees of freedom (DOFs) on which the modal identification study is based, the fit algorithm will include some additional poles that arise from local modes, out of plane and non-linear effects, or other unwanted effects. An automated algorithm is thus necessary to sort the poles generated by the autoregressive models that minimizes the distance between a set of candidate poles and the pole locations determined from the modal analysis study.

Using multiple data sets to populate pole clusters for both the baseline and test conditions of the structure will help to minimize the effect of environmental variability, noise, and sorting error. The algorithm tracks changes in pole locations, as identified by individual sensors, and classifies their severity based on their statistics. Significant migration of pole cluster locations is identified as an indication of damage. That damage estimate is normalized by the variance in identified pole location giving the algorithm a

statistical basis. Results realized from multiple sensors are combined in a weighted average based on an estimate of sensor-to-noise ratio corresponding to individual modes of the structure. This weighted average yields a network-level measure of damage. The division of sensor-level and network-level computing tasks is detailed in the next section (section 5.2.4).

### *5.2.4. Sensor-Level and Network-Level Data Processing*

For potential damage cases, structural response data (*e.g.*, acceleration) is collected by wireless sensors located throughout the structure. For input/output cases, input data (*e.g.*, base acceleration) is transmitted to the entire network while output data is held locally. The sensors then execute the recursive least-squares algorithms previously described to determine the time-series weighting coefficients (*i.e.*, coefficients of the ARX model for input/output and coefficients of the ARMA model for output-only) based on local output observations, and fit using 4096 data points. With those coefficients determined, Z-domain locations of the identified system poles are determined at the sensor level, as described in the previous section (section 5.2.3). These values are stored and the process is repeated 10 to 25 times over a short period of time during which, it is assumed that the damage level remains constant. Each repetition of the process yields a new set of poles that are similar to the previous set but not a perfect replica. Pole clusters form corresponding to modes of the structure and are assumed to have a Gaussian distribution. Thus, based on poles segregated to one cluster, a Gaussian distribution is fit to the pole locations on the complex plane. This distribution yields both the mean of the cluster as well as its variance. The mean of each cluster

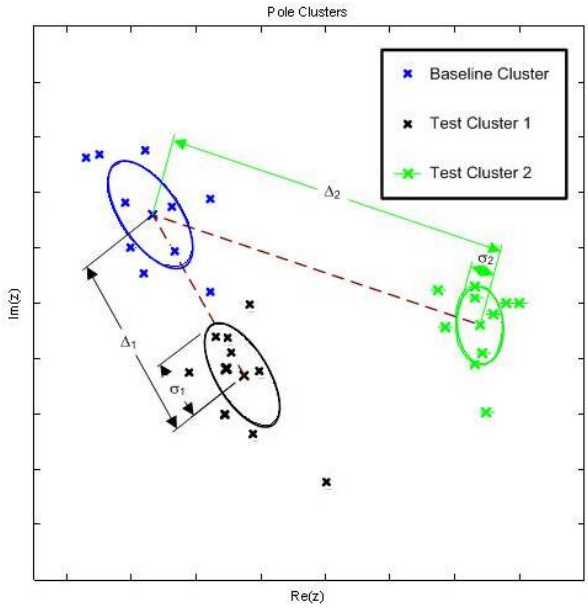


**Figure 5.2.** Mean separation distance criterion.

associated with a mode is then compared to a corresponding cluster generated from baseline data (*e.g.*, from the undamaged structure). A damage index is devised, based on the separation distance between the mean of the unknown state cluster and the baseline cluster for a given pole cluster. The mean separation distance associated with the $i^{th}$ sensor and $j^{th}$ mode is defined as $\Delta_{i,j}$. The damage index also takes into account uncertainty through the derived standard deviation of the identified pole locations, $\sigma_{i,j}$ (Figure 5.2). The final resulting index is the separation distance divided by the standard deviation value:

$$DI_{i,j} = \frac{\Delta_{\mathrm{i,j}}}{\sigma_{\mathrm{i,j}}} \tag{5.23}$$

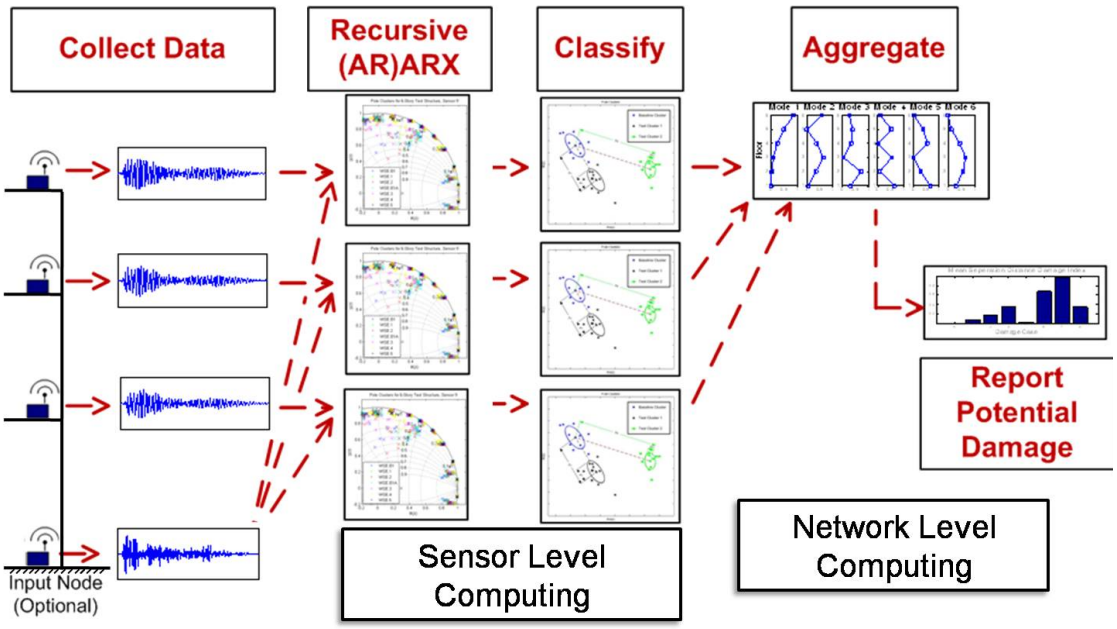


**Figure 5.3.** Graphical overview of sensor-level identification and network-level integration tasks.

At the sensor-level, every unit in the network will identify a damage index value corresponding to each identified system pole cluster (the number of pole clusters is defined by the user). However, because pole cluster correspond to mode, which is a global characteristic of the system, it is prudent to combine the pole cluster information over all measurement locations. Hence, these individual damage indices must be integrated into a network-level damage level characterization (Figure 5.3). This end is accomplished using a weighted average of the individual damage index results. The weighting factors are taken from the observability grammian, $\boldsymbol{W_O}$ (Chen 1999):

$$\boldsymbol{W_O} = \int_0^\infty e^{\boldsymbol{A}^{\mathrm{T}}\tau}\boldsymbol{C}^{\mathrm{T}}\boldsymbol{C}e^{\boldsymbol{A}\tau}\,d\tau \tag{5.24}$$

where $\boldsymbol{A}$ is the state-space state matrix, $\boldsymbol{C}$ is the state-space observer matrix, and $\tau$ is a variable of integration. The observability grammian is a relative measure of the average amount of energy one might expect to measure from a system for a given sensor configuration (Chen 1999). In sensor (or actuator) placement problems, the relative "size" of the observability (or controllability) grammian (as measured by its trace) is used as an indication of the effectiveness of one sensor (or actuator) layout versus another (Hac and Liu 1993; Mirza and Van Niekerk 2003). If the sensors used in the network have similar noise characteristics, then the size of the single-sensor observability grammian characterized by:

$$\boldsymbol{W}_{\boldsymbol{O}_i} = \int_0^\infty e^{\boldsymbol{A}^{\mathrm{T}}\tau} \boldsymbol{C}_i{}^{\mathrm{T}} \boldsymbol{C}_i e^{\boldsymbol{A}\tau}\, d\tau \tag{5.25}$$

where $\boldsymbol{C}_i$ is the $i^{\text{th}}$ row of $\boldsymbol{C}$ and yields a relative estimate of the signal-to-noise ratio realized at the $i^{\text{th}}$ sensor given the sensor's location and the dynamic properties of the structure. By decomposing the observability grammian into modal coordinates through a simple change-of-basis operation:

$$\overline{\boldsymbol{W}}_{\boldsymbol{O}_i} = \boldsymbol{\Phi}^{-1} \boldsymbol{W}_{\boldsymbol{O}_i} \boldsymbol{\Phi} \tag{5.26}$$

where $\boldsymbol{\Phi}$ is the linear transformation matrix to modal coordinates (whose columns are the mode shapes or eigenvectors of the structure), the contribution from each mode of the system, $\boldsymbol{w}_{i,j}$, may be decoupled from the remaining modes in 2x2 blocks along the

primary diagonal of the observability grammian in modal coordinates (Hac and Liu 1993):

$$\overline{\boldsymbol{W}}_{\boldsymbol{O}_i} = \begin{bmatrix} [\boldsymbol{w}_{\mathrm{i},1}] & \cdots & [\mathbf{0}] \\ \vdots & \ddots & \vdots \\ [\mathbf{0}] & \cdots & [\boldsymbol{w}_{\mathrm{i,r}}] \end{bmatrix} \tag{5.27}$$

where $r$ is the number of identified modes. This fact means that, when considering a single sensor at a time, the relative contribution to the modal grammian from each mode can be determined. These contributions found from the traces of the modal coordinate blocks (normalized across all contribution weights) are used as damage index weights for damage indices realized by each sensor within the network and for each mode (and its associated pole cluster) identified by that sensor. For a system with $s$ sensors, the aggregated damage index, $\overline{DI}$, is:

$$\overline{DI} = \sum_{i=1}^{s} \sum_{j=1}^{r} \frac{\left|\mathrm{trace}\left[\boldsymbol{w}_{\mathrm{i,j}}\right]\right|}{\sqrt{\sum_{\mathrm{k}=1}^{\mathrm{r}} \left(\mathrm{trace}\left[\boldsymbol{w}_{\mathrm{i,k}}\right]\right)^2}} * DI_{i,j} \tag{5.28}$$

By weighting contributions in this manner, measurements corresponding to high signal energy (and thus, large signal to noise ratio) are given higher priority than low-energy measurements.

**Figure 5.4.** Z24 bridge (*Photo courtesy of Verbraken (1999)*).

### 5.3. Z24 Bridge

Dynamic data for a large number of damage cases is available for the Z24 Bridge from the System Identification to Monitor Civil Engineering Structures (SIMCES) project (Wenzel and Pichler 2005). In 1998, the Z24 Bridge located between Utzenstorf and Koppigen in Switzerland (Figure 5.4) was heavily instrumented and monitored as it was progressively damaged to provide researchers with vibrational data corresponding to those progressive damage levels. The bridge is a three span bridge with exterior spans of 14 m each and a center span of 30 m with concrete piers between. The bridge is constructed using prestressed, two-cell box girders with tendons located in the webs of the girder. A description of the SIMCES Z24 Bridge project is available by De Roeck, *et al.* (2000) with a description of the progressive damage states provided by Krämer, *et al.* (1999). Peeters and Ventura (2002) have compiled a comparison of several modal

analysis techniques employed on the Z24 bridge data set including peak picking (Womack and Hodson 2001), frequency domain decomposition (FDD) (Luscher*, et al.* 2001), rational fraction polynomial (Schwartz and Richardson 2001), ARMA two-stage least squares (Fassana*, et al.* 2001), and subspace identification (Luscher*, et al.* 2001; Marchesiello*, et al.* 2001). A number of health monitoring methods have also been proposed using the Z24 Bridge data set for validation including finite element model updating (Garibaldi*, et al.* 2003; Teughels and De Roeck 2004), control charts (Kullaa 2003), modal frequencies and shapes (Maeck and De Roeck 2003), and subspace identification models (Mevel*, et al.* 2003). Intrinsic in these methods is the assumption that a centralized data server is available for data archival and processing. In a wireless sensor network, distributed data processing is preferred in order to avoid unnecessary and power draining transmissions of raw data from every sensor in the network (Lynch and Loh 2006).

The best practice for system identification requires division of the data into fit and validation sets. The fit set is used to build the model (in this study, the ARX and ARMA models) and choose its size. The validation set is then used to check the veracity of the model against new data to help avoid over fitting the data and its noise. Furthermore, the health monitoring aspect of this study requires additional data once the model size and structure has been determined. One set of data is required to choose weights for the damage index terms and another set of data is required to test those weights to determine their effectiveness in separating damaged cases from undamaged cases. In this study, sensor data is taken from four locations located near the center of the span and along the edges of the bridge. Because the bridge is very densely instrumented, accelerometers are

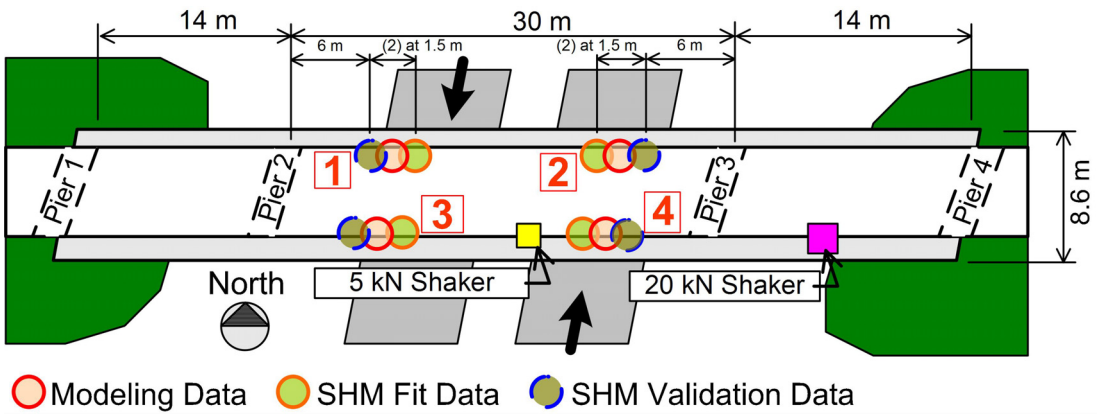


**Figure 5.5.** Sensor Layout of accelerometers on the Z24 bridge.

very close together: 1.5 m apart. During each test, 65,536 data points are collected from each sensor. To allow for 10 poles per cluster and an adequate number of data points to fit per pole, adjacent accelerometers are considered to be located at approximately the same location. This practice allows use of the entire time history from a sensor location for modeling. An adjacent sensor may then be used to fit the damage index terms while the adjacent sensor on the other side provides the final validation data for the health monitoring application. The locations of the vertical accelerometers used in this study are depicted in Figure 5.5.

### *5.3.1. Z24 Bridge Progressive Damage Tests*

The Z24 Bridge progressive damage tests offer an unprecedented opportunity for comparison of the vibrational characteristics of a single structure under a wide array of damage and distress conditions. The bridge is heavily instrumented with accelerometers and excited vertically by the use of two hydraulic shakers located on the bridge deck, the first being a SCHENK POKK/N capable of producing forces between ±5 kN in a

frequency band between 2.3 and 100 HZ; the second shaker is a SCHENK PLz 25 N Q 160 capable of generating ±20 kN between 1.5 and 60 Hz. Both shakers were configured to output random, broadband signals. Two HBM C2 force transducers were available to record the force imparted by each of the shakers to the structure; the force signal is taken as the input to the system. The outputs considered are the vertical accelerations (recorded by Kinematics, Inc. FBA 11 uniaxial force balanced accelerometers) of the deck at sensor locations 1, 2, 3, and 4 (Figure 5.5). The sampling rate used is 100 Hz.

Progressive damage tests are executed strategically with reversible and less extensive forms of damage inflicted on the structure first, and more extensive, irreversible damage inflicted on the structure later. First, a hinge is added in one pier (Pier 3) to facilitate reversible damage of the form of pier foundation settlement or rotation. This case is regarded as the baseline case to which the other progressive damage cases are compared. Following the installation of the hinge, the pier is progressively lowered by 20 mm, 40 mm, 80 mm, and 95 mm. Audible and visible cracking is observed between the 40 mm level and the 80 mm level with additional cracking occurring between the 80 mm and 95 mm levels (Krämer*, et al.* 1999). Once the pier is restored, the footing is rotated resulting in a 15 mm differential settlement from one side to the other. Upon completion of these progressive damage tests, the pier is restored to its original position and the irreversible damage tests are undertaken. Spalling of concrete and a landslide at the East abutment are simulated, followed by a cut in the concrete connection between one pier column and the box girder to simulate a concrete hinge failure (Pier 4). Finally, the pretension system is attacked by destroying 2 and then 4 anchor heads, and then with 2 and 4 tendons (54

**Table 5.2.** Description of progressive damage tests.

| Test Number | Description (Reversible Damage) | Test Number | Description (Irreversible Damage) |
|---|---|---|---|
| 1 | No Damage (missing/corrupted data) | 9 | Concrete Spalling: 12 $m^2$ |
| 2 | No Damage, Pier Hinge Added (Baseline) | 10 | Concrete Spalling: 24 $m^2$ |
| 3 | Pier 3 Settlement: 20 mm | 11 | Landslide at Abutment |
| 4 | Pier 3 Settlement: 40 mm | 12 | Concrete Hinge Failure |
| 5 | Pier 3 Settlement: 80 mm | 13 | Anchor Head Failure (2) |
| 6 | Pier 3 Settlement: 95 mm | 14 | Anchor Head Failure (4) |
| 7 | Pier 3 Foundation Tilt | 15 | Tendon Wire Failure (54/2) |
| 8 | No Damage, Pier 3 Restored | 16 | Tendon Wire Failure (100/4) |

and 100 wires respectively) cut. A summary of the 16 progressive damage tests is resented in Table 5.2 (Krämer*, et al.* 1999).

Of particular interest are progressive damage tests 5 and 6 in which the pier settlement is greatest. Besides the audible and visual cracking reported during the lowering of the pier to these points, noticeable changes in the eigenvalues of the system are observed between these cases and the baseline case. Previous studies of the Z24 Bridge data set using more computationally intensive algorithms have demonstrated that these damage cases are very detectible by more traditional methods (Garibaldi*, et al.* 2003; Kullaa 2003; Maeck and De Roeck 2003; Mevel*, et al.* 2003; Teughels and De Roeck 2004). Hence, the method presented in this study must also be able to detect damage for these cases in order to have merit.

### *5.3.2. Modeling of the Z24 Bridge*

The modeling data set is taken from the baseline set (progressive damage test 2) and is divided in half with the first half used to build time-series models of increasing sizes and the second half reserved as validation data to confirm the model size. ARX models

are automatically fit for *m* and *n* coefficients (Equation 5.1) ranging from 2 to 100 and the resulting transfer function compared to the experimental transfer function from the validation data set in the frequency domain. During the course of the investigation, models with direct transmission terms (where *m* and *n* are equal) produce the lowest mean-squared (LMS) error between theoretical and experimental transfer functions. Plotting the LMS error versus model size yields Figure 5.6. Ultimately, a 60 pole, 60 zero model is selected that achieves good improvement in LMS error versus lower order models compared with the increase in computational complexity. The transfer function comparison is presented in Figure 5.7. Because the structure is excited simultaneously by two shakers, a multiple input single output (MISO) least squares ARX model is fit to the input data and single-node output.

Poles that are highly consistent in their locations are most useful for automated health monitoring. For a structure of this type, this fact makes less desirable poles that the algorithm places on the real axis as well as higher order poles. Analysis of the baseline data from a number of sensors demonstrated that the least-squares algorithm occasionally placed pairs of poles on the real axis. The health monitoring algorithm is programmed to ignore those poles. The remaining poles occur as complex conjugate pairs and are distributed around (and inside of) the unit circle. Additionally, higher-order poles are found to cluster poorly, exhibiting much larger deviations than lower order poles and therefore, are not used by the health monitoring algorithm. Once time-series models are assembled for the test cases, the identified poles must be automatically sorted. The sorting is accomplished by a sorting algorithm that minimizes the LMS error, or the distance between a set of poles and the baseline means. When a set of 60 pole clusters is

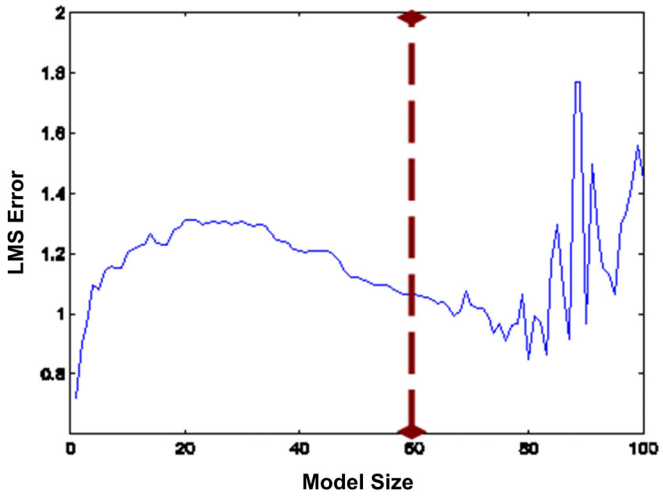


**Figure 5.6.** Frequency domain error versus ARX model size (where $m = n$).

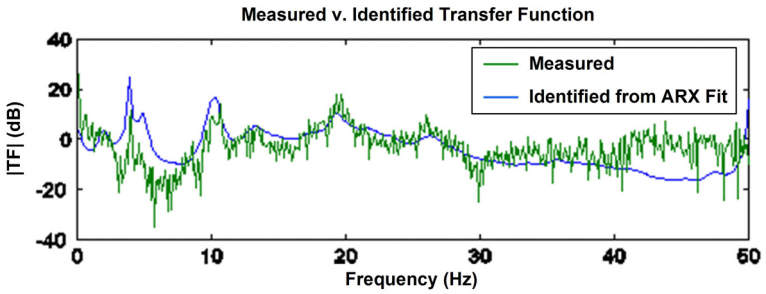


**Figure 5.7.** Experimental and identified transfer functions.

generated, the sorting algorithm first discards any poles on or below the real axis (poles below the real axis are redundant). Then it searches every ordered list of the remaining poles, looking for the permutation that yields the smallest LMS error of the distance between poles. In total, there are 12 unique pole clusters (see Figure 5.8), with 10 poles per cluster, that are realized from 6000 samples per set of poles. This process is repeated for every progressive damage test.

**Table 5.3.** List of modal frequencies of baseline poles used in health monitoring algorithm.

| Mode Number | Modal Frequency (Hz) | Identified in Peeters and Ventura (2002)? |
|---|---|---|
| 1 | 1.97 | |
| 2 | 3.88 | Yes |
| 3 | 4.94 | Yes |
| 4 | 7.22 | |
| 5 | 9.78 | Yes |
| 6 | 10.27 | Yes |
| 7 | 12.62 | Yes |
| 8 | 13.66 | Yes |
| 9 | 15.68 | |
| 10 | 17.34 | Yes |
| 11 | 19.29 | Yes |
| 12 | 19.87 | Yes |

### *5.3.3. Z24 Bridge SHM Results*

The first twelve pairs of poles (those with the lowest eigenvalue) identified by the automated ARX algorithm are selected for structural health monitoring and are summarized in Table 5.3. The mean pole location for the baseline cluster defines the location of these poles. These poles have modal frequencies ranging from 1.97 to 19.87 Hz; nine of these poles are identified in the comparative study of modal analysis techniques for the Z24 Bridge conducted by Peeters and Ventura (2002). Pole clusters along with first standard deviation level curves are presented for the twelve baseline poles in Figure 5.8. The operation deflection shapes at the sensor locations for the twelve poles of interest are calculated.

Movement of pole clusters can be observed qualitatively as the damage tests progress. First, looking at the reversible progressive damage tests [Figure 5.9(a), 5.9(d), and 5.9(g)] and focusing on the closely spaced pole clusters 5 and 6, small changes can be observed in the pole locations between tests 2-4. Larger movement is observed for tests 5 and 6

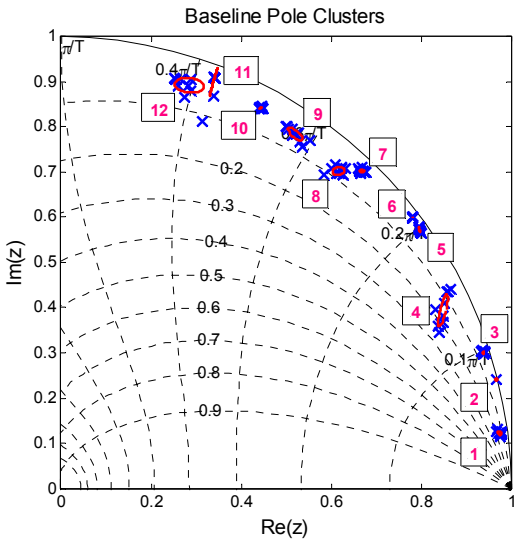


**Figure 5.8.** Twelve identified pole clusters used for structural health monitoring of the Z24 Bridge.

with the pole clusters returning back near the original baseline location during tests 7 and 8. Second, looking at the irreversible progressive tests [Figure 5.9(b-c), 5.9 (e-f), and 5.9 (h-i)] and again focusing on pole clusters 5 and 6, shows less overall movement of the pole clusters as the damage tests progress but a discernable jump is observed during damage case 12 with future progressive damage tests yielding pole clusters centered close to this new location.

Applying the damage index terms provides a quantitative assessment of pole movement during the damage test cases. Using the modal grammian weighting factors, individual damage index values computed from individual sensing nodes (one for each mode on each sensor) can be combined. The combined mean separation distance criterion shows a very large discrepancy between the poles of progressive damage tests 5 and 6 and the rest of the progressive damage tests. This result can be seen in Figure 5.10 where higher damage index values suggest a greater probability of damage. Here,

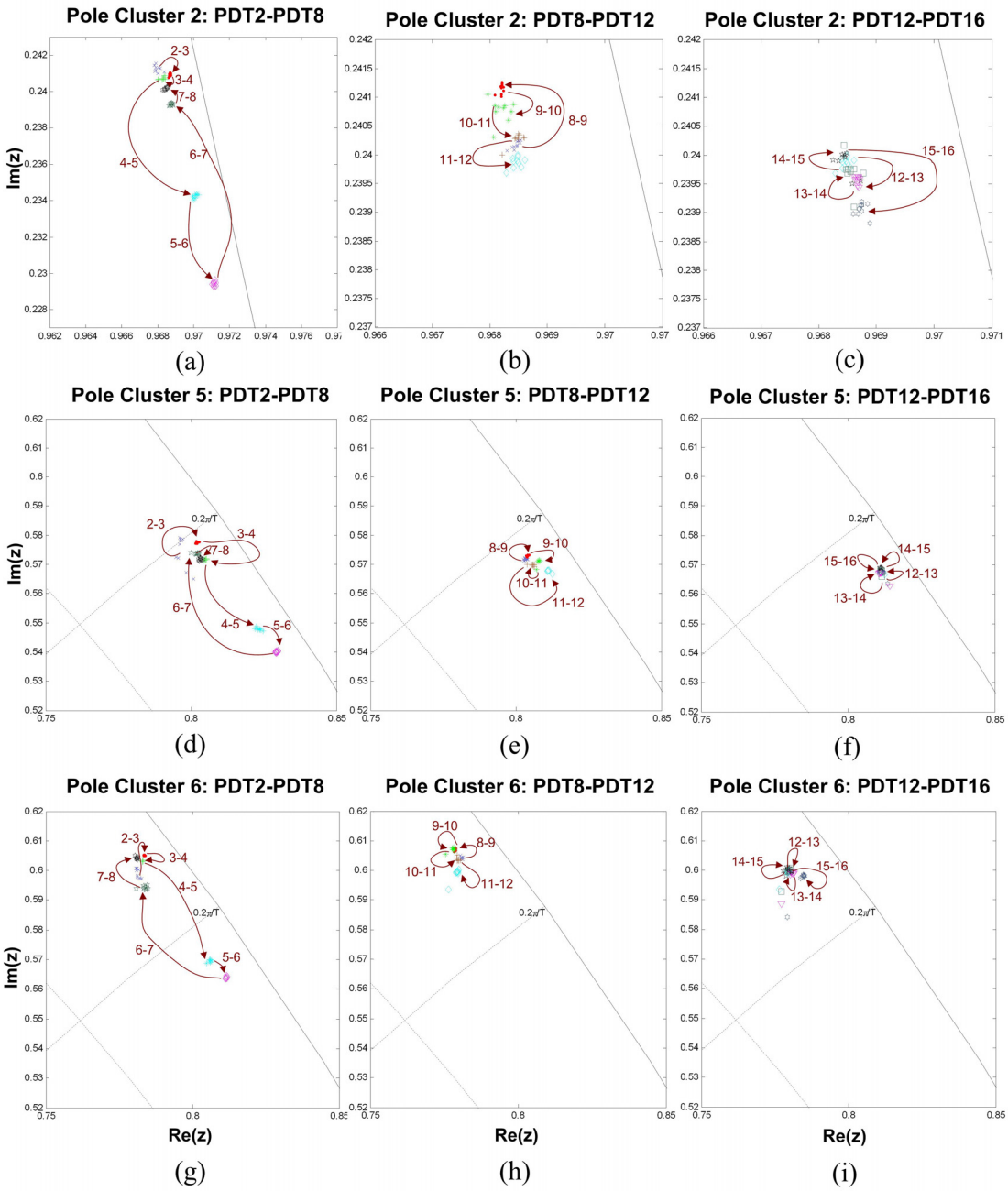


**Figure 5.9.** Sample pole clusters at Pole Cluster 2 (a-c), Pole Cluster 5 (d-f), and Pole Cluster 6 (g-i).

progressive damage tests 5 and 6 show very high damage indices indicating very high probability of damage where progressive damage tests 7 and 12 (and all subsequent tests) show elevated damage indices indicating an increased probability of damage. The

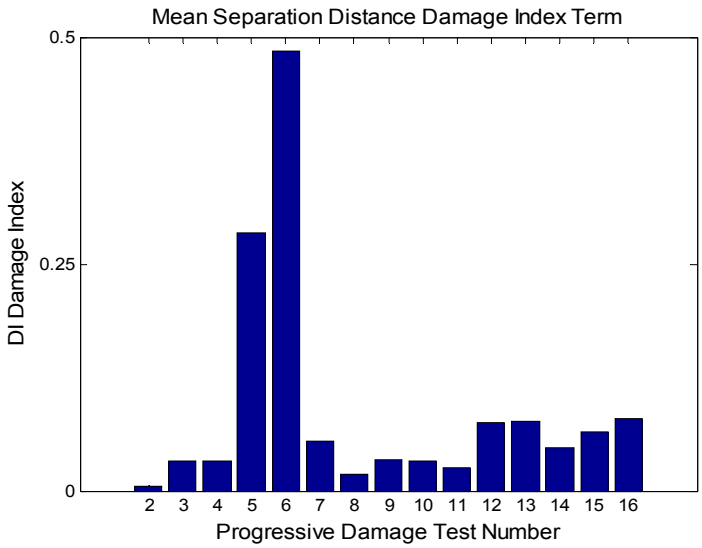


**Figure 5.10.** Z24 bridge damage index results from all damage cases.

vibrational properties of the restored pier (progressive damage test 8), as measured by the damage index, appear to be quite similar to the original baseline properties. It also appears that there is very little change in the linear behavior of the system after progressive damage test 12.

### 5.4. Six-Story Sear Structure

The test structure that is the subject of this study is a six-story, one-third scale, steel building located at the National Center for Research in Earthquake Engineering (NCREE) at National Taiwan University (NTU). The structure has a floor-to-floor height of 1.0 m, width of 1.0 m, and depth of 1.5 m. Floors are 2.0 cm thick plates supported on four sides by 5 cm x 5 cm L-sections. The L-sections are bolted to 2.5 cm x 15 cm bar columns that run continuously the entire height of the structure (Figure 5.11).

**Figure 5.11.** Six-story laboratory steel test specimen.

The structure is placed on a 5 m x 5 m, 6 degree of freedom (DOF) shaking table to simulate earthquake excitation. The structure is then instrumented with a network of 19 *Narada* wireless sensors with accelerometers attached, two on each floor measuring acceleration in the weak lateral direction of the structure, one on each floor measuring acceleration in the strong lateral direction of the structure, and one at the base measuring lateral ground motion. The base unit is configured to broadcast ground motion measurements to the rest of the network to be used as the input signal and, as such, is supplied with a permanent power supply, whereas the remote units rely on battery packs for power. A tethered data acquisition system is also installed on the structure for comparison to the wireless system results. Operation of the wireless system was done

through a laptop computer with its own CC2420 transmitter. Test runs consist of unidirectional (lateral weak direction) and bidirectional (both lateral directions) broad spectrum excitations of the structure using the shaking table. Migration of the system poles is measured through use of the migration index.

### *5.4.1. Simulation of Damage to the Six-story Structure*

To simulate damage, first the structure is stiffened. Relatively stiff chevron bracing is installed between all adjacent floors. At the bottom of each brace, stiffness elements consisting of 1.0 cm x 10.5 cm plates, loaded in their weak direction are connected between the bracing and the floor below. This stiffened structure is considered to be the baseline, or initial, undamaged structure, that the control models are to be based upon. Damage is then introduced by replacing original stiffness elements (designated B3) with weaker elements (designated B2 or B1) to simulate reduced story stiffness due to damage. Alternatively, stiffness elements may be removed altogether. B2 represents a loss of story stiffness of approximately 20% versus B3, B1 represents a loss of approximately 30%, and the removal of the stiffener represents a loss of approximately 40% versus B3. By changing stiffness in this manner, reversible simulated damage may be introduced into the structure without causing any long-term harm to an expensive test specimen. The use of reversible damage is critical for validation of structural health monitoring methods as it allows the baseline case to be repeated to assure that the damage feature extracted from the response data is correlated to damage and not just by the collection of different data or the passage of time. With this motivation in mind, damage case D1 represents the baseline case, with the strongest stiffness element

**Table 5.4.** Damage case bracing element schedule.

| FLOOR | D1 | D2 | D3 | D4 | D5 | D6 | D7 | D8 |
|---|---|---|---|---|---|---|---|---|
| 6F | B3 | B3 | B3 | B3 | B3 | B3 | B1 | B3 |
| 5F | B3 | B3 | B3 | B3 | B3 | B3 | B3 | B3 |
| 4F | B3 | B3 | B3 | B3 | B3 | Removed | Removed | Removed |
| 3F | B3 | B3 | B3 | B2 | B3 | B3 | B3 | B3 |
| 2F | B3 | B3 | B2 | B1 | B3 | B3 | B3 | B3 |
| 1F | B3 | B2 | B1 | Removed | B3 | Removed | Removed | B3 |

installed at each floor. Damage cases D2-D4 depict loss of stiffness spreading from the base upwards. For damage case D5, the strongest stiffness elements are reinstalled and the baseline case is repeated. Finally, damage cases D6-D8 represent sparse damage cases with large degrees of damage occurring at on isolated floors. Table 5.4 tabulates which braces are used in each damage case (case 1 through 5), Fig. 5.12 depicts the weak bracing elements, while Table 5.5 summarizes the size of the brace elements used.

### *5.4.2. Modeling of the Six-story Structure*

Input/output and output only models are constructed from acceleration data collected by the wireless sensors from this structure during applied uniaxial, lateral white noise table motions (scaled such that the peak acceleration amplitude is 0.5 m/s$^2$). Model order is selected from the input/output data. Multiple ARX models with equal numbers of inputs and outputs (that is $m$ is equal to $n$ in Equation 5.1) are constructed from the six-story test structure acceleration data. The poles identified by those models are compared to theoretical modes computed based on the structural properties of the specimen. A model order employing 36 poles is required to cause the lower frequency poles to converge to the theoretical values. This convergence is verified by use of a stability diagram, Figure 5.13. The poles corresponding to the lowest set of six resonant

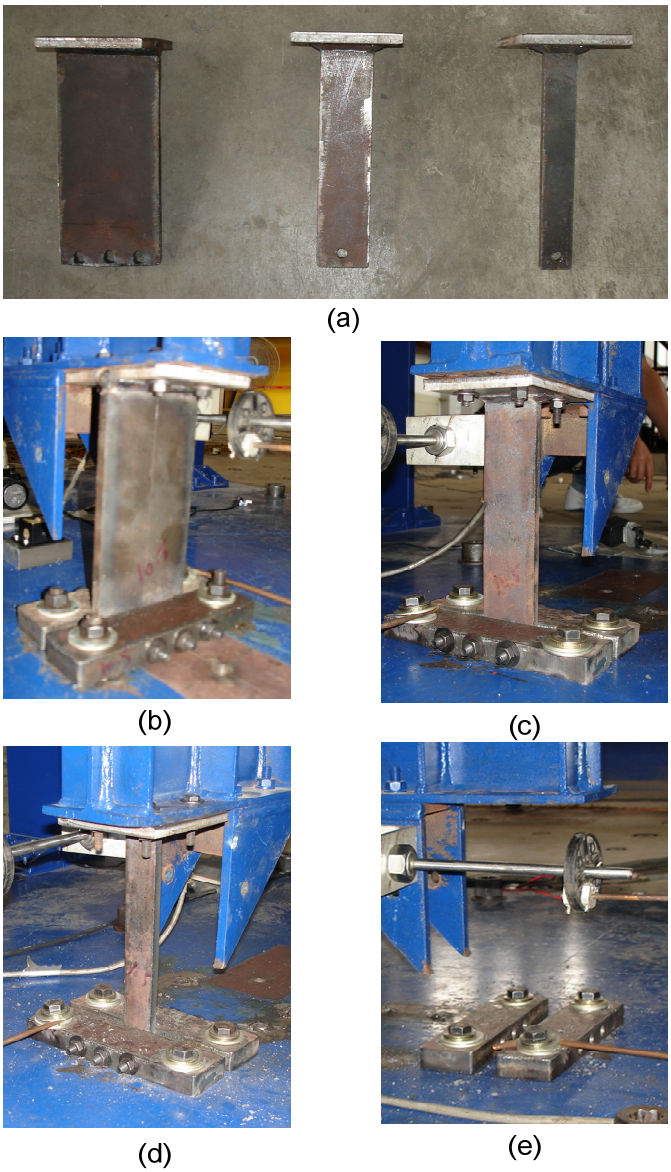


**Figure 5.12.** Bracing elements, (a) left to right, B3, B2, and B1, (b) B3 installed, (c) B2 installed, (d) B1 installed, (e) braces removed.

**Table 5.5.** Bracing description.

| | Length (cm) | Width (cm) | Thickness (cm) |
|---|---|---|---|
| Columns | 95 | 15 | 2.5 |
| Brace B1 | 21 | 3 | 1 |
| Brace B2 | 21 | 5 | 1 |
| Brace B3 | 21 | 10 | 1 |

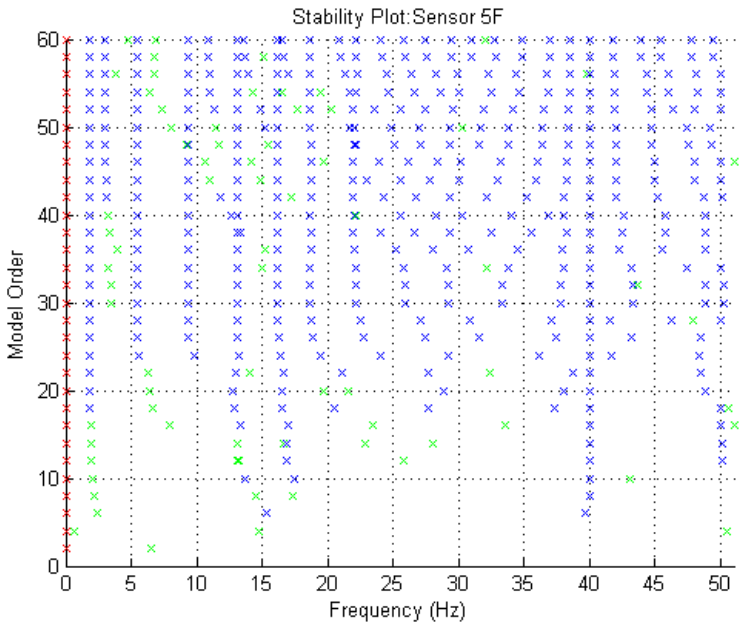


**Figure 5.13.** Stability diagram generated by the 5th floor, front sensor.

frequencies are selected (ignoring apparent poles that are mathematical artifacts of the least-squares fit process identified by unrealistically high damping ratios) for migration tracking as these poles correspond to the strong-axis lateral deflections of the structure stories, see Figure 5.14. The remaining poles are not used for health monitoring, only convergence of the time-series model. This model order is then used for the input/output model and for the lower-order ARX step of the output only model fit.

*5.4.3. Six-story Shear Structure Results*

Pole clusters are obtained from output measured at each floor for all damage cases under both input/output (ARX) and output-only (ARMA) regimens. The clusters obtained at each damage case are compared to the undamaged case, D1, via the mean

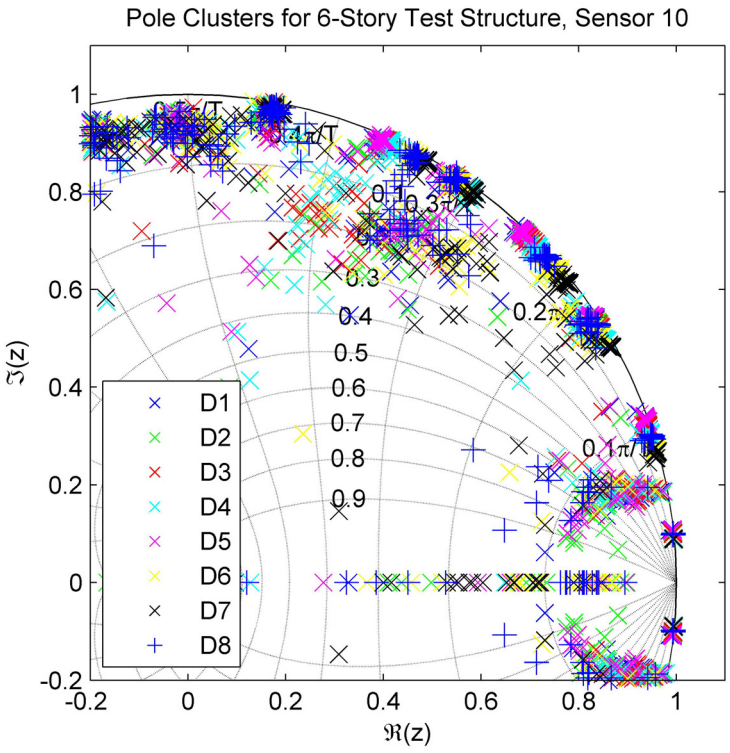


**Figure 5.14.** Identified poles in the upper right quadrant of the unit circle for damage cases 1-8.

separation distance damage index. Results from all of the sensors are then averaged, and weighted by contribution to the observability grammian (Figure 5.15). Sample pole clusters from the input/output regimen are presented in Figure 5.16 to demonstrate their migration in the z-plane. The degree of migration from the original baseline location to the test location is dependent upon the severity of the damage (loss of stiffness). Note that the cluster associated with damage case D5 returns to its original location as expected, since D5 is a repeat of the baseline case. Some poles shown in Figure 5.16 appear to be poorly fit and lie relatively far outside of their pole cluster. These discrepancies are due to inadequate excitation during data measurement, transient

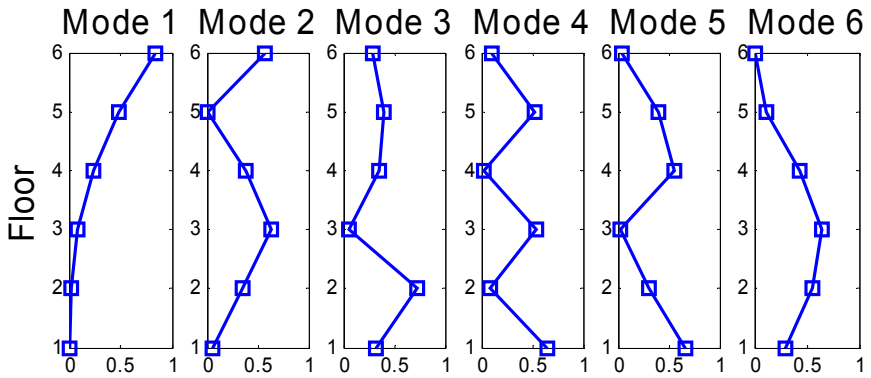


**Figure 5.15.** Modal grammian weighting factors for damage index aggregation.

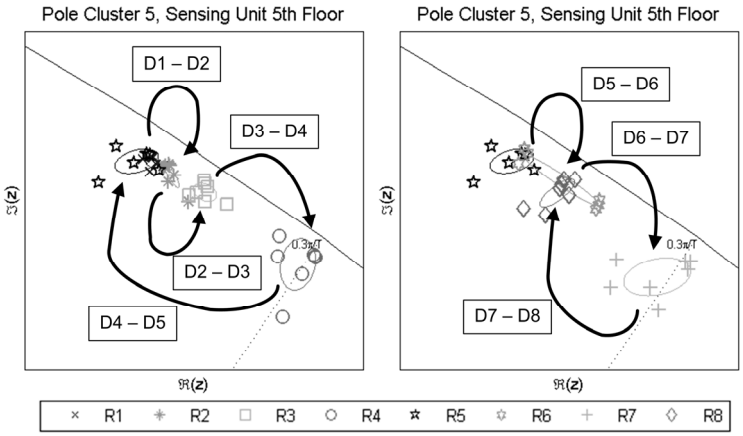


**Figure 5.16.** Pole migration of pole cluster 5 measured by the 5th floor sensing unit; left: damage cases D1-D5; right: damage cases D5-D8.

numerical issues in the algorithm, or sorting errors, all of which are relatively rare. The inherent redundancy of the health monitoring method, namely taking results from multiple data runs, multiple modes, and multiple sensors, helps to mitigate the effects of these errors so that the final damage index reported by the network is accurate. For this study, the average damage indicies reported by the network reflect well the level of damage inflicted upon the structure. The damage indicies for the input/output case are presented in Figure 5.17(a), and those of the output-only case are presented in Figure

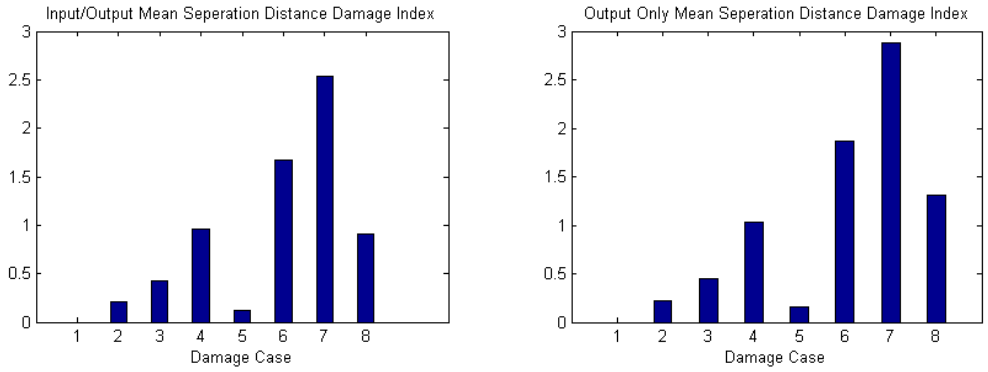


(a) (b)

**Figure 5.17.** Network-level damage indices; (a) input/output identification; (b) output-only identification.

5.17(b). Both the input/output and output-only cases return elevated damage index levels in the presence of damage, though the output-only method does so at the expense of the extra computation step fitting the ARMA model.

## 5.5. Structural Health Monitoring Conclusions

This chapter presents a simple set of algorithms for health monitoring of civil structures that is suitable for distributed implementation within a wireless sensing network and which provides physical meaningful interpretation (based on the observability grammian) to explain differing damage estimates realized from different nodes within the wireless sensor network. This method takes full advantage of the distributed computing power available within a wireless network without requiring the power and bandwidth intensive centralization and transmission of raw data from the sensor data nodes. The wireless nodes are free to do most of their computations independently of the network and only conferring to produce the final damage index value that would potentially trigger the alarm. Basing the damage detection algorithm on

the locations of system poles in the z-plane gives the network information about not only changes in frequency, but also damping of the monitored structure. By taking into account both the input and the output of the system, variability in the pole locations due to inconsistent excitation can be significantly reduced over output-only or ambient monitoring methods. If output-only is necessary, the two step ARMA model can significantly reduce variability in the identified model parameters due to inconsistent excitation.

The method is successfully applied to two validation structures: the Z24 bridge data set and a six-story laboratory steel structure. On the Z24 bridge data set, a high-order ARX model (60 poles and 60 zeros) produces poles that are consistent enough that an automated sorting algorithm can properly form pole clusters for the first 12 modal frequencies that are the basis of the health monitoring algorithm. The method is found to be effective in detecting damage due to large settlement of the pier (progressive damage tests 5 and 6) with the restored pier pole locations returning to their baseline locations (progressive damage test 8), as well as concrete hinge failure (progressive damage test 12). Detection of progressive damage tests that had little impact on stiffness and damping proved to be more challenging. The method could be tested using the *Narada* wireless sensor on the six-story laboratory steel structure. There, simulated damage in the form of replaceable weak stiffness elements could be easily detected by the method and the relative degree of damage identified. Because the method relies on global properties of the system, localization of damage is also an ongoing effort. Also, incorporation of correction factors for environmental variability (*e.g.*, temperature and humidity effects) is a necessary future step for practical implementation.

While this method is not intended as a replacement for hands-on inspection techniques or sound engineering judgment, it can provide autonomous early warnings for damage that affects dynamic performance. The method is based on global modes of the structure and is effective in identifying relatively severe damage that would be associated with extreme loading events (*e.g.*, large earthquakes). Further work in application of the method to local modes (*e.g.*, Lamb or Rayleigh wave modes) is necessary to detect more subtle and localized damage. Ultimately, a hybrid global/local damage detection scheme would provide maximum coverage of the entirety of the structure as well as maximum sensitivity to structural damage. Potentially, a structure may be characterized by both closely spaced modes and very large migration of poles due to the effects of damage, and the automated pole sorting algorithm is likely to return excessive errors that may have unpredictable effects on the damage estimate returned by sensors within the network.

To minimize the effect of unusual transient loading conditions, as well as data and sorting errors, this method combines and averages results from multiple sensors to increase its reliability and reduce the frequency of false alarms. By assigning very low weights to results derived from sensor/mode combinations that are characterized by poor excitation, the effect of low sensitivity damage information on the final network-level damage estimate is minimized. With its embedded computation of system poles, the method could also be used to update feedback control algorithms such as that proposed in the following chapter. Finally, future work to bring this structural health monitoring method into an adaptive control paradigm would be very productive and will be discussed further in *Chapter 7, Conclusions and Future Trends*.

# CHAPTER 6

## STRATEGIC NETWORK UTILIZATION IN A WIRELESS STRUCTURAL CONTROL SYSTEM FOR SEISMICALLY EXCITED STRUCTURES

The benefits associated with structural control include the mitigation of undesired structural responses and reduction in the probability of damage to structural components during seismic events. Structural control systems in current use depend on extensive wired communication systems to connect sensors and actuators with a centralized controller. While wired architectures are appropriate when control systems are small, the cost and installation complexity of tethered systems increases as the control system grows large (*i.e.*, defined by hundreds of nodes). Alternatively, wireless sensors are proposed for use in large-scale structural control systems to keep costs low and to improve system scalability. Wireless sensors are capable of collecting state data from sensors, communicating data between themselves, calculating control actions, and commanding actuators in a control system. However, bandwidth and range limitations of the wireless communication channel render traditional centralized control solutions impractical for the wireless setting. While computational abilities embedded with each wireless sensor permit fully-decentralized control architectures to be implemented, strategic utilization of

the wireless channel can improve the performance of the wireless control system. Towards this end, this chapter presents a partially-decentralized linear quadratic regulation control scheme that employs redundant state estimation as a means of minimizing the need for the communication of state data between sensors. The method is validated using numerical simulations of a seismically excited six-story building model with ideal actuators. Additional experimental validation is conducted using a full-scale physical realization of the six-story building. A wireless sensor network commanding magnetorheological (MR) dampers is shown to be effective in controlling a multi-story structure using the partially decentralized control architecture proposed.

## 6.1. Wireless Control Introduction

While it has been shown that structural control systems can be effective in mitigating the dynamic response of large-scale structures (Soong 1990; Housner, *et al.* 1997; Spencer and Nagarajaiah 2003), system costs and long-term reliability concerns still remain as barriers to widespread adoption of such systems. Semi-active structural control devices have recently been developed to address these cost and reliability concerns. Compared to large active actuators, semi-active structural control devices such as magnetrorheological (MR) dampers (Dyke, *et al.* 1998; Hatada, *et al.* 2000; Gavin, *et al.* 2001), electrorheological (ER) dampers (McMahon and Makris 1997), variable-orifice dampers (Kurino, *et al.* 2003), and variable-stiffness devices (Nagarajaiah and Mate 1998) are relatively inexpensive to design and fabricate, require little power, and can be powered from battery power supplies (Kurata, *et al.* 1999).

Semi-active control systems have been successfully deployed in numerous structural applications (Spencer and Nagarajaiah 2003; Kajima-Corporation 2006). The forces achievable with these semi-active devices are smaller in magnitude than those achievable by an active device (*e.g.,* active mass damper). However, a highly effective control system can be produced when a large number of semi-active devices are installed in a single structure. Recently completed structures employing semi-active control technology include the 54-story Mori Tower employing 356 semi-active hydraulic dampers (SHD), the 38-story Nihonbashi Mitsui Tower employing 96 SHD, and the Shiodome Tower, employing 88 SHD, all located in Tokyo, Japan (Kajima Corporation 2006). As the number of control devices increases, the vulnerability of the control system as an entity to the failure of a single control device is reduced.

Use of semi-active control devices in a centralized control system may not be a complete solution to the aforementioned cost and reliability problems often associated with structural control. While semi-active devices are less costly than active actuators, as the number of control devices grows, the cost savings realized by use of semi-active devices quickly erodes due to the high cost of the extensive wiring needed between sensors, actuators, and controllers. Additionally, centralized computation of command forces requires a central computer to collect data, calculate control forces, and command actuators in a short time frame; these calculations get more difficult to complete in the allocated time as the system grows. One solution to these two problems is achieved in Kajima Corporation's HiDAX system which is a fully-decentralized control system; SHD devices are distributed throughout a structure to independently provide control forces between consecutive floors (Kajima Corporation 2006). No communication is offered

between SHD devices with each device calculating a control action based solely on its collocated sensor output. The actions of these controllers are derived globally, but in operation they act independently, not sharing data.

Improving coordination between distributed controllers would obviously improve the results their use yields. Wireless sensors have been successfully employed for monitoring civil structures (Lynch*, et al.* 2004; Lynch and Loh 2006). Wireless sensors can be installed without the expense of cable installation, providing a low cost link between distributed elements of the monitoring system. Wireless sensors with embedded computational power are able to perform on-board data interrogation, eliminating the need to transmit raw data to centralized servers (Straser and Kiremidjian 1998). Recent work has demonstrated the ability of wireless sensors to act as active sensors (Chintalapudi*, et al.* 2005) and controllers (Kawka and Alleyne 2004). As controllers, wireless sensors are responsible for collecting sensor data, calculating desired control forces, and commanding actuators for centralized (Wang*, et al.* 2006a; Loh*, et al.* 2007) and decentralized (Wang*, et al.* 2006b; Lin*, et al.* 2007; Loh*, et al.* 2007) control architectures.

Wireless control systems, have inherent limitations that prevent them from functioning as perfect replacements for cable-based control systems. For example, wireless data transmissions add latency, thereby reducing sampling frequencies and the overall effectiveness of the controller. Another concern is data loss. Self-acknowledging protocols for data transmission (*e.g.,* TCP/IP) guarantee data transmission but also introduce additional delay. Several established transmission protocols used in real-time wireless feedback control, including polling, time division multiple access (TDMA),

random access (RA) with and without acknowledgement, and carrier sensing multiple access/collision avoidance (CSMA/CA), have been evaluated (Liu and Goldsmith 2004). Wireless feedback schemes using the IEEE 802.11b protocol are proposed with sample rate adaptation used to overcome the effects of communication latency (Colandairaj*, et al.* 2007). However, this approach introduces random, lengthy delays into the communications. Network protocols without acknowledgement (*e.g.,* UDP) can eliminate this source of latency entirely, but require a control algorithm that is tolerant of data loss (Ploplys*, et al.* 2004). Another functional constraint of wireless communications is that the available communication bandwidth is fixed (Arms*, et al.* 2004). In large control systems, care must therefore be taken not to exceed the channel capacity. The range of the wireless signal is also limited. Finally, wireless communication is power-intensive. Especially for battery powered wireless sensors, wireless radios have greater power requirements than any other hardware component (Lynch and Loh 2006; Nagayama*, et al.* 2007).

To overcome these wireless sensor limitations, a partially-distributed control scheme is proposed that is tolerant of data loss and in which the available wireless bandwidth is strategically leveraged to improve control performance. The proposed system is an adaptation of a partially-distributed control scheme developed for networked control by Yook *et al*. (2002). In it, wireless sensors with actuation capabilities (*i.e*., Narada units) are responsible both for collecting sensor output and supplying actuator commands based on linear quadratic regulation. In addition, each are embedded with identical estimators, in this case, steady-state Kalman estimators. The resulting state estimates are compared to locally available measured data and used for feedback control force computation when

errors between measured and estimated state data are small. Only when the error exceeds a threshold value specified by the designer are the measured values wirelessly transmitted to the network of sensors, allowing other sensors to update their own estimates. Detailed derivation of the method is presented in the following section followed by a review of wireless sensing for civil infrastructure. Then, results from simulations and an experimental study using *Narada* wireless sensor units to control and actuate MR dampers for seismic disturbance rejection in a six-story building model are presented and discussed.

### 6.2. Redundant Estimator Network Control Architecture

As opposed to traditional centralized systems (Figure 6.1(a)) where system outputs are communicated to a single controller for formulation of control actions, a wireless control system is assembled from a network of wireless sensors that serve as a coordinated set of distributed controllers. Each wireless sensor is responsible for measuring system outputs, calculating control actions, and issuing command signals to actuators. The resulting architecture (Figure 6.1(b)) differs significantly from the centralized approach in that: (1) the centralized controller is abandoned for an architecture in which each actuator has its own controller (*i.e.*, a wireless sensor); and (2) the dedicated wired communication system is replaced by a flexible wireless communication channel.

There are challenges associated with real-time control on a wireless network including power consumption (Lynch and Loh 2006) and fixed bandwidth (Arms*, et al.* 2004). One possible approach to addressing these limitations is to fully decentralize the

control system by eliminating the communication between controllers. Such an approach has proven effective for semi-active hydraulic dampers deployed in large civil structures (Kurino*, et al.* 2003). However, decentralization does not take advantage of the benefits offered by communication between controllers. Alternatively, a centralized control system can be replicated upon a wireless control system by forcing all wireless sensors to broadcast their measurements at every time step. Unfortunately, this approach places a hefty demand on the available communication bandwidth; hence, the approach is not scalable for large wireless sensor networks. Past work in wireless structural control reveals low-sample rates are required to ensure reliable data delivery when implementing a centralized wireless control system (Lynch*, et al.* 2008).

A partially-decentralized distributed control algorithm is proposed to achieve an optimal compromise between the decentralized and centralized control approaches. The benefits associated with data exchange between wireless sensors are preserved, while use of the communication channel is minimized both to keep channel performance high and power demands at the individual sensors low. A redundant estimation framework first proposed by Yook, *et al*. (2002) for networked control systems is adopted. As shown in Figure 6.1(b), each wireless sensor employs a Kalman filter to estimate the full state response, $\bar{\mathbf{z}}$, based upon the measured system output, $y_i$, at the sensor's degree-of-freedom. If the control system is decentralized, the state estimate would be used to calculate the control action, $u_i$. In contrast, the redundant estimation framework proposed herein compares the estimated, $\bar{y}$, and measured output, $y$, to quantify the error inherent in the estimator. If the estimated state variable at the $i^{th}$ measurement degree-of-freedom is inaccurate, then the estimators executed at the other degrees-of-freedom (that are

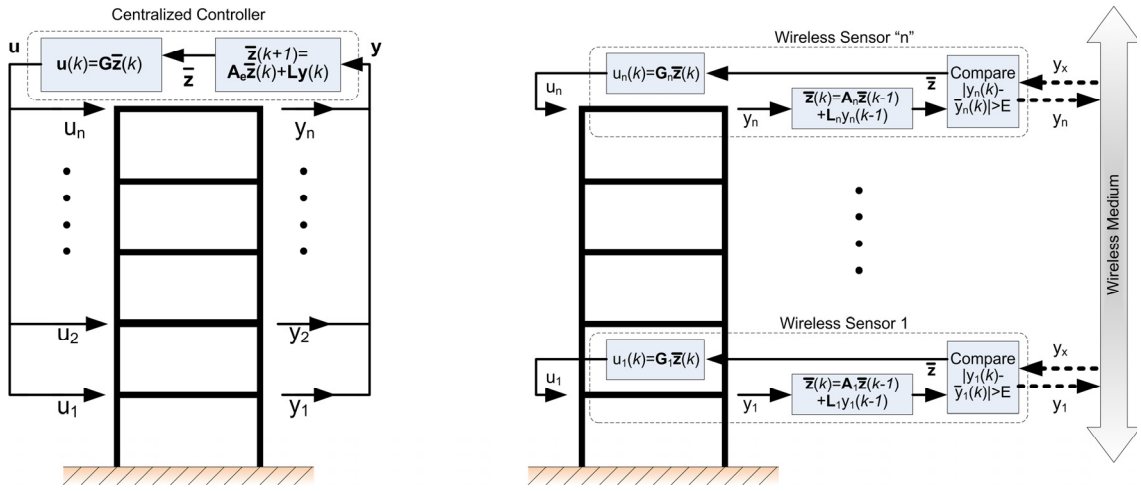


(a) (b)

**Figure 6.1.** (a) Classical centralized controller approach to structural control; (b) proposed distributed control system assembled from a network of wireless sensors serving as controllers.

derived from the same model) will also have inaccurate estimates of the $i^{th}$ degree-of-freedom's state variables. If the error is above a threshold, the $i^{th}$ wireless sensor broadcasts the measured state variables. Upon receipt of the true measured output from the $i^{th}$ degree-of-freedom, the other wireless sensors update their estimated states before calculating the control force to be applied. In essence, wireless bandwidth is strategically leveraged to improve decentralized control performance as is described in the following sections.

### *6.2.1. State-Space System Model*

The base-excited structural system is modeled in continuous-time as an $n$-degree-of-freedom (DOF) linear time-invariant, lumped mass shear structure whose equation of motion is:

$$\mathbf{M}\ddot{\mathbf{x}}(t)+\mathbf{C_d}\dot{\mathbf{x}}(t)+\mathbf{K}\mathbf{x}(t)=-\mathbf{M}\boldsymbol{\ell}\ddot{x}_g(t)+\mathbf{L}\mathbf{u}(t) \tag{6.1}$$

with $\mathbf{M}$, $\mathbf{C_d}$, and $\mathbf{K} \in \mathbf{R}^{n\text{x}n}$ corresponding to the mass, damping, and stiffness matrices, respectively. The displacement vector relative to the base of the structure is $\mathbf{x} \in \mathbf{R}^{n\text{x}1}$, ground displacement is $x_g$, and $\boldsymbol{\ell} \in \mathbf{R}^{n\text{x}1}$ is a vector in which each term is unitary. If control forces, $\mathbf{u} \in \mathbf{R}^{m\text{x}1}$, are applied to the system then the actuator locations are described by the location matrix, $\mathbf{L} \in \mathbf{R}^{n\text{x}m}$. The variable $t$ represents continuous time.

The equation of dynamic equilibrium described by Equation 6.1 can be reformulated in state-space as

$$\dot{\mathbf{z}}(t)=\mathbf{A}\mathbf{z}(t)+\mathbf{B}\mathbf{u}(t)+\mathbf{E}\ddot{x}_g(t) \tag{6.2}$$

where the state is $\mathbf{z}^{\mathrm{T}} = \{\mathbf{x}^{\mathrm{T}}\ \dot{\mathbf{x}}^{\mathrm{T}}\} \in \mathbf{R}^{2n\text{x}1}$ and

$$\mathbf{A}=\begin{bmatrix}\mathbf{0} & \mathbf{I}\\ -\mathbf{M}^{-1}\mathbf{K} & -\mathbf{M}^{-1}\mathbf{C_d}\end{bmatrix}\in\mathbf{R}^{2n\text{x}2n},$$

$$\mathbf{B}=\begin{bmatrix}\mathbf{0}\\ \mathbf{M}^{-1}\mathbf{L}\end{bmatrix}\in\mathbf{R}^{2n\text{x}m},\quad \mathbf{E}=\begin{bmatrix}\mathbf{0}\\ -\boldsymbol{\ell}\end{bmatrix}\in\mathbf{R}^{2n\text{x}1}$$

With sensors installed in the structure, the measurable system output, $\mathbf{y} \in \mathbf{R}^{p\text{x}1}$, is represented by a linear sum of the state of the system and the applied control forces:

$$\mathbf{y}(t)=\mathbf{C}\mathbf{z}(t)+\mathbf{D}\mathbf{u}(t)+\mathbf{F}\ddot{x}_g(t) \tag{6.3}$$

with $\mathbf{C} \in \mathbf{R}^{p\text{x}2n}$, $\mathbf{D} \in \mathbf{R}^{p\text{x}m}$, and $\mathbf{F} \in \mathbf{R}^{p\text{x}1}$.

Before a digital control system can be implemented, the continuous-time state-space model (Equation 6.2) is converted into the discrete-time domain with time step $T_s$ using the zero order hold (ZOH) discretization method (Franklin*, et al.* 2002):

$$\mathbf{z}(k+1)=\boldsymbol{\Phi}\mathbf{z}(k)+\boldsymbol{\Gamma}\mathbf{u}(k)+\boldsymbol{\Lambda}\ddot{x}_g(k) \tag{6.4}$$

where

$$\mathbf{\Phi} = e^{\mathbf{A}T_S} \in \mathbf{R}^{2nx2n},$$

$$\mathbf{\Gamma} = \left(\int_0^{T_S} e^{\mathbf{A}\tau} d\tau\right)\mathbf{B} \in \mathbf{R}^{2nxm}, \quad \mathbf{\Lambda} = \left(\int_0^{T_S} e^{\mathbf{A}\tau} d\tau\right)\mathbf{E} \in \mathbf{R}^{2nx1}$$

*6.2.2. Optimal LQR Control*

The linear quadratic regulation (LQR) control strategy is widely employed in the structural control field because it offers an optimal control solution minimizing the response of the structure, **y**, while simultaneously minimizing control effort. The LQR control solution determines the optimal control force trajectory, **u**, by minimizing the scalar cost function, *J*:

$$J(\mathbf{u}) = \sum_{k=1}^{\infty}\left(\mathbf{z}^T(k)\mathbf{Q}_1\mathbf{z}(k) + \mathbf{u}^T(k)\mathbf{Q}_2\mathbf{u}(k)\right) \tag{6.5}$$

where $\mathbf{Q}_1$ is equal to $\mathbf{C_{LQR}}^{\mathrm{T}}\mathbf{C_{LQR}}$, $\mathbf{C_{LQR}}$ being a linear mapping between the state and a response to be regulated ($\tilde{\mathbf{y}} = \mathbf{C_{LQR}}\mathbf{z}$), and $\mathbf{Q}_2 \in \mathbf{R}^{pxp}$ is a symmetric positive definite matrix that weighs the relative importance of control effort against the structure output. The matrices $\mathbf{Q}_1$ and $\mathbf{Q}_2$ are often termed the state cost matrix and input cost matrix, respectively (Franklin, *et al.* 2002).

To ensure the optimal control trajectory is physically feasible, minimization of the LQR cost function is constrained by Equation 6.4 through the use of Lagrangian multipliers (Stengle 1994). The full derivation of the LQR control law may be found in any standard control text, *e.g.,* (Bryson and Ho 1975). The resulting linear control law is:

$$\mathbf{u}(k) = \left[\left[\mathbf{Q}_2 + \mathbf{\Gamma}^T\mathbf{P}\mathbf{\Gamma}\right]^{-1}\mathbf{\Gamma}^T\mathbf{P}\mathbf{\Phi}\right]\mathbf{z}(k) = \mathbf{G}\mathbf{z}(k) \tag{6.6}$$

with $\mathbf{G} \in \mathbf{R}^{m\text{x}2n}$, the linear gain matrix, and the Riccati matrix, $\mathbf{P} \in \mathbf{R}^{2n\text{x}2n}$, derived from the solution to the algebraic Riccati equation:

$$\mathbf{P} = \mathbf{\Phi}^T \left[ \mathbf{P} - \mathbf{P\Gamma} \left[ \mathbf{Q}_2 + \mathbf{\Gamma}^T \mathbf{P\Gamma} \right]^{-1} \mathbf{\Gamma}^T \mathbf{P} \right] \mathbf{\Phi} + \mathbf{Q}_1 \tag{6.7}$$

*6.2.3. Kalman State Estimation*

To calculate the optimal control forces using the LQR control law proposed in Equation 6.6, the entire state vector, $\mathbf{z}(k)$, is needed at each time step. For most structural control systems, measurement of the complete state of the system is not an economical option. Rather, the measured output of the structure, $\mathbf{y}(k)$, is communicated to a centralized controller where an estimator is implemented for estimation of the state, $\hat{\mathbf{z}}$. Amongst the many methods available for state estimation, Kalman filtering is the most widely implemented by the structural control community (Soong 1990; Chu*, et al.* 2005).

The Kalman estimator assumes the structure is disturbed at its base by the broad-band excitation, $w(k)$, with a zero mean and covariance of $R_w$.

$$\mathbf{z}(k+1) = \mathbf{\Phi z}(k) + \mathbf{\Gamma u}(k) + \mathbf{\Lambda} w(k) \tag{6.8}$$

Furthermore, the output measurement of the system is corrupted by white noise, $\mathbf{v}(k) \in \mathbf{R}^{p\text{x}1}$ with covariance, $\mathbf{R}_\text{v} \in \mathbf{R}^{p\text{x}p}$:

$$\mathbf{y}(k) = \mathbf{C}\mathbf{z}(k) + \mathbf{v}(k) \tag{6.9}$$

The estimation problem seeks to minimize the state estimation error covariance, $\mathbf{P}_\mathbf{e}$:

$$\mathbf{P}_\mathbf{e} = \lim_{t \to \infty} \left[ (\mathbf{z} - \hat{\mathbf{z}})(\mathbf{z} - \hat{\mathbf{z}})^T \right] \in \mathbf{R}^{2n\text{x}2n} \tag{6.10}$$

First, given an estimate of the state at the last time step, $\hat{\mathbf{z}}(k\text{-}1)$, the state at the current time step can be predicted:

$$\bar{\mathbf{z}}(k) = \mathbf{\Phi}\hat{\mathbf{z}}(k-1) + \mathbf{\Gamma}\mathbf{u}(k-1) \tag{6.11}$$

However, the estimate can be improved by taking into account the measurement error at the current step:

$$\hat{\mathbf{z}}(k) = \bar{\mathbf{z}}(k) + \mathbf{L}(k)(\mathbf{y}(k) - \mathbf{C}\bar{\mathbf{z}}(k)) \tag{6.12}$$

The estimator gain matrix, $\mathbf{L}(k) \in \mathbf{R}^{2nxp}$, is intended to minimize the error inherent to state estimation by considering the error in the measurement. The estimator gain is time variant but will settle to a steady state value over the course of the control system execution (Franklin*, et al.* 2002). As a result, the steady state estimator gain is implemented in most control systems to keep the implementation of the Kalman filter simple. Derivation of the steady-state estimator gain matrix mimics that of the linear quadratic regulator with a nonlinear Riccati equation recursively solved for the steady-state error covariance, $\mathbf{P_e}$.

### *6.2.4. Redundant Estimation and State Recovery*

An independent Kalman estimator is designed for each degree-of-freedom of the system as shown in Figure 6.1(b). To ensure the estimation states are identical across the system, the same model of the system (**Γ, Φ**, and **Λ**), disturbance covariance, $R_w$ and noise covariance, $R_v$, are employed in deriving each Kalman estimator. The only difference in the derivations is the output matrix, **C**, that is uniquely defined for each degree-of-freedom.

With an estimator embedded in each wireless sensor, the sensors can locally calculate a control force, $u$, based upon their state estimate, $\bar{\mathbf{z}}$. Should a pure decentralized architecture be adopted, the control system performance would be limited by the quality of the estimator. Hence, the performance of the decentralized control system can be improved if the wireless communication channel is utilized. In the redundant estimator framework, state recovery is proposed as a mechanism by which estimator performance can be improved without placing a hefty burden on the wireless channel (Yook*, et al.* 2002).

State recovery consists of estimators exchanging measurement data when estimation errors are large. Each estimator in the control system compares its locally measured system output, $\mathbf{y}_i$, to that estimated, $\bar{\mathbf{y}}_i$, where:

$$\bar{\mathbf{y}}_i(k) = \mathbf{C}_i \bar{\mathbf{z}}(k) \tag{6.13}$$

The error between the measured and estimated state response is defined as:

$$\mathbf{E} = \bar{\mathbf{y}}_i - \mathbf{y}_i \tag{6.14}$$

where $\mathbf{E} \in \mathbf{R}^{p\text{x}1}$. Should the error exceed a predefined threshold, then the wireless sensor replaces the estimated state variables with those measured. Additionally, the measurement is transmitted to the wireless sensor network, thus allowing other estimators to "recover" the accurate (*i.e.,* measured) state value. In this manner, state estimates are synchronized throughout the wireless network to be within an allowable error range. State recovery allows a wirelessly networked control system to attain a higher level of performance compared to a purely decentralized system in which controllers do not communicate.

For example, the estimator at the $i^{th}$ degree-of-freedom makes an estimate based on the measured output of the system:

$$\mathbf{y}_i = \{x_i \quad \dot{x}_i\}^T \tag{6.15}$$

Using this measurement, an estimate for the full state is made using Equations 6.11 and (6.12). The estimator then compares the estimate $\bar{\mathbf{y}}_i$, to the measured system output, $\mathbf{y}_i$. If the difference is greater than the established error bound, $H$:

$$\begin{aligned} &\text{Transmit } x_i \text{ if } \bar{x}_i - x_i > H_d \\ &\text{Transmit } \dot{x}_i \text{ if } \bar{\dot{x}}_i - \dot{x}_i > H_v \end{aligned} \tag{6.16}$$

After transmission, the updated state vector, $\bar{\mathbf{z}}^*$, at each degree-of-freedom in the system becomes:

$$\bar{\mathbf{z}}^* = \{\bar{x}_1 \ \cdots \ \bar{x}_{i-1} \ \ x_i \ \ \bar{x}_{i+1} \ \cdots \ \bar{x}_n \ \ \bar{\dot{x}}_1 \ \cdots \ \bar{\dot{x}}_{i-1} \ \ \dot{x}_i \ \ \bar{\dot{x}}_{i+1} \ \cdots \ \bar{\dot{x}}_n\}^T \tag{6.17}$$

The calculation of the control force is then $u_i = \mathbf{G}_i \bar{\mathbf{z}}^*$ where $\mathbf{G}_i \in \mathbf{R}^{1x2n}$ is the $i^{th}$ row of the global LQR gain matrix, $\mathbf{G}$.

The difference between the true state response and the updated state estimate can be expressed:

$$\bar{\mathbf{z}}^* = \mathbf{z} + \mathbf{e} \tag{6.18}$$

where

$$\mathbf{e} = \{e_1 \ \cdots \ e_{i-1} \ \ 0 \ \ e_{i+1} \ \cdots \ e_n \ \ \dot{e}_1 \ \cdots \ \dot{e}_{i-1} \ \ 0 \ \ \dot{e}_{i+1} \ \cdots \ \dot{e}_n\}^T \tag{6.19}$$

Each term of the vector represents the error between the estimated and true state variable; however, if the estimate is updated by the state recovery algorithm, then the corresponding error is zero. Through state recovery, the error inherent to the estimator is

bounded by the threshold vector, **H**. Hence, the calculated control force vector for the global system, **u**, is:

$$\mathbf{u} = \mathbf{G}\bar{\mathbf{z}}^{*} = \mathbf{Gz} + \mathbf{Ge} \tag{6.20}$$

In essence, the estimation error amplified by the feedback gain represents a bounded disturbance on the control force with the bound dictated by the thresholds, *H*, used (Yook*, et al.* 2002).

### 6.3. Operating System Requirements for Wireless Control Applications

For maximum flexibility, a multi-threaded operating system (OS) and application software were developed. A fully functional physical (PHY) layer, controlling physical parameters of the radio (channel selection, unit and network identification, and modulation of data on the carrier frequency), and medium access control (MAC) layer, defining timing and access to wireless communications, were written to conform to the IEEE 802.15.4 wireless communication standard. For structural control applications, the IEEE 802.15.4 MAC layer introduces excessive latency, requiring up to 16 ms per data transmission. A simplified, though less adaptable, MAC layer is developed for this study using an unacknowledged TDMA communication scheme to keep data transmission times below 2 ms. In total, the calculations of state vector estimates, determination of control forces, and the transmission of state data (when necessary) occurs within 33 ms. As will be shown, clock drift and jitter during the course of the test occasionally disrupt the TDMA scheme leading to randomly lost packets, most especially when demand for the available bandwidth is high. Finally, taking advantage of the multi-threaded OS, the

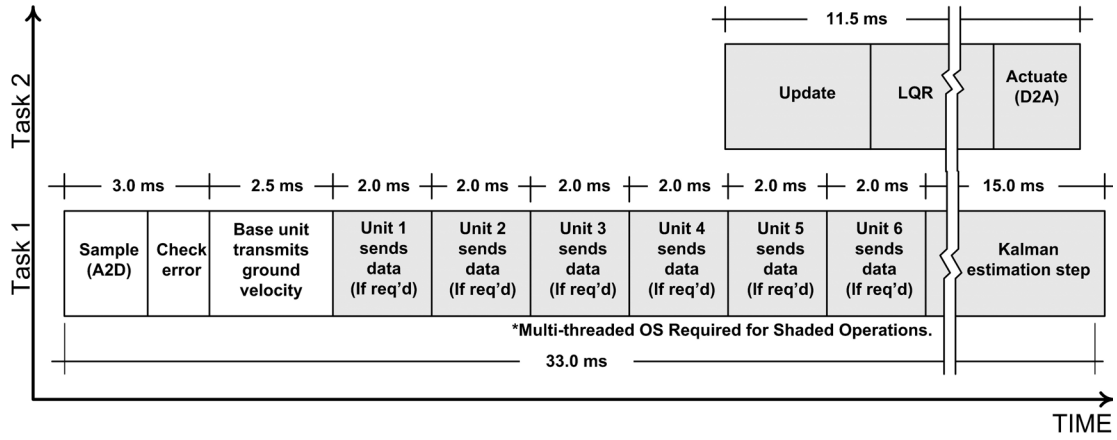


**Figure 6.2.** Typical wireless sensor operation during each time step of the discrete-time control system.

desired control force can be calculated as the unit is in communication with the wireless sensor network. The timing of a typical control step is presented in Figure 6.2.

### 6.4. Verification of the Control Strategy

The structure (Figure 6.3) that is the subject of both the simulation and experimental phases of this study is a partial scale, single-bay, six-story building. The floor height is 1.0 m per story and the bays are 1.0 m wide by 1.5 m deep. The columns are 15 cm x 2.5 cm rectangular steel sections oriented in their flexurally weak direction. Steel floor plates are 2 cm thick and are supported on four sides by 0.5 cm thick L-section beams with equal 5 cm legs. The floor plates are connected to the beams by means of welded connections while the beams are connected to the columns via bolted connections. Wide flange H100x100x6x8 steel section V-braces are provided as the connection points for the MR dampers (Figure 6.4) installed on every floor of the structure. The damping coefficient of the MR dampers varies with input current. As the current changes, the

resulting magnetic field aligns ferrous particles suspended in a viscous fluid within the damper. A stronger magnetic field results in stronger particle alignment yielding higher damping ratios. The hysteretic, bi-linear, bi-viscous MR damper model in this study was developed by Lin, *et al*. (2005). The MR damper employed (Lord Corp. RD-1005-3) saturates at ±2.0 kN, has a 20 mm stroke, an input range of 0 to 2 A, and is powered by an independent 24 V power supply.

Each actuator has an associated *Narada* wireless sensor; the wireless sensor measures the lateral response of the structure using Tokyo Sokushin VSE-15D velocity meters. The VSE-15 has a sensitivity constant of 10 V/(m/s) and voltage output between ±10 V. Its maximum measurable velocity is 1 m/s within a 0.1 to 70 Hz frequency band. A signal conditioning circuit shifts the mean from 0 V to 2.5 V and de-amplifies the sensitivity by a factor of 4 such that the velocity meters output is within the input range (0-5 V) of the wireless sensor's ADC. An additional wireless sensor is located on the table to measure and broadcast the reference (ground) motion to the network. Wireless sensors are used to calculate control forces and to command the MR dampers with voltage outputs ranging from 0 to 0.8 V. The aforementioned bi-linear, bi-viscous model is used to convert the desired control force into an appropriate command voltage (Lynch*, et al.* 2008). Desired control forces, with few and minor exceptions, are in the direction opposing motion. For any desired control force not opposing motion (which the MR damper cannot supply) the voltage output is set to 0 V (corresponding to minimum damping). The command voltage output by the sensor is converted by the damper power supply into a proportional amperage that falls within the operating range of the MR

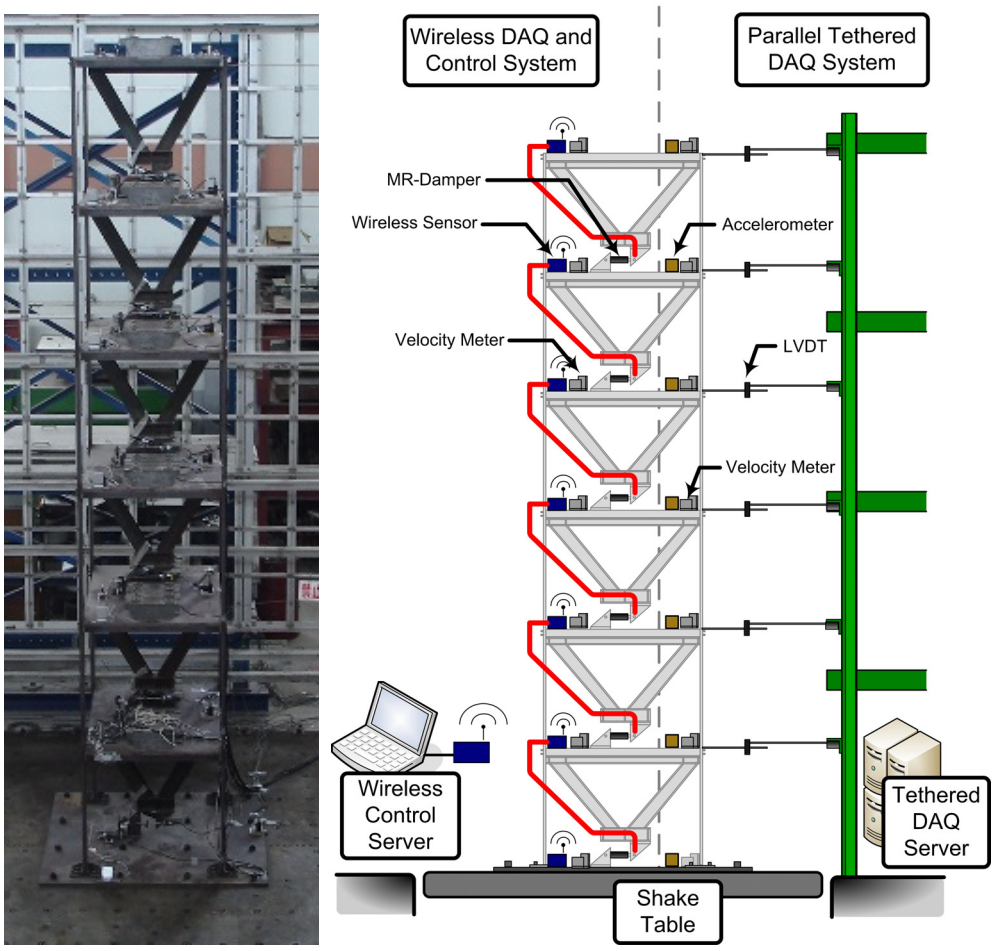


(a) (b)

**Figure 6.3.** Test structure for the validation of the wireless control system: (a) structure mounted to the shake table; (b) instrumentation strategy.

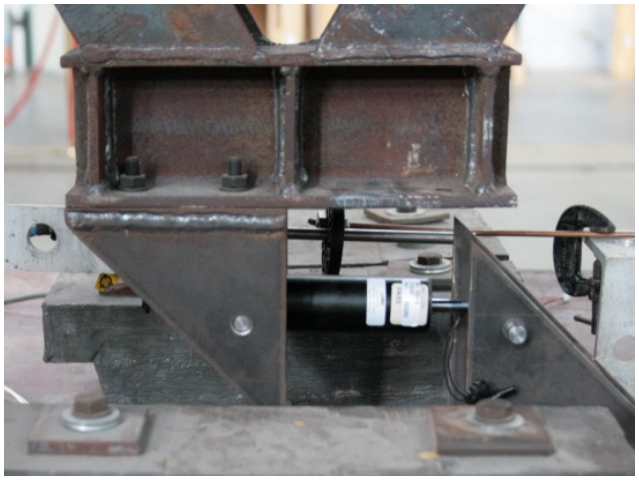

**Figure 6.4.** MR damper (Courtesy of K.-C. Lu).

damper. Transmissions of state data occur only when the estimated state errors exceed the preset threshold.

The command to begin testing is sent from a personal computer (PC) via a Chipcon CC2420DBK development board connected through the PC's serial port. No further communication with the PC occurs until the test is over, at which time the wireless sensors transmit data back to the PC for offline analysis. The velocity response of the structure (relative to base), estimated velocity, and desired control force values recorded by the wireless sensors are reported back to the PC. Redundant cable based sensors record the displacement (Temposonics II position sensors) and velocity (Tokyo Sokushin VSE-15-AM) of the structure. Refer to Figure 6.3(b) for a full schematic of the structure with the wireless and wired data acquisition systems detailed. The configuration of the MR dampers, unfortunately, do not allow for the use of load-cells at the present time.

### *6.4.1. Control Performance Evaluation*

As the state recovery error threshold is varied, control performance changes. Eight cost functions, $J_1$ through $J_8$, are used to characterize the controller performance as a function of error threshold. The first six cost functions, adapted from Ohtori, *et al*. (2004), characterize the ability of controllers to reduce seismic responses important to design: interstory drift, floor acceleration, and base shear all normalized to the uncontrolled structural response due to the same ground excitation signal. Interstory drift minimization is important to reduce the likelihood of damage to the building system, especially to non-structural elements such as windows, doors, and partitions. Floor acceleration is related to the force exerted on the structure and its occupants during a

seismic event. Base shear is an important design parameter in sizing columns and footings. A pair of cost functions measures each of these parameters; one cost function compares single point absolute maximum values, while another compares the vector norm response over the entire test period.

$$J_1 = \frac{\max_{Floor,t}(|\,\mathbf{d}_{\mathbf{controlled}}\,|)}{\max_{Floor,t}(|\,\mathbf{d}_{\mathbf{uncontrolled}}\,|)} \tag{6.21}$$

where $\mathbf{d} \in \mathbf{R}^{n \times N}$ is interstory drift (where N is the total number of time steps),

$$J_2 = \frac{\text{norm}(|\,\mathbf{d}_{\mathbf{controlled}}\,|)}{\text{norm}(|\,\mathbf{d}_{\mathbf{uncontrolled}}\,|)} \tag{6.22}$$

$$J_3 = \frac{\max_{Floor,t}(|\,\ddot{\mathbf{x}}_{\mathbf{controlled}}\,|)}{\max_{Floor,t}(|\,\ddot{\mathbf{x}}_{\mathbf{uncontrolled}}\,|)} \tag{6.23}$$

$$J_4 = \frac{\text{norm}(|\,\ddot{\mathbf{x}}_{\mathbf{controlled}}\,|)}{\text{norm}(|\,\ddot{\mathbf{x}}_{\mathbf{uncontrolled}}\,|)} \tag{6.24}$$

$$J_5 = \frac{\max(|\,\ddot{\mathbf{x}}_{\mathbf{controlled}}\mathbf{W}\,|)}{\max(|\,\ddot{\mathbf{x}}_{\mathbf{uncontrolled}}\mathbf{W}\,|)} \tag{6.25}$$

where $\boldsymbol{W} \in \mathbf{R}^{n \times 1}$ is the seismic mass vector. Finally,

$$J_6 = \frac{\text{norm}(|\,\ddot{\mathbf{x}}_{\mathbf{controlled}}\mathbf{W}\,|)}{\text{norm}(|\,\ddot{\mathbf{x}}_{\mathbf{uncontrolled}}\mathbf{W}\,|)} \tag{6.26}$$

$J_7$ characterizes the average strain and kinetic energies in the system during the earthquake. Clearly, $J_7$ should be minimized to reduce the undesirable response energy of the system due to seismic excitation:

$$J_7 = \frac{\left[\frac{1}{N}\sum_{i=1}^{N}\mathbf{z}_i^{\mathrm{T}}\begin{bmatrix}\mathbf{K} & \mathbf{0}\\ \mathbf{0} & \mathbf{M}\end{bmatrix}\mathbf{z}_i\right]_{controlled}}{\left[\frac{1}{N}\sum_{i=1}^{N}\mathbf{z}_i^{\mathrm{T}}\begin{bmatrix}\mathbf{K} & \mathbf{0}\\ \mathbf{0} & \mathbf{M}\end{bmatrix}\mathbf{z}_i\right]_{uncontrolled}} \tag{6.27}$$

The wireless bandwidth utilized by the wireless control system is characterized in $J_8$, which is the total number of data transmissions during the time of the ground motion

divided by the total possible number of transmissions per sensor ($N$) times the total number of sensors ($n$).

$$J_8 = \frac{(\#\ \ Data\ \ \ Transmissions\ \ \ Sent)}{N \times n} \tag{6.28}$$

For centralized control, $J_8$ would be 1 while for fully-decentralized control, $J_8$ would be 0; a number between 0 and 1 is an indirect measurement of where the partially decentralized control system falls on the spectrum between centralized and decentralized. These cost functions form the basis for comparing simulation and experimental results over a range of error threshold levels.

### *6.4.2. Simulation*

To demonstrate the proposed control method, a numerical simulation is preformed in MATLAB using a model based on the six-story test structure. Specifically, the structure is modeled as a lumped-mass building with the mass of each floor equal to 862.85 kg. The identified stiffness for all stories is approximately 1.24 MN/m. The structure is lightly damped and is modeled using 0.5% Rayleigh damping. Wireless sensing units, assumed to be on each floor, record velocity measurements from collocated velocity meters while a seventh unit measures and broadcasts ground velocity to the network. Sensor noise is added to the signal in the form of Gaussian white noise with a standard deviation of 0.5 mm/s. The units compute the estimation error of the locally measured state data and compare it to the error threshold, retaining the estimate in cases where the error is below the threshold, otherwise replacing it with the measured value and transmitting that measured value to the rest of the network in cases where the error exceeds the threshold. Both perfect and lossy communications are simulated. For lossy

communication, the chance of a dropped packet is modeled by use of a zero-mean, Gaussian random variable with unity standard deviation. A packet is considered to be "dropped" whenever the magnitude of the random variable exceeds an experimentally derived threshold. The magnitude of the random variable is multiplied by the number of neighboring units that choose to utilize the broadcast medium at the current step hence, the probability of a dropped packet increases when nearby units transmit and is zero when none of the neighboring units transmit.

Finally, the units calculate and apply the LQR control force and update the state estimate for the next time step. In the simulation, idealized skyhook actuators are assumed. To keep desired control forces below the limits of realistic semi-active actuators (*e.g.*, MR dampers), the following values of $\boldsymbol{C_{LQR}}$ and $\boldsymbol{Q_2}$ are selected in the LQR formulation (Equation 6.6).

$$\mathbf{C}_{\mathrm{LQR}} = \begin{bmatrix} \begin{bmatrix} 1 & -1 & & 0 \\ 0 & 1 & \ddots & \\ \vdots & & \ddots & -1 \\ 0 & & & 1 \end{bmatrix} & 0.01*\mathbf{I} \end{bmatrix}, \quad \mathbf{Q}_2 = 10^{-9}\mathbf{I} \tag{6.29}$$

The numerical simulation performs average Newmark integration of Equation 6.1. The model is subjected to two different earthquake ground acceleration records: El Centro 1940 NS (USGS Station 117), Chi-Chi 1999 NS (TCU Station 076). The records are normalized to obtain absolute maximum accelerations of 1.0 m/s$^2$ (100 gals). The simulation is repeated with the error threshold of the state recovery algorithm altered. The velocity state values are compared at each degree of freedom with 25 error thresholds (that are logarithmically equally spaced between 0 m/s and 5 m/s) applied in successive runs. Clearly, the 0 m/s threshold effectively triggers communications at each

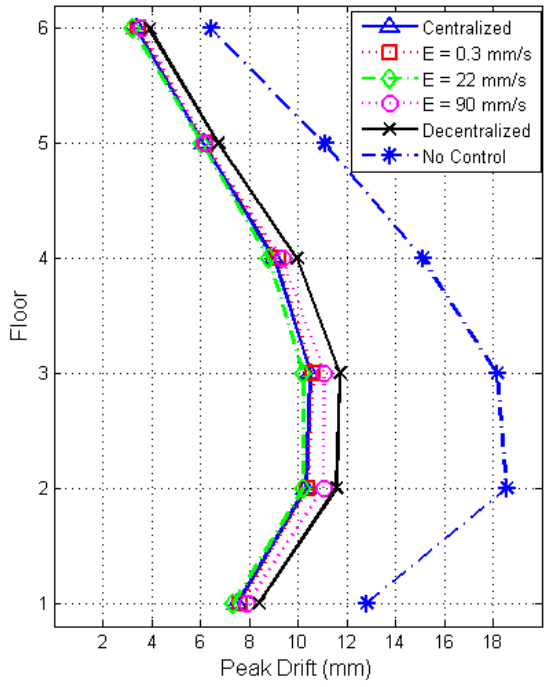


**Figure 6.5.** El Centro (100 gals) simulation results: peak interstory drift by floor.

step resembling a centralized control system. Likewise, the 5 m/s threshold is so large that the threshold is never exceeded leading to a decentralized control system.

The ability of the controllers to reduce the seismic response of the structure changes as the error threshold varies. Maximum interstory drift as a function of floor is presented for a relevant set of error thresholds in Figure 6.5 for the El Centro record (assuming perfect communication). In the simulation, the peak drift per floor increases monotonically with error threshold. The control performance, measured by error thresholds $J_1$ through $J_8$, as a function of error threshold is presented in Figure 6.6 for both the perfect and lossy communication cases (El Centro and Chi-Chi). In the perfect communication case, performance generally transitions smoothly from centralized to fully-decentralized control results as error threshold increases; the transition is

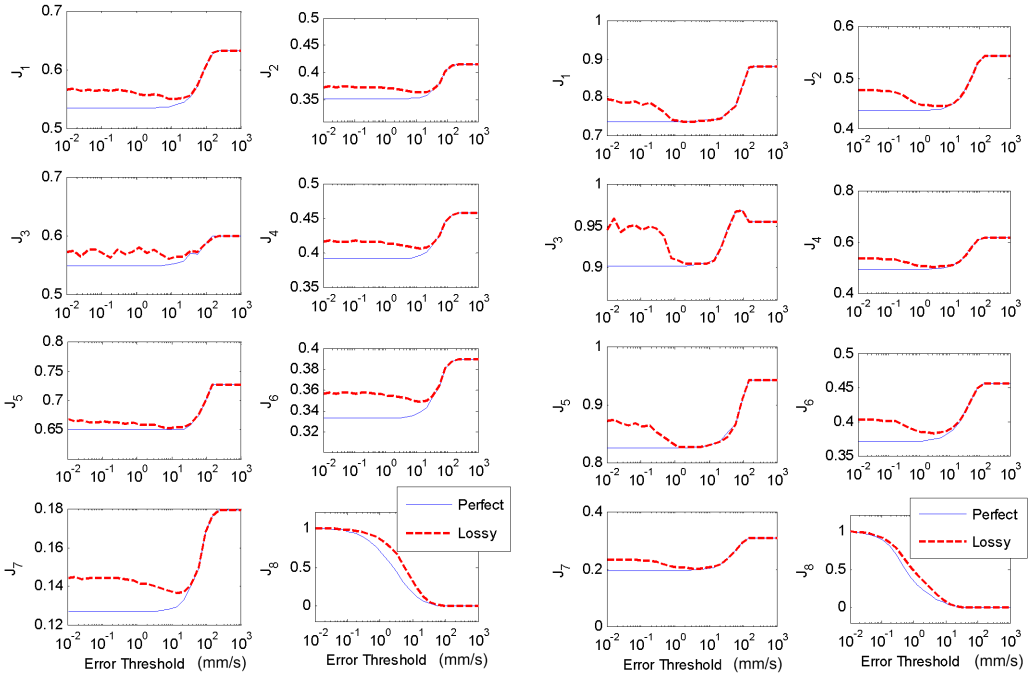


**Figure 6.6.** Simulation results: (a) El Centro (100 gals) cost functions; (b) Chi-Chi (100 gals) cost functions.

characterized by a sigmoidal shaped function, as expected for $J_1$ through $J_7$. However, in the case of lossy transmission, as bandwidth utilization decreases (as seen by $J_8$), the control performance generally improves slightly since fewer data packets are lost to collisions common in a centralized control system. This effect causes the error functions to actually go down as error threshold is initially increased. Eventually however, the error threshold becomes so large that the overall control performance degrades due to estimation error and performance begins to approach that of the fully-decentralized case. In that case, the error threshold function rises with cost function values identical to the perfect communication case. These plots suggest an optimal error threshold level for performance in the case of lossy communications where enough data is transmitted to

improve performance, but not too much to cause excessive packet collisions. For El Centro, this optimal error threshold is at 10 mm/s, while for the Chi-Chi earthquake, it is from 1 to 10 mm/s.

### *6.4.3. Experimental Results*

Uniaxial lateral excitation is applied to the test structure by the shaking table corresponding to the ground motion record for El Cento and Chi-Chi normalized to 1.0 $m/s^2$ (100 gals) peak acceleration. *Narada* wireless sensing units operate autonomously to run the control network once the test has begun and interact with a PC server only at the end of a test to report data. The measurement performance of the Narada wireless sensor is presented in Figure 6.7 with the wirelessly measured velocity comparing well to that of the wired system. In one day of testing, a ground motion record is repeated over an approximately logarithmically distributed error threshold domain. As shown in Table 6.1, in total, 17 independent tests are conducted with increasing error thresholds. The 0 m/s threshold corresponds to a centralized case because at each time step, the threshold is exceeded forcing every sensor to communicate. Tests 2 through 16 increase the error threshold so as to render the system increasingly more decentralized. Test 17 is completely decentralized since the error threshold is so high, it is never exceeded.

Figure 6.8 depicts the experimentally derived maximum drift response by floor for the El Centro record. Evident in the peak drift plots is the effectiveness of the wireless control system. The greatest peak drifts are witnessed for the structure without dampers installed. With the MR dampers installed but placed in a passive state (minimum and maximum damping settings), reduction in the interstory drifts are observed. However,

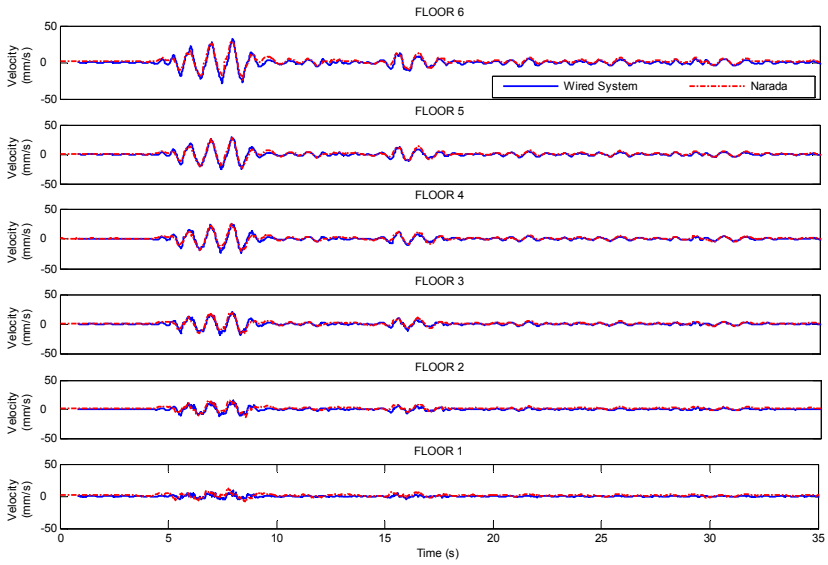


**Figure 6.7.** Narada measured velocity output of the test structure excited by El Centro (100 gals) with cabled system response overlaid for comparison.

**Table 6.1.** State recovery error thresholds experimentally tested.

| Test # | Velocity Error | Test # | Velocity Error |
|---|---|---|---|
| 1 | 0 m/s (Centralized) | 10 | 0.008 m/s |
| 2 | 0.00002 m/s | 11 | 0.02 m/s |
| 3 | 0.00005 m/s | 12 | 0.05 m/s |
| 4 | 0.00008 m/s | 13 | 0.08 m/s |
| 5 | 0.0002 m/s | 14 | 0.2 m/s |
| 6 | 0.0005 m/s | 15 | 0.5 m/s |
| 7 | 0.0008 m/s | 16 | 0.8 m/s |
| 8 | 0.002 m/s | 17 | 5 m/s (Decentralized) |
| 9 | 0.005 m/s | | |

the best performance occurs when the dampers are operated by the wireless control system. In general, as the error threshold is lowered, the redundant estimator framework yields better performance with respect to the peak interstory drift profile of the structure. This fact is more apparent when considering the cost functions $J_1$-$J_8$ that are presented in Figure 6.9 for both the El Centro and Chi-Chi earthquake records (the El Centro results are an average of the two days of testing). The experimental results observed for both ground motion records are consistent with those obtained in simulation (Figure 6.6). It

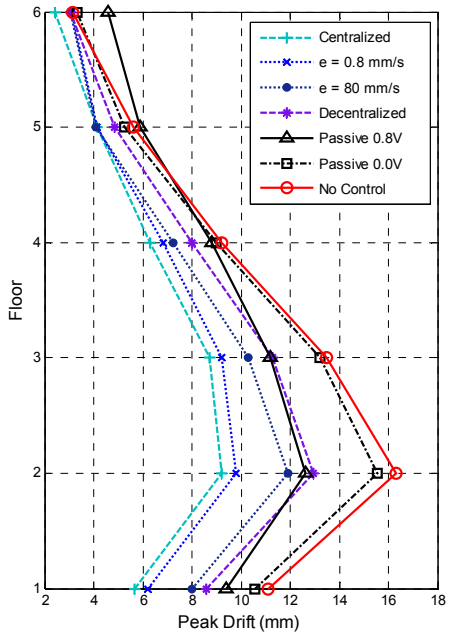


**Figure 6.8.** El Centro (100 gals) experimental results: peak interstory drift by floor.

should be noted that, due to time constraints during testing, $J_8$ was not logged for the Chi-Chi record. The majority of the cost functions initially decline as the error threshold is raised suggesting that the system performance improves initially because partial decentralization results in less data loss in the wireless channel (despite the TDMA communications). While initial gains are derived by alleviating the demand for the wireless channel, such gains are eroded as the error threshold is raised further due to decentralization of the control system. As a result, the cost functions begin to increase until is plateaus at large threshold values (essentially, when it is decentralized). This result lends further credence to the view advanced in the simulation phase that there exists an optimum error threshold level for control performance. For both earthquake records, it is likely that the optimal threshold is from 1 to 10 mm/s.

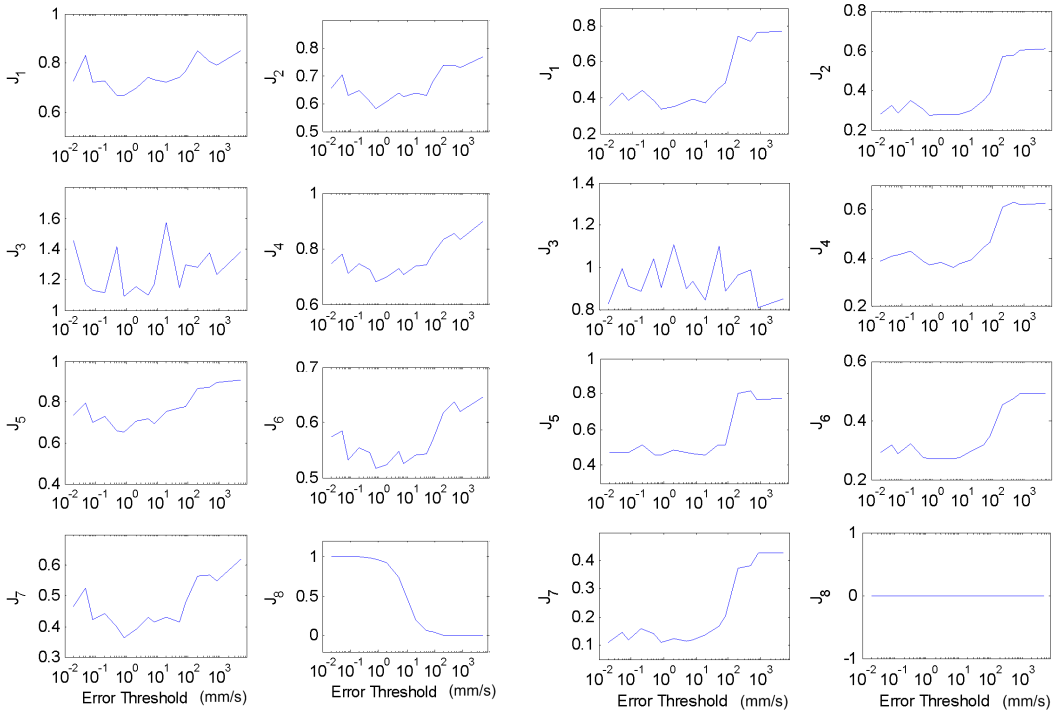


(a) (b)

**Figure 6.9.** Experimental results: (a) El Centro (100 gals) cost functions; (b) Chi-Chi (100 gals) cost functions.

## 6.5. Conclusions

Transmission of every raw data point within a wireless control system increases delay, degrading the control performance, and drastically reducing battery life of the wireless sensors. Strategic use of wireless bandwidth can help to overcome some of the limitations of wireless control. An embedded estimator with embedded control force computation can be used for control in an actuator network whose size makes centralized control impractical due to bandwidth limitations. Limitations on the performance of fully-distributed control make some sharing of data between units attractive. By sharing the most critical measured data points, those most different from their corresponding estimated data points, limited bandwidth can be utilized in an efficient manner.

Furthermore, the performance of the controller varies from that of centralized control to that of distributed control as the error threshold is varied from low to high. Even for conservative communication models (*e.g.*, TDMA) however, there appears to be data loss resulting in a decline in performance for excessively low error threshold levels (suggesting an optimal threshold level between centralized and fully-decentralized control). This effect may become more pronounced under less conservative communications models (*e.g.*, CSMA-CA), a prospect that warrants further investigation. One might also wonder about the efficacy of the base unit responsible for relaying ground motion data to the rest of the network as this data is critical for proper operation at any level of centralization. For this study, a larger time window is allocated to the base wireless sensor for communications, resulting in near perfect reception. Additionally, as the height of controlled structures increase, the ability of the base unit to transmit to sensing and actuation nodes located on upper floors will be compromised. Further work to address the effect is warranted. Also, as the number of floors increase, the number of embedded floating-point math operations required to compute the estimation updates as well as the control forces increase. Eventually, the latency introduced by these computations will introduce unacceptable losses in control performance making reduced order models more attractive.

In this study, a so-called "optimal" threshold was determined experimentally, but an *a priori* means of establishing an error threshold would have more appeal. To identify the optimal threshold, first characterization of the behavior of the wireless system is necessary (*e.g.*, packet collisions, drop rates, range issues, *etc*.) along with an analytical model of the transmission success rate as a function of utilized bandwidth. Second, an

analytical model of the system performance as error accumulates (with a realistic estimation of sensor noise and disturbances) is necessary so that an acceptable level of control performance that is achievable by the wireless system can be identified. Further investigation is also warranted in control force derivation. It is implicit in the LQR approach used in this study that the applied control force will be the exact desired control force to guarantee optimality. Also, all models used in the LQR derivation assume linearity of the system. These assumptions are often unrealistic for civil structures due to the large forces required and the complicated dynamics of semi-active actuators such as MR dampers. Additional investigation is also warranted in error handling algorithms within the communications protocol derived for this study. Additionally, an adaptive error threshold may yield better results than the static threshold and should be investigated. Finally, organizing sensors into hierarchal clusters may reduce bandwidth usage, allow multi-channel utilization, and improve data flow in large control systems.

# CHAPTER 7

# CONCLUSIONS AND FUTURE DIRECTIONS

## 7.1. Summary of Thesis

The main focus of this thesis was to present a wireless framework for low-cost smart structure technology that goes beyond just simple monitoring activities and leverages collocated computing and actuation to make civil infrastructure safer and its management more economical. This framework emphasized autonomous operation, embedded computing, and the reactive abilities of sensor-enabled structural systems. This framework mandated the development and validation of a wireless sensing platform tailored to meet the particular challenges of sensing, embedded computing, and actuation in civil infrastructure environments. More so however, this framework required a new way of looking at engineering algorithms (*e.g.*, monitoring, algorithms for structural health monitoring, and structural control) so that they can run effectively within a distributed sensor network, characterized by distributed memory, processing, and data resources, not to mention non-trivial costs associated with data transmission between nodes (namely, in terms of energy and quality-of-service realized by the network's

wireless communication bandwidth). Thus, this thesis emphasized sensor-level, local data processing to preserve both battery life and wireless communication bandwidth, as well as to eliminate the potential accumulation of unprocessed raw data that tends to exist in monitoring applications where data processing resources are limited. This thesis also presented embedded computing frameworks for tasks necessary to the smart structure paradigm including monitoring, feature extraction (load estimation and structural health monitoring), and structural control.

*Chapter 2* introduced the wireless sensing platform, termed *Narada*, that facilitated the wireless smart structure framework of this thesis. *Chapter 2* began with a detailed discussion of both the advantages and challenges inherent within a wireless sensor network relative to a traditional cable-based system. Following that, was a discussion of the hardware requirements necessary for wireless sensor design as well as a discussion of wireless sensors that were precursors to *Narada* from both academia and industry as well as contemporary wireless sensor nodes. The *Narada* wireless senor was then introduced with descriptions of both its hardware and firmware (embedded software) features and a discussion of the design decisions that affected its effectiveness in civil infrastructure applications. The *Narada* wireless sensor had a number of features that made it unique. These features included a high-resolution sensing interface, that made it well suited for monitoring of civil structures excited by low-level, ambient environmental loading, a low-power radio designed for use in scalable, ad-hoc personal area networks, and an actuation interface that allowed it to form and participate in active sensing and control networks. *Chapter 2* also presented a power-amplified transceiver interface for Narada,

followed by a discussion of data collection issues including network formation, data buffering, and synchronization.

A validation study of the suitability of the *Narada* wireless sensing system for long-term autonomous monitoring applications was presented in *Chapter 3*. A novel hybrid wired/wireless sensing network was deployed as a hull monitoring system aboard the FSF-1 Sea Fighter, a unique, experimental littoral combat vessel commissioned by the U.S. Navy. The Sea Fighter was composed of twin aluminum catamaran-style hulls, which made it an exotic design from the Navy's point of view. This fact lead to the vessel serving as an ideal test-bed for the wireless sensing system because an existing seakeeping hull monitoring system was available for comparison purposes (and the vessel's crew was accustomed to accommodating research activities). In this study, 20 *Narada* wireless sensors were installed aboard Sea Fighter collecting hull response data from accelerometers and metal-foil strain gauges. The hybrid wired/wireless network, consisting of three wireless subnets linked to the existing shipboard Ethernet local area network through wireless access points on its main working deck, was presented in detail. By using wireless technology, to economically consolidate sensor data from transducers that were spatially dispersed within the main ship compartment, and wired technology, to communicate large quantities of data through bulkheads, the relative strengths of each technology were leveraged while significantly mitigating the relative weaknesses of each. Reliability of the wireless hull monitoring system was discussed in detail and wirelessly collected data was used to characterize modal properties of the vessel.

In *Chapter 4*, an embedded feature extraction algorithm was introduced for load estimation of wind turbine structures. Load estimation of wind turbines continues to be

an open problem regardless of sensor type or network topology. The wind load estimation method of *Chapter 4* was designed for use with output-only wireless sensing data, relying on low-order input-output mathematical models (often associated with system identification and control applications) to extract loading information from the measured structural response of the turbine. In this method, sensor data was used to update a model of the turbine tower which in turn was used to estimate the loading input from the tower response. The method was described in detail and then demonstrated using a laboratory validation structure with known parameters and measurable input. Finally, a field instrumentation campaign measuring the response of operational turbines using *Narada* was presented with application of the method to data obtained from one of the operational turbine towers.

With the ability of the online system to identify and extract relevant features from data established in *Chapter 4*, *Chapter 5* presented a structural health monitoring framework for the *Narada* network based on the tracking of changes in identified system poles. In this method, distributed computing resources were leveraged to process distributed data using primarily sensor-level computing. Both input/output and output-only approaches were presented. In the input/output approach, the sensor node with access to input data broadcasted it for use by the entire network, but raw output data was not transmitted. A recursive linear least-squares algorithm was used to identify a linear difference equation that described the system; from the linear difference equation, system poles were extracted. In the output-only approach, sensors used purely locally measured output data in a recursive, pseudo-linear least-squares algorithm to find the denominator of the linear difference equation that yielded an estimate of the same system poles.

Statistically significant changes in pole locations were correlated to damage in both a pre-stressed concrete box-girder bridge and six-story steel building frame application. In both the input/output and output only approaches used, results from all sensors in the network were aggregated using weights derived from the observation grammian. Because the observation grammian is a measurement of energy at a sensor due to the effect of the vibrational modes of a structure, it provided physical insight into the differing levels of sensitivity to damage observed by different sensors from the identified poles. Furthermore, it gave a rational basis for integrating the sensor-level results across the network. By transmitting primarily results of the data processing algorithms between units (as opposed to raw data), the energy and communication bandwidth demands placed on the wireless network by the structural health monitoring algorithm were constrained.

In *Chapter 6*, a similar balance between local processing and communication using the network's wireless communication bandwidth was considered for wireless structural control. A key aspect of the smart structure system proposed was its ability not only to sense external stimuli, but to react to them as well through feedback control. Wireless networks introduce additional latency into feedback control systems that is both deterministic (*e.g.*, delay due to computational overhead) and non-deterministic (*e.g.*, transmission delays due to dropped packets). Because increased use of the wireless communication channel tends to degrade the performance of units accessing that channel, a means for intelligently leveraging scarce communication bandwidth in wireless control systems that was adapted from network control (Yook*, et al.* 2002) was developed and presented in Chapter 6. Here, wireless sensors responsible for sensing the response of the structure, calculating control forces, and commanding collocated, semi-active actuators

ran redundant state estimators. Local estimation errors were tracked and large errors triggered communication of measured state data between sensing nodes. In this way, only the most critical sensor data points were transmitted, reducing network dependency on the wireless communication network and preserving bandwidth.

## 7.2. Contributions

Despite many possible benefits, adoption of smart structure technology for management of civil infrastructure systems has still not occurred on a wide scale. This thesis identified three key areas in which smart structure technology would be highly advantageous for protection of both the public and its infrastructure investments. Namely, this thesis identified deterioration, exposure to extreme loading events, and inadequate load characterization as problems within the civil engineering community that could be largely addressed by application of smart structure technologies. Key barriers to the application of smart structure technologies in mitigating these problems are cost and perceived benefit. This thesis presented wireless sensing systems characterized by sensors with collocated sensing, computing power, and actuation abilities as a means by which the benefits of smart structures (*i.e.*, embedded capabilities within the structure to sense external stimuli, interrogate their own condition, and react in order to reduce the effects of undesirable events) might be realized at a significantly reduced cost versus traditional cable-based sensor networks.

To accomplish this goal, a new wireless sensing platform was required, tailored to meet the needs of smart structure applications in the civil engineering realm. The sensing system, termed *Narada*, was designed to be low-cost and to promote use in high-density

sensor networks. It was designed to be low-power, to operate effectively on battery energy, to form scalable, adaptable networks of varying sizes, to be computationally capable, to be able to perform embedded distributed engineering algorithms, and equipped with actuation capabilities allowing it to command collocated actuators as well as respond autonomously to large loading events. Meeting these design criteria, *Narada* represents a new paradigm in active sensors for civil infrastructure systems. In addition, as a part of its development, the Narada wireless sensing system was extensively field tested as a structural monitoring system. The hybrid wired/wireless hull monitoring system presented in *Chapter 3* represents a novel approach to combine the cost benefits of wireless signal routing for spatially dispersed transducers, and the high-throughput rates of wired signal routing of the wirelessly aggregated data.

Most interestingly, this thesis presented a framework for distributed, embedded data processing within wireless civil smart structure sensor networks. Because computing resources and data are distributed throughout wireless sensor networks, novel data processing approaches are particularly valuable for the efficient execution of engineering algorithms. While a wireless network is capable of sharing data between nodes, data transmission comes at the expense of power consumption (an important issue in battery powered wireless networks) and bandwidth utilization (which can impose limits on system scalability due to constraints on the wireless communication bandwidth available to wireless networks). Data processing algorithms that rely primarily on local sensor-level processing make the most sense in wireless sensor networks because they preserve power and bandwidth. This thesis presented algorithms that fit this framework for three important smart structure applications, namely load estimation from measured dynamic

response, structural health monitoring, and structural control. These algorithms relied predominantly on sensor-level computing and access to the wireless communication channel was restricted to transmission of only limited amounts of strategically selected data that provide maximum benefit to their associated algorithm. These algorithms were then validated in laboratory studies as well as in field instrumentation campaigns.

### 7.3. Future Work

This thesis presented a framework for wireless civil smart structures that relied on embedded, sensor-level data processing, a sensor platform capable of realizing that framework, and application algorithms for design load estimation, structural health monitoring, and structural control that fit within that framework. While these results represent a significant step forward, future research efforts along these lines are still warranted. More recent advances in low-power commercial electronics now provide significantly greater memory and computational power within individual wireless devices for relatively modest increases in power consumption and cost. Properly implemented, these advances have the potential to increase the computational burden that may be assumed by individual sensors within a network and the speed at which engineering algorithms can be executed. A new generation of the *Narada* wireless sensing platform, built on the latest digital signal processor (DSP) technology, will allow embedded system identification algorithms (that are at the heart of both the load estimation and structural health monitoring methods) to operate faster, larger models to be used, and larger data sets to be processed. With significantly greater speeds for floating-point matrix math operations involving floating-point numbers, new DSP technology will also allow for

significant improvements in the speed at which wireless control operations can be run (the speed of these algorithms directly affects their effectiveness) and will serve to increase the desirability of embedded sensor-level computation as the latency due to embedded math operations decreases and the latency due to communication remains fixed.

Besides simply leveraging new technology to improve the capabilities of the wireless platform, future work is warranted to improve the specific algorithms also presented as part of this thesis. Model based load estimation for wind turbines is a relatively new area of investigation and provides many additional opportunities for improvement. The method presented in this thesis for load estimation of wind turbine towers could be extended. In future studies, arranging access to the turbine blades will be very important. With the ability to place sensors concurrently within the turbine blades and the tower, the interplay between the turbine blades and the tower could be characterized. Vibrational measurements of points within the turbine blades could be used to identify blade models that, combined with the tower model, could separate the influence of vibrational modes of the blades from the wind loading itself and improve the estimate of the wind load itself. Also, additional sensing modalities could be of great value to enhance the estimate of the loading derived from the vibrational response of the turbine. Measurements of air velocity at the tower, though disturbed by the blades, could provide additional insight into the loading environment when coupled with a sufficiently sophisticated model of the wind/structure interactions.

In the area of structural health monitoring, characterization of the structural parameters with respect to environmental changes is necessary before wide spread

adoption is practical. To accomplish this goal, additional long-term field monitoring campaigns of operational structures will be necessary. Wireless sensors will be instrumental in collecting and processing this data. In addition, load estimation methods developed earlier in this thesis could prove valuable in identification of more accurate system models that form the basis of the structural health monitoring method. Output-only methods presented are effective in producing models that show demonstrable variation for the damage scenarios investigated however, more refined models should yield greater sensitivity to detectible damage modalities.

Just as the fusion of load estimation and embedded structural health monitoring shows promise for improved performance, fusion of the online model identification methods developed for structural health monitoring could be used to improve structural control applications. The method for leveraging bandwidth in a partially decentralized structural control framework is highly model dependent. Modeling uncertainties or changes in structural or actuator parameters over time will affect the accuracy of the estimators, the degree of wireless communication bandwidth consumed, and ultimately, system performance. An embedded adaptive control system would help to alleviate these concerns. Adaptive control systems operate in two parts: a control law and a recursive model identification algorithm. In high processor power applications, these steps can be implemented on the same device; and a constant update of the control law can be provided. In resource constrained wireless networks, the recursive system identification process may be executed instead on a parallel wireless network programmed to compute and transmit control law updates only when certain conditions are met, for instance when significant discrepancies in structural properties are observed.

Finally, additional smart structure embedded computing frameworks for use in civil sensor networks (wired or wireless) could provide great benefit for management of civil infrastructure assets. Data usage is a critical issue regardless of how data is transmitted within a network. Resources for manual data processing (namely, qualified technicians and engineers) are in ever decreasing supply due to pressures to contain asset management costs. Discrepancies between data collection capacities and data processing capacities lead to the inundation of raw data stored in centralized servers that may never be utilized. Public monetary resources expended to collect data that goes unused either to provide for more efficient resource management or to enhance public safety are, for all practical purposes, wasted resources. Autonomous data processing algorithms that are executed within microprocessors that are directly collocated with sensors eliminate this possibility. These embedded computing tools can provide benefits in many area of civil infrastructure management including smart transportation networks (automotive or rail), monitoring of environmental pollutants, building environmental control systems, power distribution grids, drinking water supply networks, storm/waste water management systems, and even construction project administration.

## REFERENCES


Abidi, K., Sabanovic, A. and Yesilyurt, S., "Sliding mode control based disturbance compensation and external force estimation for a piezoelectric actuator", Proceedings of the 8th IEEE International Workshop on Advanced Motion Control, Piscataway, NJ, USA, (2004).

ACI Committee 345, *345.1R-06: Guide for Maintenance of Concrete Bridge Members*, American Concrete Institute, Farmington Hills, MI, (2006).

Adeli, H. and Saleh, A., *Control, Optimization, and Smart Structures: High-Performance Bridges and Buildings of the Future*, John Wiley & Sons, Inc., New York, NY, (1999).

Agre, J.R., Clare, L.P., Pottie, G.J. and Romanov, N.P., "Development platform for self-organizing wireless sensor networks", Proceedings of the Conference on Unattended Ground Sensor Technologies and Applications, Orlando, FL, (1999).

Aizawa, S., Kakizawa, T. and Masahiko, H., "Case studies of smart materials for civil structures", *Smart Materials and Structures*, 7(5), pp. 617-626, (1997).

Allemang, R., *Vibrations: Experimental Modal Analysis. Course Notes*, Technical Report UC-SDRL-CN-20-263-663/664, Structural Dynamics Research Laboratory, University of Cincinnati, Cincinnati, OH, (1999).

Allemang, R.J. and Brown, D.L., "A correlation coefficient for modal vector analysis", Proceedings of the 1st International Modal Analysis Conference, Orlando, FL, (1982).

Allen, D.W., Software for Manipulating and Embedding Data Interrogation Algorithms into Integrated Systems, Blacksburg, VA, Virginia Polytechnic Institute and State University, M.S., (2004).

Aoki, S., Fujino, Y. and Abe, M., "Intelligent bridge maintenance system using MEMS and network technology", Smart Systems and NDE for Civil Infrastructures, San Diego, CA, March 3–6, (2003).

Arms, S.W., Townsend, C.P., Churchill, D.L., Hamel, M.J., Galbreath, J.H. and Mundell, S.W., "Frequency-agile wireless sensor networks", *Proceedings of SPIE*, 5389, pp. 468-475, (2004).

ASCE, *Minimum Design Loads for Buildings and Other Structures, ASCE/SEI 7-05*, American Society of Civil Engineers, New York, NY, (2005).

ASCE, *2009 Report Card for America's Infrastructure*, American Society of Civil Engineers, Washington, D.C., (2009).

Atmel, *Atmega128/Atmega128L 8-bit AVR Microcontroller with 128K Bytes In-System Programmable Flash*, Atmel Corporation, San Jose, CA, (2009).

Bachman, R.J., Woolaver, D.A. and Powell, M.D., *Sea Fighter (FSF-1) Seakeeping Measurements*, Technical Report NSWCCD-50-TR-2007/010, Naval Surface Warefare Center Carderock Division, West Bethesda, MD, (2007).

Bennett, R., Hayes-Gill, B., Crowe, J.A., Armitage, R., Rodgers, D. and Hendroff, A., "Wireless monitoring of highways", Smart Systems for Bridges, Structures, and Highways, Newport Beach, CA, March 1–2, (1999).

Bensky, A., *Short-Range Wireless Communication*, Elsevier, Amsterdam, The Netherlands, (2004).

Bhalla, S. and Soh, C.K., "Structural health monitoring by piezo--impedance transducers. II: applications", *Journal of Aerospace Engineering*, 17(4), pp. 166-175, (2004).

Binde, S., "A numerically stable fast transversal filter with leakage correction", *IEEE Signal Processing Letters*, 2(6), pp. 114-116, (1995).

Brei, D., *Lecture 1, Course Notes: ME559 Smart Materials and Structures*, Department of Mechanical Engineering, University of Michigan, Ann Arbor, MI, (2007).

Brincker, R., Andersen, P., Kirkegaard, P.H. and Ulfkjaer, J.P., "Damage detection in laboratory concrete beams", Proceedings of the 13th International Modal Analysis Conference, Nashville, TN, (1995a).

Brincker, R., Kirkegaard, P.H., Andersen, P. and Martinez, M.E., "Damage detection in an offshore structure", Proceedings of the 13th International Modal Analysis Conference, Nashville, TN, (1995b).

Brincker, R., Zhang, L. and Andersen, P., "Modal identification of output-only systems using frequency domain decomposition", *Smart Materials and Structures*, 10(3), pp. 441-445, (2001).

Broch, J., Maltz, D.A., Johnson, D.B., Hu, Y.-C. and Jetcheva, J., A performance comparison of multi-hop wireless ad hoc network routing protocols, Dallas, Texas, United States, ACM, (1998).

Brownjohn, J.M.W., "Structural health monitoring of civil infrastructure", *Philosophical Transactions of the Royal Society A*, 365(1851), pp. 589-622, (2007).

Bryson, A.E. and Ho, Y.C., *Applied Optimal Control: Optimization, Estimation, and Control*, Hemisphere Publishing, New York, NY, (1975).

Burr-Brown, *DAC7612 Dual, 12-Bit Serial Input Digital-to-Analog Converter*, Burr-Brown, Corporation, Tuscon, AZ, (1999).

Butterfield, S., Sheng, S. and Oyague, F., "Wind energy's new role in supplying the world's energy: what role will structural health monitoring play?" Proceedings of the 7th Annual Workshop on Structural Health Monitoring, Stanford, CA, September 9-11, 2009, (2009).

Callaway, E.H., *Wireless Sensor Networks: Architectures and Protocols*, CRC Press, Boca Raton, FL, (2003).

Camp, T.R., Morris, M.J., van Rooij, R., van der Tempel, J., Zaaijer, M.B., Henderson, A.R., Argyriadis, A., Schwartz, S., Just, H., Grainger, W. and Pearce, D., *Design Methods for Offshore Wind Turbines at Exposed Sites—Hydrodynamic Loading on Offshore Wind Turbines*, Delft University of Technology Section Wind Energy, Delft, The Netherlands, (2003).

Carden, E.P. and Fanning, P., "Vibration Based Condition Monitoring: A Review", *Structural Health Monitoring*, 3(4), pp. 355-377, (2004).

Caughey, T., "Classical normal modes in damped linear systems", *Journal of Applied Mechanics*, 27, pp. 269–271, (1960).

Celebi, M., *Seismic Instrumentation of Buildings (with Emphasis on Federal Buildings)*, Technical Report 0-7460-68170, United States Geologic Survey (USGS), Menlo Park, CA, (2002).

Chang, P.C., Flatau, A. and Liu, S.C., "Review Paper: Health Monitoring of Civil Infrastructure", *Structural Health Monitoring*, 2(3), pp. 257-267, (2003).

Chen, C.-T., *Linear System Theory and Design*, Oxford University Press, New York, NY, (1999).

Chen, W.-F. and Scawthorn, C., *Earthquake Engineering Handbook*, CRC Press, Boca Raton, FL, (2003).

Cheng, F.Y., Jiang, H. and Lou, K., *Smart Structures:Innovative Systems for Seismic Control*, CRC Press, Taylor & Francis Group, Boca Raton, FL, (2008).

Chintalapudi, K., Johnson, E.A. and Govindan, R., "Structural damage detection using wireless sensor-actuator networks", 13th Mediterranean Conference on Control and Automation, Limassol, Cyprus, (2005).

Cho, S., Gordon, P., Moore, J.E., Richardson, H.W., Shinozuka, M. and Chang, S., "Integrating transportation network and regional economic models to estimate the costs of a large urban earthquake", *Journal of Regional Science*, 41(1), pp. 39-65, (2002).

Chong, S.-L., "Preventing corrosion in steel bridges", *Public Roads*, (2004).

Chopra, I., "Review of state of art of smart structures and integrated systems", *AIAA Journal*, 40(11), pp. 2145-2187, (2002).

Chu, S.Y., Soong, T.T. and Reinhorn, A.M., *Active, Hybrid, and Semi-Active Structural Control: a Design and Implementation Handbook*, Wiley, New York, NY, (2005).

Chung, H.-C., Enomoto, T., Shinozuka, M., Chou, P., Park, C., Yokoi, I. and Morishita, S., "Real-time visualization of structural response with wireless MEMS sensors", Proceedings of the 13th World Conference on Earthquake Engineering, Vancouver, BC, Canada, (2004).

Cioffi, J.M. and Kailath, T., "Fast, recursive-least-squares transversal filters for adaptive filtering", *IEEE Transactions on Accoustics, Speech, and Signal Processing*, ASSP-32(2), pp. 304-337, (1984).

Clayton, E.H., Lu, C., Koh, B.-H., Xing, G. and Fok, C.-L., "Damage detections and correlation-based localization using wireless mote sensors", 20th IEEE International Symposium on Intelligent Control, ISIC '05 and the 13th Mediterranean Conference on Control and Automation, MED '05, Limassol, Cyprus, (2005).

Colandairaj, J., Irwin, G.W. and Scanlon, W.G., "Wireless networked control systems with QoS-based sampling", *IET Control Theory & Applications*, 1(1), pp. 430-438, (2007).

Crossbow Technology, "Imote2 Datasheet, Document Part Number: 6020-0117-02 Rev A", Retrieved October 8, 2009, from http://www.xbow.com/Products/Product_pdf_files/Wireless_pdf/Imote2_Datasheet.pdf, (2007).

Culshaw, B., Michie, C., Gardiner, P. and McGown, A., "Smart structures and applications in civil engineering", *Proceedings of the IEEE*, 84(1), pp. 78-86, (1996).

De Roeck, G., Peeters, B. and Maeck, J., "Dynamic monitoring of civil engineering structures", Proceedings of IASS-IACM 2000, Computational Methods for Shell and Spatial Structures, Chania, Greece, (2000).

DOE, *Wind Energy Multiyear Program Plan for 2007-2012*, U.S. Department of Energy (DOE), Washington D. C., (2006).

Doebling, S.W., Farrar, C.R. and Cornwell, P.J., "DIAMOND: a graphical interface toolbox for comparative modal analysis and damage identification", the 6th International Conference on Recent Advances in Structural Dynamics, Southampton, UK, (1997).

Doebling, S.W., Farrar, C.R. and Prime, M.R., "A summary review of vibration-based damage identification methods", *Shock and Vibration Digest*, 30(2), pp. 91-105, (1998).

Donald, J.K., *Fracture Mechanics Characterization of Aluminum Alloys for Marine Structural Applications*, Technical Report SSC-448, Ship Structure Committee, U.S. Coast Guard, Washington, D.C., (2007).

Dyke, S.J., Spencer, B.F., Jr. and Sain, M.K., "An experimental study of MR dampers for seismic protection", *Smart Materials and Structures*, 7(1), pp. 693-703, (1998).

Edelman, A. and Murakami, H., "Polynomial roots from companion matrix eigenvalues", *Mathematics of Computation*, 64(210), pp. 763-776, (1995).

Elliott, R.S., *Antenna Theory & Design*, John Wiley & Sons, Hoboken, NJ, (2003).

Ellis, B.R. and Littler, J.D., "Response of cantilever grandstands to crowd loads. Part 2: load estimation", *Proceedings of the Institution of Civil Engineers. Structures and buildings*, 157(5), pp. 297-307, (2004).

Encyclopedia Mythica, "Narada", *Encyclopedia Mythica: mythology, folklore, and religion* Retrieved Sept. 1, 2009, from http://www.pantheon.org/articles/n/narada.html, (1997).

Enright, M.P. and Frangopol, D.M., "Service-life prediction of deteriorating concrete bridges", *Journal of Structural Engineering*, 124(3), pp. 309-317, (1998).

Farrar, C.R., Allen, D.W., Ball, S., Masquelier, M.P. and Park, G., "Coupling sensing hardware with data interrogation software for structural health monitoring", Proceedings of the 6th International Symposium on Dynamic Problems of Mechanics (DINAME), Ouro Preto, Brazil, (2005).

Farrar, C.R. and Lieven, A.J., "Damage prognosis: the future of structural health monitoring", *Philosophical Transactions of the Royal Society A*, 365(1851), pp. 623-632, (2007).

Farrar, C.R., Park, G., Allen, D.W. and Todd, M.D., "Sensor network paradigms for structural health monitoring", *Journal of Structural Control and Health Monitoring*, 13(1), pp. 210-225, (2006).

Farrar, C.R., Sohn, H., Hemez, F.M., Anderson, M.C., Bement, M.T., Cornwell, P.J., Doebling, S.W., Schultze, J.F., Lieven, N. and Robertson, A.N., *Damage prognosis: current status and future needs: Technical Report No. LA-14051-MS*, Los Alamos National Laboratory, Los Alamos, NM, (2003).

Farrar, C.R. and Worden, K., "An introduction to structural health monitoring", *Philosophical Transactions of the Royal Society A*, 365(1851), pp. 303-315, (2007).

Fassana, A., Garibaldi, L., Giorcelli, E. and Sabia, D., "Z24 Bridge dynamic data analysis by time domain methods", Proceedings of IMAC 19, the International Modal Analysis Conference, Kissimmee, FL, (2001).

Fassois, S.D. and Sakellariou, J.S., "Time-series methods for fault detection and identification in vibrating structures", *Philosophical Transactions of the Royal*

*Society A: Mathematical, Physical and Engineering Sciences*, 365(1851), pp. 411-448, (2007).

Feld, J. and Carper, K.L., *Construction Failure*, John Wiley & Sons, Inc., New York, NY, (1997).

Finkenzeller, K., *RFID Handbook: Radio Frequency Identification Fundamentals and Applications*, Chichester, UK, John Wiley and Sons, (1999).

Franklin, G.F., Powell, J.D. and Emami-Naeini, A., *Feedback Control of Dynamic Systems*, Prentice Hall, Upper Saddle River, NJ, (2002).

Galbreath, J.H., Townsend, C.P., Mundell, S.W., Hamel, M.J., Esser, B., Huston, D. and Arms, S.W., "Civil structure strain monitoring with power-efficient, high-speed wireless sensor networks", Proceedings of the 4th International Workshop on Structural Health Monitoring, Stanford, CA, September 15–17, (2003).

Gandhi, M.D. and Thompson, B.S., *Smart Materials and Structures*, Chapman and Hall, London, UK, (1992).

Gao, Y. and Spencer, B.F., Jr., *Structural Health Monitoring Strategies for Smart Sensor Networks*, Technical Report NSEL-011, Newmark Structural Engineering Laboratory, Department of Civil and Environmental Engineering, University of Illinois, Urbana-Champaign, IL, (2008).

Gao, Y., Spencer, B.F., Jr. and Ruiz-Sandoval, M., "Distributed computing strategy for structural health monitoring", *Structural Control and Health Monitoring*, 13(1), pp. 488-507, (2006).

Garibaldi, L., Marchesiello, S. and Bonisoli, E., "Identification and up-dating over the Z24 benchmark", *Mechanical Systems and Signal Processing*, 17(1), pp. 153-161, (2003).

Gavin, H., Hoagg, J. and Dobossy, M., "Optimal design of MR dampers", U.S.-Japan Workshop on Smart Structures for Improved Seismic Performance in Urban Regions, Seattle, WA, (2001).

Gibson, A.O. and Stein, J.L., "Linear observer based approach for estimating spindle bearing loads", Atlanta, GA, USA, (1996).

Ginsberg, J.H., *Mechanical and Structural Vibrations : Theory and Applications*, Wiley, New York, NY, (2001).

Greening, D.R., "Parallel simulated annealing techniques", *Physica D*, 42, pp. 293–306, (1990).

Grisso, B.L., Martin, L.A. and Inman, D.J., "A wireless active sensing system for impedance-based structural health monitoring", Proceedings of the 23rd International Modal Analysis Conference, Orlando, FL, USA, (2005).

Hac, A. and Liu, L., "Sensor And Actuator Location In Motion Control Of Flexible Structures", *Journal of Sound and Vibration*, 167(2), pp. 239-261, (1993).

Harvey, A.F., *Microwave Engineering*, Academic Press, London, UK, (1963).

Hatada, T., Kobori, T., Ishida, M. and Niwa, N., "Dynamic analysis of structures with Maxwell model", *Earthquake Engineering and Structural Dynamics*, 29(2), pp. 159-176, (2000).

Hau, E., *Wind Turbines: Fundamentals, Technologies, Applications, and Economics*, Springer, Berlin, Germany, (2006a).

Hau, E., *Wind Turbines: Fundamentals, Technologies, Applications, Economics*, Springer, Berlin, Germany, (2006b).

Haykin, S., *Adaptive Filter Theory*, Prentice Hall, Englewood Clifs, NJ, (1991).

Haykin, S., *Adaptive Filter Theory*, Prentice Hall, Upper Saddle River, NJ, (1996).

Henderson, A.R. and Zaaijer, M.B., "Hydrodynamic loading on offshore wind turbines", Proceedings of the OWEMES Conference, Naples, Italy, (2003).

Hess, P.E., "Structural health monitoring for high-speed naval ships", 7th International Workshop on Structural Health Monitoring, Stanford, CA, (2007).

Holmes, J.D., *Wind Loading of Structures*, Taylor and Francis, New York, NY, (2007).

Hou, T.-C. and Lynch, J.P., "Electrical impedance tomographic methods for sensing strain fields and crack damage in cementitious structures", *Journal of Intelligent Material Systems and Structures*, 20(11), pp. 1363-1379, (2009).

Hou, T.-C., Lynch, J.P. and Parra-Montesinos, G., "Local-based damage detection of cyclically loaded bridge piers using wireless sensing units", *Proceedings of SPIE*, 5768, pp. 85-96, (2005).

Housner, G.W., Bergman, L.A., Caughey, T.K., Chassiakos, A.G., Claus, R.O., Masri, S.F., Skelton, R.E., Soong, T.T., Spencer, B.F., Jr. and Yao, J.T.P., "Structural control: past, present, and future", *Journal of Engineering Mechanics*, 123(9), pp. 897-971, (1997).

Huang, J.D., Yeh, C.S., Chen, C.S., Lee, C.K. and Wu, W.J., "Design and implementation of a wireless sensor network for smart living spaces", Proceedings of the Sensors and Smart Structures Technologies for Civil, Mechanical, and Aerospace Systems 2008, San Diego, California, USA, (2008).

Hwang, J.-S., Kareem, A. and Kim, W.-J., "Estimation of modal loads using structural response", *Journal of Sound and Vibration*, 326(3-5), pp. 522-539, (2009).

ICC, *International Building Code*, International Code Council, Inc., Country Club Hills, IL, (2006).

IEEE, *802.15.4: Standard for Information technology--Telecommunications and information exchange between systems--Local and metropolitan area networks--Specific requirements Part 15.4: Wireless Medium Access Control (MAC) and Physical Layer (PHY) Specifications for Low Rate Wireless Personal Area Networks (LR-WPANs)*, IEEE Standards Association, New York, NY, (2006).

Inaudi, D., "SOFO sensors for static and dynamic measurements", Proceedings of the 1st FIG International Symposium on Engineering Surveys for Construction Works and Structural Engineering, Nottingham, UK, (2004).

Janocha, H., Ed. *Adaptronics and Smart Structures*, Springer, Berlin, Germany, (1999).

Jia, J., Chen, J., Chang, G. and Tan, Z., "Energy efficient coverage control in wireless sensor networks based on multi-objective genetic algorithm", *Computers & Mathematics with Applications*, 57(11-12), pp. 1756-1766, (2009).

Juang, J.-N., *Applied System Identification*, Prentice Hall, Upper Saddle River, NJ, (1994).

Kajima-Corporation, *Advanced Structural Control Technologies, HiDAX: High Damping System in the Next Generation*, Kajima Corporation, Tokyo, Japan, (2006).

Kajima Corporation, *Advanced Structural Control Technologies, HiDAX: High Damping System in the Next Generation*, Kajima Corporation, Tokyo, Japan, (2006).

Karlof, C., Sastry, N. and Wagner, D., TinySec: a link layer security architecture for wireless sensor networks, Baltimore, MD, ACM, (2004).

Karlof, C. and Wagner, D., "Secure routing in wireless sensor networks: attacks and countermeasures", *Ad Hoc Networks*, 1(2-3), pp. 293-315, (2003).

Katsas, S., Nikolaou, J. and Papadimitriou, G., "Corrosion resistance of repair welded naval aluminum alloys", *Materials and Design*, 28(3), pp. 831-836, (2007).

Kattell, J. and Eriksson, M., *Bridge Scour Evaluation: Screening, Analysis, & Countermeasures*, Technical Report 9877 1207—SDTDC, United States Department of Agriculture Forest Service Technology & Development Program, San Dimas, CA, (1998).

Kawka, P.A. and Alleyne, A.G., "Stability and feedback control of wireless networked systems", 2005 American Control Conference, Portland, OR, (2004).

Kessler, S.S., Spearing, S.M. and Soutis, C., "Damage detection in composite materials using Lamb wave methods", *Smart Materials and Structures*, 11(2), pp. 269-278, (2002).

Kim, D.-H., Hong, K.-S. and Yi, K., "Driving load estimation with the use of an estimated turbine torque", *JSME International Journal, Series C: Mechanical Systems, Machine Elements and Manufacturing*, 49(1), pp. 163-171, (2006).

Kim, S., Pakzad, S., Culler, D., Demmel, J., Fenves, G., Glaser, S. and Turon, M., Health monitoring of civil infrastructures using wireless sensor networks, Cambridge, Massachusetts, USA, ACM, (2007).

Kiremidjian, A.S., Straser, E.G., Meng, T.H., Law, K. and Soon, H., "Structural damage monitoring for civil structures", Proceedings of the International Workshop on Structural Health Monitoring, Stanford, CA, (1997).

Kirkpatrick, S., Gelatt, C.D., Jr. and Vecchi, M.P., "Optimization by simulated annealing", *Science*, 220, pp. 671–680, (1983).

Kling, R., "Intel motes: advanced sensor network platforms and applications", *Microwave Symposium Digest, 2005 IEEE MTT-S International*, pp. 365-368, (2005).

Kling, R.M., "Intel mote: an enhanced sensor network node", Proceedings of the International Workshop on Advanced Sensors, Structural Health Monitoring and Smart Structures, Tokyo, Japan, (2003).

Kottapalli, V.A., Kiremidjian, A.S., Lynch, J.P., Carryer, E., Kenny, T.W., Law, K.H. and Lei, Y., "Two-tiered wireless sensor network architecture for structural health monitoring", Smart Structures and Materials, San Diego, CA, March 3–6, (2003a).

Kottapalli, V.A., Kiremidjian, A.S., Lynch, J.P., Carryer, E., Kenny, T.W., Law, K.H. and Lei, Y., "Two-tiered wireless sensor network architecture for structural health monitoring", Proceedings of the 10th Annual International Symposium on Smart Structures and Materials, San Diego, CA, (2003b).

Krämer, C., De Smet, C.A.M. and De Roeck, G., "Z24 bridge damage detection tests", Proceedings of IMAC 17, the International Modal Analysis Conference, Kissimmee, FL, (1999).

Kullaa, J., "Damage detection of the Z24 bridge using control charts", *Mechanical Systems and Signal Processing*, 17(1), pp. 163-170, (2003).

Kurata, N., Kobori, T., Takahashi, M., Niwa, N. and Midorikawa, H., "Actual seismic response controlled building with semi-active damper system", *Earthquake Engineering and Structural Dynamics*, 28(11), pp. 1427-1447, (1999).

Kurata, N., Spencer, B.F., Jr. and Ruiz-Sandoval, M., "Risk monitoring of buildings with wireless sensor networks", *Structural Control & Health Monitoring*, 12(3), pp. 315-327, (2005).

Kurata, N., Spencer Jr., B.F., Ruiz-Sandoval, M., Miyamoto, Y. and Sako, Y., "A study on building risk monitoring using wireless sensor network MICA-Mote", First International Conference on Structural Health Monitoring and Intelligent Infrastructure, Tokyo, Japan, November 13–15, (2003).

Kurino, H., Tagami, J., Shimizu, K. and Kobori, T., "Switching oil damper with built-in controller for structural control", *Journal of Structural Engineering*, 129(7), pp. 895-904, (2003).

Law, S.S., Bu, J.Q. and Zhu, X.Q., "Time-varying wind load identification from structural responses", *Engineering Structures*, 27(10), pp. 1586-1598, (2005).

Leopold, G., "U.S. wind power is rising, but will it fly?" *EE Times*, June, (2007).

LeRose, C., "The collapse of the silver bridge", *West Virginia Historical Society Quarterly*, 15(4), (2001).

Levis, P., *TinyOS Programming*, TinyOS Alliance, (2006).

Levis, P., Madden, S., Gay, D., Polastre, J., Szewczyk, R., Woo, A., Brewer, E. and Culler, D., "The emergence of networking abstractions and techniques in TinyOS", Proceedings of the First Symposium on Networked Systems Design and Implementation (NSDI '04), (2004).

Li, Y.-Q. and Tamura, Y., "Equivalent static wind load estimation in wind-resistant design of single-layer reticulated shells", *Wind and Structures*, 8(6), pp. 443-54, (2005).

Lian, F.-L., Moyne, J.R. and Tilbury, D.M., Network protocols for networked control systems. *Handbook of Networked and Embedded Control Systems*. D. Hristu-Varsakelis and W. S. Levine. Boston, MA, USA, Birkhäuser, pp. 651-675, (2005).

Lin, L., Dyke, S. and Veto, R., "Wireless sensing and control of structural vibration from earthquake", 26th Chinese Control Conference, Zhangjiajie, Hunan, China, (2007).

Lin, P.-Y., Roschke, P.N. and Loh, C.-H., "System identification and real application of a smart magneto-rheological damper", 2005 International Symposium on Intelligent Control, Limassol, Cyprus, (2005).

Liu, J.-J., Ma, C.-K., Kung, I.-C. and Lin, D.-C., "Input force estimation of a cantilever plate by using a system identification technique", *Computer Methods in Applied Mechanics and Engineering*, 190(11-12), pp. 1309-22, (2000).

Liu, X. and Goldsmith, A., "Wireless medium access control in networked control systems", 2004 American Controls Conference, Boston, MA, (2004).

Lively, K.A., Seman, A.J. and Kirkpatrick, M., "Human systems integration and advanced technology in engineering department workload and manpower reduction", *Naval Engineers Journal*, 115(1), pp. 57-66, (2008).

Ljung, L., *System Identification, Theory for the User*, Prentice Hall, Upper Saddle River, NJ, (1999).

Loh, C.-H., Lynch, J.P., Lu, K.-C., Wang, Y., Chang, C.-M., Lin, P.-Y. and Yeh, T.-H., "Experimental verification of a wireless sensing and control system for structural

control using MR dampers", *Earthquake Engineering and Structural Dynamics*, 36(10), pp. 1303-1328, (2007).

Lu, Y. and Gao, F., "A novel time-domain auto-regressive modelfor structural damage diagnosis", *Journal of Sound and Vibration*, 283(3-5), pp. 1031-1049, (2005).

Luscher, D.J., Brownjohn, J.M.W., Sohn, H. and Farrar, C.R., "Modal parameter extraction of Z24 Bridge data", Proceedings of IMAC 19, the International Modal Analysis Conference, Kissimmee, FL, (2001).

Lynch, J.P., "Linear classification of system poles for structural damage detection using piezoelectric active sensors", SPIE 11th Annual International Symposium on Smart Structures and Materials, San Diego, CA, (2004).

Lynch, J.P., "Damage characterization of the IASC-ASCE structural health monitoring benchmark structure by transfer function pole migration", 2005 ASCE Structures Congress, New York, NY, (2005).

Lynch, J.P. and Hou, T.-C., "Conductivity-based strain and damage monitoring of cementitious structural components", Proceedings of the SPIE 12th Annual International Symposium on Smart Structures and Materials, San Diego, CA, March 6-10, (2005).

Lynch, J.P., Law, K.H., Kiremidjian, A.S., Carryer, E., Farrar, C.R., Sohn, H., Allen, D.W., Nadler, B. and Wait, J.R., "Design and performance validation of a wireless sensing unit for structural monitoring applications", *Structural Engineering & Mechanics*, 17(3), pp. 393-408, (2004a).

Lynch, J.P., Law, K.H., Kiremidjian, A.S., Carryer, E., Kenny, T.W., Partridge, A. and Sundararajan, A., "Validation of a wireless modular monitoring system for

structures", Smart Structures and Materials: Smart Systems for Bridges, Structures, and Highways, San Diego, CA, March 17–21, (2002a).

Lynch, J.P., Law, K.H., Kiremidjian, A.S., Kenny, T.W. and Carryer, E., "A wireless modular monitoring system for civil structures", Proceedings of the 20th International Modal Analysis Conference (IMAC XX), Los Angeles, CA, (2002b).

Lynch, J.P., Law, K.H., Kiremidjian, A.S., Kenny, T.W., Carryer, E. and Partridge, A., "The design of a wireless sensing unit for structural health monitoring", Proceedings of the 3rd International Workshop on Structural Health Monitoring, Stanford, CA, (2001).

Lynch, J.P. and Loh, K.J., "A summary review of wireless sensors and sensor networks for structural health monitoring", *The Shock and Vibration Digest*, 38(2), pp. 91-128, (2006).

Lynch, J.P., Partridge, A., Law, K.H., Kenny, T.W., Kiremidjian, A.S. and Carryer, E., "Design of piezoresistive MEMS-based accelerometer for integration with wireless sensing unit for structural monitoring", *Journal of Aerospace Engineering*, 16(3), pp. 108-114, (2003a).

Lynch, J.P., Sundararajan, A., Law, K.H., Kiremidjian, A.S. and Carryer, E., "Embedding damage detection algorithms in a wireless sensing unit for attainment of operational power efficiency", *Smart Materials and Structures, IOP*, 13(4), pp. 800-810, (2004b).

Lynch, J.P., Sundararajan, A., Law, K.H., Kiremidjian, A.S., Carryer, E., Sohn, H. and Farrar, C.R., "Field Validation of a wireless structural monitoring system on the Alamosa Canyon Bridge", *Proceedings of SPIE*, 5057, pp. 267-278, (2003b).

Lynch, J.P., Sundararajan, A., Law, K.H., Kiremidjian, A.S., Kenny, T.W. and Carryer, E., "Embedment of structural monitoring algorithms in a wireless sensing unit", *Structural Engineering and Mechanics*, 15(3), pp. 285-297, (2003c).

Lynch, J.P., Sundararajan, A., Law, K.H., Sohn, H. and Farrar, C.R., "Design and performance validation of a wireless active sensing unit", Proceedings of the International Workshop on Advanced Sensors, Structural Health Monitoring, and Smart Structures, Tokyo, Japan, (2003d).

Lynch, J.P., Sundararajan, A., Law, K.H., Sohn, H. and Farrar, C.R., "Design of a wireless active sensing unit for structural health monitoring", Proceedings of the 11th Annual International Symposium on Smart Structures and Materials, San Diego, CA, March 14–18, (2004c).

Lynch, J.P., Wang, Y., Loh, K., Yi, J. and Yun, C.-B., "Performance monitoring of the Geumdang Bridge using a dense network of high-resolution wireless sensors", *Smart Materials and Structures, IOP*, 15(6), pp. 1561-1575, (2006a).

Lynch, J.P., Wang, Y., Lu, K.-C., Hou, T.-C. and Loh, C.-H., "Post-seismic damage assessment of steel structures instrumented with self-interrogating wireless sensors", Proceedings of the 8th National Conference on Earthquake Engineering (8NCEE), San Francisco, CA, April 18-21, (2006b).

Lynch, J.P., Wang, Y., Swartz, R.A., Lu, K.-C. and Loh, C.-H., "Implementation of a closed-loop structural control system using wireless sensor networks", *Journal of Structural Control and Health Monitoring*, (2008).

Ma, C.K., Chang, J.M. and Lin, D.C., "Input forces estimation of beam structures by an inverse method", *Journal of Sound and Vibration*, 259(2), pp. 387-407, (2003).

MacGillivray, P. and Goddard, K., "Advanced sensor technology for marine propulsion control systems", Proceedings of the 11th Ship Control Systems Symposium, Southampton, UK, (1997).

Maeck, J. and De Roeck, G., "Damage assessment using vibration analysis on the Z24-Bridge", *Mechanical Systems and Signal Processing*, 17(1), pp. 133-142, (2003).

Mahin, S.A., "Lessons from damage to steel buildings during the Northridge earthquake", *Engineering Structures*, 20(4-6), pp. 261-270, (1998).

Marchesiello, S., Piombo, B.A.D. and Sorrentino, S., "Application of the CVA-BR method to the Z24 Bridge vibration data", Proceedings of IMAC 19, the International Modal Analysis Conference, Kissimmee, FL, (2001).

Maróti, M., Kusy, B., Simon, G. and Lédeczi, Á., "The flooding time synchronization protocol", Proceedings of the 2nd International Conference on Embedded Networked Sensor Systems, Baltimore, MD, (2004).

Mascarenas, D.L., Todd, M.D., Park, G. and Farrar, C.R., "Development of an impedance-based wireless sensing node for structural health monitoring", *Smart Materials and Structures*, 16, pp. 2137-2145, (2007a).

Mascarenas, D.L., Todd, M.D., Park, G. and Farrar, C.R., "Development of an impedance-based wireless sensor node for structural health monitoring", *Smart Materials and Structures*, 16(6), pp. 2137-2145, (2007b).

Mastroleon, L., Kiremidjian, A.S., Carryer, E. and Law, K.H., "Design of a new power-efficient wireless sensor system for structural health monitoring", Non-destructive Detection and Measurement for Homeland Security II, San Diego, CA, March 16–17, (2004).

McMahon, S. and Makris, N., "Large-scale ER-damper for seismic protection", *Proceedings of SPIE*, 3045, pp. 140-147, (1997).

Merovitch, L., *Elements of Vibration Analysis*, McGraw-Hill, New York, NY, (1986).

Metropolis, N., Rosembluth, A., Rosembluth, M., Teller, A. and Teller, E., "Equation of state calculations by fast computing machines", *Journal Chemical Physics*, 21, pp. 1087-1092, (1953).

Mevel, L., Goursat, M. and Basseville, M., "Stochastic subspace-based structural identification and damage detection and localisation-application to the Z24 bridge benchmark", *Mechanical Systems and Signal Processing*, 17(1), pp. 143-151, (2003).

Mirza, M.A. and Van Niekerk, J.L., "Optimal actuator placement for active vibration control with known disturbances", *Journal of Vibration and Control*, 5(5), pp. 709-724, (2003).

Mitchell, K., Rao, V.S. and Pottinger, H.J., "Lessons learned about wireless technologies for data acquisition", Proceedings of the SPIE Smart Structures and Materials 2002: Smart Electronics, MEMS, and Nanotechnology, San Diego, CA, March 18–21, (2002).

Mittag, L., "Magic in the air", *Embedded Systems Programming*, 14(10), pp. 49-60, (2001).

Montalvao, D., Maia, N.M.M. and Ribeiro, A.M.R., "A review of vibration-based structural health monitoring with special emphasis on composite materials", *The Shock and vibration digest*, 38(4), pp. 295, (2006).

Moyo, P., Brownjohn, J.M.W. and Omenzetter, P., "Highway bridge live loading assessment and load carrying capacity estimation using a health monitoring system", *Structural Engineering & Mechanics*, 18, pp. 609–626, (2004).

Mufti, A.A., Tadros, G. and Jones, P.R., "Field assessment of fibre-optic Bragg grating strain sensors in the Confederation Bridge", *Canadian Journal of Civil Engineering*, 24, pp. 963–966, (1997).

Musiani, D., Lin, K. and Rosing, T.S., "Active sensing platform for wireless structural health monitoring", 7th International Conference on Information Processing in Sensor Networks, Cambridge, MA, April 25–27, (2007).

Nagarajaiah, S. and Mate, D., "Semi-active control of continuously variable stiffness system", 2nd World Conference of Structural Control, New York, NY, (1998).

Nagarajaiah, S. and Narasimhan, S., "Smart base-isolated benchmark building. Part II: phase I sample controllers for linear isolation systems", *Structural Control & Health Monitoring*, 13, pp. 589-604, (2006).

Nagayama, T., Structural Health Monitoring Using Smart Sensors, Urbana, IL, University of Illinois at Urbana-Champaign, Ph. D., (2007).

Nagayama, T. and Spencer, B.F., Jr., *Structural Health Monitoring Using Smart Sensors*, Technical Report NSEL-001, University of Illinois, Urbana, IL, (2007).

Nagayama, T., Spencer, B.F., Jr. and Rice, J.A., "Structural health monitoring utilizing Intel's Imote2 wireless sensor platform", *Proceedings of SPIE--Sensors and Smart Structures Technologies for Civil, Mechanical, and Aerospace Systems 2007*, 6529(2), pp. 6592943, (2007).

Nurung, S., Magsino, K.C. and Nilkhamhang, I., "Force estimation using piezoelectric actuator with adaptive control", Proceedings of the 6th International Conference on Electrical Engineering/Electronics, Computer, Telecommunications and Information Technology (ECTI-CON), Piscataway, NJ, USA, (2009).

Ohtori, Y., Christenson, R.E. and Spencer, B.F., Jr. , "Benchmark control problems for seismically excited nonlinear buildings", *Journal of Engineering Mechanics*, 130(4), pp. 366-385, (2004).

Ou, J., Li, H. and Yu, Y., "Development and performance of wireless sensor network for structural health monitoring", Smart Structures and Materials, San Diego, CA, March 15–18, (2004).

Pakzad, S.N., Fenves, G.L., Kim, S. and Culler, D.E., "Design and Implementation of Scalable Wireless Sensor Network for Structural Monitoring", *Journal of Infrastructure Systems*, 14(1), pp. 89-101, (2008).

Park, G., Cudney, H.H. and Inman, D.J., "An integrated health monitoring technique using structural impedance sensors", *Journal of Intelligent Material Systems and Structures*, 11(6), pp. 448-455, (2000).

Park, G., Kabeya, K., Cudney, H.H. and Inman, D.J., "Impedance-based structural health monitoring for temperature varying applications", *JSME International Journal, Series A: Solid Mechanics and Material Engineering*, 42(2), pp. 249-258, (1999).

Park, G., Sohn, H., Farrar, C.R. and Inman, D.J., "Overview of piezoelectric impedance-based health monitoring and path forward", *The Shock and vibration digest*, 35(6), pp. 451-463, (2003).

Park, G., Sohn, H., Farrar, C.R. and Inman, D.J., "Overview of piezoelectric impedance-based health monitoring and path forward", *The Shock and Vibration Digest*, 35(6), pp. 451-463, (2007).

Peeters, B. and Ventura, C.E., "Comparative study of modal analysis techniques for bridge dynamic characteristics", *Mechanical Systems and Signal Processing*, 17(5), pp. 965-988, (2002).

Pei, J.-S., Kapoor, C., Graves-Abe, T.L., Sugeng, Y. and Lynch, J.P., "Critical design parameters and operating conditions of wireless sensor units for structural health monitoring", Proceedings of the 23rd International Modal Analysis Conference (IMAC XXIII), Orlando, FL, (2005).

Perrig, A., Stankovic, J. and Wagner, D., "Security in wireless sensor networks", *Commun. ACM*, 47(6), pp. 53-57, (2004).

Perrig, A., Szewczyk, R., Tygar, J.D., Wen, V. and Culler, D.E., "SPINS: security protocols for sensor networks", *Wireless Networks*, 8(5), pp. 521-534, (2002).

Pitchford, C., Grisso, B.L. and Inman, D.J., "Impedance-based structural health monitoring of wind turbine blades", *Proceedings of SPIE*, 6532, pp. 653211-1-653211-11 (2007).

Ploplys, N.J., Kawka, P.A. and Alleyne, A.G., "Closed-loop control over wireless networks", *IEEE Control Systems Magazine*, 24(3), pp. 58-71, (2004).

Pran, K., Johnson, G., Jensen, A.E., Hegstad, K.A., Sagvolden, G., Farsund, O., Chang, C.-C., Malsawma, L. and Wang, G., "Instrumentation of a high-speed surface effect ship for structural response characterization during seatrials", *Proceedings of SPIE*, 3986, pp. 372-379, (2002).

Press, W.H., Flannery, B.P., Teukolsky, S.A. and Vetterling, W.T., *Numerical Recipes in C: The Art of Scientific Computing*, Cambridge University Press, Cambridge, UK, (1992).

Proakis, J.G. and Manolakis, D.G., *Digital Signal Processing: Princlipes, Algorithms, and Applications*, Prentice Hall, Upper Saddle River, NJ, (1996).

Raghavan, A. and Cesnik, C.E.S., "Review of guided-wave structural health monitoring", *The Shock and vibration digest*, 39(2), pp. 91-114, (2007).

Raghavendra, C.S., Sivalingam, K.M. and Znati, T.F., *Wireless Sensor Networks*, Springer, New York, NY, (2004).

Rappaport, T.S., *Wireless Communications: Principles and Practice*, Prentice-Hall, Englewood Cliffs, NJ, (2002).

Rice, J.A. and Spencer, B.F., Jr., "Structural health monitoring sensor development for the Imote2 platform", Proceedings of the SPIE Smart Structures/NDE 2008, San Diego, CA, (2008).

Rolfes, R., Gerasch, G., Haake, G., Reetz, J. and Zerbst, S., "Early damage detection system for tower and rotor blades of offshore wind turbines", The 3rd European Workshop on Structural Health Monitoring, Granada, Spain, (2006).

Rolfes, R., Zerbst, S., Haake, G., Reetz, J. and Lynch, J.P., "Integral SHM-system for offshore wind turbines using smart wireless sensors", The 6th International Workshop on Structural Health Monitoring, Stanford, CA, (2007).

Ronkanen, P., Kallio, P. and Koivo, H.N., "Simultaneous actuation and force estimation using piezoelectric actuators", Proceedings of the IEEE International Conference on Mechatronics and Automation, Piscataway, NJ, USA, (2007).

Ruiz-Sandoval, M., Tomonori, N. and Spencer, B.F., "Sensor development using Berkeley mote platform", *Journal of Earthquake Engineering*, 10(2), pp. 289-309, (2006).

Sazonov, E., Janoyan, K. and Jha, R., "Wireless intelligent sensor network for autonomous structural health monitoring", Smart Structures and Materials: Smart Sensor Technology and Measurement Systems, San Diego, CA, March 15–17, (2004).

Schueeller, G.I., Hirtz, H. and Booz, G., "Effect of uncertanties in wind load estimation on reliability assessments", *Journal of Wind Engineering and Industrial Aerodynamics*, 14(1-3), pp. 15-26, (1983).

Schulz, M.J. and Sundaresan, M.J., *Smart Sensor System for Structural Condition Monitoring of Wind Turbines*, Technical Report NREL/SR-500-40089, National Renewable Energy Laboratory, Golden, CO, (2006).

Schwartz, B. and Richardson, M., "Post-processing ambient and forced response bridge data to obtain modal parameters", Proceedings of IMAC 19, the International Modal Analysis Conference, Kissimmee, FL, (2001).

Scruggs, J.T., "An optimal stochastic control theory for distributed energy harvesting networks", *Journal of Sound and Vibration*, 320(4-5), pp. 707-725, (2009).

Shinozuka, M., "Homeland security and safety", Proceedings of the International Conference on Structural Health Monitoring and Intelligent Infrastructure, Tokyo, Japan, (2003).

Sielski, R.A., "Research needs in aluminum structure", Proceedings of the 10th International Symposium on Practical Design of Ships and Other Floating Structures, Houston, TX, (2007).

Slaughter, S.B., Cheung, M.C., Sucharski, D. and Cowper, B., *State of the Art in Hull Monitoring Systems*, Technical Report SSC-401, Ship Structure Committee, U.S. Coast Guard, Washington D. C., (1997).

Slock, D.T.M. and Kailath, T., "Numerically stable fast transversal filters for recursive least squares adaptive filtering", *IEEE Transactions on Signal Processing*, 39(1), pp. 92-114, (1991).

Smith, D.A., Harris, M., Coffey, A.S., Mikkelsen, T., Jørgensen, H.E., Mann, J. and Danielian, R., "Wind lidar evaluation at the Danish wind test site in Høvsøre", *Wind Energy*, 9(1-2), pp. 87-93, (2006).

Sobanjo, J.O., Stukhart, G. and James, R.W., "Evaluation of projects for rehabilitation of highway bridges", *Journal of Structural Engineering*, 120(1), pp. 81-99, (1994).

Sodano, H.A., Inman, D.J. and Park, G., "A review of power harvesting from vibration using piezoelectric materials", *Shock and Vibration Digest*, 36(3), pp. 197-205, (2004).

Sodano, H.A., Inman, D.J. and Park, G., "Generation and Storage of Electricity from Power Harvesting Devices", *Journal of Intelligent Material Systems and Structures*, 16(1), pp. 67-75, (2005).

Soh, C.K., Tseng, K.K.-H., Bhalla, S. and Gupta, A., "Performance of smart piezoceramic transducers in health monitoring of RC bridge", *Smart Materials and Structures*, 9, pp. 553–542, (2000).

Soh, J.K. and Douglas, S.C., "Analysis of the stabilized FTF algorithm with leakage correction", 1996 30th Asilomar Conference on Signals, Systems & Computers, Pacific Grove, CA, (1997).

Sohn, H. and Farrar, C.R., "Damage diagnosis using time series analysis of vibration signals", *Smart Materials and Structures*, 10(3), pp. 446-451, (2001).

Sohn, H., Farrar, C.R., Hemez, F.M., Shunk, D.D., Stinemates, D.W., Nadler, B.R. and Czarnecki, J.J., *A Review of Structural Health Monitoring Literature 1996-2001*, Los Alamos National Laboratory, Los Alamos, NM, (2003).

Song, G., Ma, N. and Li, H.N., "Review of applications of shape memory alloys in civil structures", *Smart Structures and Vibrations*, 153(78), pp. 559-566, (2004).

Song, G., Sethi, V. and Li, H.-N., "Vibration control of civil structures using piezoceramic smart materials: A review", *Engineering Structures*, 28(11), pp. 1513-1524, (2006).

Soong, T.T., *Active Structural Control: Theory and Practice*, Longman Scientific and Technical, Essex, England, (1990).

Southern, A., "Michigan goes green", *dBusiness*, November, (2007).

Spencer, B.F., Jr., Ruiz-Sandoval, M.E. and Kurata, N., "Smart sensing technology: opportunities and challenges", *Structural Control & Health Monitoring*, 11, pp. 349-368, (2004).

Spencer, B.F. and Nagarajaiah, S., "State of the art of structural control", *Journal of Structural Engineering*, 129(7), pp. 845-856, (2003).

Stengle, R.F., *Optimal Control and Estimation*, Dover Publications Inc., Mineola, NY, (1994).

Stevens, K.K., "Force identification problems: an overview", Proceedings of the 1987 SEM Spring Conference on Experimental Mechanics, Houston, TX, (1987).

Storch, J. and Strang, G., "Paradox lost: natural boundry conditions in the Ritz-Galerkin method", *International Journal for Numerical Methods in Engineering*, 26, pp. 2255-2266, (1988).

Straser, E. and Kiremidjian, A.S., *Modular, Wireless Damage Monitoring System for Structures*, Technical Report 128, John A. Blume Earthquake Engineering Center, Stanford, CA, (1998).

Sun, M., Li, Z. and Song, X., "Piezoelectric effect of hardened cement paste", *Cement and Concrete Composites*, 26(6), pp. 717-720, (2004).

Swartz, R.A., Jung, D., Lynch, J.P., Wang, Y., Shi, D. and Flynn, M.P., "Design of a wireless sensor for scalable distributed in-network computation in a structural health monitoring system", 5th International Workshop on Structural Health Monitoring, Stanford, CA, (2005).

Symans, M.D. and Constantinou, M.C., "Semi-active control systems for seismic protection of structures: a state-of-the-art review", *Engineering Structures*, 21, pp. 469-487, (1999).

Tanner, N.A., Farrar, C.R. and Sohn, H., "Structural health monitoring using wireless sensing system with embedded processing ", *Proceedings of SPIE*, 4704, pp. 215-224, (2002).

Teughels, A. and De Roeck, G., "Structural damage identification of the highway bridge Z24 by FE model updating", *Journal of Sound and Vibration*, 278, pp. 589-610, (2004).

Texas Instruments, *ADS8341 16-Bit, 4-Channel Serial Output Sampling Analog-to-Digital Converter*, Texas Instruments Incorporated, Dallas, TX, (2003).

Texas Instruments, *CC2420 2.4 GHz IEEE 802.15.4 / ZigBee-ready RF Transceiver*, Texas Instruments Incorporated, Dallas, TX, (2008).

Todd, M.D., Nichols, J.M., Trickey, S.T., Seaver, M., Nichols, C.J. and Virgin, L.N., "Bragg grating-based fibre optic sensors in structural health monitoring", *Philosophical Transactions of the Royal Society A*, 365(1851), pp. 317-343, (2007).

Turner, A., Graver, T.W., Rumsey, M.A. and Mendez, A., "Wind turbine structural health monitoring using optical biber based sensors", Proceedings of the 7th International Workshop on Structural Health Monitoring, Stanford, CA, (2009).

Tweedie, K., "Wind farm fears as blade snaps", *The Times*, April 16, (2005).

Uematsu, Y., Kuribara, O., Yamada, M., Sasaki, A. and Hongo, T., "Wind-induced dynamic behavior and its load estimation of a single-layer latticed dome with a long span", *Journal of Wind Engineering and Industrial Aerodynamics*, 89(14-15), pp. 1671-1687, (2001).

Uematsu, Y., Yamada, M. and Sasaki, A., "Wind-induced dynamic response and resultant load estimation for a flat long-span roof", *Journal of Wind Engineering and Industrial Aerodynamics*, 65(1-3), pp. 155-166, (1996).

Veers, P.S. and Butterfield, S., "Extreme Load Estimation for Wind Turbines: Issues and Opportunities for Improved Practice", Proceedings of 2001 ASME Wind Energy Symposium, Reno, NV, (2001).

Wang, M.L., Gu, H., Lloyd, G.M. and Zhao, Y., "A multichannel wireless PVDF displacement sensor for structural monitoring", Proceedings of the International

Workshop on Advanced Sensors, Structural Health Monitoring and Smart Structures, Tokyo, Japan, (2003).

Wang, Y., Wireless Sensing and Decentralized Control for Civil Structures: Theory and Implementation, Stanford, CA, USA, Stanford University, Ph.D., (2007).

Wang, Y., Lynch, J.P. and Law, K.H., "Wireless structural sensors using reliable communication protocols for data acquisition and interrogation", Proceedings of the 23rd International Modal Analysis Conference (IMAC XXIII), Orlando, FL, USA, (2005).

Wang, Y., Swartz, A., Lynch, J.P., Law, K.H., Lu, K.-C. and Loh, C.-H., "Wireless feedback structural control with embedded computing", Proceedings of SPIE--11th International Symposium on Nondestructive Evaluation for Health Monitoring and Diagnostics, San Diego, CA, (2006a).

Wang, Y., Swartz, R.A., Lynch, J.P., Law, K.H., K.-C., L. and C.-H., L., "Decentralized civil structural control using a real-time wireless sensing and control system", 4th World Conference on Structural Control and Monitoring (4WCSCM), San Diego, CA, (2006b).

Wenzel, H. and Pichler, D., *Ambient Vibration Monitoring*, John Wiley & Sons, West Sussex, UK, (2005).

Whelan, M.J., Gangone, M.V., Janoyan, K.D., Cross, K. and Jha, R., "Reliable high-rate bridge monitoring using dense wireless sensor arrays", International Workshop on Structural Health Monitoring, Stanford, CA, (2007).

White, J.R., Adams, D.E. and Rumsey, M.A., "Operational load estimation of a smart wind turbine rotor blade", Proceedings of the SPIE 7295 - Health Monitoring of Structural and Biological Systems 2009, San Diego, CA, (2009).

Wie, Z., Yam, L.H. and Cheng, I., "NARMAX model representation and its application to damage detection for multi-layer composites", *Composite Structures*, 68, pp. 109-117, (2005).

Window, A.L., Ed. *Strain Gauge Technology*, Elsevier Applied Science, London, UK, (1992).

Wiser, R. and Bolinger, M., *Annual Report on U.S. Wind Power Installation, Costruction and Performance Trends: 2006*, U.S. Department of Energy (DOE), Washington D. C., (2007).

Womack, K. and Hodson, J., "System identification of the Z24 Swiss bridge", Proceedings of IMAC 19, the International Modal Analysis Conference, Kissimmee, FL, (2001).

Yan, G., Dyke, S.J. and Song, W., "Structural damage localization with tolerance to large time synchronization errors in WSNs", Proceedings of the 2009 American Control Conference, St. Louis, MO, (2009).

Yao, J.T.P., "Concept of structural control", *Journal of the Structural Division*, 98(7), pp. 1567-1574, (1972).

Yi, F. and Dyke, S.J., "Performance of smart structures", *Smart Structures and Materials 2000: Smart Systems for Bridges, Structures, and Highways, Proceedings of SPIE*, 3968, pp. 94-104, (2000).

Ying, L., Anne, S.K., Nair, K.K., Jerome, P.L. and Kincho, H.L., "Algorithms for time synchronization of wireless structural monitoring sensors", *Earthquake Engineering & Structural Dynamics*, 34(6), pp. 555-573, (2005).

Yoe, J.G., Raja, M.K.R.V., Hardesty, R.M., Brewer, W.A., Moore, B., III, Ryan, J.M., Hays, P.B., Nardell, C.A., Gentry, B.M., Day, M. and Rancourt, K., "GroundWinds 2000 field campaign: demonstration of new Doppler lidar technology and wind lidar data intercomparison", Lidar Remote Sensing for Industry and Environment Monitoring III, Hangzhou, China, (2003).

Yook, J.K., Tilbury, D.M. and Soparkar, N.R., "Trading computation for bandwidth: reducing communication in distributed control systems using state estimators", *IEEE Transactions on Control Systems Technology*, 10(4), pp. 503-518, (2002).

Yu, L. and Chan, T.H.T., "Recent research on identification of moving loads on bridges", *Journal of Sound and Vibration*, 305(1-2), pp. 3-21, (2007).

Zhang, Y. and Lu, L.-W., "Introducing smart structures technology into civil engineering curriculum: education development at Lehigh University", *Journal of Professional Issues in Engineering Education and Practice*, 134(1), pp. 41-48, (2008).

Zhao, F. and Guibas, L.J., *Wireless Sensor Networks an Information Processing Approach*, Morgan Kaufmann Publishers, San Francisco, CA, (2004).

Zhao, Z. and Haldar, A., "Bridge fatigue damage evaluation and updating using non-destructive inspections", *Engineering Fracture Mechanics*, 53(5), pp. 775-788, (1996).

Zimmerman, A.T. and Lynch, J.P., "A parallel simulated annealing architecture for model updating in wireless sensor networks", *IEEE Sensors Journal, IEEE*, 9(11), pp. 1503-1510, (2009).

Zimmerman, A.T., Shiraishi, M., Swartz, R.A. and Lynch, J.P., "Automated modal parameter estimation by parallel processing within wireless monitoring systems", *Journal of Infrastructure Systems*, 14(1), pp. 102-113, (2008).

Zoughi, R. and Kharkovsky, S., "Microwave and millimetre wave sensors for crack detection", *Fatigue & Fracture of Engineering Materials & Structures*, 31(8), pp. 695-713, (2008).